frontiers | Research Topics

Molecular pathogenesis and novel treatments for inherited cardiomyopathies

Edited by
Michael T. Chin, John Lynn Jefferies and Hilary Vernon

Published in
Frontiers in Cardiovascular Medicine

ISSN 1664-8714
ISBN 978-2-8325-3517-2
DOI 10.3389/978-2-8325-3517-2

About Frontiers

Frontiers is more than just an open access publisher of scholarly articles: it is a pioneering approach to the world of academia, radically improving the way scholarly research is managed. The grand vision of Frontiers is a world where all people have an equal opportunity to seek, share and generate knowledge. Frontiers provides immediate and permanent online open access to all its publications, but this alone is not enough to realize our grand goals.

Frontiers journal series

The Frontiers journal series is a multi-tier and interdisciplinary set of open-access, online journals, promising a paradigm shift from the current review, selection and dissemination processes in academic publishing. All Frontiers journals are driven by researchers for researchers; therefore, they constitute a service to the scholarly community. At the same time, the *Frontiers journal series* operates on a revolutionary invention, the tiered publishing system, initially addressing specific communities of scholars, and gradually climbing up to broader public understanding, thus serving the interests of the lay society, too.

Dedication to quality

Each Frontiers article is a landmark of the highest quality, thanks to genuinely collaborative interactions between authors and review editors, who include some of the world's best academicians. Research must be certified by peers before entering a stream of knowledge that may eventually reach the public - and shape society; therefore, Frontiers only applies the most rigorous and unbiased reviews. Frontiers revolutionizes research publishing by freely delivering the most outstanding research, evaluated with no bias from both the academic and social point of view. By applying the most advanced information technologies, Frontiers is catapulting scholarly publishing into a new generation.

What are Frontiers Research Topics?

Frontiers Research Topics are very popular trademarks of the *Frontiers journals series*: they are collections of at least ten articles, all centered on a particular subject. With their unique mix of varied contributions from Original Research to Review Articles, Frontiers Research Topics unify the most influential researchers, the latest key findings and historical advances in a hot research area.

Find out more on how to host your own Frontiers Research Topic or contribute to one as an author by contacting the Frontiers editorial office: frontiersin.org/about/contact

Molecular pathogenesis and novel treatments for inherited cardiomyopathies

Topic editors

Michael T. Chin — Tufts Medical Center, United States

John Lynn Jefferies — University of Tennessee Health Science Center (UTHSC), United States

Hilary Vernon — The Johns Hopkins Hospital, Johns Hopkins Medicine, United States

Citation

Chin, M. T., Jefferies, J. L., Vernon, H., eds. (2023). *Molecular pathogenesis and novel treatments for inherited cardiomyopathies*. Lausanne: Frontiers Media SA. doi: 10.3389/978-2-8325-3517-2

Table of contents

frontiers | Frontiers in Cardiovascular Medicine

TYPE Editorial
PUBLISHED 06 September 2023
DOI 10.3389/fcvm.2023.1282852

OPEN ACCESS

EDITED AND REVIEWED BY
Neil Morgan,
University of Birmingham, United Kingdom

*CORRESPONDENCE
Michael T. Chin
✉ Michael.t.chin@tuftsmedicine.org

RECEIVED 24 August 2023
ACCEPTED 28 August 2023
PUBLISHED 06 September 2023

CITATION
Chou C, Vemon HJ, Jefferies JL and Chin MT (2023) Editorial: Molecular pathogenesis and novel treatments for inherited cardiomyopathies.
Front. Cardiovasc. Med. 10:1282852.
doi: 10.3389/fcvm.2023.1282852

Editorial: Molecular pathogenesis and novel treatments for inherited cardiomyopathies

Chun Chou[1], Hilary J. Vemon[2], John L. Jefferies[3] and Michael T. Chin[1,4]*

[1]Department of Medicine, Tufts University School of Medicine, Boston, MA, United States, [2]Department of Genetic Medicine, Johns Hopkins University School of Medicine, Baltimore, MD, United States, [3]Division of Cardiology, Department of Medicine, University of Tennessee Health Sciences Center, Memphis, TN, United States, [4]Molecular Cardiology Research Institute, Tufts Medical Center, Boston, MA, United States

KEYWORDS

inherited cardiomyopathy, hypertrophic cardiomyopathy, dilated cardiomyopathy, iron overload cardiomyopathy, rasopathy, arrhythmogenic cardiomyopathy

Editorial on the Research Topic
Molecular pathogenesis and novel treatments for inherited cardiomyopathies

Inherited cardiomyopathies have diverse genetic etiologies, but together are major contributors to cardiac disease that affect patients of all ages, typically with early onset in childhood or adolescence. While inherited cardiomyopathies are currently classified according to functional and morphologic features, finer resolution of these categories has been made possible with the aid of modern genetics. However, despite the identification of many disease-causing variants, effective therapies for the majority of inherited cardiomyopathies remains scarce. In this issue, a collection of original research and review articles unveil and summarize the pathogenic mechanisms and gene expression signatures of various inherited cardiomyopathies as well as novel and extant therapeutic strategies in treating selected subsets of inherited cardiomyopathies.

While genetic evaluation of family with a cardiomyopathy is increasingly common, in clinical practice, molecular insights do not supersede the clinical phenotyping and classification of inherited cardiomyopathies since different mutations in the same gene can result in distinct disorders. This is best exemplified in a review by Hilal et al. which discusses in detail how mutations in RAS genes underlie phenotypically diverse cardiomyopathies in addition to distinct systemic syndromology. Notably, one must cautiously distinguish cardiomyocyte-intrinsic from extrinsic effects of RAS hyperactivation. While several *in vitro* studies demonstrated that ectopic RAS activation results in cardiomyocyte hypertrophy, cardiomyocyte-specific expression of gain-of-function RAS variants did not result in HCM despite cardiomyocyte hypertrophy seen in neonatal mice carrying the same germline mutation in the RAS gene (1). Whether other RAS variants promote cardiomyopathy in a cardiomyocyte-extrinsic mechanism has not been exhaustively tested.

As the affordability of multiple "omics" technologies have increased in recent years, whole-exome sequencing has become the new standard to identify novel genetic variants. Recently, a variant of crystallin alpha B, R123W, was identified in a pair of homozygotic twins who develop concordant HCM (2). Chou et al. further demonstrated that mice

carrying the *Cryab*^{R123W} indeed recapitulates several key features of human HCM. Mechanistically, this CRYAB variant promotes pathologic calcium signaling through an unexpected protein-protein interaction with calcineurin, uncovering yet another sarcomere-independent mechanism of HCM pathogenesis. Also included in this issue was a case report by Liu et al. who identified a novel variant of DSG2 in a pediatric patient with arrhythmogenic cardiomyopathy misdiagnosed as myocarditis. Although both CRYAB^{R123W} and DSG2 c.1592T > G are rare variants, they nevertheless provided novel insights into previously unappreciated pathogenic mechanisms of inherited cardiomyopathies.

In addition to mutations in protein-coding genes, non-coding genetic variants have increasingly been recognized as potential modifiers or primary contributors towards pathogenic processes. Htet et al. reviewed known associations between non-coding genetic mutations and various inherited cardiomyopathies. In addition to splice site variants which affect function of encoded protein, mutations in other regulatory elements, such as untranslated regions and microRNAs, are also reviewed. Cao and Yuan further uncovered that three distinct lncRNAs were differentially expressed between control and HCM patients regardless of sarcomere mutation. Intriguingly, expression of mRNA co-expressed with these lncRNA is not consistently different between HCM patients and controls. Thus, the mechanism by which the three lncRNAs are differentially regulated during HCM pathogenesis is unclear. As with other omics studies, whether differential expression of lncRNA is biologically relevant remains to be tested.

In addition to identifying genetic mutations associated with various inherited cardiomyopathies, mechanistic studies that elucidate the molecular consequences of these genetic mutations are also underway. Considering that adult hearts almost solely utilize fatty acid oxidation to generate ATP, Gaar-Humphreys et al. reviewed how biological processes associated with lipid metabolism are altered in various inherited cardiomyopathies. Intriguingly, disrupted metabolism is present in inherited cardiomyopathies regardless of the pathogenic DNA variant or phenotypes, though etiology- and phenotype-specific alterations in lipid metabolism also exist. Notably, expression of PPAR family transcription factors, key regulators of fatty acid uptake and oxidation, is generally suppressed in both DCM and HCM. Although how PPAR affects DCM and HCM pathogenesis remains unclear, several well-established PPAR agonists are readily available for pre-clinical studies.

Lastly, a series of seminal studies and reviews summarize recent advances in diagnostic tools and medical therapies for various inherited cardiomyopathies. While increasing evidence suggest that additional etiologies, aside from the canonical monogenic mechanism, for HCM are prevalent, sarcomere gene mutations leading to contractile dysfunction still represents a prevailing model of HCM pathogenesis. Extensive translational research over the past decades has thus focused on developing therapies to reverse sarcomere defects. A mini review by Sewanan and Shimada summarizes the results of clinical trials assessing efficacy of myosin-targeted agents, including mavacamten in HCM patients with LVOT obstruction. Whether mavacamten also delays cardiac remodeling in patient without LVOT obstruction is currently being tested. Furthermore, considering that cardiomyocyte hypertrophy is a defining feature of HCM regardless of sarcomere gene mutations, it would be intriguing to evaluate whether myosin-modulators also exert similar beneficial effect in patients without sarcomere mutations, using subgroup analysis of existing trials.

The structural changes associated with cardiac remodeling predispose HCM patients to ventricular arrythmias. However, there has not been a practical biomarker to predict who is most at risk of developing arrythmia. Zhang et al. analyzed EKG patterns in a cohort of Chinese population with HCM who has also received ICD implantation, and identified QTc duration > 464 ms and long or deep S wave in V4 lead as predictive markers for appropriate ICD shocks. Future retrospective studies to assess how well these EKG abnormalities predict first ventricular arrythmias in patients without ICD as secondary prevention would be valuable in guiding timing of ICD implantation.

Considering that diagnosis of DCM is often delayed until signs and symptoms of heart failure manifest, Zhang et al. performed multi-model machine learning on existing microarray data from DCM patients and healthy controls to develop a predictive model that may facilitate early DCM diagnosis. Notably, three DCM signature genes were identified and reassuringly, the plasma levels of proteins encoded by all three genes were indeed altered in an independent patient cohort. It is, however, surprising that three genes are sufficient to identify DCM in a testing dataset. A few caveats remain: the severity of disease in patients from the testing dataset is unclear and whether the "healthy controls" contain patients with undiagnosed DCM also remains unclear. Additionally, whether the expression pattern of these three genes is specific to DCM needs to be tested.

Another form of inherited cardiomyopathy, iron overload cardiomyopathy (IOC), represents a major co-morbidity of genetic hemochromatosis as well as secondary iron overload. A recent clinical trial demonstrated that amlodipine and chelation combination therapy significantly lowers intracardiomyocyte iron deposition. Mechanistically, amlodipine appears to block the L-type calcium channel, which otherwise provides a major route for iron entry into the cardiomyocyte. Zhabyeyev et al. demonstrated that a genetic mouse model of primary hemochromatosis when fed with high iron diet recapitulates histological, electrical and echocardiographic defects seen in patients with primary hemochromatosis. Furthermore, such phenotypes were markedly reversed with amlodipine treatment. Although the study does not provide further mechanistic insights, it nevertheless highlights a translatable mouse model that may serve as platform for development of future IOC therapies.

Over the past decades, the identification of genes in which pathogenic variants are associated with inherited cardiomyopathies has raised expectations for new therapies. Advances in genomic editing technology hold promise for directly targeting pathogenic variants, and have the potential for shifting the paradigm for treatment in genetic medicine. Other approaches harnessing natural genetic modifying mechanisms

that suppress the penetrance of pathogenic variants may also be useful. While the incomplete penetrance of inherited cardiomyopathies often complicates the genetic evaluations of families with cardiomyopathies, the observation that many mutation carriers remain disease free in fact provides paradoxical hope that disease-modifying therapeutics may be achievable. Future omics studies comparing transcriptome and proteome between clinically active and silent mutation carriers may thus uncover novel therapeutic approaches to delaying disease onset. In parallel, development of additional genetic animal models that approximate human cardiomyopathies will enable rigorous mechanistic studies that potentiate development of therapeutic agents.

Author contributions

CC: Writing – original draft. HV: Writing – review & editing. JJ: Writing – review & editing. MC: Writing – review & editing.

Conflict of interest

The authors declare that the research was conducted in the absence of any commercial or financial relationships that could be construed as a potential conflict of interest.

The author(s) declared that they were an editorial board member of Frontiers, at the time of submission. This had no impact on the peer review process and the final decision.

Publisher's note

References

1. Dalin MG, Zou Z, Scharin-Tang M, Safari R, Karlsson C, Bergo MO. Myocardial KRAS(G12D) expression does not cause cardiomyopathy in mice. *Cardiovasc Res*. (2014) 101:229–35. doi: 10.1093/cvr/cvt260

2. Maron BJ, Rowin EJ, Arkun K, Rastegar H, Larson AM, Maron MS, et al. Adult monozygotic twins with hypertrophic cardiomyopathy and identical disease expression and clinical course. *Am J Cardiol*. (2020) 127:135–8. doi: 10.1016/j.amjcard.2020.04.020

frontiers | Frontiers in Cardiovascular Medicine

ORIGINAL RESEARCH
published: 12 May 2022
doi: 10.3389/fcvm.2022.882662

Association of QTc Interval and V4-S Wave With Appropriate ICD Therapy in Hypertrophic Cardiomyopathy

Nixiao Zhang[1,2†], Sijing Cheng[2†], Hongxia Niu[2], Min Gu[2], Hui Peng[1], Zhijun Sun[1], Xi Liu[2], Yu Deng[2], Xuhua Chen[2] and Wei Hua[2*]*

[1] Department of Cardiology, Cardiovascular Center, Beijing Friendship Hospital, Capital Medical University, Beijing, China, [2] Cardiac Arrhythmia Center, Fuwai Hospital, National Center for Cardiovascular Diseases, Chinese Academy of Medical Sciences and Peking Union Medical College, Beijing, China

OPEN ACCESS

Edited by:
Paolo Emilio Puddu,
Université de Caen Normandie, France

Reviewed by:
Emanuele Bertaglia,
Clinica Cardiologica - Azienda Ospedale Università, Italy
Michele Schiariti,
Sapienza University of Rome, Italy

***Correspondence:**
Wei Hua
drhuaweifw@sina.com
Hui Peng
liumanyi2005@sina.cn

[†] These authors have contributed equally to this work

Specialty section:
This article was submitted to Cardiovascular Epidemiology and Prevention, a section of the journal Frontiers in Cardiovascular Medicine

Received: 24 February 2022
Accepted: 14 April 2022
Published: 12 May 2022

Citation:
Zhang N-X, Cheng S-J, Niu H-X, Gu M, Peng H, Sun Z-J, Liu X, Deng Y, Chen X-H and Hua W (2022) Association of QTc Interval and V4-S Wave With Appropriate ICD Therapy in Hypertrophic Cardiomyopathy. Front. Cardiovasc. Med. 9:882662. doi: 10.3389/fcvm.2022.882662

Background: Ventricular arrhythmias in patients with hypertrophic cardiomyopathy (HCM) may lead to sudden cardiac death (SCD). We aimed to investigate the relationship between electrocardiogram (ECG) indicators and the risk of appropriate implantable cardioverter-defibrillator (ICD) therapy in HCM.

Methods: The HCM patients receiving ICD implantation were enrolled consecutively. QT interval correction (QTc) was calculated using Bazett's formula. Long or deep S wave in V4 lead was defined as duration time >50 ms and/or voltage amplitude >0.6 mV. The endpoint in our study was at least one ICD appropriate therapy triggered by ventricular tachyarrhythmia (VT) or ventricular fibrillation (VF), including anti-tachyarrhythmia pacing (ATP) and electrical shock.

Results: A total of 149 patients with HCM (mean age 53 ± 14 years, male 69.8%) were studied. Appropriate ICD therapies occurred in 47 patients (31.5%) during a median follow-up of 2.9 years. Cox regression analysis showed that long or deep S wave in V4 lead [hazard ratio (HR) 1.955, 95% confidence interval (CI) 1.017–3.759, $P = 0.045$] and QTc interval (HR 1.014, 95% CI 1.008–1.021, $P < 0.001$) were independent risk factors for appropriate ICD therapy. The ROC showed that the optimal cut-off point value for the QTc interval to predict the appropriate ICD therapy was 464 ms, and the AUC was 0.658 (95% CI 0.544–0.762, $P = 0.002$). The AUC for S wave anomalies in V4 lead was 0.608 (95% CI 0.511–0.706, $P = 0.034$). We developed a new model that combined the QTc interval and S wave anomalies in V4 lead based on four patient groups. Patients with QTc ≥464 ms and long or deep V4-S wave had the highest risk of developing appropriate ICD therapy (log-rank $P < 0.0001$). After adding QTc interval and V4-S wave anomalies into the HCM-risk-SCD model, the prediction effect of the new model was significantly improved, and the NRI was 0.302.

Conclusions: In this HCM cohort, QTc and S wave anomalies in V4 lead were found to be significant and strong predictors of the risk of appropriate ICD therapy.

Patients with QTc ≥464 ms and long or deep S wave had the highest risk. After QTc interval and V4-S wave anomalies adding to the HCM-risk-SCD model, the prediction effect is significantly improved.

Keywords: hypertrophic cardiomyopathy, implantable cardioverter-defibrillator, appropriate therapy, electrocardiogram, sudden cardiac death (SCD)

INTRODUCTION

The pathophysiological characteristics of hypertrophic cardiomyopathy (HCM) are cardiomyocyte hypertrophy, interstitial fibrosis and disorder of the cardiomyocyte fiber arrangement, which increase the risk of sudden cardiac death (SCD) (1). These structural changes may explain the abnormality in the electrical activity of the left ventricle, including depolarization and repolarization on the surface electrocardiogram (ECG) (1, 2). The ECG patterns showed non-specific change in 75 to 95% of HCM patients (3). Recent studies found that the severity of ECG abnormalities was associated with structural and functional findings in cardiac magnetic resonance (CMR), including left ventricular mass, myocardial hypertrophy, and fibrosis (4–7). However, whether these ECG abnormalities are related to electrical instability and could identify patients with a higher risk of ventricular arrhythmia (VT) or SCD is still not determined. The HCM risk-SCD model recommended by 2014 European Society of Cardiology guidelines was widely used in clinical practice. The HCM risk-SCD model included family history of SCD, maximal left ventricular wall thickness, syncope, non-sustained ventricular tachyarrhythmias (NSVT), age, left atrial diameter (LAD), and maximal left ventricular outflow tract gradient (LVOTG) (8). In 2019, the enhanced American College of Cardiology/American Heart Association guideline incorporated novel high-risk markers, such as extensive late gadolinium enhancement (LGE), systolic dysfunction and left apical ventricular aneurysms (9). These models provide essential value for the selection of patients suitable for implantable cardioverter defibrillator (ICD).

However, there are some controversies regarding the effect of these two assessment methods (10, 11). These two methods were not ideal for predicting the risk of SCD when applied to Chinese patients (11). Therefore, it is complicated to determine the risk stratification of the patients and make a decision on ICD implantation.

Standard 12-lead ECG is a simple, reproducible and inexpensive test that could be used by cardiologists and general practitioners and is one of the non-invasive tools for HCM patients (12, 13). Fragmented of the QRS complex (fQRS) on the ECG was the manifestation of abnormal cardiac depolarization and was associated with myocardial fibrosis (14). Studies have found that fQRS was the independent risk factor of arrhythmic events in ischemic cardiomyopathy and non-ischemic cardiomyopathy (15). It was also the marker of the substrate for spontaneous ventricular fibrillation in Brugada syndrome patients and was the diagnostic marker of arrhythmogenic right ventricular dysplasia (16, 17). QT prolongation was the arrhythmogenic substrate in long QT syndrome and drug-induced QT prolongation (18). Several studies evaluating the role of QTc prolongation in HCM did not have homogenous findings (4, 19, 20). HCM patients could have huge T-wave inversion in ECG (TWI). However, it is still unknown whether the TWI is secondary to depolarization abnormality or repolarization abnormality. The prediction value of TWI for SCD risk was still controversial (21, 22). Recently, Lyon et al. (23) used mathematical modeling and computational clustering to analyze the 12-lead Holter ECGs for the prediction of the risk of SCD. This study included 85 patients and 38 healthy volunteers and had found that primary TWI may increase SCD risk in HCM. Our aim was to investigate whether 12-lead ECG could predict ICD therapy in a Chinese HCM cohort.

METHODS

Study Population

This is a retrospective single-center observational study. One hundred and sixty four HCM patients who successfully implanted ICD in Fuwai hospital between June 2007 and August 2020 were included. Patients had the indication for ICD when they had at least one of the following risk factors (24): (1) history of resuscitation of cardiac arrest, (2) history of premature HCM- related sudden death in one or more first-degree relatives, (3) documented non-sustained ventricular fibrillation, (4) documented ventricular events or unexplained syncope, or decision regarding the risk status and ICD implantation was made at the discretion of the managing cardiovascular specialists (usually involving electrophysiologists) using established risk stratification for primary or secondary prevention of SCD. Fifteen patients were excluded as follows: (1) need for ventricular pacing ($n = 5$), (2) lost to follow-up ($n = 3$), (3) low-quality ECG ($n = 7$). The study conformed to the principles of the Declaration of Helsinki. Written informed consent was obtained from each patient.

Diagnosis of HCM

HCM was defined as left ventricular thickness ≥15 mm (or ≥13 mm if family history of HCM was present) in one or more ventricular myocardial segments measured by echocardiography, cardiac magnetic resonance (CMR) or computed tomography (CT) in the absence of another cause of hypertrophy (25).

ECG Diagnosis and Analysis

We retrospectively analyzed the 12-lead ECG of HCM patients prior to ICD implantation. ECG was measured at 25 mm/s paper speed, 10 mm/mV amplitude and 0.05-100 Hz filter setting. We only analyzed clearly recorded ECG. The ECG signals were calculated as the mean of three consecutive beats by an ECG

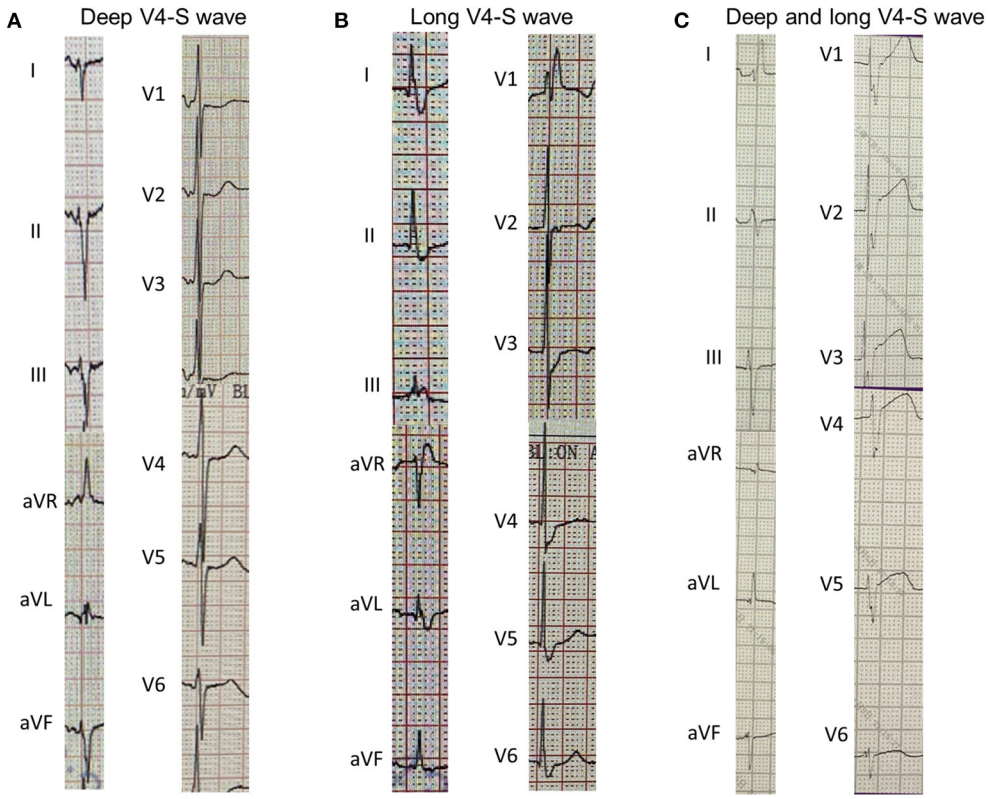

FIGURE 1 | Three cases of long or deep V4-S wave in 12-lead electrocardiogram. **(A)**, V4-S wave depth >0.6 mV; **(B)**, V4-S wave duration >50 ms; **(C)**, V4-S wave is wide and deep.

caliper through an electronic medical recording system. The signals were measured and averaged by two researchers (NX Zhang and SJ Cheng) in the same ECG, who were blinded to the patients' medical status.

The signals we analyzed included heart rate, complete left bundle branch block (cLBBB), complete right bundle branch block (cRBBB), atrioventricular block (AVB), left ventricular high voltage (LVHV), fQRS, deep S wave or long S wave in V4, TWI, P wave duration, PR duration, QRS duration and corrected QT interval (QTc). The signals except the S wave were measured in lead II, V5 or V6.

The cLBBB was defined as QRS duration >120 ms, QS or rS in lead V1, wide R wave with the absence of Q wave in lead I or lead V6, notched or slurred QRS in more than two leads of V1, V2, V5, V6, I, aVL. The cRBBB was defined as a late R (R') in V1 or V2, with slurred wide S wave in leads I and V5/V6 and QRS duration >120 ms. LVHV was based on Cornell criteria (S wave amplitude in V3 plus R wave amplitude in aVL ≥20 mm in female and ≥28 mm in male) or Sokolow-Lyon criteria (S wave amplitude in V1 or V2 plus R wave amplitude in V5 or V6 ≥35 mm). fQRS was defined as RSR' morphology (an additional R wave or notching in the nadir of the S wave) in more than two contiguous leads. Long or deep S wave was defined as prolongation of S wave (S wave duration >50 ms in V4 lead) and/or S wave amplitude deepening (>0.6 mV) (Three cases of patients with long or deep S wave were listed in **Figure 1**). TWI was defined as the amplitude of T wave >0.1 mV, and huge TWI was defined as amplitude >1.0 mV. PR duration was measured between the start of the P wave and the beginning of the QRS complex. QRS duration was measured between the start of the QRS complex and the J point. QT interval was measured between the start of the QRS complex and the end of the T wave. QTc was calculated according to Bazett's formula ($QTc = QT/(RR)^{1/2}$). The end of the T wave was defined as the intersection between the tangent of the descending limb of the T wave and the isoelectric line. If there was a U wave after the T wave, the end of the T wave was the intersection of the tangent of the steepest part of the T wave descending limb and the isoelectric line.

ICD Therapy and Follow-Up

We regularly implanted transvenous ICD. In patients without venous access, with the difficult crossing of the tricuspid valve, or after tricuspid valve replacement, S-ICD was implanted. Type and programming parameters of ICD were based on the decision-making of patients and doctors. The appropriate ICD therapy was defined as delivering anti-tachycardia pacing (ATP) or shock for sustained ventricular tachycardia (VT) or ventricular fibrillation (VF). We documented the occurrence of ICD therapy for VT or VF via stored electrograms and reviewed by an experienced electrophysiologist. For patients without program information,

we obtained the ICD therapy information via the medical calls. The censored date was January 31th, 2021.

HCM-risk-SCD Model

HCM-risk-SCD model was calculated as follows: 5-year risk = 1-0.998 exp (prognosis index), where prognosis index = [0.15939858*Maximal wall thickness (mm)]– [0.00294271*Maximal wall thickness^2(mm^2)] + [0.826391195*NSVT] + [0.0259082*LAD (mm)]+ [0.00446131*maximal LVOTG (mmHg)] + [0.71650361* unexplained syncope] + [0.4583082* family history of SCD] – [0.01799934*age at evaluation (years)] (8).

Statistical Analysis

All analysis were done using SPSS version 25.0 and R version 3.6. Continuous variables were presented with mean and standard deviation or median and interquartile range according to distribution. Student's *t*-test or Mann-Whitney *U*-test was used to compare groups as appropriate. Categorical variables were presented with count and percentage, and Chi-square was used to compare. Receiver operating characteristic (ROC) curves were generated to evaluate the prediction efficacy of factors for SCD and calculate the best cutoff value of QTc. The prediction efficacy was presented with the area under the curve (AUC), and the larger the AUC was, the greater the prediction efficacy was. We used the Cox regression model to select the prediction factor for SCD. We included all variables that showed a trend toward an association with effect at uni-variable Cox regression analysis ($P < 0.1$). And we also included the use of amiodarone as it could affect the QTc. Pearson correlation test was used to analyze the relationship between QTc and MWT, and the Spearman correlation test for the relationship between QTc and LVOTG. Net reclassification index (NRI) was used to evaluate the change of prediction efficacy. *P*-value < 0.05 were considered significant.

RESULTS

Characteristics of the Patient

One hundred forty-nine HCM patients were enrolled in our study. Among these, 9 of 149 patients (6.0%) had apical hypertrophic cardiomyopathy (APHCM), 102 patients (68.5%) implanted ICD for primary prevention, while 47 patients (31.5%) implanted ICD for secondary prevention. Among these patients, 23 (15.4%) had coronary heart disease. The mean HCM- SCD risk score was 5±3%. For ECG indicators, 37 patients (24.8%) had LVHV; 19 patients (12.8%) had fQRS; 73 patients (49%) had long or deep S wave; and 65 patients (43.6%) had TWI, of whom six patients (4.0%) had huge TWI. The mean duration of P wave, PR duration, QRS complex and QTc interval was 105 ± 36 ms, 168 ± 51 ms, 111 ± 27 ms, and 445 ± 45 ms, respectively (**Table 1**).

Follow-Up

The median follow-up was 2.9 years (IQR: 1.7–5.6 years). Forty Seven patients (31.5%) received ICD appropriate therapy. The characteristics of patients who received appropriate ICD and who did not receive appropriate ICD therapy are presented in **Table 1**. The baseline characteristics and echocardiography parameters were similar between the two groups, except for a higher proportion of patients with atrial fibrillation (AF) without appropriate ICD therapy (34.3 vs. 17.0%, $P = 0.03$). There was a higher proportion of patients with long or deep S wave in V4 among patients with appropriate ICD therapy (63.8 vs. 42.2%, $P = 0.021$). Moreover, patients with appropriate ICD therapy had longer QTc (464 ms ± 56 ms vs. 436 ± 36 ms, $P = 0.003$).

Cox Regression Analysis

In univariate Cox regression analysis, long or deep S wave was significantly associated with appropriate ICD therapy (HR 2.197, 95%CI 1.197–4.035, $P = 0.011$). QTc at baseline and RBBB were also significantly associated with ICD appropriate therapy (HR 1.014, 95%CI 1.008–1.021, $P < 0.001$; HR 3.196, 95%CI 1.342–7.613, $P = 0.009$, respectively). In multivariate analysis, we included AF, RBBB, long or deep S wave, QTc, HCM-risk SCD score and history of amiodarone. We did not include age, family history of SCD, or LVOTG due to the presence of these parameters in the HCM-risk-SCD score. After adjusting for confounding factors, long or deep S wave and QTc were independent predictors for ICD appropriate therapy (HR 1.955, 95%CI 1.017–3.759, $P = 0.045$; HR 1.014, 95%CI 1.008–1.021, $P < 0.001$, respectively). The HCM-risk-SCD score was also an independent risk factor in our cohort (HR 1.110, 95%CI 1.003–1.229, $P = 0.043$) (**Table 2**).

Relationship Between QTc and MWT and LVOTG

QTc interval was not correlated with MWT (r=0.095, P=0.251) nor LVOTG ($r = -0.070$, $P = 0.394$).

The Prediction Efficacy of the Combination of QTc and V4-S Wave

ROC curves were presented in **Figure 2** to investigate the prediction efficacy of QTc and long or deep S wave in V4. In ROC curves, AUC in HCM-risk-SCD score for ICD appropriate therapy was 0.517 (95%CI 0.412–0.623, $P = 0.735$). As shown in **Figure 2A**, the two ECG indicators achieved a high prediction value, with an AUC of 0.608 (95%CI 0.511–0.706, $P = 0.034$) for S wave anomalies and 0.658 (95%CI 0.554–0.762, $P = 0.002$) for QTc with the optimal cutoff value of 464 ms. We demonstrated that the risk of appropriate ICD therapy was higher in patients with QTc≥464 ms than QTc <464 ms (Log-rank $P < 0.0001$) (**Figure 3A**). Similarly, the risk of ICD appropriate therapy was higher in patients with long or deep S wave in V4 (Log-rank $P = 0.009$) (**Figure 3B**).

Association of S Wave and QTc With Appropriate ICD Therapy

In this study, 73 patients (49.0%) presented long or deep S wave. Compared with patients without long or deep S wave, patients with long or deep S wave had a higher rate of fQRS (20.5 vs. 5.3%, $P = 0.006$), longer QRS duration (118 ms ± 29 ms vs. 103 ms ± 22 ms, $P = 0.002$), and lower usage of amiodarone (43.8 vs. 60.5%, $P = 0.041$). There was no significant difference in QTc duration, HCM-risk-SCD score and rate of ICD implantation for secondary prevention between the two groups. The rate of

TABLE 1 | Baseline characteristics of HCM patients with and without appropriate ICD therapy.

Variable	All patients (n = 149)	Patients without appropriate ICD therapy (n = 102)	Patients with appropriate ICD therapy (n = 47)	*P*
Demographic characteristics				
Age (y)	53 ± 14	54 ± 14	51 ± 19	0.288
Male (%)	104 (69.8)	72 (70.6)	32 (68.1)	0.848
BMI (kg/m^2)	25 ± 3	25 ± 3	25 ± 4	0.277
SBP (mmHg)	119 ± 14	119 ± ± 15	120 ± 14	0.818
DBP (mmHg)	72 ± 9	72 ± 9	72 ± 9	0.984
Comorbidity				
Diabetes mellitus (%)	25 (16.8)	19 (18.6)	6 (12.8)	0.482
Hypertension (%)	55 (36.9)	38 (37.3)	17 (36.2)	>0.999
AF (%)	43 (28.9)	35 (34.3)	8 (17.0)	0.030
Coronary artery disease (%)	23 (15.4)	18 (17.6)	5 (10.6)	0.335
ICD prevention				0.451
Primary prevention (%)	102 (68.5)	72 (70.6)	30 (63.8)	-
Secondary prevention (%)	47 (31.5)	30 (29.4)	17 (36.2)	-
Family history of SCD	38 (25.5)	25 (24.5)	13 (27.7)	0.690
Syncope, *n* (%)	88 (59.1)	60 (58.8)	28 (59.6)	>0.999
NSVT, *n* (%)	60 (40.3)	41 (40.2)	19 (40.4)	>0.999
APHCM, *n* (%)	9 (6.0)	7 (6.9)	2 (4.3)	0.72
HOCM, *n* (%)	28 (18.8)	22 (21.6)	6 (12.8)	0.261
ASA, *n* (%)	2 (1.3)	1 (1.0)	1 (2.1)	0.533
MORROW, *n* (%)	3 (2.0)	3 (2.9)	0	0.552
SCD risk score, %	5 ± 3	5 ± 3	5 ± 3	0.562
Echocardiography				
LAD, mm	42 ± 6	43 ± 6	41 ± 6	0.143
LVMT, mm	22 ± 6	22 ± 6	21 ± 5	0.268
Maximal LVOTG, mmHg	6.8 (4.8-10.6)	6.8 (4.8-16.0)	6.8 (4.8-10.2)	0.562
LVEDD, mm	47 ± 8	47 ± 7	49 ± 8	0.110
LVEF, %	60 ± 11	60 ± 12	59 ± 10	0.474
RVD, mm	21 ± 3	21 ± 3	21 ± 3	0.869
Ventricular aneurysm, (%)	4 (2.7)	3 (2.9)	1 (2.1)	>0.999
ECG indicators				
Heart rate, bpm	66 ± 14	67 ± 14	66 ± 13	0.937
cLBBB, *n* (%)	4 (2.7)	4 (3.9)	0	0.308
cRBBB, *n* (%)	8 (5.4)	2 (2.0)	6 (12.8)	0.020
LVHV, *n* (%)	37 (24.8)	28 (27.5)	9 (19.1)	0.314
fQRS, *n* (%)	19 (12.8)	12 (11.8)	7 (14.9)	0.604
S wave abnormality, *n* (%)	73 (49.0)	43 (42.2)	30 (63.8)	0.021
TWI, *n* (%)				0.327
TWI>0.1, <1.0 mV	65 (43.6)	48 (47.1)	17 (36.2)	-
Giant TWI	6 (4.0)	5 (4.9)	1 (2.1)	-
P wave duration, ms	105 ± 36	106 ± 39	102 ± 29	0.592
PR interval, ms	168 ± 51	163 ± 53	179 ± 45	0.099
QRS complex, ms	111 ± 27	107 ± 22	118 ± 33	0.058
QTc, ms	445 ± 45	436 ± 36	464 ± 56	0.003
Drug usage, *n* (%)				
β-block	139 (93.3)	95 (93.1)	44 (93.6)	>0.999

(Continued)

TABLE 1 | Continued

Variable	All patients ($n = 149$)	Patients without appropriate ICD therapy ($n = 102$)	Patients with appropriate ICD therapy ($n = 47$)	*P*
Amiodarone	78 (52.3)	56 (54.9)	22 (46.8)	0.382
ACEI/ARB	60 (40.3)	43 (42.2)	17 (36.2)	0.590

Values are presented as mean ± SD or median (IQR), or as n (%).
HCM, hypertrophic cardiomyopathy; ICD, implantable cardioverter-defibrillator; BMI, body mass index; SBP, systolic blood pressure; DBP, dilated blood pressure; AF, atrial fibrillation; SCD, sudden cardiac death; NSVT, non-sustained ventricular tachyarrhythmia; APHCM, apical hypertrophic cardiomyopathy; HOCM, hypertrophic obstructive cardiomyopathy; ASA, alcohol septal ablation; LAD, left atrial diameter; LVMT, left ventricular maximum thickness; LVOTG, left ventricular outflow tract gradient; LVEDD, left ventricular end-diastolic diameter; LVEF, left ventricular ejection fraction; RVD, right ventricular diameter; ECG, electrocardiogram; cLBBB, complete left bundle branch block; cRBBB, complete right bundle branch block; LVHV, left ventricular high voltage; TWI, T wave inversion; ACEI/ARB, angiotensin converting enzyme inhibitor/ angiotensin receptor blocker.

TABLE 2 | Univariable and multivariable models for predictors of appropriate ICD therapies.

Variable	Univariable analysis		Multivariable analysis	
	Hazard ratio (95%CI)	*P*	Hazard ratio (95%CI)	*P*
AF	0.472 (0.220–1.011)	0.053	0.459 (0.203–1.040)	0.062
HCM-risk-SCD	1.024 (0.932–1.126)	0.620	1.110 (1.003–1.229)	0.043
cRBBB	3.196 (1.342–7.613)	0.009	2.022 (0.813–5.026)	0.130
S wave abnormality	2.197 (1.197–4.035)	0.011	1.955 (1.017–3.759)	0.045
QTc	1.013 (1.007–1.019)	<0.001	1.014 (1.008–1.021)	<0.001
Amiodarone	0.770 (0.432–1.374)	0.377	0.893 (0.471–1.693)	0.729

ICD, implantable cardioverter-defibrillator; AF, atrial fibrillation; HCM, hypertrophic cardiomyopathy; SCD, sudden cardiac death; cRBBB, complete right bundle branch block.

patients with long or deep S wave receiving appropriate ICD therapy was higher than patients without long or deep S wave (41.1 vs. 22.4%, $P = 0.014$).

There were 99 patients (66.4%) with QTc <464 ms, while 50 patients (33.6%) had a QTc ≥464 ms. The rate of ICD implantation for secondary prevention was significantly higher in patients with QTc≥464 ms (23/50, 46%) than in patients with QTc <464 ms (24/99, 24.2%). There were significant differences in QRS complex duration (119 ms ≥ 30 ms vs. 107 ≥ 24 ms, $P = 0.017$) and usage of amiodarone (34/50 (68%) vs. 44/99 (44.4%), $P = 0.007$) in patients with QTc ≥464 ms compared with patients with QTc <464 ms. The rate of long or deep S wave was similar in the two groups (24/50 (48%) in QTc ≥464 ms vs. 49/99 (49.5%) in QTc <464 ms, $P = 0.863$). The rate of patients with QTc ≥464 ms receiving appropriate ICD therapy was higher compared with patients with QTc <464 ms (27/50 (54%) vs. 20/99 (20.2%), $P < 0.0001$) (**Table 3**).

We divided our patients into four groups according to QTc and long or deep S wave:(1) without long or deep S wave (-) and QTc <464 ms ($n = 50$); (2) with long or deep S wave (+) and QTc <464 ms ($n = 49$); (3) without long or deep S wave (-) and QTc ≥464 ms ($n = 26$); (4) with long or deep S wave (+) and QTc ≥464 ms ($n = 24$). There were 6 (12.0%), 14 (28.6%), 11 (42.3%), and 16 (66.7%) patients receiving appropriate ICD therapy, respectively (**Figure 4**). Kaplan-Meier analysis demonstrated that there was a significant difference among the four groups ($P < 0.0001$) (**Figure 5**). Pairwise comparison analysis showed that there were differences between group1 and group 2 ($P = 0.026$), group 1 and group 3 ($P = 0.002$), group 1 and group 4 ($P < 0.0001$), and group 2 and group 4 ($P = 0.004$). The highest appropriate ICD therapy rate was in group 4.

Improvement of Prediction Efficacy of HCM-risk-SCD After Inclusion of New Parameters

We added long or deep S wave in V4 to the HCM-risk-SCD model, and the C- statistics of the new model 1 was 0.625 (95%CI 0.526–0.723, $P = 0.015$). The new model improved reclassification with the net reclassification index (NRI) of 0.011. Then, we added QTc into the HCM-risk-SCD model. The C-statistics of the new model 2 was 0.659 (95%CI 0.552-0.765), and the NRI was 0.193. Finally, we added long or deep S wave in V4 and QTc in the HCM-risk-SCD model simultaneously. The C-statistics of new model 3 was 0.702 (95%CI 0.607–0.796), and the NRI was 0.302 (**Figure 6A**).

Subgroups With Primary and Secondary Prevention

Figures 2B,C demonstrated ROC curves of S-wave anomalies and QTc interval stratified according to primary and secondary prevention.

In the primary prevention patients, S wave anomalies and QTc yielded AUC of 0.592 (95%CI 0.470–0.713, $P = 0.146$) and 0.678 (95%CI 0.548–0.808, $P = 0.06$), respectively. While the HCM-risk-SCD model yield AUC of 0.613 (95%CI 0.490–0.735, $P =$

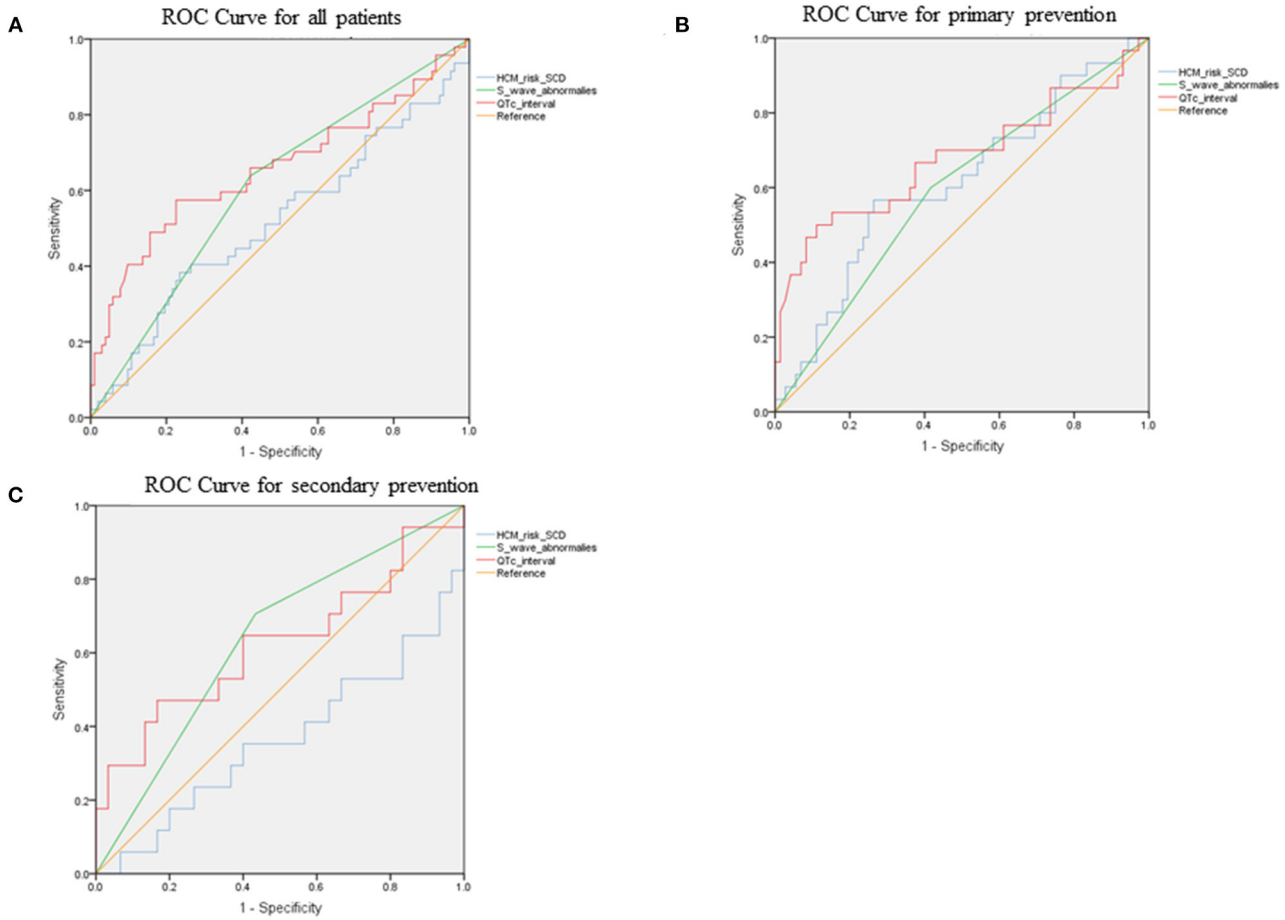

FIGURE 2 | The ROC curves for predicting appropriate ICD therapies by HCM-risk-SCD model, QTc interval, and V4-S wave. **(A)** for all patients, **(B)** for primary prevention, and **(C)** for secondary prevention. ROC, receiver operating curve; ICD, implantable cardioverter-defibrillator; HCM, hypertrophic cardiomyopathy; SCD, sudden cardiac death.

0.074) as shown in **Figure 6B**, the addition of long or deep S wave and QTc into the HCM-risk SCD model showed reclassification improvement (NRI 0.306).

In the secondary prevention patients, S wave anomalies and QTc yielded AUC of 0.636 (95%CI 0.471–0.801, P =0.124) and 0.624 (95%CI 0.444–0.803, P = 0.163), respectively. While the HCM-risk-SCD model yield AUC of 0.363 (95%CI 0.188–0.537, P = 0.121, **Figure 6C**). And the addition of long or deep S wave and QTc into the HCM-risk SCD model resulted in reclassification improvement (NRI 0.135, **Figure 6C**).

DISCUSSION

In this study, we demonstrated that: (1) long or deep S wave in V4 and QTc ≥464 ms were independent factors of appropriate ICD therapy in HCM patients implanted with ICD; (2) Patients with QTc ≥464 ms and long or deep V4-S wave had the highest risk of appropriate ICD therapy; (3) addition of QTc and long or deep S wave improved the prediction efficacy of HCM-risk-SCD model (NRI: 0.302).

QTc in HCM Patients

Approximately 75–95% of HCM patients had abnormal 12-lead ECG (3). However, not all abnormal ECG patterns were associated with ventricular arrhythmias. QT interval is defined from the beginning of the QRS complex to the end of the T wave and contains the sum of the duration of myocardium depolarization and repolarization. Several studies have demonstrated that QTc was associated with severity of left ventricular hypertrophy, LVOTG, potential pathogenic mutations (mutations may affect sodium and potassium channels involved in depolarization and repolarization), and activity of sympathetic nerve (19, 20, 26). Furthermore, myocardial fibrosis, myocardium arrangement disorder and/or microvascular ischemia may affect the QTc in HCM patients. Many studies investigated the influence of QTc on the prognosis of HCM patients (20, 27). In our study population, 33.6% of patients had a QTc ≥464 ms, compared to the 13% of patients in a previous study (27). The numerically higher prevalence in our study may be due to the inclusion the patients with the usage of amiodarone which could prolong the QTc. A previous study has demonstrated that the patients with QTc ≥460 ms

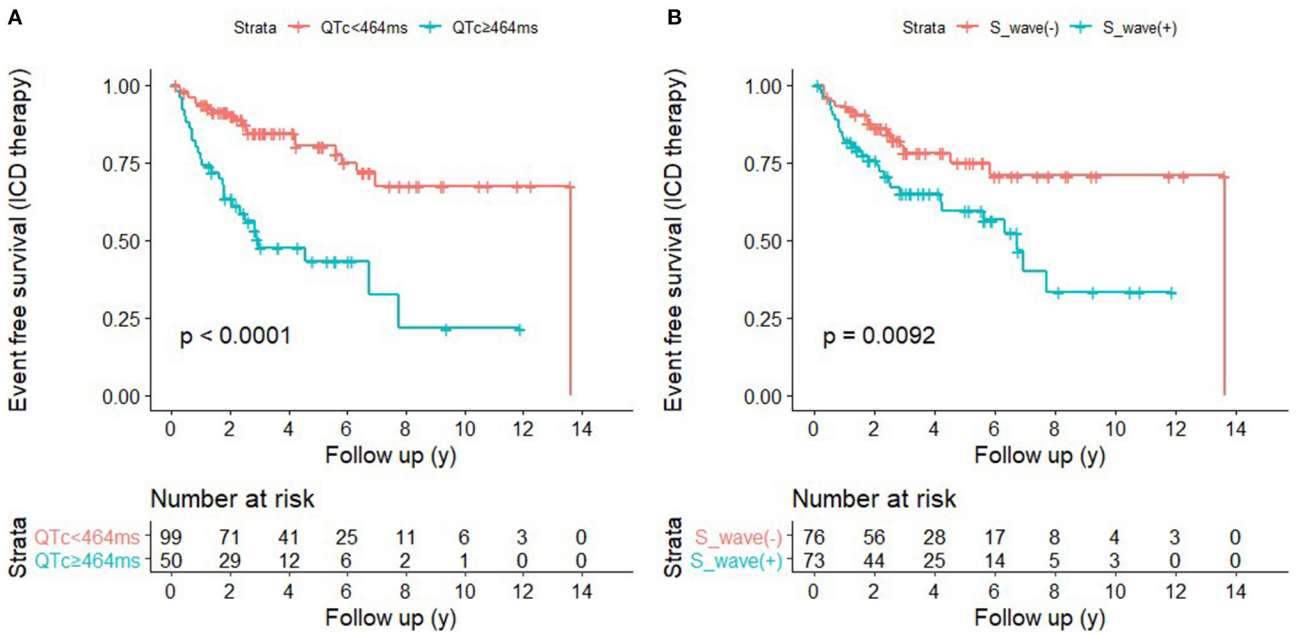

FIGURE 3 | Kaplan-Meier survival analysis based on QTc interval **(A)** and wide or deep V4- S wave **(B)**.

had a 3-fold increased risk of VA or SCD (27). Gray et al. (28) found that the risk for appropriate ICD therapy was >3-fold in patients with QTc ≥464 ms compared with patients without QTc prolongation after adjustment for LVWT and sex. Similarly, QTc prolongation had an arrhythmogenic effect in our study. Maron et al. demonstrated that QTc prolongation and greater QT dispersion were present in HCM patients but were not predictors for SCD (29). This result may be due to differences in population, genetic background, and outcomes between the two studies.

A possible explanation for the lack of correlation between QTc interval and the increase in left ventricular wall thickness is that prolonged QTc interval is associated with myocardial fibrosis. Studies have found that, in addition to myocardial hypertrophy, interstitial fibrosis and myocardial fibrosis may lead to prolonged QTc interval, which is the substrate of arrhythmia (30). Riza Demir et al. (4) enrolled 74 HCM patients and underwent CMR. They found that QTc in HCM patients with myocardial fibrosis was longer than in patients without fibrosis (455 ± 38 ms vs. 430 ± 29ms, $P = 0.002$). And QTc could predict LGE in CMR (OR 1.024, 95%CI 1.007–1.040, $P = 0.004$). On the contrary, Delcrè et al. (19) demonstrated no correlation between QTc prolongation and prevalence of LGE ($p = 0.08$). We did not assess the relationship between myocardial fibrosis, QTc and appropriate ICD therapy. Thus, this potential mechanism needs further investigation.

The prolonged QTc interval of HCM patients may also be related to genetic factors. HCM and long QT syndrome (LQTS) are heart diseases caused by abnormal proteins encoded by two sets of disease-causing genes (31, 32). Studies have shown that these two sets of inheritance may be related to each other. HCM patients may have some mutations in LQTS, which may lead to the prolongation of the QT interval and the occurrence of arrhythmia events (31). Nevertheless, we did not perform genetic testing on patients, so any genetic evaluation of the LQTS gene was not possible.

V4-S Wave in HCM Patients

S wave is the terminal part of the QRS complex and represents the depolarization vector of the right ventricle and the posterosuperior late left ventricular. Arrhythmogenic cardiomyopathy (ACM) mainly involves the right ventricle (delay in the right ventricular activation or conduction), in which ECG may manifest as a delay in terminal activation delay (TAD) in the right chest lead. TAD >55 ms is a predictor of right ventricular dilatation and dysfunction (33). Right ventricular insufficiency was a prediction factor of SCD in patients with ACM (34). Recently, more and more studies have begun to explore the effect of right ventricular involvement on HCM patients. Wu et al. compared the right ventricular function and the exercise tolerance of 76 HCM patients and 30 healthy people and found that a higher proportion of right ventricular dysfunction and reduction of contractile reserve in HCM patients (35). Seo et al. included 256 HCM patients and found that right ventricular involvement (CMR showed that the free wall thickness of the right ventricle ≥7 mm) was related to abnormal left ventricular structure and biventricular dysfunction. Right ventricular involvement and impaired right ventricular strain were predictors of composite endpoints (all-cause death, cardiac transplantation, and cardiovascular hospitalization) (36). Lyon

TABLE 3 | Patients stratified according to QTc interval and S wave anomalies.

Variable	S wave abnormality (-) (*n* = 76)	S wave abnormality (+) (*n* =73)	QTc <464 ms (*n* = 99)	QTc ≥464 ms (*n* = 50)	*P*-value*	*P*-value#
Demographic characteristics						
Age (y)	54 ± 14	52 ± 16	54 ± 15	52 ± 17	0.401	0.573
Male (%)	49 (64.5)	55 (75.3)	73 (73.7)	31 (62.0)	0.149	0.141
BMI (kg/m^2)	25 ± 3	25 ± 4	25 ± 3	24 ± 4	0.576	0.089
SBP, mmHg	119 ± 15	119 ± 13	120 ± 14	118 ± 15	0.835	0.630
DBP, mmHg	72 ± 9	72 ± 9	71 ± 9	73 ± 9	0.656	0.221
Comorbidity						
Diabetes Mellitus (%)	16 (21.1)	9 (12.3)	17 (17.2)	8 (16.0)	0.154	0.857
Hypertension (%)	25 (32.9)	30 (41.1)	39 (39.4)	16 (32.0)	0.300	0.377
AF (%)	25 (32.9)	18 (24.7)	27 (27.3)	16 (32.0)	0.267	0.548
Coronary heart disease (%)	8 (10.5)	15 (20.5)	12 (12.1)	11 (22.0)	0.091	0.115
Family history of SCD, *n* (%)	21 (27.6)	17 (23.3)	27 (27.3)	11 (22.0)	0.543	0.486
Syncope, *n* (%)	48 (63.2)	40 (54.8)	58 (58.6)	30 (60.0)	0.299	0.868
NSVT, n (%)	34 (44.7)	26 (35.6)	43 (43.4)	17 (34.0)	0.256	0.268
APHCM, *n* (%)	3 (3.9)	6 (8.2)	6 (6.1)	3 (6.0)	0.321	>0.999
HOCM, *n* (%)	15 (19.7)	13 (17.8)	20 (20.2)	8 (16.0)	0.763	0.535
ASA, *n* (%)	1 (1.3)	1 (1.4)	0	2 (4.0)	>0.999	0.111
MORROW, *n* (%)	2 (2.6)	1 (1.4)	1 (1.0)	2 (4.0)	>0.999	0.261
HCM-risk-SCD, %	5 ± 3	5 ± 3	5 ± 3	5 ± 3	0.185	0.768
ICD prevention, *n* (%)					0.487	0.007
Primary prevention	54 (71.1)	48 (65.8)	75 (75.8)	27 (54.0)	-	-
Secondary prevention	22 (28.9)	25 (34.2)	24 (24.2)	23 (46.0)	-	-
Echocardiography						
LAD, mm	42 ± 6	42 ± 7	42 ± 7	42 ± 5	0.963	0.964
LVMT, mm	22 ± 5	22 ± 6	22 ± 5	23 ± 6	0.453	0.260
Maximal LVOTG, mmHg	6.8 (4.8-9.0)	6.8 (4.9-11.3)	6.8 (4.8-14.4)	6.8 (4.8-9.0)	0.638	0.595
LVEDD, mm	47 ± 8	48 ± 7	48 ± 7	47 ± 8	0.204	0.599
LVEF, %	61 ± 11	59 ± 12	60 ± 11	58 ± 11	0.364	0.232
RVD, mm	21 ± 3	22 ± 3	22 ± 3	21 ± 3	0.298	0.177
Ventricular aneurysm	4 (5.3)	0	2 (2.0)	2 (4.0)	0.120	0.602
ECG indicators						
Heart rate, bpm	66 ± 13	66 ± 14	65 ± 14	69 ± 12	0.983	0.067
LBBB, *n* (%)	2 (2.6)	2 (2.7)	3 (3.0)	1 (2.0)	>0.999	>0.999
RBBB, *n* (%)	1 (1.3)	7 (9.6)	5 (5.1)	3 (6.0)	0.031	>0.999
LVHV, *n* (%)	17 (22.4)	20 (27.4)	25 (25.3)	12 (24.0)	0.478	0.867
fQRS, *n* (%)	4 (5.3)	15 (20.5)	14 (14.1)	5 (10.0)	0.006	0.474
S wave abnormality, *n* (%)	-	-	49 (49.5)	24 (48.0)	-	0.863
TWI, *n* (%)					0.323	0.864
TWI >0.1, <1.0 mV	33 (43.4)	32 (43.8)	45 (45.5)	20 (40.0)	-	-
Giant TWI	5 (6.6)	1 (1.4)	4 (4.0)	2 (4.0)	-	-
P wave duration, ms	110 ± 43	99 ± 25	101 ± 36	111 ± 34	0.096	0.199
PR interval, ms	161 ± 54	175 ± 46	166 ± 48	172 ± 56	0.147	0.571
QRS duration, ms	103 ± 22	118 ± 29	107 ± 24	119 ± 30	0.002	0.017
QTc, ms	443 ± 40	447 ± 50	421 ± 28	493 ± 32	0.584	<0.0001
QTc <464 ms	50 (65.8)	49 (67.1)	-	-	0.863	-
Drug usage, *n* (%)						
β-block	70 (92.1)	69 (94.5)	93 (93.9)	46 (92.0)	0.794	0.655

(Continued)

TABLE 3 | Continued

Variable	S wave abnormality (-) (*n* = 76)	S wave abnormality (+) (*n* =73)	QTc <464 ms (*n* = 99)	QTc ≥464 ms (*n* = 50)	*P*-value*	*P*-value#
Amiodarone	46 (60.5)	32 (43.8)	44 (44.4)	34 (68.0)	0.041	0.007
ACEI/ARB	27 (35.5)	33 (45.2)	43 (43.4)	17 (34.0)	0.228	0.268
Appropriate ICD therapy, *n* (%)	17 (22.4)	30 (41.1)	20 (20.2)	27 (54.0)	0.014	<0.0001

**P represented the comparison between patients with S wave abnormality and without S wave abnormality.*
#P represented the comparison between Patients with QTc ≥464 ms and QTc< 464 ms.
Values are presented as mean ± SD or median (IQR), or as n (%).
HCM, hypertrophic cardiomyopathy; ICD, implantable cardioverter-defibrillator; BMI, body mass index; SBP, systolic blood pressure; DBP, dilated blood pressure; AF, atrial fibrillation; SCD, sudden cardiac death; NSVT, non-sustained ventricular tachyarrhythmia; APHCM, apical hypertrophic cardiomyopathy; HOCM, hypertrophic obstructive cardiomyopathy; ASA, alcohol septal ablation; LAD, left atrial diameter; LVMT, left ventricular maximum thickness; LVOTG, left ventricular outflow tract gradient; LVEDD, left ventricular end-diastolic diameter; LVEF, left ventricular ejection fraction; RVD, right ventricular diameter; ECG, electrocardiogram; cLBBB, complete left bundle branch block; cRBBB, complete right bundle branch block; LVHV, left ventricular high voltage; TWI, T wave inversion; ACEI/ARB, angiotensin converting enzyme inhibitor/angiotensin receptor blocker.

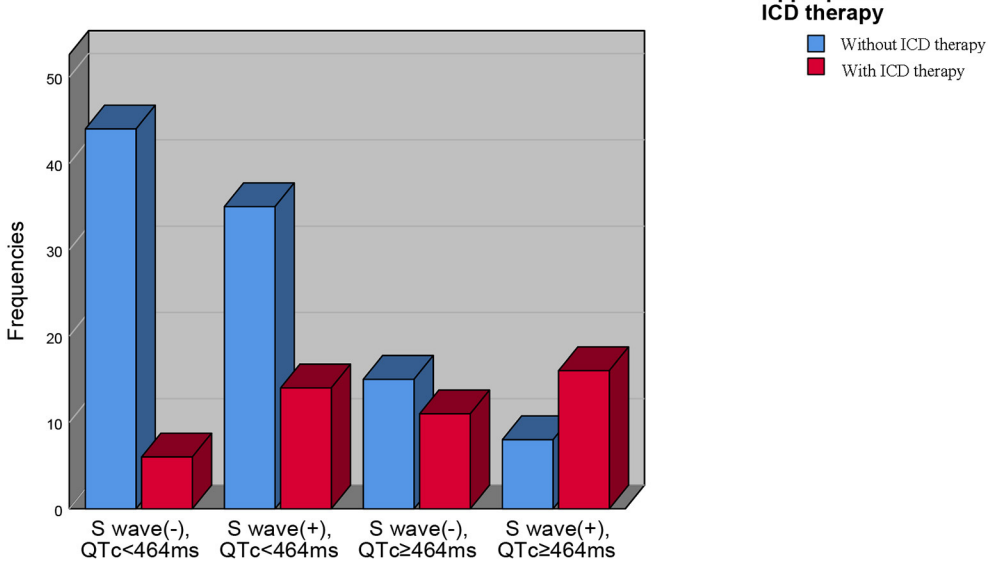

FIGURE 4 | The prevalence of appropriate ICD therapies in four subgroups based on QTc interval and V4-S wave. ICD, implantable cardioverter-defibrillator.

et al. used machine learning algorithms to regroup HCM patients based on baseline characteristics to investigate the risk of arrhythmia and the severity of myocardial hypertrophy. Researchers found that the algorithm automatically divided HCM into three groups based on QRS morphology: group 1 with normal QRS morphology; group 2 with low R wave amplitude in lead V4 and large S wave amplitude; and group 3 with low R wave amplitude in lead V4-V6, wide S wave, and left axis deviation. However, the study found no significant differences in the risk of arrhythmia and the severity of myocardial hypertrophy (23). And the study did not further explore the relationship between the differences in ECG of the three groups and SCD.

In this study, we could not explore the effect of these factors on the appropriate treatment of ICD due to the absence of CMR examination. Although there was no significant difference in the anteroposterior diameter of the right ventricle between patients with appropriate ICD therapy and patients without appropriate ICD therapy, more subtle changes in the structure and function of the right ventricle, such as myocardial fibrosis, right ventricular strain, etc. could be found. Some subclinical impairments of the right ventricular myocardium may appear before the reduced right ventricular function (37). However, subclinical impairments in the right ventricle were likely to affect the ECG vector. Therefore, we measured the S wave in lead V4 and found that the long or deep V4-S wave was an independent predictor of the appropriate ICD therapy. And after it was added to the HCM-risk-SCD model, the prediction effect of the model was significantly increased. In univariate Cox regression, both long or deep S wave and RBBB were correlated with ICD therapy, but in multivariate Cox regression,

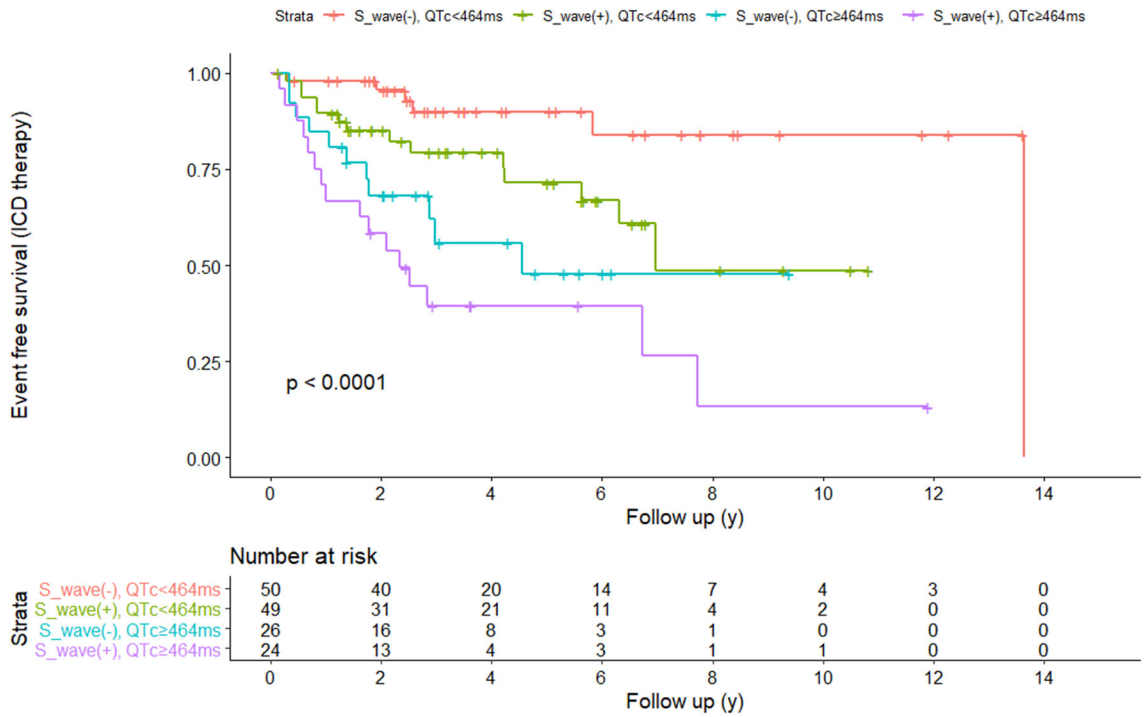

FIGURE 5 | Kaplan-Meier survival analysis curves were compared among the four subgroups.

the correlation between long or deep V4-S wave and appropriate ICD therapy was independent of RBBB. Most patients with RBBB were accompanied with deep and wide S-wave in lead V4, so to a certain extent long or deep S-wave could represent or contain most RBBB. Therefore, RBBB was not significant in multivariate regression.

Subgroup Analysis

In this study, we did not restrict the analysis to patients in primary prevention but also included patients with secondary prevention. Prior study has shown that not all patients implanted ICD for secondary prevention would receive ICD therapy during follow-up (38), thus it was also essential to identify patients in this indication who had a higher risk of appropriate therapy. In our study, there was no interaction between indications for ICD and whether to receive ICD therapy. And analysis according to the indication demonstrated that S wave anomalies and QTc improved the risk stratification in both subgroups.

LIMITATIONS

This study has several limitations. Firstly, this was a single-center retrospective study with a small sample size. A prospective trial with a large sample size was needed to verify the relationship between the long or deep S wave in V4 and the appropriate ICD therapy. Secondly, the patients in this study did not routinely undergo pathogenic genetic tests. Thirdly, in our research V4-S wave was a categorical variable defined based on manual measurement, and we did not measure the precise time duration and amplitude of the S wave. More research is needed to measure and explore the optimal cut-off value for prediction accurately. Fourthly, as CMR data are not available for this study, no further conclusion can be drawn on whether MRI, especially LGE could be related to appropriate ICD therapy in this population. Fifthly, approximate 50% of patients in our study were on therapy with amiodarone. Our results might only suggest that longer QTc could predict SCD, but cannot suggest a widely applicable cut-off value. However, it is indeed impossible to determine a fixed QTc cut-off value in HCM populations with different amiodarone utilization rates. Lastly, appropriate ICD therapy, associated with the programming of the device, is not equal to SCD. Nevertheless, the findings of this study are still meaningful.

CONCLUSION

QTc duration and long or deep V4-S wave were independent predictors of appropriate ICD therapy in HCM patients with ICD. Patients with QTc $\geq$464 ms and long or deep V4-S wave had the highest risk of appropriate ICD therapy. The addition of QTc duration and long or deep V4-S wave to HCM-risk-SCD improved the prediction efficacy. These two ECG parameters might help better stratify HCM patients with ICD.

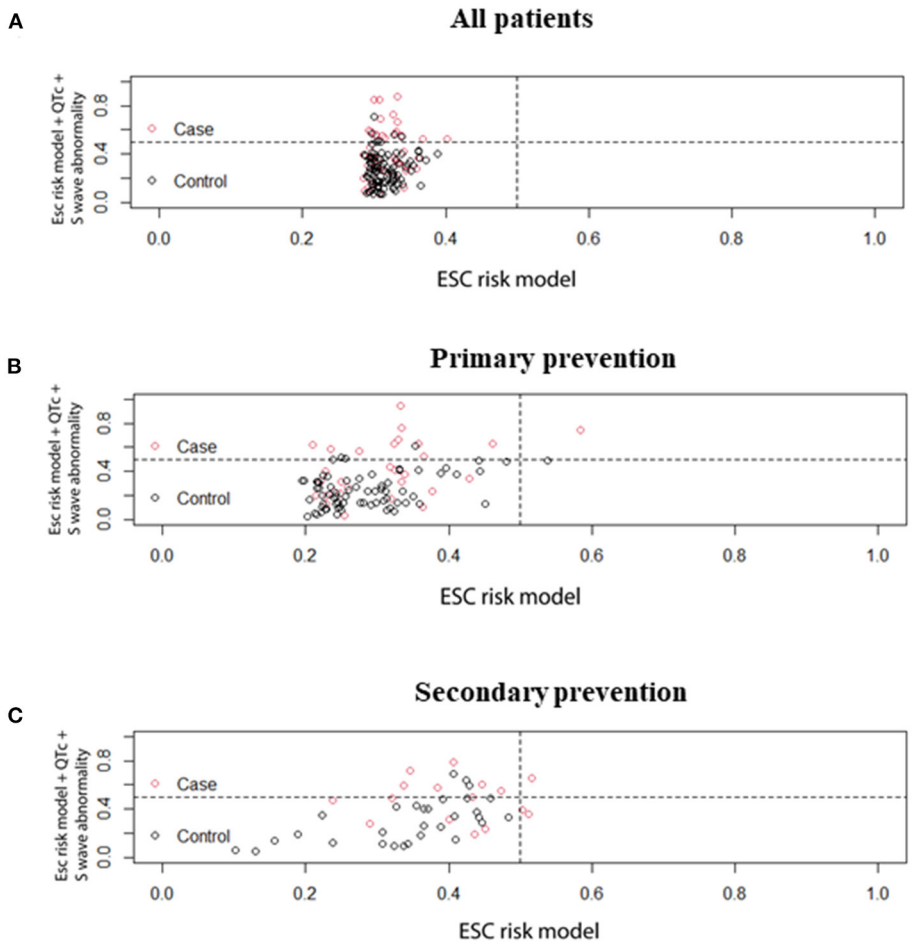

FIGURE 6 | Comparison of prediction effect of HCM-risk-SCD model before and after adding QTc and V4-S wave simultaneously. **(A)** for all patients, **(B)** for primary patients, and **(C)** for secondary patients. HCM, hypertrophic cardiomyopathy; SCD, sudden cardiac death.

DATA AVAILABILITY STATEMENT

The raw data supporting the conclusions of this article will be made available by the authors, without undue reservation.

ETHICS STATEMENT

The studies involving human participants were reviewed and approved by the Ethics Committee of Fuwai Hospital. The patients/participants provided their written informed consent to participate in this study.

AUTHOR CONTRIBUTIONS

NZ and SC contributed to conception and design of the study and organized the database. NZ performed the statistical analysis and wrote the first draft of the manuscript. SC wrote sections of the manuscript. All authors contributed to manuscript revision, read, and approved the submitted version.

REFERENCES

1. Maron BJ, Maron MS. Hypertrophic cardiomyopathy. *Lancet*. (2013) 381:242–55. doi: 10.1016/S0140-6736(12)60397-3
2. Dumont CA, Monserrat L, Soler R, Rodríguez E, Fernandez X, Peteiro J, et al. Interpretation of electrocardiographic abnormalities in hypertrophic cardiomyopathy with cardiac magnetic resonance. *Eur Heart J.* (2006) 27:1725–31. doi: 10.1093/eurheartj/ehl101
3. Maron BJ. Hypertrophic cardiomyopathy: a systematic review. *JAMA*. (2002) 287:1308–20. doi: 10.1001/jama.287.10.1308
4. Riza Demir A, Celik Ö, Sevinç S, Uygur B, Kahraman S, Yilmaz E, et al. The relationship between myocardial fibrosis detected by cardiac magnetic resonance and Tp-e interval, 5-year sudden cardiac death risk score in hypertrophic cardiomyopathy patients. *Ann Noninvasive Electrocardiol.* (2019) 24:e12672. doi: 10.1111/anec.12672
5. Dohy Z, Vereckei A, Horvath V, Czimbalmos C, Szabo L, Toth A, et al. How are ECG parameters related to cardiac magnetic resonance

images? Electrocardiographic predictors of left ventricular hypertrophy and myocardial fibrosis in hypertrophic cardiomyopathy. *Ann Noninvasive Electrocardiol.* (2020) 25:e12763. doi: 10.1111/anec.12763
6. Österberg AW, Östman-Smith I, Jablonowski R, Carlsson M, Green H, Gunnarsson C, et al. High ECG risk-scores predict late gadolinium enhancement on magnetic resonance imaging in HCM in the young. *Pediatr Cardiol.* (2021) 42:492–500. doi: 10.1007/s00246-020-02506-9
7. Matsuki A, Kawasaki T, Kawamata H, Sakai C, Harimoto K, Kamitani T, et al. Ventricular late potentials and myocardial fibrosis in hypertrophic cardiomyopathy. *J Electrocardiol.* (2020) 58:87–91. doi: 10.1016/j.jelectrocard.2019.10.003
8. O'Mahony C, Jichi F, Pavlou M, Monserrat L, Anastasakis A, Rapezzi C, et al. A novel clinical risk prediction model for sudden cardiac death in hypertrophic cardiomyopathy (HCM risk-SCD). *Eur Heart J.* (2014) 35:2010–20. doi: 10.1093/eurheartj/eht439
9. Maron MS, Rowin EJ, Wessler BS, Mooney PJ, Fatima A, Patel P, et al. Enhanced American college of cardiology/American heart association strategy for prevention of sudden cardiac death in high-risk patients with hypertrophic cardiomyopathy. *JAMA Cardiol.* (2019) 4:644–57. doi: 10.1001/jamacardio.2019.1391
10. Maron BJ, Casey SA, Chan RH, Garberich RF, Rowin EJ, Maron MS. Independent assessment of the European society of cardiology sudden death risk model for hypertrophic cardiomyopathy. *Am J Cardiol.* (2015) 116:757–64. doi: 10.1016/j.amjcard.2015.05.047
11. Liu J, Wu G, Zhang C, Ruan J, Wang D, Zhang M, et al. Improvement in sudden cardiac death risk prediction by the enhanced American college of cardiology/American heart association strategy in Chinese patients with hypertrophic cardiomyopathy. *Heart Rhythm.* (2020) 17:1658–63. doi: 10.1016/j.hrthm.2020.04.017
12. Savage DD, Seides SF, Clark CE, Henry WL, Maron BJ, Robinson FC, et al. Electrocardiographic findings in patients with obstructive and non-obstructive hypertrophic cardiomyopathy. *Circulation.* (1978) 58:402–8. doi: 10.1161/01.cir.58.3.402
13. Ryan MP, Cleland JG, French JA, Joshi J, Choudhury L, Chojnowska L, et al. The standard electrocardiogram as a screening test for hypertrophic cardiomyopathy. *Am J Cardiol.* (1995) 76:689–94. doi: 10.1016/s0002-9149(99)80198-2
14. Basaran Y, Tigen K, Karaahmet T, Isiklar I, Cevik C, Gurel E, et al. Fragmented QRS complexes are associated with cardiac fibrosis and significant intraventricular systolic dyssynchrony in non-ischemic dilated cardiomyopathy patients with a narrow QRS interval. *Echocardiography.* (2011) 28:62–8. doi: 10.1111/j.1540-8175.2010.01242.x
15. Das MK, Maskoun W, Shen C, Michael MA, Suradi H, Desai M, et al. Fragmented QRS on twelve-lead electrocardiogram predicts arrhythmic events in patients with ischemic and non-ischemic cardiomyopathy. *Heart Rhythm.* (2010) 7:74–80. doi: 10.1016/j.hrthm.2009.09.065
16. Morita H, Kusano KF, Miura D, Nagase S, Nakamura K, Morita ST, et al. Fragmented QRS as a marker of conduction abnormality and a predictor of prognosis of Brugada syndrome. *Circulation.* (2008) 118:1697–704. doi: 10.1161/CIRCULATIONAHA.108.770917
17. Peters S, Trummel M, Koehler B, QRS. fragmentation in standard ECG as a diagnostic marker of arrhythmogenic right ventricular dysplasia- cardiomyopathy. *Heart Rhythm.* (2008) 5:1417–21. doi: 10.1016/j.hrthm.2008.07.012
18. Goldenberg I, Moss AJ, Peterson DR, McNitt S, Zareba W, Andrews ML, et al. Risk factors for aborted cardiac arrest and sudden cardiac death in children with the congenital long-QT syndrome. *Circulation.* (2008) 117:2184–91. doi: 10.1161/CIRCULATIONAHA.107.701243
19. Delcrè SD, Di Donna P, Leuzzi S, Miceli S, Bisi M, Scaglione M, et al. Relationship of ECG findings to phenotypic expression in patients with hypertrophic cardiomyopathy: a cardiac magnetic resonance study. *Int J Cardiol.* (2013) 167:1038–45. doi: 10.1016/j.ijcard.2012.03.074
20. Johnson JN, Grifoni C, Bos JM, Saber-Ayad M, Ommen SR, Nistri S, et al. Prevalence and clinical correlates of QT prolongation in patients with hypertrophic cardiomyopathy. *Eur Heart J.* (2011) 32:1114–20. doi: 10.1093/eurheartj/ehr021
21. Sherrid MV, Cotiga D, Hart D, Ehlert F, Haas TS, Shen WK, et al. Relation of 12-lead electrocardiogram patterns to implanted defibrillator-terminated ventricular tachyarrhythmias in hypertrophic cardiomyopathy. *Am J Cardiol.* (2009) 104:1722–6. doi: 10.1016/j.amjcard.2009.07.056
22. Ostman-Smith I, Wisten A, Nylander E, Bratt EL. Granelli Ad, Oulhaj A, et al. Electrocardiographic amplitudes: a new risk factor for sudden death in hypertrophic cardiomyopathy. *Eur Heart J.* (2010) 31:439–49. doi: 10.1093/eurheartj/ehp443
23. Lyon A, Ariga R, Mincholé A, Mahmod M, Ormondroyd E, Laguna P, et al. Distinct ECG phenotypes identified in hypertrophic cardiomyopathy using machine learning associate with arrhythmic risk markers. *Front Physiol.* (2018) 9:213. doi: 10.3389/fphys.2018.00213
24. Maron BJ, Spirito P, Shen WK, Haas TS, Formisano F, Link MS, et al. Implantable cardioverter-defibrillators and prevention of sudden cardiac death in hypertrophic cardiomyopathy. *JAMA.* (2007) 298:405–12. doi: 10.1001/jama.298.4.405
25. Ommen SR, Mital S, Burke MA, Day SM, Deswal A, Elliott P, et al. 2020 AHA/ACC guideline for the diagnosis and treatment of patients with hypertrophic cardiomyopathy: executive summary: a report of the American College of cardiology/American heart association joint committee on clinical practice guidelines. *Circulation.* (2020) 142:e533–57. doi: 10.1161/CIR.0000000000000938
26. Jouven X, Hagege A, Charron P, Carrier L, Dubourg O, Langlard JM, et al. Relation between QT duration and maximal wall thickness in familial hypertrophic cardiomyopathy. *Heart.* (2002) 88:153–7. https://doi.org/10.1136/heart.88.2.153
27. Debonnaire P, Katsanos S, Joyce E, VAN DEN Brink OV, Atsma DE, Schalij MJ, et al. QRS Fragmentation and QTc duration relate to malignant ventricular Tachyarrhythmias and sudden cardiac death in patients with hypertrophic cardiomyopathy. *J Cardiovasc Electrophysiol.* (2015) 26:547–55. doi: 10.1111/jce.12629
28. Gray B, Ingles J, Medi C, Semsarian C. Prolongation of the QTc interval predicts appropriate implantable cardioverter-defibrillator therapies in hypertrophic cardiomyopathy. *JACC Heart Fail.* (2013) 1:149–55. doi: 10.1016/j.jchf.2013.01.004
29. Maron BJ, Leyhe MJ III, Casey SA, Gohman TE, Lawler CM, Crow RS, et al. Assessment of QT dispersion as a prognostic marker for sudden death in a regional non-referred hypertrophic cardiomyopathy cohort. *Am J Cardiol.* (2001) 87:114–5. doi: 10.1016/s0002-9149(00)01285-6
30. Sen-Chowdhry S, McKenna WJ. Sudden death from genetic and acquired cardiomyopathies. *Circulation.* (2012) 125:1563–76. doi: 10.1161/CIRCULATIONAHA.111.025528
31. Kapplinger JD, Tester DJ, Salisbury BA, Carr JL, Harris-Kerr C, Pollevick GD, et al. Spectrum and prevalence of mutations from the first 2,500 consecutive unrelated patients referred for the FAMILION long QT syndrome genetic test. *Heart Rhythm.* (2009) 6:1297–303. doi: 10.1016/j.hrthm.2009.05.021
32. Darbar D. Is it time to develop a "pathogenicity" score to distinguish long QT syndrome causing mutations from "background" genetic noise? *Heart Rhythm.* (2009) 6:1304–5. doi: 10.1016/j.hrthm.2009.06.027
33. De Lazzari M, Zorzi A, Cipriani A, Susana A, Mastella G, Rizzo A, et al. Relationship between electrocardiographic findings and cardiac magnetic resonance phenotypes in arrhythmogenic cardiomyopathy. *J Am Heart Assoc.* (2018) 7:e009855. doi: 10.1161/JAHA.118.009855
34. Cadrin-Tourigny J, Bosman LP, Nozza A, Wang W, Tadros R, Bhonsale A, et al. A new prediction model for ventricular arrhythmias in arrhythmogenic right ventricular cardiomyopathy. *Eur Heart J.* (2019) 40:1850–8. doi: 10.1093/eurheartj/ehz103
35. Wu XP Li YD, Wang YD, Zhang M, Zhu WW, Cai QZ, et al. Impaired right ventricular mechanics at rest and during exercise are associated with exercise capacity in patients with hypertrophic cardiomyopathy. *J Am Heart Assoc.* (2019) 8:e011269. doi: 10.1161/JAHA.118.011269
36. Seo J, Hong YJ, Kim YJ, Lkhagvasuren P, Cho I, Shim CY, et al. Prevalence, functional characteristics, and clinical significance of right ventricular involvement in patients with hypertrophic cardiomyopathy. *Sci Rep.* (2020) 10:21908. doi: 10.1038/s41598-020-78945-4
37. Li X, Shi K, Yang ZG, Guo YK, Huang S, Xia CC, et al. Assessing right ventricular deformation in hypertrophic cardiomyopathy patients with preserved right ventricular ejection fraction: a 3. 0-T cardiovascular magnetic resonance study. *Sci Rep.* (2020) 10:1967. doi: 10.1038/s41598-020-58775-0

38. Borleffs CJ, van Erven L, Schotman M, Boersma E, Kiès P, van der Burg AE, et al. Recurrence of ventricular arrhythmias in ischaemic secondary prevention implantable cardioverter defibrillator recipients: long-term follow-up of the Leiden out-of-hospital cardiac arrest study (LOHCAT). *Eur Heart J.* (2009) 30:1621–6. doi: 10.1093/eurheartj/ehp234

Conflict of Interest: The authors declare that the research was conducted in the absence of any commercial or financial relationships that could be construed as a potential conflict of interest.

Publisher's Note: All claims expressed in this article are solely those of the authors and do not necessarily represent those of their affiliated organizations, or those of the publisher, the editors and the reviewers. Any product that may be evaluated in this article, or claim that may be made by its manufacturer, is not guaranteed or endorsed by the publisher.

frontiers | Frontiers in Cardiovascular Medicine

TYPE Original Research
PUBLISHED 04 August 2022
DOI 10.3389/fcvm.2022.946229

OPEN ACCESS

EDITED BY
Yan Zhang,
Peking University, China

REVIEWED BY
Quanyi Zhao,
Chinese Academy of Medical Sciences, China
Mao Zhang,
Stanford University, United States

*CORRESPONDENCE
Lei Yuan
yuanlei33@csu.edu.cn

SPECIALTY SECTION
This article was submitted to General Cardiovascular Medicine, a section of the journal Frontiers in Cardiovascular Medicine

RECEIVED 17 May 2022
ACCEPTED 08 July 2022
PUBLISHED 04 August 2022

CITATION
Cao J and Yuan L (2022) Identification of key genes for hypertrophic cardiomyopathy using integrated network analysis of differential lncRNA and gene expression.
Front. Cardiovasc. Med. 9:946229.
doi: 10.3389/fcvm.2022.946229

Identification of key genes for hypertrophic cardiomyopathy using integrated network analysis of differential lncRNA and gene expression

Jing Cao[1] and Lei Yuan[2]*

[1]Department of Cardiovascular Medicine, Third Xiangya Hospital, Central South University, Changsha, China, [2]Department of Medical Affairs, Xiangya Hospital, Central South University, Changsha, China

Objective: Hypertrophic cardiomyopathy (HCM) is a complex heterogeneous heart disease. Recent reports found that long non-coding RNAs (lncRNAs) play an important role in the progression of cardiovascular diseases. The present study aimed to identify the novel lncRNAs and messenger RNAs (mRNAs) and determine the key pathways involved in HCM.

Methods: The lncRNA and mRNA sequencing datasets of GSE68316 and GSE130036 were downloaded from the Gene Expression Omnibus (GEO) database. An integrated co-expression network analysis was conducted to identify differentially expressed lncRNAs and differentially expressed mRNAs in patients with HCM. Then, gene ontology (GO) and Kyoto Encyclopedia of Genes and Genomes (KEGG) pathway enrichment analyses were explored to identify the biological functions and signaling pathways of the co-expression network. Protein–protein interaction (PPI) and hub gene networks were constructed by using Cytoscape software. Plasma samples of patients with HCM and the GSE89714 dataset were used to validate the bioinformatics results.

Results: A total of 1,426 differentially expressed long non-coding RNAs (lncRNAs) and 1,715 differentially expressed mRNAs were obtained from GSE68316, of which 965 lncRNAs and 896 mRNAs were upregulated and 461 lncRNAs and 819 mRNAs were downregulated. A total of 469 differentially expressed lncRNAs and 2,407 differentially expressed mRNAs were screened from GSE130036, of which 183 lncRNAs and 1,283 mRNAs were upregulated and 286 lncRNAs and 1,124 mRNAs were downregulated. A co-expression network was constructed and contained 30 differentially expressed lncRNAs and 63 differentially expressed mRNAs, which were primarily involved in 'G-protein beta/gamma-subunit complex binding,' 'polyubiquitin modification-dependent protein binding,' 'Apelin signaling pathway,' and 'Wnt signaling pathway.' The 10 hub genes in the upregulated network [G Protein Subunit Alpha I2 (GNAI2), G Protein Subunit Alpha I1 (GNAI1), G Protein Subunit Alpha I3 (GNAI3), G Protein Subunit Gamma 2 (GNG2), G Protein Subunit Beta 1 (GNB1), G Protein Subunit Gamma 13 (GNG13), G Protein Subunit Gamma Transducin 1 (GNGT1), G Protein

Subunit Gamma 12 (GNG12), AKT Serine/Threonine Kinase 1 (AKT1) and GNAS Complex Locus (GNAS)] and the 10 hub genes in the downregulated network [Nucleotide-Binding Oligomerization Domain Containing Protein 2 (NOD2), Receptor-Interacting Serine/Threonine Kinase 2 (RIPK2), Nucleotide-Binding Oligomerization Domain Containing Protein 1 (NOD1), Mitochondrial Antiviral Signaling Protein (MAVS), Autophagy Related 16-Like 1 (ATG16L1), Interferon Induced With Helicase C Domain 1 (IFIH1), Autophagy Related 5 (ATG5), TANK-Binding Kinase 1 (TBK1), Caspase Recruitment Domain Family Member 9 (CARD9), and von Willebrand factor (VWF)] were screened using cytoHubba. The expression of LA16c-312E8.2 and RP5-1160K1.3 in the plasma of patients with HCM was elevated, and the expression of the MIR22 host gene (MIR22HG) was decreased, which was consistent with our analysis, while the expression of LINC00324 and Small Nucleolar RNA Host Gene 12 (SNHG12) was not significantly different between the two groups. Verification analyses performed on GSE89714 showed the upregulated mRNAs of Chloride Voltage-Gated Channel 7 (CLCN7), N-Acetylglucosamine-1-Phosphate Transferase Subunit Gamma (GNPTG), Unk Like Zinc Finger (UNKL), Adenosine Monophosphate Deaminase 2 (AMPD2), GNAI3, WD Repeat Domain 81 (WDR81), and Serpin Family F Member 1 (SERPINF1) and downregulated mRNAs of TATA-Box Binding Protein Associated Factor 12 (TAF12) co-expressed with five crucial lncRNAs. Moreover, GNAI2, GNAI3, GNG12, and vWF were upregulated and GNAS was downregulated in the top 10 hub genes of upregulated and downregulated PPI networks.

Conclusion: These findings from integrative biological analysis of lncRNA-mRNA co-expression networks explored the key genes and pathways and provide new insights into the understanding of the mechanism and discovering new therapeutic targets for HCM. Three differentially expressed pivotal lncRNAs (LA16c-312E8.2, RP5-1160K1.3, and MIR22HG) in the co-expression network may serve as biomarkers and intervention targets for the diagnosis and treatment of HCM.

KEYWORDS

hypertrophic cardiomyopathy, differentially expressed long non-coding RNAs, differentially expressed mRNAs, co-expression network, bioinformatics analysis

Introduction

Hypertrophic cardiomyopathy (HCM) is a complex heterogeneous heart disease that has been recognized to be a significant cause of atrial fibrillation, heart failure, and arrhythmic sudden death and is one of the main causes of sudden cardiac death in young adults (1). Epidemiological investigations have shown that the prevalence of phenotypic expression of HCM in the adult general population was about 0.2% (1:500) (2, 3). HCM is characterized by myocardial hypertrophy, asymmetrical ventricular septal hypertrophy, ventricular narrowing, and abnormal myocardial cell hypertrophy. In the absence of other cardiac or systemic diseases, such as hypertension or aortic stenosis, echocardiography of a hypertrophic but undilated left ventricle is the easiest and most reliable method for the clinical diagnosis of HCM (4). The pathogenesis of HCM is strongly associated with the mutation of the genes encoding proteins of thick and thin myofilament contractile components of the cardiac sarcomere or Z-disk (5, 6). Although myosin heavy chain 7 (MYH7) and myosin binding protein C3 (MYBPC3), which encode β-myosin heavy chain and myosin binding protein C, are the two most common mutations (7, 8), the great heterogeneity and diversity in the molecular pathways make the exact mechanism of HCM remain indistinct.

About 99% of genomic sequences in the human genome do not encode proteins, but they are highly transcriptional and produce a broad spectrum of non-coding RNAs (ncRNAs) that show regulatory and structural functions. The encyclopedia of DNA elements (ENCODE) project and other studies showed

that limiting the pathogenesis analysis of diseases to the protein-coding regions of the human genome is insufficient since many non-coding variations are associated with important human diseases (9–11). The most studied ncRNAs in the heart are microRNAs, and little is known about the other ncRNAs (12–14). Long non-coding RNAs (lncRNAs) are defined as RNAs with transcripts >200 nucleotides that do not encode protein. Recent reports demonstrated that lncRNAs play an important role in the progression of several cardiovascular diseases, such as acute myocardial infarction, heart failure, and atrial fibrillation (15–17). In HCM, lncRNAs are verified to be involved in vital biological processes of myocardial fibrosis, myocardial hypertrophy, and atherosclerosis (18, 19). For example, the overexpression of cardiomyocyte-specific non-coding repressor of factor of Nuclear factor of activated T-cells (NFAT) (NRON) exacerbated transverse aortic constriction (TAC)-induced hypertrophy in mice heart (19), and ROR sponges miR-133 to cause the re-expression of atrial natriuretic peptide and B-type natriuretic peptide, leading to the exacerbation of cardiac hypertrophy eventually (20). However, the role of lncRNAs in the progression of HCM remains to be further explored.

Currently, big data mining and precision medicine have gained considerable attention. In this study, we aimed to perform in-depth data mining based on former microarray studies. We identified differentially expressed lncRNAs and mRNAs in HCM progression by a comprehensive analysis of the public datasets GSE68316 and GSE13036, including 35 patients with HCM and 14 controls. Subsequently, we constructed the co-expression network of lncRNA-mRNA and performed gene ontology (GO) and Kyoto Encyclopedia of Genes/Genomes (KEGG) pathway enrichment analyses on the differentially expressed genes in the network. Finally, we constructed the protein–protein interaction (PPI) network of the differentially expressed genes to reveal the potential role of HCM-related mRNAs and lncRNAs. This study will provide useful information to explore the potential candidate biomarkers for HCM diagnosis, prognosis, and intervention targets.

Materials and methods

Data of gene expression profiles

The expression profile data of LncRNA and mRNA with the sequence numbers GSE68316 and GSE130036 were obtained from the Gene Expression Omnibus (GEO, http://www.ncbi.nlm.nih.gov/geo/) database. The left ventricular tissues of 35 patients with HCM and 14 healthy donors along with their clinical data were obtained, including 7 HCM and 5 healthy donors from GSE68316 and 28 HCM and 9 healthy donors from GSE130036. Gene expression profile dataset GSE89714 was collected from the GEO database to verify the key genes involved in HCM, which included the left ventricular tissues of 5 patients with HCM and 4 healthy donors. The characteristics of these expression profiles are presented in Supplementary Table 1.

Screening of differentially expressed lncRNAs and mRNAs

R language was used to analyze the initial data and identify differential lncRNAs and mRNAs. The Affy package was applied to perform data normalization, including converting the data to raw data and correcting the background. The limma software package was performed to screen the data for differentially expressed lncRNAs and mRNAs. The thresholds were |log2 (fold change) |>1 with the adjusted p-value < 0.05, and the genes that met the criteria were considered as differentially expressed lncRNAs and mRNAs. The gglot2 and heatmap packages were used to create volcano maps and heatmaps of differentially expressed lncRNAs and mRNAs to make them visible.

Co-expression network analysis of differentially expressed lncRNAs and mRNAs in patients with HCM

The Pearson correlation analysis of the differentially expressed lncRNAs and mRNAs was performed by the cor () function in the R language. The absolute value of the Pearson correlation coefficient ≥0.75 of lncRNA-mRNA pairs was considered to be significantly correlated and selected in the co-expression network. Subsequently, the co-expression network was visualized using Cytoscape software.

Gene ontology (GO) enrichment and Kyoto Encyclopedia of genes and genomes (KEGG) pathway analysis of genes in the network

The functions of genes enriched in the co-expression network, including cellular components, biological processes, and molecular functions, were determined by using gene ontology (GO) enrichment analysis. The enriched pathways of genes were analyzed using the Kyoto Encyclopedia of Genes and Genomes (KEGG) pathway analysis. ClusterProfiler package in R was applied to GO enrichment and KEGG pathway analyses with a threshold of adjusted p-value <0.05.

Protein–protein interaction (PPI) network analysis of genes in the network

To predict the physical and functional interactions of proteins, protein–protein interaction (PPI) networks were constructed by the online Search Tool for the Retrieval of Interacting Genes/Proteins (STRING), and the combined score >0.4 was used as the cutoff criterion. Following the construction of the PPI network, the Cytohubba plugin in Cytoscape software was adopted to calculate the degree of each protein node. In this study, the top 10 nodes were regarded to be hub genes.

Plasma collection and real-time quantitative PCR (qPCR)

The research design, protocol, and the use of human plasma samples were approved by the Medical Ethics Committee of the Xiangya Hospital of Central South University. The diagnosis of HCM was carried out according to the European Society of Cardiology Guidelines (21). 4 patients diagnosed with HCM and 4 healthy controls were included in this study. The clinical characteristics of the patients are listed in Supplementary Table 4. The peripheral whole blood of patients was collected in a tube containing an EDTA anticoagulant after overnight fasting, and plasma was separated by centrifugation. Total RNA was extracted from plasma samples using a miRNeasy Serum/Plasma Kit (Qiagen) according to the manufacturer's instructions. The quality and concentration of RNA were evaluated using NanoDrop 2000 spectrophotometer (Thermo Fisher Scientific). Complementary DNAs (cDNAs) were synthesized from the total RNA using the PrimeScript RT reagent Kit (Takara) in accordance with the manufacturer's instructions. The lncRNAs were quantified by performing real-time qPCR on a QuantStudio 5 Real-Time PCR System with SYBR Premix Ex Taq assays (Takara). The fold difference in the expression level between the two groups was calculated using the $2^{-\Delta\Delta Ct}$ method. The primer sequences are summarized in Supplementary Table 5.

Statistical analysis

The results are expressed as mean±SD. The *T*-tests or nonparametric tests were used to compare the differences between the HCM group and the control group. Graphs were constructed with R software, GraphPad Prism, and online visualization tools. A two-tailed *P*-value of < 0.05 was considered to be statistically significant. Statistical analyses were done using GraphPad Prism 8.0 and SPSS 20.0.

Results

Identification of differentially expressed lncRNAs and mRNAs in patients with HCM compared with the controls

The gene expression data of HCM were obtained from GSE68316 and GSE130036 datasets, which included 35 patients with HCM and 14 controls, and the basic information of the datasets is presented in Supplementary Table 1. After normalization, a total of 1,426 differential expressed lncRNAs and 1,715 differential expressed mRNAs were obtained from GSE68316 (adjusted $P < 0.05$, fold change >2). Among them, 965 lncRNAs were upregulated and 461 lncRNAs were downregulated; 896 mRNAs were upregulated and 819 mRNAs were downregulated. The volcano plots of differentially expressed genes are shown in Figures 1A,C, and the cluster heatmaps are shown in Figures 2A,C. A total of 469 differentially expressed lncRNAs and 2,407 differentially expressed mRNAs were obtained from GSE130036, of which 183 lncRNAs and 1,283 mRNAs were upregulated and 286 lncRNAs and 1,124 mRNAs were downregulated (adjusted $P < 0.05$, fold change >2). The volcano plots of differentially expressed genes in GSE130036 are shown in Figures 1B,D, and the cluster heatmaps are shown in Figures 2B,D. The top 10 differentially expressed lncRNAs involved in the HCM of the two datasets are listed in Table 1, and the top 10 differentially expressed mRNAs are listed in Table 2.

Subsequently, the Venn diagrams of upregulated and downregulated genes are shown in Figure 3. A total of 34 common differentially expressed lncRNAs with 15 upregulated and 19 downregulated lncRNAs (Figures 3A,C) and a total of 54 common differentially expressed mRNAs with 25 upregulated and 29 downregulated mRNAs (Figures 3B,D) were thus identified.

Differential lncRNA-mRNA co-expression network construction and analysis

To determine the function of differentially expressed lncRNAs and their role in HCM, a gene co-expression network between lncRNAs and mRNAs was constructed. Then, Pearson's correlation coefficients in all samples were calculated for correlation analysis of mRNAs and lncRNAs, and lncRNA-mRNA pairs with a coefficient of ≥0.75 were selected. A total of 63 lncRNA-mRNA pairs were observed to be involved in 30 differentially expressed lncRNAs (13 upregulated and 17 downregulated) and 63 differentially expressed mRNAs (27 in upregulated network and 36 in downregulated network). In the upregulated co-expression network, 27 lncRNA-mRNA pairs were observed with 13 differentially expressed lncRNAs

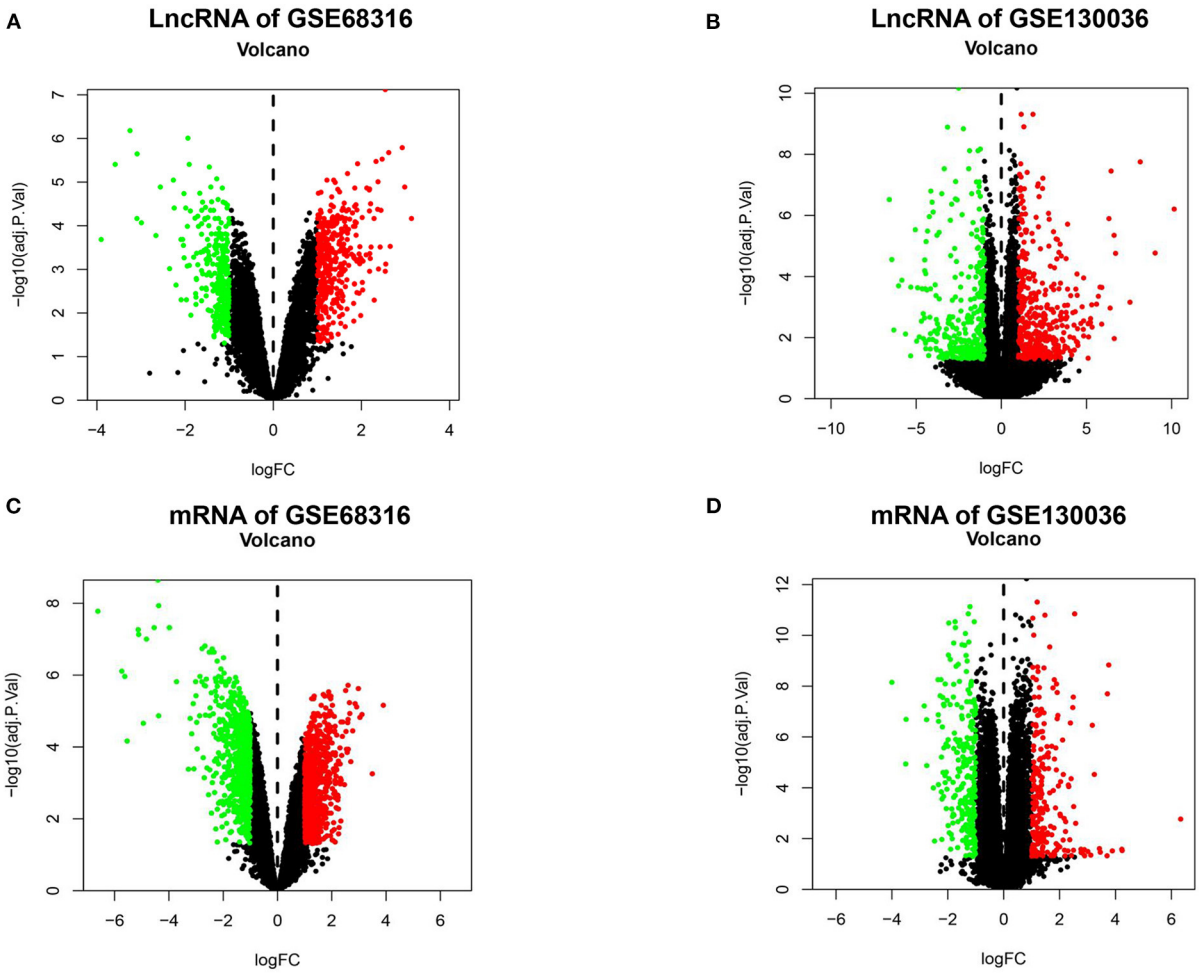

FIGURE 1
A Volcano plot of all the differentially expressed lncRNAs and mRNAs between patients with HCM and the controls. **(A)** A volcano plot of differentially expressed lncRNAs in the GSE68316 dataset. **(B)** A volcano plot of differentially expressed lncRNAs in the GSE130036 dataset. **(C)** A volcano plot of differentially expressed mRNAs in the GSE68316 dataset. **(D)** A volcano plot of differentially expressed mRNAs in GSE130036 dataset. Green dots represent differentially expressed genes with log-fold change <-1, red dots represent differentially expressed genes with log-fold change >1, and black spots represent genes with no significant difference in expression, adjusted *p*-value <0.05.

and 27 mRNAs (Figure 4A). About 36 lncRNA-mRNA pairs were observed in the downregulated co-expression network, including 17 differentially expressed lncRNAs and 36 mRNAs (Figure 4B).

GO function enrichment analysis of genes in the co-expression network

Furthermore, to ascertain the potential functions of the identified differentially expressed lncRNAs and mRNAs in the co-expression network, GO function enrichment analysis was performed (Figure 5). GO analysis mainly described three categories of results: 'molecular functions' (MF), 'cellular components' (CC), and 'biological processes' (BP). The analyses exhibited the top 10 significant enrichment of MF, CC, and BP in terms of upregulated and downregulated genes in the co-expression network. As shown in Figure 5A, the enrichment analysis of upregulated co-expression network related to molecular functions was primarily enriched in G-protein beta/gamma-subunit complex binding ($P = 0.0002$), GDP binding ($P = 0.0031$), and GTPase activity ($P = 0.0055$), and the analysis related to cellular components were mainly enriched in heterotrimeric G-protein complex ($p = 0.0006$), GTPase complex ($P = 0.0006$), and the extrinsic component of the cytoplasmic side of the plasma membrane ($P = 0.0005$). Additionally, the analysis of biological processes showed that genes were mainly involved in the positive regulation of cholesterol metabolic process ($P = 0.0112$), endothelial cell chemotaxis to fibroblast growth factor (P

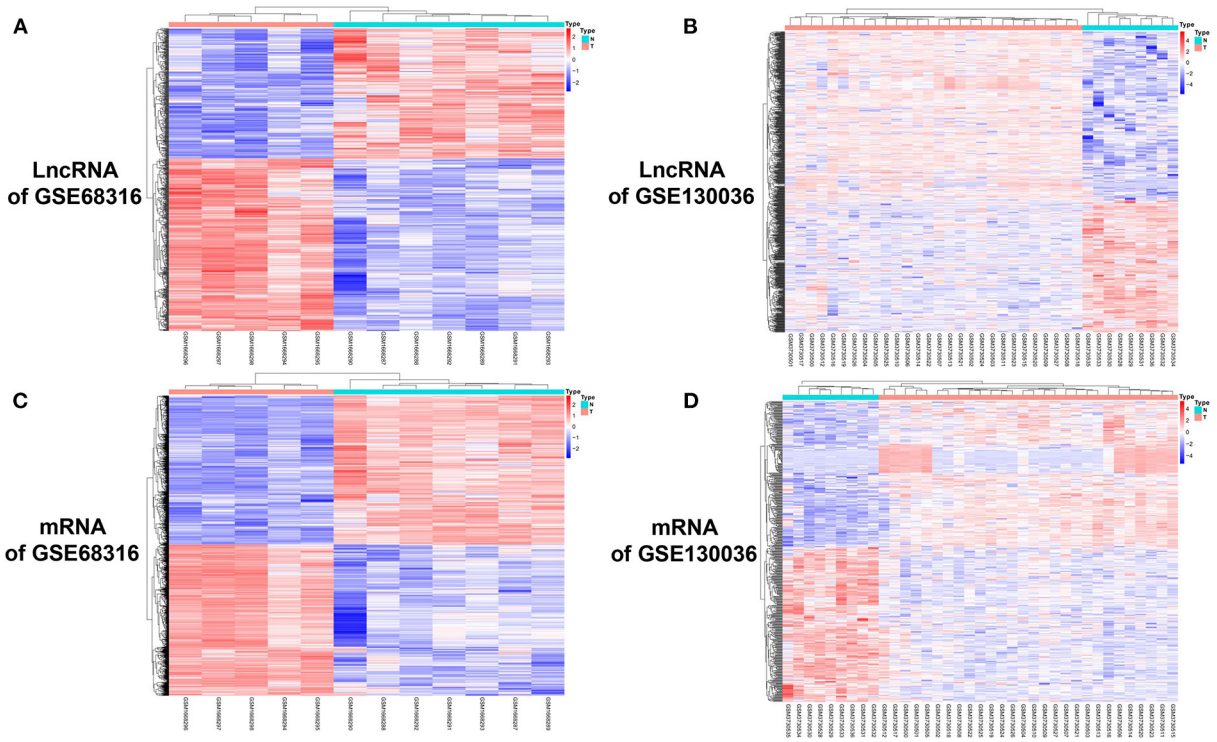

FIGURE 2
A cluster heat map of differentially expressed lncRNAs and mRNAs between HCM patients and the controls. **(A)** A heat map of differentially expressed lncRNAs in the GSE68316 dataset. **(B)** A heat map of differentially expressed lncRNAs in the GSE130036 dataset. **(C)** A heat map of differentially expressed mRNAs in the GSE68316 dataset. **(D)** A heat map of differentially expressed mRNAs in the GSE130036 dataset. The gradient color change from blue to red represents the changing process from downregulation to upregulation.

= 0.0112), and miRNA catabolic process (P = 0.0112). On the other hand, the enrichment analysis related to the molecular functions of downregulated co-expression network focused on K63-linked polyubiquitin modification-dependent protein binding (P = 0.0007), polyubiquitin modification-dependent protein binding (P = 0.0041), and serine-type endopeptidase inhibitor activity (P = 0.0132). Also, the cellular components were primarily enriched in mitotic spindle midzone (P = 0.0002), spindle midzone (P = 0.0015), and myelin sheath (P = 0.0030). In regard to biological process enrichment analysis of downregulated co-expression network, genes were mainly involved in the hydrogen peroxide biosynthetic process (P = 0.0004), the antibiotic biosynthetic process (P = 0.0007), and glutamate secretion (P = 0.0029) (Figure 5B).

KEGG pathway enrichment analysis of genes in the co-expression network

To further identify the biological processes associated with genes in the co-expression networ, KEGG pathway enrichment analyses were performed. As shown in Figure 6A, a total of nine key pathways were found through the KEGG pathway enrichment analysis of upregulated genes, which were primarily enriched in the Apelin signaling pathway (P = 0.0095), the Rap1 signaling pathway (P = 0.0215), and the regulation of the actin cytoskeleton (P = 0.0223). However, the downregulated genes in the co-expression network were significantly enriched in the Wnt signaling pathway (P = 0.0347), the folate biosynthesis pathway (P = 0.0473), and the transcriptional misregulation pathway (P = 0.0483) (Figure 6B).

PPI network construction analysis

The PPI network analysis aims to study disease-related molecular mechanisms in co-expression networks and identify novel therapeutic targets from a systematic perspective. Consequently, a PPI network analysis of differentially expressed genes in the co-expression network was conducted with the STRING database. A total of 65 nodes and 362 edges were screened in the upregulated PPI network (Figure 7A). Nodes with high topological scores were considered to likely play an important role in disease, and G Protein Subunit

TABLE 1 Top 10 upregulated and downregulated long noncoding RNAs in the myocardial tissues of patients with HCM in GSE68316 and GSE130036.

GSE68316					GSE130036				
Ensembl_Gene_ID	Gene symbol	Adjust P	Regulation	Log2 FC	Ensembl Gene_ID	Gene symbol	Adjust P	Regulation	Log2 FC
ENST00000445814	XIST	0.12802	up	3.89686	ENST00000624710	AC008522.1	0.01136	up	6.80673
ENST00000440196	LOC101928626	3.48E-21	up	3.69278	ENST00000611237	RP5-881P19.7	0.01272	up	6.62029
ENST00000588634	CTC-510F12.2	1.01E-15	up	3.32935	ENST00000619449	MALAT1-215	0.01494	up	4.98358
ENST00000472913	PLCH1-AS2	5.11E-19	up	3.05175	ENST00000489821	B3GALT5-AS1	0.02867	up	4.88654
ENST00000453100	LINC00570	8.53E-14	up	2.79108	ENST00000553348	CTD-2243E23.1	7.79E-06	up	4.73740
ENST00000549241	RP11-449P15.1	1.23E-15	up	2.74094	ENST00000507108	LINC02433	0.00069	up	4.67747
ENST00000558994	CTD-2308G16.1	1.37E-08	up	2.58255	ENST00000554055	RP11-841O20.2	0.01226	up	4.22569
ENST00000524768	CTD-2530H12.2	7.62E-13	up	2.52511	ENST00000425630	LINC00200	0.01358	up	4.16374
ENST00000456450	AC010907.2	2.23E-20	up	2.47399	ENST00000562361	AC018767.2	0.00044	up	3.90221
ENST00000420902	RP1-29C18.8	3.55E-10	up	2.47292	ENST00000554759	RP11-588P7.2	0.00076	up	3.78938
ENST00000450016	LINC01952	1.92E-07	down	2.81115	ENST00000634611	AC107068.2	0.00149	down	5.39759
ENST00000443565	LINC01781	0.00021	down	2.73194	ENST00000446593	AC093642.6	0.00292	down	5.27501
ENST00000376482	AC073842.19	4.56E-16	down	2.53420	ENST00000552470	RP11-632B21.1	9.28E-06	down	5.10923
ENST00000563833	AF213884.2	3.97E-09	down	2.33589	ENST00000430181	TSPEAR-AS1	4.24E-07	down	4.10253
ENST00000475250	PPP1R35-AS1	0.00086	down	2.29869	ENST00000555146	RP11-110A12.2	0.00019	down	3.97233
ENST00000424948	RP1-92O14.3	1.30E-06	down	2.21711	ENST00000453554	RP11-108M9.3	1.27E-14	down	3.88847
ENST00000570843	RP11-473M20.16	1.43E-16	down	2.20565	ENST00000330490	TSPEAR-AS2	4.76E-12	down	3.57308
ENST00000367477	STXBP5	0.00368	down	2.20057	ENST00000521558	RP11-1081M5.1	1.69E-24	down	3.49851
ENST00000507727	ALG14	4.59E-09	down	2.16974	ENST00000533578	FAM167A-AS1	0.03743	down	3.43473
ENST00000549023	AC010173.1	4.11E-08	down	2.14412	ENST00000467995	LINC00881	2.62E-16	down	3.42541

Log2 FC, Log2-fold change; adjust P, adjusted P-value; XIST, X Inactive Specific Transcript; PLCH1-AS2, PLCH1 Antisense RNA 2; PPP1R35-AS1, PPP1R35 Antisense RNA 1; STXBP5, Syntaxin Binding Protein 5; ALG14, ALG14 UDP-N-Acetylglucosaminyltransferase Subunit; MALAT1, metastasis-associated lung adenocarcinoma transcript 1; B3GALT5-AS1, B3GALT5 Antisense RNA 1; TSPEAR-AS1, TSPEAR Antisense RNA 1; TSPEAR-AS2, TSPEAR Antisense RNA 2; FAM167A-AS1, FAM167A Antisense RNA 1.

Alpha I2 (GNAI2), G Protein Subunit Alpha I1 (GNAI1), G Protein Subunit Alpha I3 (GNAI3), G Protein Subunit Gamma 2 (GNG2), G Protein Subunit Beta 1 (GNB1), G Protein Subunit Gamma 13 (GNG13), G Protein Subunit Gamma Transducin 1 (GNGT1), G Protein Subunit Gamma 12 (GNG12), AKT Serine/Threonine Kinase 1 (AKT1), and GNAS Complex Locus (GNAS) were the top 10 hub genes in the PPI network of upregulated genes (Figure 7B, Supplementary Table 2). A total of 69 nodes and 314 edges were screened in the downregulated PPI network (Figure 7C). Nucleotide-Binding Oligomerization Domain Containing Protein 2 (NOD2), Receptor-Interacting Serine/Threonine Kinase 2 (RIPK2), Nucleotide-Binding Oligomerization Domain Containing 1 (NOD1), Mitochondrial Antiviral Signaling Protein (MAVS), Autophagy Related 16-Like 1 (ATG16L1), Interferon Induced With Helicase C Domain 1 (IFIH1), Autophagy Related 5 (ATG5), TANK Binding Kinase 1 (TBK1), Caspase Recruitment Domain Family Member 9 (CARD9), and von Willebrand factor (VWF) were the top 10 hub genes in the PPI network of downregulated genes (Figure 7D, Supplementary Table 2).

Verification of crucial lncRNAs and mRNAs in patients with HCM

In addition to expressing in specific tissues, lncRNA also exists stably in the circulating peripheral blood and hence can be used as biomarkers for the diagnosis and treatment of diseases (22). In order to verify the key lncRNAs and their diagnostic value for HCM, we collected plasma samples of patients with HCM and evaluated the level of five crucial lncRNAs (two upregulated and three downregulated) in the co-expression network by real-time qPCR. As shown in Figure 8A, lncRNA LA16c-312E8.2 (control: 0.99 ± 0.42 vs. HCM: 2.44 ± 0.93, $P = 0.0303$) and RP5-1160K1.3 (control: 1.15 ± 0.42 vs HCM: 2.97 ± 1.10, $P = 0.0219$) were upregulated and lncRNA MIR22 host gene (MIR22HG) (control: 1.19 ± 0.46 vs. HCM: 0.49 ± 0.23, $P = 0.0360$) was downregulated in patients with HCM, which was consistent with our previous analysis results. However, the levels of LINC00324 (control: 1.11 ± 0.46 vs. HCM: 0.93 ± 0.48, $P = 0.6037$) and Small Nucleolar RNA Host Gene 12 (SNHG12) (control: 1.14 ± 0.40 vs. HCM: 0.88 ± 0.53, $P = 0.4657$) were not significantly different between the two groups.

TABLE 2 Top 10 upregulated and downregulated mRNAs in the myocardial tissues of patients with HCM in GSE68316 and GSE130036.

GSE68316					GSE130036				
Ensembl_Gene_ID	Gene symbol	Adjust P	Regulation	Log2 FC	Ensembl Gene_ID	Gene symbol	Adjust P	Regulation	Log2 FC
ENST00000463664	SELENBP1	2.22E-17	up	6.481273	ENST00000368742	LORICRIN	2.26E-33	up	24.72548
ENST00000171887	TNS1	1.91E-13	up	6.36043	ENST00000437231	PCBP2	4.21E-34	up	24.54893
ENST00000330597	HBG1	3.36E-06	up	5.848873	ENST00000252244	KRT1	7.45E-28	up	23.59247
ENST00000380327	TROAP	6.80E-17	up	5.734056	ENST00000553458	ALDH6A1	6.28E-23	up	22.89827
ENST00000555156	LOC100506767	4.26E-17	up	5.246619	ENST00000396934	BTN3A2	3.58E-23	up	22.85187
ENST00000397027	EPB42	1.72E-18	up	5.11782	ENST00000425460	MYH14	3.93E-19	up	22.57398
ENST00000523022	CA1	1.24E-13	up	5.066804	ENST00000368295	ECHDC1	1.45E-16	up	22.04711
ENST00000399246	SLC4A1	8.42E-15	up	4.797823	ENST00000611477	ZNF16	6.11E-09	up	21.68905
ENST00000472539	HBM	2.08E-18	up	4.557216	ENST00000357992	ELK4	4.60E-08	up	21.62953
ENST00000537904	PDE4DIP	7.35E-19	up	4.386079	ENST00000585156	PDE4DIP	5.98E-08	up	21.46707
ENST00000463664	COMMD6	2.02E-19	down	3.84337	ENST00000504584	CORIN	1.42E-12	down	25.772
ENST00000309170	P2RY14	7.18E-13	down	3.299083	ENST00000509536	TECRL	1.54E-11	down	25.6542
ENST00000435402	CCDC7	4.90E-17	down	3.080423	ENST00000327705	BTNL9	1.10E-10	down	24.6503
ENST00000356719	KIAA1841	1.26E-19	down	3.010909	ENST00000360162	ADD3	3.04E-10	down	24.1061
ENST00000480956	LSM5	2.31E-17	down	2.997625	ENST00000613142	SELENOI	6.17E-10	down	23.7528
ENST00000293842	RPL26	6.68E-20	Down	2.935435	ENST00000503821	CORIN	0.00211	down	10.5294
ENST00000467106	RPS24	6.91E-19	down	2.902729	ENST00000370046	KCNIP2	0.000273	down	9.13034
ENST00000460380	C17orf108	1.51E-13	down	2.793557	ENST00000618099	FURIN	3.10E-06	down	8.64193
ENST00000496387	UQCRH	5.80E-17	down	2.764366	ENST00000392179	NDUFS2	0.002885	down	8.56594
ENST00000552548	PFDN5	2.17E-17	down	2.682237	ENST00000343195	KCNIP2	7.95E-05	down	8.36729

Log2 FC, Log2-fold change; adjust P, adjusted P-value; SELENBP1, Selenium Binding Protein 1; TNS1, Tensin 1; HBG1, Hemoglobin Subunit Gamma 1; TROAP, Trophinin Associated Protein; EPB42, Erythrocyte Membrane Protein Band 4.2; CA1, Carbonic Anhydrase 1; SLC4A1, Solute Carrier Family 4 Member 1; HBM, Hemoglobin Subunit Mu; PDE4DIP, Phosphodiesterase 4D Interacting Protein; COMMD6, COMM Domain Containing 6; P2RY14, Phosphodiesterase 4D Interacting Protein; CCDC7, Coiled-Coil Domain Containing 7; RPL26, Ribosomal Protein L26; RPS24, Ribosomal Protein S24; C17orf108, LYR Motif Containing 9, LYRM9; UQCRH, Ubiquinol-Cytochrome C Reductase Hinge Protein; PFDN5, Prefoldin Subunit 5; PCBP2, Poly(RC) Binding Protein 2; KRT1, Keratin 1; ALDH6A1, Aldehyde Dehydrogenase 6 Family Member A1; BTN3A2, Butyrophilin Subfamily 3 Member A2; MYH14, Myosin Heavy Chain 14; ECHDC1, Ethylmalonyl-CoA Decarboxylase 1; ZNF16, Zinc Finger Protein 16; ELK4, ETS Transcription Factor ELK4; CORIN, Corin, Serine Peptidase; TECRL, Trans-2,3-Enoyl-CoA Reductase Like; BTNL9, Butyrophilin Like 9; ADD3, Adducin 3; SELENOI, Selenoprotein I; KCNIP2, Potassium Voltage-Gated Channel Interacting Protein 2; FURIN, Furin, Paired Basic Amino Acid Cleaving Enzyme; NDUFS2, NADH: Ubiquinone Oxidoreductase Core Subunit S2.

In addition to verify the expression of lncRNAs in peripheral blood, we selected GSE89714 as the validation dataset to verify the expression levels of mRNAs (co-expressed with five crucial lncRNAs) in the co-expression network and the top 10 hub genes in the PPI network between HCM and healthy control cardiac tissues. As seen in Figure 8B, Chloride Voltage-Gated Channel 7 (CLCN7), N-Acetylglucosamine-1-Phosphate Transferase Subunit Gamma (GNPTG), and Unk Like Zinc Finger (UNKL), which co-expressed with LA16c-312E8.2, were upregulated in the cardiac tissue of patients with HCM, whereas Coiled-Coil Domain Containing 154 (CCDC154), Proline and Glutamate Rich with Coiled Coil 1 (PERCC1), and C16orf91 showed no significant differences between the two groups; LncRNA RP5-1160K1.3 co-expressed mRNAs Adenosine Monophosphate Deaminase 2 (AMPD2) and GNAI3 were upregulated, and G Protein Subunit Alpha Transducin 2 (GNAT2) and G Protein-Coupled Receptor 61 (GPR61) showed no significant changes. In the co-expressed mRNAs of MIR22HG, WD Repeat Domain 81 (WDR81) and Serpin Family F Member 1 (SERPINF1) were upregulated in the HCM group, and TLC Domain Containing 2 (TLCD2), Pre-mRNA Processing Factor 8 (PRPF8), and Serpin Family F Member 2 (SERPINF2) showed no significant differences. In the co-expressed mRNAs of SNHG12, TATA-Box Binding Protein Associated Factor 12 (TAF12) was downregulated in HCM cardiac tissues, and other genes like Regulator of Chromosome Condensation 1 (RCC1), TRNA Selenocysteine 1 Associated Protein 1 (TRNAU1AP), and RAB42 showed no significant differences. Unfortunately, there were no significant differences in the expression of LINC00324 co-expressed mRNAs, which include CST telomere replication complex component 1 (CTC1), Phosphoribosylformylglycinamidine synthase (PFAS), Transmembrane Protein 107 (TMEM107), Aurora Kinase B (AURKB), and C17orf59, compared with the control group. In regard to the top 10 hub genes, the analysis of the dataset GSE89714 found that GNAI2, GNAI3, and AKT1 were upregulated, whereas GNAS was downregulated in the upregulated PPI network. Other genes, including GNAI1,

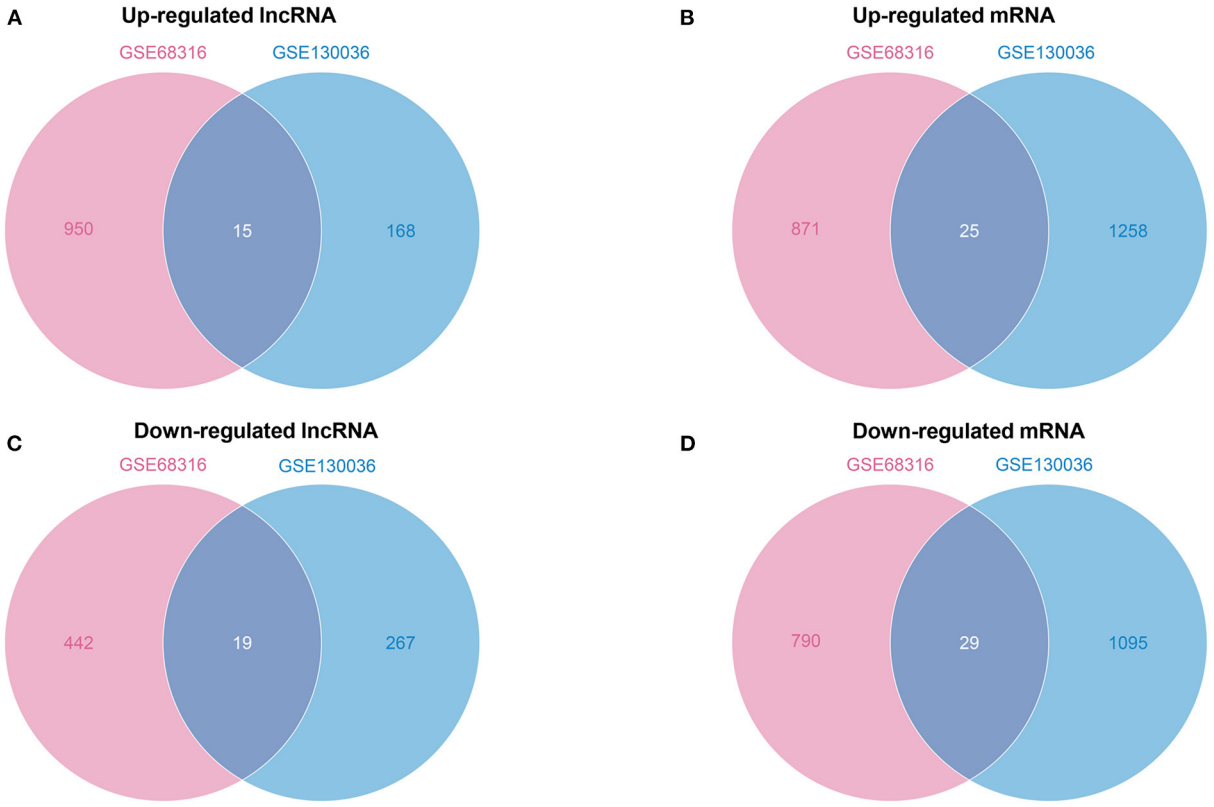

FIGURE 3
A Venn diagram of common differentially expressed lncRNAs and mRNAs. **(A)** A Venn diagram of upregulated common differentially expressed lncRNAs. **(B)** A Venn diagram of upregulated common differentially expressed mRNAs. **(C)** A Venn diagram of downregulated common differentially expressed lncRNAs. **(D)** A Venn diagram of downregulated common differentially expressed mRNAs.

GNG2, GNB1, GNG13, GNGT1, and GNG12, showed no significant differences between HCM and control cardiac tissue. In the downregulated network, only one gene (vWF) was statistically different (Figure 8C).

Discussion

Hypertrophic cardiomyopathy, a type of hereditary cardiomyopathy, is the most common risk factor for sudden death in young people. With the emergence of next-generation sequencing (NGS) technologies, the list of variants and genes implicated in HCM is also expanding. These discoveries allow the precise identification of at-risk individuals prior to clinical diagnosis and provide novel therapeutic approaches for the modulation and prevention of HCM (23–26). A growing number of studies showed that lncRNAs play a momentous regulatory function in the pathophysiology of cardiovascular diseases, such as acute myocardial infarction, heart failure, and atrial fibrillation (15–17). Sequencing studies gradually found that lncRNAs also play an important role in the pathogenesis of HCM (27, 28), but the comprehensive evaluation of multiple datasets has not been thoroughly investigated. In the present study, we identified a total of 1,861 lncRNAs (1,133 upregulated and 728 downregulated) and 4,068 mRNAs (2,154 upregulated and 1,914 downregulated) were differentially expressed between the HCM and controls in the GSE68316 and GSE130036 datasets. Among these differentially expressed genes, 34 lncRNAs (15 upregulated and 19 downregulated) and 54 mRNAs (25 upregulated and 29 downregulated) were the commonly found differentially expressed genes. Co-expression network construction and subsequent GO enrichment and KEGG pathway analysis showed that the upregulated co-expression network was mainly enriched in G-protein beta/gamma-subunit complex binding, heterotrimeric G-protein complex, the Apelin signaling pathway, and the Rap1 signaling pathway. In addition, the downregulated network was mainly enriched in K63-linked polyubiquitin modification-dependent protein binding, mitotic spindle midzon, the Wnt signaling pathway, and the folate biosynthesis pathway. Of note, plasma sample validation of patients with

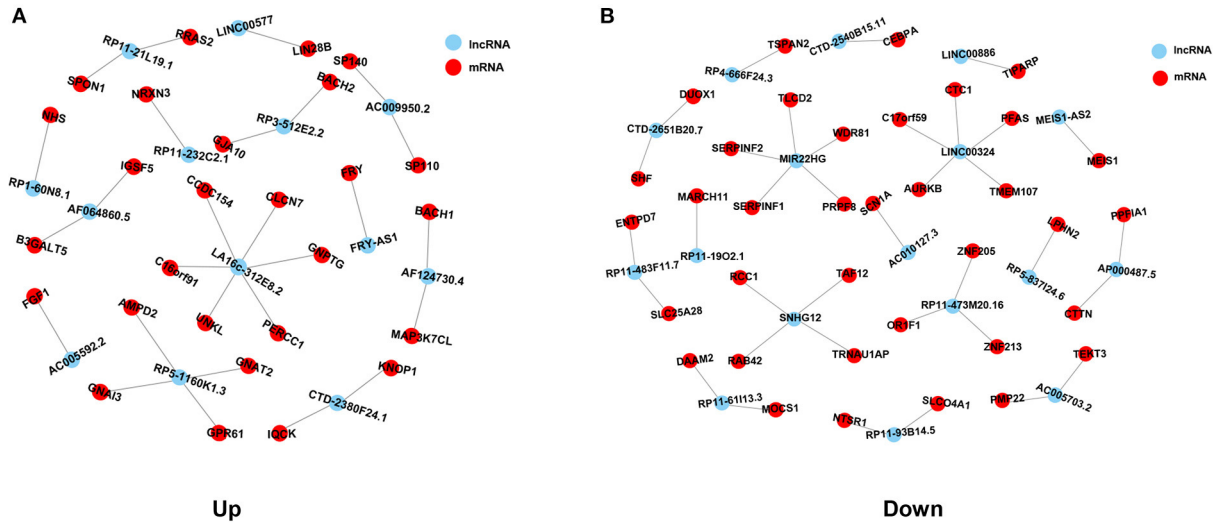

FIGURE 4
Co-expression network analysis of common differentially expressed lncRNAs and mRNAs in HCM. **(A)** Co-expression network of upregulated common differentially expressed lncRNAs and mRNAs. **(B)** Co-expression network of downregulated common differentially expressed lncRNAs and mRNAs. Red spots represent lncRNAs, blue spots represent mRNAs, and lines represent the co-expression relationships between lncRNAs and mRNAs.

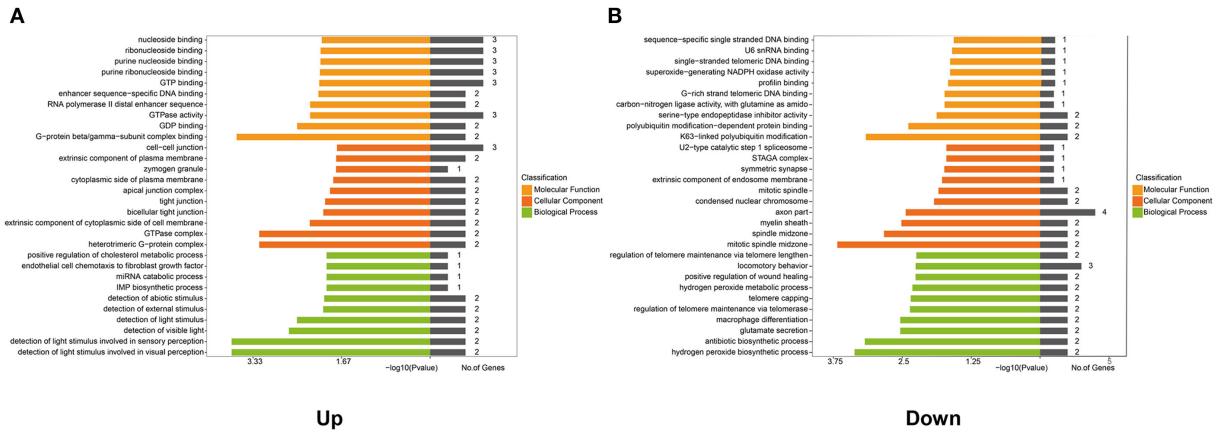

FIGURE 5
Gene Ontology (GO) analysis of genes in the co-expression network. GO analysis shows: **(A)** The top 10 enriched terms associated with the molecular function (MF), cellular component (CC), and biological process (BP) of genes in the upregulated co-expression network. **(B)** The top 10 enriched terms associated with MF, CC, and BP of genes in the downregulated co-expression network.

HCM prompts that three key lncRNAs (LA16c-312E8.2, RP5-1160K1.3, and MIR22HG) may serve as biomarkers and intervention targets in HCM. These analyses provide novel insights to explore the potential mechanisms underlying HCM progression.

LncRNA has been found to regulate cardiomyocyte hypertrophy, apoptosis, angiogenesis, atherosclerosis, and other pathophysiological processes and play an important role in the development of cardiovascular disease (29–32). In recent years, it has also been reported that lncRNA plays an important role in HCM. Janika Viereck et al. reported that LncRNA H19 is highly conserved and downregulated in the failing hearts of mice, pigs, and humans. The H19 gene therapy prevents and reverses experimental pressure-overload-induced heart failure according to interaction with the polycomb repressive complex 2, suppressing H3K27 trimethylation, which, in turn, leads to reduced NFAT expression and activity (33). On the other hand, Xiao et al. (34) found that lncRNA X Inactive Specific Transcript

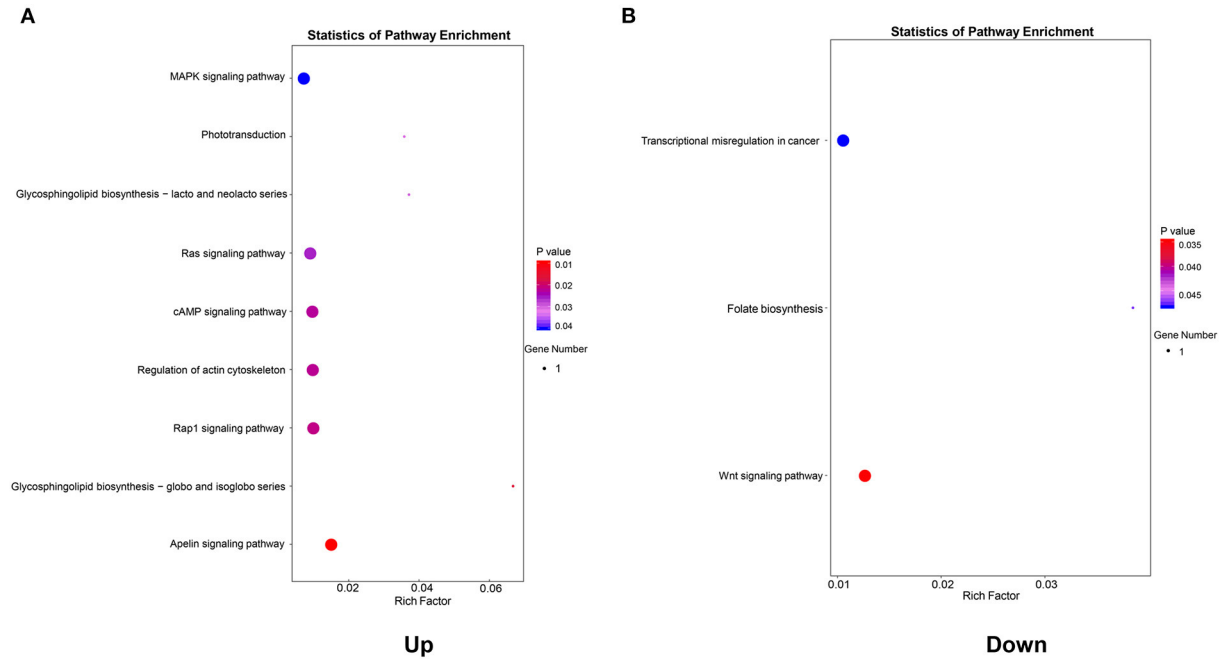

FIGURE 6
Kyoto Encyclopedia of Genes and Genomes (KEGG) pathway enrichment analysis of genes in the co-expression network. **(A)** KEGG pathways enriched by genes in the upregulated co-expression network. **(B)** KEGG pathways enriched by genes in the downregulated co-expression network.

(XIST) expression was significantly upregulated in hypertrophic mouse hearts and phenylephrine-treated cardiomyocytes. XIST promoted the progression of cardiac hypertrophy through competitively binding with miR-101 to enhance the expression of TLR2. After knocking down XIST, PE-induced cardiomyocyte hypertrophy was attenuated. In our research, a total of 1861 differentially expressed lncRNAs were identified by integrating datasets GSE68316 and GSE130036, among which 34 lncRNAs were expressed in both datasets. These common differentially expressed lncRNAs were analyzed to be co-expressed with several genes.

LncRNA LA16c-312E8.2 is also named LOC101929440. In addition to upregulated expression in HCM, LA16c-312E8.2 has also been reported to be differentially expressed in HER-2 enriched subtypes of breast cancer and pancreatic cancer (35, 36). However, the exact function and regulatory role of LA16c-312E8.2 has not yet been studied. The mRNAs co-expressed with LA16C-312E8.2 included CCDC154, CLCN7, GNPTG, PERCC1, UNKL, and C16orf91. CCDC154 is mainly involved in osteopetrosis and hypoplastic left heart syndrome (37, 38), and CLCN7 is mainly involved in osteopetrosis and angiogenesis (39). Diseases associated with GNPTG include mucolipidosis III gamma and mucolipidosis (40, 41), and those associated with PERCC1 include diarrhea 11, malabsorptive, congenital, and hepatocellular carcinoma (42–44). UNKL is associated with mucolipidosis (45), while the function and role of C16orf91 have not been reported. Among these co-expressed mRNAs, GNPTG and UNKL were involved in mucolipidosis that is associated with dilated cardiomyopathy in mucolipidosis type 2 (46), and CLCN7 was related to angiogenesis (39). These three genes are associated with cardiovascular diseases but have not been reported in HCM, which may be related to the lack of adequate research on HCM. In this study, our verification results showed that LncRNA LA16c-312E8.2 was upregulated in the plasma samples of patients with HCM compared to the controls. Besides, verification analysis of the public dataset showed that CCDC154, GNPTG, and UNKL were upregulated in the heart tissues of patients with HCM in the GSE89714 dataset, but there were no significant differences in other genes between the patients with HCM and controls.

MIR22HG, also known as C17orf91, is a downregulated lncRNA in HCM. The actions and functions of the MIR22HG gene are complex and have not been fully elucidated, but it has been reported to be involved in the regulation of cell proliferation and death according to several signaling pathways, including Wnt/β-catenin, epithelial-mesenchymal transition (EMT), notch, and STAT3 (47, 48). These pathways may promote the process of myocardial fibrosis in HCM. Previous studies reported that MIR22HG aggravates hypoxia-induced injury in cardiomyocytes and endothelial cells

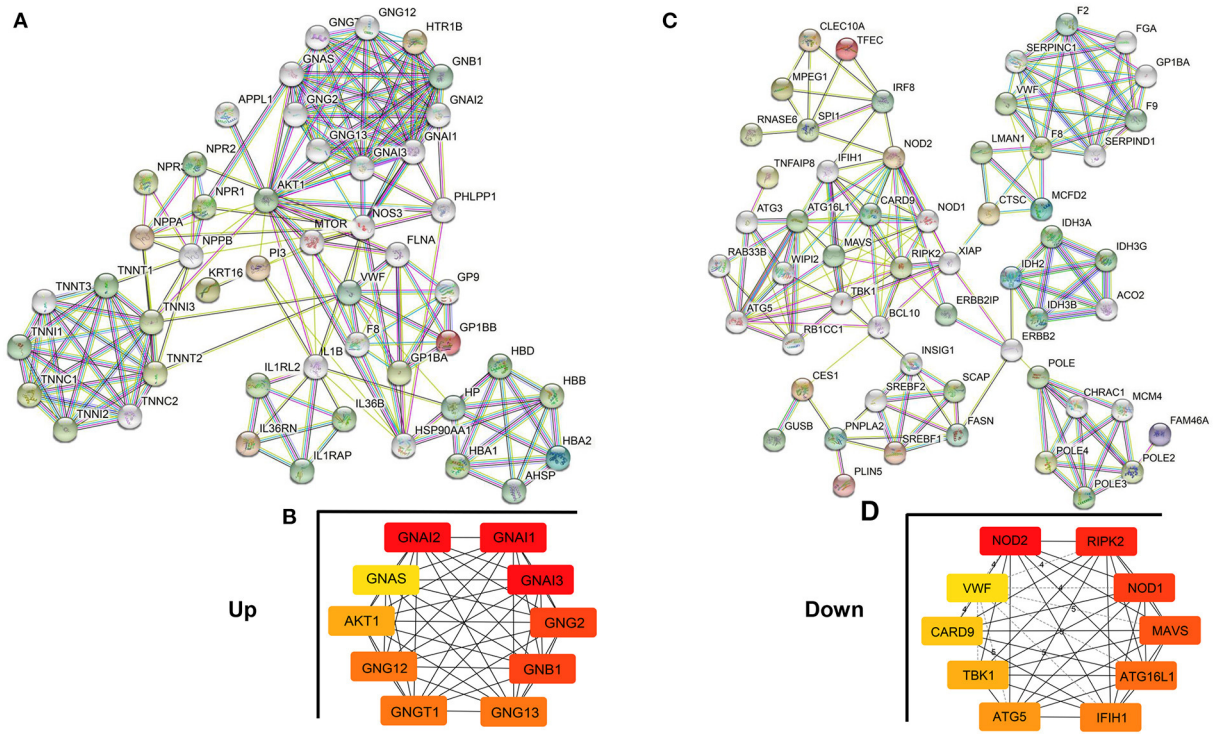

FIGURE 7
Protein–Protein Interaction (PPI) network analysis of genes in the co-expression network. **(A,B)** PPI network and hub genes in the upregulated co-expression network. **(C,D)** PPI network and hub genes in the downregulated co-expression network. The edges represent the interaction between two nodes, and the number of edges in one node is called the degree of the PPI network.

(49, 50); however, the exact mechanism of this gene in HCM has not been elucidated. MIR22HG was co-expressed with SERPINF1, SERPINF2, TLCD2, WDR81, and PRPF8. SERPINF1 and SERPINF2 are members of the serpin family. SERPINF1 strongly inhibits angiogenesis, and SERPINF2 is involved in alpha-2-plasmin inhibitor deficiency, vasculitis, and left ventricular diastolic dysfunction (51, 52). TLCD2 participates in Chromosome 17P13.3, Centromeric, Duplication Syndrome and is reported to be associated with increased left ventricular mass and cardiac hypertrophy (53). WDR81 is necessary for Purkinje and photoreceptor cell survival and has been reported to be associated with cerebellar ataxia and mental retardation. PRPF8 is essential for oxidative stress injury-induced mitophagy, which in turn leads to intracellular energy metabolism disorders (54). Although these genes have not been reported in HCM, they are involved in pathophysiological processes, including left ventricular diastolic dysfunction, myocardial hypertrophy, and disturbances in cellular energy metabolism, which are closely related to HCM. Therefore, it deserves our attention and further study.

We further analyzed the co-expression network of lncRNA-mRNA and found two hub gene networks. In the upregulated network, 10 hub genes were enumerated, which were involved in regulating the G protein-coupled receptor (GPCR) signaling pathway and GTPase activity. GPCR mediates many pathophysiological processes, such as cardiac contractility, hypertrophy, proliferation, survival, and fibrosis, which are closely correlated with HCM (55–57). Xin Liu et al. reported that ERK1/2 communicates with the GPCR signaling pathways to promote HCM upon Ang-II stimulation (58). In addition, Feng Xie et al. found that the GPCR family member APJ interacts with its ligand and promotes cardiac hypertrophy through the PI3K-autophagy and endoplasmic reticulum stress-autophagy pathways (59). Although the position of GCRP in cardiac hypertrophy is now well-recognized, the roles and mechanisms of GCRP family members in HCM remain poorly understood. Therefore, we need to focus on and study these genes and their related GPCR pathways in the next step. With regard to the downregulated network, 10 hub genes were filtered out, which were enriched in positive regulation of tumor necrosis factor production and nucleotide-binding oligomerization domain (NOD)-like receptor signaling pathway. A clinical study found that, after non-surgical septal reduction therapy for patients with hypertrophic obstructive cardiomyopathy, the expression of tumor necrosis factor-α was decreased and cardiac hypertrophy was regressed (60).

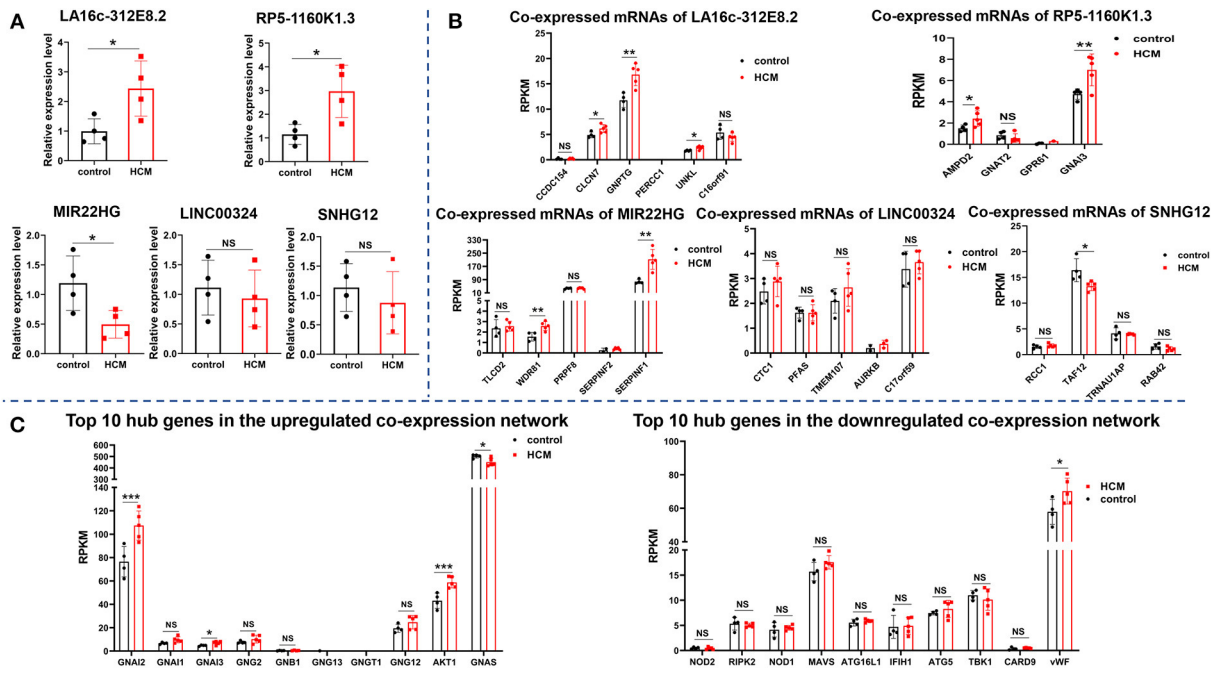

FIGURE 8
Verification of crucial lncRNAs and mRNAs in HCM patients. **(A)** The expression of five crucial lncRNAs in plasma of HCM patients and the controls were measured by real-time qPCR. **(B)** The expression level of mRNAs (co-expressed with five crucial lncRNAs) in the verification dataset GSE89714. **(C)** The expression level of the top 10 hub genes of upregulated and downregulated PPI network in the verification dataset GSE89714. ***$p < 0.001$.

Knockout of tumor necrosis factor-related protein reduced myocardial hypertrophy in mice (61). NOD leucine-rich repeat (LRR) protein family plays an important role in regulating the intracellular recognition of bacterial components by immune cells and is crucial for the maintenance of immune homeostasis (62). Jing Zong et al. found that NOD2 expression was upregulated in cardiomyocytes of aortic banding hypertrophic mice. NOD2 deficiency promoted cardiac hypertrophy and fibrosis by activating TLR4 and the MAPKs, NF-kB, and TGF-β/Smad pathways (63). Furthermore, the data showed that NOD-like receptor NLRP3 expression was downregulated in the aortic banding hypertrophic mice. NLRP3 deficiency accelerated cardiac hypertrophy, fibrosis, and inflammation responses with deteriorating cardiac dysfunction (64). Although the role of NOD in HCM is still controversial at present, its status and importance for cardiac hypertrophy have been widely recognized. Therefore, it is crucial to explore and elucidate the mechanism of these hub genes in HCM.

This study has certain limitations. Although both datasets contain several hundred differentially expressed lncRNAs and mRNAs, only a few of them overlapped. It is likely that the dominant mutant genotypes of the patients with HCM in the GSE130036 dataset were MYH7 and MYBPC3 mutations, while the dominant mutant genotypes of the patients with HCM in the GSE68316 dataset were not clear. It is well-known that numerous mutant genotypes lead to HCM, but pathophysiological processes caused by each genotype are not the same, resulting in different gene expressions in patients with different genotypes (65, 66). Notably, inconsistent sample size, sequencing methods, and baseline data of patients between the two datasets may also account for a few of the co-differentially expressed genes. In addition, due to the difficulties in obtaining cardiac tissues from patients with HCM, we did not validate the results in cardiac tissues. Finally, we could obtain limited plasma samples from patients with HCM for validation, and this may be the reason for the inconsistent results of lncRNA LINC00324 and SNHG12 between GEO analysis and our real-time qPCR data. In the future, more samples are needed to verify the abovementioned results.

Conclusion

The present study aimed to analyze and elucidate the differentially expressed lncRNAs and mRNAs by integrative biological analysis of lncRNA-mRNA co-expression networks in patients with HCM. Three key lncRNAs (LA16c-312E8.2, RP5-1160K1.3, and MIR22HG) identified in patients with HCM may

serve as biomarkers and intervention targets for HCM. These findings will provide a new thought in understanding the cause and mechanism of HCM and discovering new biomarkers or therapeutic targets for clinic treatment.

Data availability statement

The datasets presented in this study can be found in online repositories. The names of the repository/repositories and accession number(s) can be found in the article/Supplementary material.

Ethics statement

This study was reviewed and approved by the Committee at Xiangya Hospital of Central South University (IRB No. 202113548).

Author contributions

JC conducted the statistical analysis, carried out the experiments, and drafted the article. LY contributed to reviewing, editing, and revising the article. All authors contributed to manuscript revision, read, and approved the submitted version.

Funding

The work was supported by grants from Xiangya Hospital, Wei Ming Clinical, and Rehabilitation Research Fund of Peking University (No. xywmII09).

Conflict of interest

The authors declare that the research was conducted in the absence of any commercial or financial relationships that could be construed as a potential conflict of interest.

Publisher's note

All claims expressed in this article are solely those of the authors and do not necessarily represent those of their affiliated organizations, or those of the publisher, the editors and the reviewers. Any product that may be evaluated in this article, or claim that may be made by its manufacturer, is not guaranteed or endorsed by the publisher.

Supplementary material

The Supplementary Material for this article can be found online at: https://www.frontiersin.org/articles/10.3389/fcvm.2022.946229/full#supplementary-material

References

1. Veselka J, Anavekar NS, Charron P. Hypertrophic obstructive cardiomyopathy. *Lancet.* (2017) 389:1253–67. doi: 10.1016/S0140-6736(16)31321-6

2. Maron BJ, Gardin JM, Flack JM, Gidding SS, Kurosaki TT, Bild DE. Prevalence of hypertrophic cardiomyopathy in a general population of young adults. Echocardiographic analysis of 4111 subjects in the CARDIA Study. Coronary artery risk development in (Young) adults. *Circulation.* (1995) 92:785–9. doi: 10.1161/01.CIR.92.4.785

3. Zou Y, Song L, Wang Z, Ma A, Liu T, Gu H, et al. Prevalence of idiopathic hypertrophic cardiomyopathy in China: a population-based echocardiographic analysis of 8,080 adults. *Am J Med.* (2004) 116:14–8. doi: 10.1016/j.amjmed.2003.05.009

4. Geske JB, Ommen SR, Gersh BJ. Hypertrophic cardiomyopathy: Clinical Update. *JACC Heart Fail.* (2018) 6:364–75. doi: 10.1016/j.jchf.2018.02.010

5. Cirino AL, Harris S, Lakdawala NK, Michels M, Olivotto I, Day SM, et al. Role of genetic testing in inherited cardiovascular disease: a review. *Jama Cardiol.* (2017) 2:1153–60. doi: 10.1001/jamacardio.2017.2352

6. Burke MA, Cook SA, Seidman JG, Seidman CE. Clinical and mechanistic insights into the genetics of cardiomyopathy. *J Am Coll Cardiol.* (2016) 68:2871–86. doi: 10.1016/j.jacc.2016.08.079

7. Fourey D, Care M, Siminovitch KA, Weissler-Snir A, Hindieh W, Chan RH, et al. Prevalence and clinical implication of double mutations in hypertrophic cardiomyopathy: revisiting the gene-dose effect. *Circ Cardiovasc Genet.* (2017) 10:1685. doi: 10.1161/CIRCGENETICS.116.001685

8. Biagini E, Olivotto I, Iascone M, Parodi MI, Girolami F, Frisso G, et al. Significance of sarcomere gene mutations analysis in the end-stage phase of hypertrophic cardiomyopathy. *Am J Cardiol.* (2014) 114:769–76. doi: 10.1016/j.amjcard.2014.05.065

9. An integrated encyclopedia of DNA elements in the human genome. *Nature.* (2012) 489:57–74. doi: 10.1038/nature11247

10. Hoffman MM, Ernst J, Wilder SP, Kundaje A, Harris RS, Libbrecht M, et al. Integrative annotation of chromatin elements from ENCODE data. *Nucleic Acids Res.* (2013) 41:827–41. doi: 10.1093/nar/gks1284

11. Hardison RC. Genome-wide epigenetic data facilitate understanding of disease susceptibility association studies. *J Biol Chem.* (2012) 287:30932–40. doi: 10.1074/jbc.R112.352427

12. Barwari T, Joshi A, Mayr M. MicroRNAs in cardiovascular disease. *J Am Coll Cardiol.* (2016) 68:2577–84. doi: 10.1016/j.jacc.2016.09.945

13. Lu D, Thum T. RNA-based diagnostic and therapeutic strategies for cardiovascular disease. *Nat Rev Cardiol.* (2019) 16:661–74. doi: 10.1038/s41569-019-0218-x

14. Philippen LE, Dirkx E, Wit JB, Burggraaf K, de Windt LJ Da CMP. Antisense MicroRNA therapeutics in cardiovascular disease: quo vadis? *Mol Ther.* (2015) 23:1810–8. doi: 10.1038/mt.2015.133

15. Zhang Y, Jiao L, Sun L, Li Y, Gao Y, Xu C, et al. LncRNA ZFAS1 as a SERCA2a inhibitor to cause intracellular Ca(2+) overload and contractile dysfunction in a mouse model of myocardial infarction. *Circ Res.* (2018) 122:1354–68. doi: 10.1161/CIRCRESAHA.117.312117

16. Liang H, Su X, Wu Q, Shan H, Lv L, Yu T, et al. LncRNA 2810403D21Rik/Mirf promotes ischemic myocardial injury by regulating autophagy through targeting Mir26a. *Autophagy.* (2020) 16:1077–91. doi: 10.1080/15548627.2019.1659610

17. Wang LY, Shen H, Yang Q, Min J, Wang Q, Xi W, et al. LncRNA-LINC00472 contributes to the pathogenesis of atrial fibrillation (Af) by reducing expression of JP2 and RyR2 via miR-24. *Biomed Pharmacother.* (2019) 120:109364. doi: 10.1016/j.biopha.2019.109364

18. Wang L, Wang J, Li G, Xiao J. Non-coding RNAs in physiological cardiac hypertrophy. *Adv Exp Med Biol.* (2020) 1229:149–61. doi: 10.1007/978-981-15-1671-9_8

19. Hoepfner J, Leonardy J, Lu D, Schmidt K, Hunkler HJ, Biss S, et al. The long non-coding RNA NRON promotes the development of cardiac hypertrophy in the murine heart. *Mol Ther.* (2022) 30:1265–74. doi: 10.1016/j.ymthe.2021.11.018

20. Jiang F, Zhou X, Huang J. Long non-coding RNA-ROR mediates the reprogramming in cardiac hypertrophy. *PLoS ONE.* (2016) 11:e152767. doi: 10.1371/journal.pone.0152767

21. Elliott PM, Anastasakis A, Borger MA, Borggrefe M, Cecchi F, Charron P, et al. 2014 ESC Guidelines on diagnosis and management of hypertrophic cardiomyopathy: the task force for the diagnosis and management of hypertrophic cardiomyopathy of the european society of cardiology (ESC). *Eur Heart J.* (2014) 35:2733–79. doi: 10.1093/eurheartj/ehu284

22. Viereck J, Thum T. Circulating noncoding rnas as biomarkers of cardiovascular disease and injury. *Circ Res.* (2017) 120:381–99. doi: 10.1161/CIRCRESAHA.116.308434

23. Cecconi M, Parodi MI, Formisano F, Spirito P, Autore C, Musumeci MB, et al. Targeted next-generation sequencing helps to decipher the genetic and phenotypic heterogeneity of hypertrophic cardiomyopathy. *Int J Mol Med.* (2016) 38:1111–24. doi: 10.3892/ijmm.2016.2732

24. Ashley EA, Reuter CM, Wheeler MT. Genome sequencing in hypertrophic cardiomyopathy. *J Am Coll Cardiol.* (2018) 72:430–3. doi: 10.1016/j.jacc.2018.05.029

25. Chen R, Ge T, Jiang W, Huo J, Chang Q, Geng J, et al. Identification of biomarkers correlated with hypertrophic cardiomyopathy with co-expression analysis. *J Cell Physiol.* (2019) 234:21999–2008. doi: 10.1002/jcp.28762

26. Walsh R, Offerhaus JA, Tadros R, Bezzina CR. Minor hypertrophic cardiomyopathy genes, major insights into the genetics of cardiomyopathies. *Nat Rev Cardiol.* (2022) 19:151–67. doi: 10.1038/s41569-021-00608-2

27. Yuan Y, Wang J, Chen Q, Wu Q, Deng W, Zhou H, et al. Long non-coding RNA cytoskeleton regulator RNA (CYTOR) modulates pathological cardiac hypertrophy through miR-155-mediated IKKi signaling. *Biochim Biophys Acta Mol Basis Dis.* (2019) 1865:1421–7. doi: 10.1016/j.bbadis.2019.02.014

28. Gao J, Collyer J, Wang M, Sun F, Xu F. Genetic dissection of hypertrophic cardiomyopathy with myocardial RNA-Seq. *Int J Mol Sci.* (2020) 21:3040. doi: 10.3390/ijms21093040

29. Lee JH, Gao C, Peng G, Greer C, Ren S, Wang Y, et al. Analysis of transcriptome complexity through RNA sequencing in normal and failing murine hearts. *Circ Res.* (2011) 109:1332–41. doi: 10.1161/CIRCRESAHA.111.249433

30. Wang K, Long B, Zhou LY, Liu F, Zhou QY, Liu CY, et al. CARL lncRNA inhibits anoxia-induced mitochondrial fission and apoptosis in cardiomyocytes by impairing miR-539-dependent PHB2 downregulation. *Nat Commun.* (2014) 5:3596. doi: 10.1038/ncomms4596

31. Simion V, Zhou H, Haemmig S, Pierce JB, Mendes S, Tesmenitsky Y, et al. A macrophage-specific lncRNA regulates apoptosis and atherosclerosis by tethering HuR in the nucleus. *Nat Commun.* (2020) 11:6135. doi: 10.1038/s41467-020-19664-2

32. Wu R, Hu W, Chen H, Wang Y, Li Q, Xiao C, et al. A Novel human long non-coding RNA SCDAL promotes angiogenesis through SNF5-mediated GDF6 expression. *Adv Sci.* (2021) 8:e2004629. doi: 10.1002/advs.202004629

33. Viereck J, Buhrke A, Foinquinos A, Chatterjee S, Kleeberger JA, Xiao K, et al. Targeting muscle-enriched long non-coding RNA H19 reverses pathological cardiac hypertrophy. *Eur Heart J.* (2020) 41:3462–74. doi: 10.1093/eurheartj/ehaa519

34. Xiao L, Gu Y, Sun Y, Chen J, Wang X, Zhang Y, et al. The long noncoding RNA XIST regulates cardiac hypertrophy by targeting miR-101. *J Cell Physiol.* (2019) 234:13680–92. doi: 10.1002/jcp.28047

35. Rossignoli F, Spano C, Grisendi G, Foppiani EM, Golinelli G, Mastrolia I, et al. MSC-delivered soluble TRAIL and paclitaxel as novel combinatory treatment for pancreatic adenocarcinoma. *Theranostics.* (2019) 9:436–48. doi: 10.7150/thno.27576

36. Yang F, Lyu S, Dong S, Liu Y, Zhang X, Wang O. Expression profile analysis of long noncoding RNA in HER-2-enriched subtype breast cancer by next-generation sequencing and bioinformatics. *Onco Targets Ther.* (2016) 9:761–72. doi: 10.2147/OTT.S97664

37. Liao W, Zhao R, Lu L, Zhang R, Zou J, Xu T, et al. Overexpression of a novel osteopetrosis-related gene CCDC154 suppresses cell proliferation by inducing G2/M arrest. *Cell Cycle.* (2012) 11:3270–9. doi: 10.4161/cc.21642

38. Liu X, Yagi H, Saeed S, Bais AS, Gabriel GC, Chen Z, et al. The complex genetics of hypoplastic left heart syndrome. *Nat Genet.* (2017) 49:1152–9. doi: 10.1038/ng.3870

39. Peng H, He HB, Wen T, A. Novel Variant in CLCN7 Regulates the coupling of angiogenesis and osteogenesis. *Front Cell Dev Biol.* (2020) 8:599826. doi: 10.3389/fcell.2020.599826

40. Di Lorenzo G, Westermann LM, Yorgan TA, Sturznickel J, Ludwig NF, Ammer LS, et al. Pathogenic variants in GNPTAB and GNPTG encoding distinct subunits of GlcNAc-1-phosphotransferase differentially impact bone resorption in patients with mucolipidosis type II and III. *GENET MED.* (2021) 23:2369–77. doi: 10.1038/s41436-021-01285-9

41. Westermann LM, Fleischhauer L, Vogel J, Jenei-Lanzl Z, Ludwig NF, Schau L, et al. Imbalanced cellular metabolism compromises cartilage homeostasis and joint function in a mouse model of mucolipidosis type III gamma. *Dis Model Mech.* (2020) 13:6425. doi: 10.1242/dmm.046425

42. Oz-Levi D, Olender T, Bar-Joseph I, Zhu Y, Marek-Yagel D, Barozzi I, et al. Noncoding deletions reveal a gene that is critical for intestinal function. *Nature.* (2019) 571:107–11. doi: 10.1038/s41586-019-1312-2

43. Yang LY Li L, Jiang H, Shen Y, Plunkett W. Expression of ERCC1 antisense RNA abrogates gemicitabine-mediated cytotoxic synergism with cisplatin in human colon tumor cells defective in mismatch repair but proficient in nucleotide excision repair. *Clin Cancer Res.* (2000) 6:773–81.

44. Goulet O, Pigneur B, Charbit-Henrion F. Congenital enteropathies involving defects in enterocyte structure or differentiation. *Best Pract Res Clin Gastroenterol.* (2022) 56–57:101784. doi: 10.1016/j.bpg.2021.101784

45. Lores P, Visvikis O, Luna R, Lemichez E, Gacon G. The SWI/SNF protein BAF60b is ubiquitinated through a signalling process involving Rac GTPase and the RING finger protein Unkempt. *FEBS J.* (2010) 277:1453–64. doi: 10.1111/j.1742-4658.2010.07575.x

46. Carboni E, Sestito S, Lucente M, Morrone A, Zampini L, Chimenz R, et al. Dilated cardiomyopathy in mucolipidosis type 2. *J Biol Regul Homeost Agents.* (2020) 34(4 Suppl. 2):71–7. Available online at: https://www.biolifesas.org/EN/Y2020/V34/I4(S2)/71

47. Zhang L, Li C, Su X. Emerging impact of the long noncoding RNA MIR22HG on proliferation and apoptosis in multiple human cancers. *J Exp Clin Cancer Res.* (2020) 39:271. doi: 10.1186/s13046-020-01784-8

48. Xu J, Shao T, Song M, Xie Y, Zhou J, Yin J, et al. MIR22HG acts as a tumor suppressor via TGFbeta/SMAD signaling and facilitates immunotherapy in colorectal cancer. *Mol Cancer.* (2020) 19:51. doi: 10.1186/s12943-020-01174-w

49. Yan X, Hou J. miR-22 host gene enhances nuclear factor-kappa B activation to aggravate hypoxia-induced injury in AC16 cardiomyocytes. *Cell Transplant.* (2021) 30:2139983027. doi: 10.1177/0963689721990323

50. Voellenkle C, Garcia-Manteiga JM, Pedrotti S, Perfetti A, De Toma I, Da SD, et al. Implication of Long noncoding RNAs in the endothelial cell response to hypoxia revealed by RNA-sequencing. *Sci Rep.* (2016) 6:24141. doi: 10.1038/srep24141

51. Nakata I, Yamashiro K, Yamada R, Gotoh N, Nakanishi H, Hayashi H, et al. Genetic variants in pigment epithelium-derived factor influence response of polypoidal choroidal vasculopathy to photodynamic therapy. *Ophthalmology.* (2011) 118:1408–15. doi: 10.1016/j.ophtha.2010.12.011

52. Verbree-Willemsen L, Zhang YN, Ibrahim I, Ooi S, Wang JW, Mazlan MI, et al. Extracellular vesicle Cystatin C and CD14 are associated with both renal dysfunction and heart failure. *ESC Heart Fail.* (2020) 7:2240–9. doi: 10.1002/ehf2.12699

53. Harper AR, Mayosi BM, Rodriguez A, Rahman T, Hall D, Mamasoula C, et al. Common variation neighbouring micro-RNA 22 is associated with increased left ventricular mass. *PLoS One.* (2013) 8:e55061. doi: 10.1371/journal.pone.0055061

54. Xu G, Li T, Chen J, Li C, Zhao H, Yao C, et al. Autosomal dominant retinitis pigmentosa-associated gene PRPF8 is essential for hypoxia-induced mitophagy through regulating ULK1 mRNA splicing. *Autophagy.* (2018) 14:1818–30. doi: 10.1080/15548627.2018.1501251

55. Tilley DG. G protein-dependent and G protein-independent signaling pathways and their impact on cardiac function. Circ Res. (2011) 109:217–30. doi: 10.1161/CIRCRESAHA.110.231225

56. Murga C, Arcones AC, Cruces-Sande M, Briones AM, Salaices M, Mayor FJ, et al. Protein-coupled receptor Kinase 2 (GRK2) as a potential therapeutic target in cardiovascular and metabolic

diseases. *Front Pharmacol.* (2019) 10:112. doi: 10.3389/fphar.2019.00112

57. Belmonte SL, Blaxall BC, G. protein coupled receptor kinases as therapeutic targets in cardiovascular disease. *CIRC RES.* (2011) 109:309–19. doi: 10.1161/CIRCRESAHA.110.231233

58. Liu X, Lin L, Li Q, Ni Y, Zhang C, Qin S, et al. ERK1/2 communicates GPCR and EGFR signaling pathways to promote CTGF-mediated hypertrophic cardiomyopathy upon Ang-II stimulation. *BMC Mol Cell Biol.* (2019) 20:14. doi: 10.1186/s12860-019-0202-7

59. Xie F, Wu D, Huang SF, Cao JG Li HN, He L, et al. The endoplasmic reticulum stress-autophagy pathway is involved in apelin-13-induced cardiomyocyte hypertrophy in vitro. *Acta Pharmacol Sin.* (2017) 38:1589–600. doi: 10.1038/aps.2017.97

60. Nagueh SF, Stetson SJ, Lakkis NM, Killip D, Perez-Verdia A, Entman ML, et al. Decreased expression of tumor necrosis factor-alpha and regression of hypertrophy after nonsurgical septal reduction therapy for patients with hypertrophic obstructive cardiomyopathy. *Circulation.* (2001) 103:1844–50. doi: 10.1161/01.CIR.103.14.1844

61. Ma ZG, Yuan YP, Zhang X, Xu SC, Kong CY, Song P, et al. C1q-tumour necrosis factor-related protein-3 exacerbates cardiac hypertrophy in mice. *Cardiovasc Res.* (2019) 115:1067–77. doi: 10.1093/cvr/cvy279

62. Philpott DJ, Sorbara MT, Robertson SJ, Croitoru K, Girardin SE. NOD proteins: regulators of inflammation in health and disease. *Nat Rev Immunol.* (2014) 14:9–23. doi: 10.1038/nri3565

63. Zong J, Salim M, Zhou H, Bian ZY Dai J, Yuan Y, et al. NOD2 deletion promotes cardiac hypertrophy and fibrosis induced by pressure overload. *Lab Invest.* (2013) 93:1128–36. doi: 10.1038/labinvest.2013.99

64. Li F, Zhang H, Yang L, Yong H, Qin Q, Tan M, et al. NLRP3 deficiency accelerates pressure overload-induced cardiac remodeling via increased TLR4 expression. *J Mol Med (Berl).* (2018) 96:1189–202. doi: 10.1007/s00109-018-1691-0

65. Ho CY, Day SM, Ashley EA, Michels M, Pereira AC, Jacoby D, et al. Genotype and lifetime burden of disease in hypertrophic cardiomyopathy: insights from the sarcomeric human cardiomyopathy registry (SHaRe). *Circulation.* (2018) 138:1387–98. doi: 10.1161/CIRCULATIONAHA.117.033200

66. Cambronero F, Marin F, Roldan V, Hernandez-Romero D, Valdes M, Lip GY. Biomarkers of pathophysiology in hypertrophic cardiomyopathy: implications for clinical management and prognosis. *Eur Heart J.* (2009) 30:139–51. doi: 10.1093/eurheartj/ehn538

Glossary

ADD3, Adducin 3; ALDH6A1, Aldehyde Dehydrogenase 6 Family Member A1; ALG14, ALG14 UDP-N-Acetylglucosaminyltransferase Subunit; AMPD2, Adenosine Monophosphate Deaminase 2; ANP, Atrial natriuretic peptide; ATG5, Autophagy Related 5; ATG16L1, Autophagy Related 16-Like 1; AURKB, Aurora Kinase B; B3GALT5-AS1, B3GALT5 Antisense RNA 1; BNP, Brain Natriuretic Peptide; BP, Biological processes; BTN3A2, Butyrophilin Subfamily 3 Member A2; BTNL9, Butyrophilin Like 9; C16orf91, Chromosome 16 Open Reading Frame 91; C17orf108, LYR Motif Containing 9, LYRM9; CA1, Carbonic Anhydrase 1; CARD9, Caspase Recruitment Domain Family Member 9; CCDC7, Coiled-Coil Domain Containing 7; CCDC154, Coiled-Coil Domain Containing 154; CLCN7, Chloride Voltage-Gated Channel 7; COMMD6, COMM Domain Containing 6; CORIN, Corin, Serine Peptidase; CTC1, CST telomere replication complex component 1; ECHDC1, Ethylmalonyl-CoA Decarboxylase 1; ELK4, ETS Transcription Factor ELK4; ENCODE, Encyclopedia of DNA Elements; EPB42, Erythrocyte Membrane Protein Band 4.2; FAM167A-AS1, FAM167A Antisense RNA 1; FURIN, Furin, Paired Basic Amino Acid Cleaving Enzyme; GEO, Gene Expression Omnibus; GO, Gene Ontology; GNAI1, G Protein Subunit Alpha I1; GNAI2, G Protein Subunit Alpha I2; GNAI3, G Protein Subunit Alpha I3; GNAT2, G Protein Subunit Alpha Transducin 2; GNB1, G Protein Subunit Beta 1; GNG2, G Protein Subunit Gamma 2; GNG12, G Protein Subunit Gamma 12; GNG13, G Protein Subunit Gamma 13; GNGT1, G Protein Subunit Gamma Transducin 1; GNAS, GNAS Complex Locus; GNPTG, N-Acetylglucosamine-1-Phosphate Transferase Subunit Gamma; HCM, Hypertrophic cardiomyopathy; HBG1, Hemoglobin Subunit Gamma 1; HBM, Hemoglobin Subunit Mu; IFIH1, Interferon Induced With Helicase C Domain 1; KEGG, Kyoto Encyclopedia of Genes and Genomes; KRT1, Keratin 1; KCNIP2, Potassium Voltage-Gated Channel Interacting Protein 2; LncRNAs, Long noncoding RNAs; LRR, leucine rich repeat; MF, molecular function; MAVS, Mitochondrial antiviral-signaling protein; MIR22HG, MIR22 Host Gene; MYBPC3, Myosin Binding Protein C3; MYH7, Myosin Heavy Chain 7; MYH14, Myosin Heavy Chain 14; ncRNA, noncoding RNA; NOD, Nucleotide-Binding Oligomerization Domain; NOD1, Nucleotide-Binding Oligomerization Domain Containing Protein 1; NOD2, Nucleotide-Binding Oligomerization Domain Containing 2; NDUFS2, NADH: Ubiquinone Oxidoreductase Core Subunit S2; P2RY14, Phosphodiesterase 4D Interacting Protein; PDE4DIP, Phosphodiesterase 4D Interacting Protein; PERCC1, Proline and Glutamate Rich with Coiled Coil 1; PFAS, Phosphoribosylformylglycinamidine synthase; PFDN5, Prefoldin Subunit 5; PLCH1-AS2, PLCH1 Antisense RNA 2; PPI, Protein–protein interaction; PPP1R35-AS1, PPP1R35 Antisense RNA 1; PCBP2, Poly(RC) Binding Protein 2; PRPF8, pre-mRNA processing factor 8; RCC1, Regulator of Chromosome Condensation 1; RIPK2, Receptor-Interacting Serine/Threonine Kinase 2; RPL26, Ribosomal Protein L26; RPS24, Ribosomal Protein S24; SELENBP1, Selenium Binding Protein 1; SERPINF1, Serpin Family F Member 2; SERPINF2, Serpin Family F Member 2; SLC4A1, Solute Carrier Family 4 Member 1; SELENOI, Selenoprotein I; STXBP5, Syntaxin Binding Protein 5; TAF12, TATA-Box Binding Protein Associated Factor 12; TBK1, TANK Binding Kinase 1; TECRL, Trans-2,3-Enoyl-CoA Reductase Like; TLCD2, TLC Domain Containing 2; TMEM107, Transmembrane Protein 107; TRNAU1AP, TRNA Selenocysteine 1 Associated Protein 1; TSPEAR-AS1, TSPEAR Antisense RNA 1; TSPEAR-AS2, TSPEAR Antisense RNA 2; TNS1, Tensin 1; TROAP, Trophinin Associated Protein; UNKL, Unk Like Zinc Finger; UQCRH, Ubiquinol-Cytochrome C Reductase Hinge Protein; VWF, von Willebrand factor; WDR81, WD Repeat Domain 81; XIST, X Inactive Specific Transcript; ZNF16, Zinc Finger Protein 16.

frontiers | Frontiers in Cardiovascular Medicine

TYPE Mini Review
PUBLISHED 18 October 2022
DOI 10.3389/fcvm.2022.1051564

OPEN ACCESS

EDITED BY
Michael T. Chin,
Tufts Medical Center, United States

REVIEWED BY
Daniel Yang,
University of Washington,
United States

*CORRESPONDENCE
Yuichi J. Shimada
ys3053@cumc.columbia.edu

SPECIALTY SECTION
This article was submitted to Cardiovascular Genetics and Systems Medicine, a section of the journal Frontiers in Cardiovascular Medicine

RECEIVED 23 September 2022
ACCEPTED 06 October 2022
PUBLISHED 18 October 2022

CITATION
Sewanan LR and Shimada YJ (2022) Prospects for remodeling the hypertrophic heart with myosin modulators.
Front. Cardiovasc. Med. 9:1051564.
doi: 10.3389/fcvm.2022.1051564

Prospects for remodeling the hypertrophic heart with myosin modulators

Lorenzo R. Sewanan[1] and Yuichi J. Shimada[2]*

[1]Department of Medicine, Columbia University Irving Medical Center, New York, NY, United States, [2]Division of Cardiology, Department of Medicine, Columbia University Irving Medical Center, New York, NY, United States

Hypertrophic cardiomyopathy (HCM) is a complex but relatively common genetic disease that usually arises from pathogenic variants that disrupt sarcomere function and lead to variable structural, hypertrophic, and fibrotic remodeling of the heart which result in substantial adverse clinical outcomes including arrhythmias, heart failure, and sudden cardiac death. HCM has had few effective treatments with the potential to ameliorate disease progression until the recent advent of inhibitory myosin modulators like mavacamten. Preclinical investigations and clinical trials utilizing this treatment targeted to this specific pathophysiological mechanism of sarcomere hypercontractility in HCM have confirmed that myosin modulators can alter disease expression and attenuate hypertrophic remodeling. Here, we summarize the state of hypertrophic remodeling and consider the arguments for and against salutary HCM disease modification using targeted myosin modulators. Further, we consider critical unanswered questions for future investigative and therapeutic avenues in HCM disease modification. We are at the precipice of a new era in understanding and treating HCM, with the potential to target agents toward modifying disease expression and natural history of this most common inherited disease of the heart.

KEYWORDS

hypertrophic cardiomyopathy, remodeling, myosin modulator, mavacamten, hypertrophy, fibrosis, reverse remodeling

Introduction

Hypertrophic cardiomyopathy (HCM) is a structural heart disease historically characterized by left ventricular outflow tract obstruction (LVOTO) and cardiomegaly with severe eccentric hypertrophy (1). At the tissue level, HCM often features cardiomyocyte hypertrophy, myocyte disarray, myofibrillar disarray, interstitial fibrosis, which can result sudden cardiac death, early-onset heart failure with preserved ejection fraction, and end-stage heart disease. Since its discovery, it has come to be recognized as the most common inherited disease of the myocardium which typically results from mutations to the molecular machinery in the cardiac sarcomere (2). Many mechanisms have been proposed that most frequently link mutations to aberrant contractile function and regulation at the level of the sarcomere (3–7).

Conventional agents such as anti-arrhythmics and neurohormonal blocking agents to treat HCM have provided only symptomatic relief though have not modified disease progression. In particular, no therapy has yet been shown to mitigate adverse structural remodeling like hypertrophy and fibrosis. The recently discovered cardiac myosin specific modulator, mavacamten, has been shown in the largest prospective phase 3 trial in HCM to be overall effective in reducing LVOTO gradient and improving objective exercise tolerance [i.e., peak oxygen consumption (pVO_2)] (8). The efficacy of myosin modulations agents in HCM further raises questions about the potential for reversal or attenuation of adverse structural changes in the hypertrophic heart.

Pathophysiology and clinical features of HCM

HCM is known to have significant variability in disease course and adverse outcomes in both of its forms, obstructive (oHCM) and non-obstructive (nHCM). In the largest HCM registry to date [SHaRe (Sarcomeric Human Cardiomyopathy Registry)], mortality of younger patients with HCM (age 20–29) was at least 4-fold higher than the general population and 3-fold higher in older patients (age 50–69), indicating that HCM even with contemporary management has death that remains unmitigated and not yet completely preventable (9). Electrical arrhythmias including 20% with atrial fibrillation and 6% with ventricular arrhythmias were quite common as well, with implantable cardioverter-defibrillator (ICD) present in 21% of patients with HCM. Strikingly, 22% of patients developed New York Heart Association (NYHA) III/IV heart failure (HF), especially if diagnosed before the age of 40, and more than 80% of those with HF had left ventricular ejection fraction (LVEF) $>$ 55%. Indeed, HF with preserved ejection fraction and atrial fibrillation were the most common outcomes in HCM patients in this large cohort. A prospective study of 225 patients with nHCM suggested that a 5-year mortality was similar to age-matched and sex-matched general US population (10). However, these patients showed at least a 10% risk of developing NYHA III/IV HF over a median follow-up of 6.5 years. Similar to SHaRe, about 3% of patients developed end-stage heart disease requiring transplantation, even though none had oHCM. Indeed, the progression to left ventricular systolic dysfunction (LVSD) with LVEF $<$ 50% has been documented to occur in 8% of patients with 11% of these patients progressing to cardiac transplant and 2% progressing to left ventricular assist device (LVAD) implantation, a total need for advanced therapy of 13% compared to $<$1% of the patients without LVSD (11). The progression of nHCM in HF and arrhythmias does demonstrate overall that HCM structural remodeling of the ventricle and of the atria even without LVOTO remains a significant issue driving disease-related morbidities. Similarly, an HCM imaging registry demonstrating that profound cardiac structural changes with hypertrophy and fibrosis [50% had at least some late gadolinium enhancement (LGE)] in even the milder forms of HCM suggests a need to focus on remodeling as a significant feature driving outcomes of disease from an early stage (12).

The underlying pathophysiology driving HCM cardiac remodeling is complex but must be grounded in an initial understanding of the proximal etiology of HCM. At this time, the mechanisms driving non-sarcomeric HCM remain poorly elucidated, even though sarcomeric mutations than can be linked in a Mendelian fashion to about 40–50% of HCM. However, recent work notes that some HCM may be complex polygenic phenotype with non-sarcomeric disease modifying genes as well as modifiable risk factors such as diastolic blood pressure (13). Lastly, syndromic disease including HCM phenocopies are not at all fully understood but may differ profoundly in their mechanisms (14). Several important observations could be made from a wealth of studies that have accumulated over the last 30 years using biophysical, biochemical, and animal models of disease (15), specifically that HCM-linked sarcomeric mutations tend to increase myofilament calcium sensitivity, increase the crossbridge duty cycle, and increase energy cost of tension generation, leading to a hypercontractile state in cardiac muscle (3–7, 16–36).

Recent translational investigations, for instance, using proteomics and transcriptomics have started to reveal pathways upregulated that could account for hypertrophy and fibrosis in HCM, including ERK, MAPK, AMPK, TGF-β, amongst others (37). Such work further is corroborated by some human iPSC and animal models of disease that show direct linkages between molecular changes caused by genetic changes to the sarcomere and the upregulation of pathways leading to hypertrophy and fibrosis (38–40). These linkages are not fully explained at this time, but they do not necessarily correspond to a typical paradigm of afterload causing hypertrophy and fibrosis as in hypertensive heart disease and valvular heart disease (41, 42). The mechanobiology and mechanisms seem to be somewhat distinctive.

Myocardial remodeling in HCM

Remodeling in HCM is primarily noted as thickened heart walls which occurs spontaneously and presumably progressively over the life of an individual to the time they present clinically (43). Studies of genotype positive, phenotype negative individuals have demonstrated that the hypertrophy can be subclinically present in many adolescents. A study of 39 children with HCM showed that 22 patients progressed with up to 12 mm wall thickening by 19 years of age (44). However, a similar study of 65 adult patients with HCM demonstrated that continued hypertrophic remodeling rarely occurred in adults (45). Some reverse remodeling of cardiac thickening and even thinning

without LVSD does spontaneously occur in some patients though no evidence shows this to have negative clinical impact (43). However, patients can sometimes develop progressive adverse remodeling with LVSD and extensive fibrosis, essentially burnt out heart disease, with poor outcomes (46). Therapies in patients with established HCM therefore would need to address structural remodeling, though it remains to be determined whether reversal of hypertrophy and fibrosis would be more beneficial than preventing hypertrophy and fibrosis at an initial state in the disease course.

Conventional medical therapies for HCM have had limited efficacy in disease modification though have proven useful in particular scenarios with oHCM in reduction of LVOTO and improvement of overall heart function (47). Selective β-blockers are commonly used as they are known to reduce LVOTO gradient with exercise provocation (48). Calcium channel blockers like diltiazem and the sodium channel blocker disopyramide are used for their negative inotrope effect by overall reduction of intracellular calcium, which leads to suppression of sarcomeric activity. Overall, these agents can be effective in reducing LVOTO, controlling symptoms, and even exercise tolerance, though have limited effect structurally. For instance, early administration of diltiazem was not found to be effective in patients with preclinical HCM in preventing progression and development of clinical HCM though only small studies have been conducted at this time. Several agents have been investigated for their potential effect on remodeling with mixed results including perhexiline and trimetazidine (49), ranolazine and eleclazine (50), losartan (51, 52), and spironolactone (53). It appears that many preclinical studies that suggested an effect on HCM through indirect pathways have not panned out in their *in vivo* application, potentially due to a combination of inability of animal models to capture human pathophysiology, differences in HCM pathophysiology across patients and mutations, difficulty in assessing when patients should be treated at an early enough stage to reverse disease, and perhaps a lack of targeting the proximal mechanism of HCM itself.

With regards to evidence for treatment during an early stage of disease, the VANISH trial investigated whether using valsartan for preclinical HCM would have a beneficial effect and was designed on the premise that animal models demonstrate that use of ARBs can inhibit TGF-β dependent remodeling in HCM hearts if treated prior to establishment of disease. With this specifically in mind, the trial enrolled 178 participants with a mean age of 23 and an initial LV wall thickness of 16 mm into a randomized phase 2 clinical trial in which they received either valsartan or placebo for 2 years (54). The endpoint of the study evaluated a complex nine-measure composite endpoint of z score-normalized cardiac magnetic resonance (CMR), echocardiographic, and biomarkers relating to diastolic function, hypertrophy, and myocardial injury. The trial met its endpoint showing that the patients who received valsartan showed less progression in these parameters; specifically, the NT-proBNP and diastolic measures as well as LV wall thickness worsened in the placebo group compared to the treatment group. This demonstrates a therapeutic paradigm of early treatment to prevent HCM complications rather than palliation.

Some of the sickest patients remain those with oHCM, many of whom require progression to septal reduction therapy (SRT) despite medical therapy as no medical therapy has been shown to prevent progression but rather to be temporizing at this time. SRT is indicated when patients have persistent LVOT gradient >50 mmHg and NYHA functional class III/IV or recurrent syncope with maximal medical therapy that can be tolerated (55). In terms of the effect on myocardial structure, it would be hopeful that relief of obstruction and the high afterload state would lead to some degree of remodeling, similar to that of treatment of hypertension, with some improvement in LV systolic function, diastole, and energetics. An early echocardiographic-based retrospective study of 60 patients who underwent septal myectomy showed a reduction of mean LV gradient of 67 mmHg to 12 mmHg, with EF decreasing from 74 to 67% on average, with expected reductions in septal wall thickness and left ventricular end systolic diameter (LVED) (56). Over the course of 2 years, left ventricular end diastolic diameter (LVEDD) was unchanged, but posterior wall thickness decreased mildly by 1 mm and left atrial diameter (LAD) decreased by 3 mm on average. Importantly, LV mass overall decreased from about 300 to 250 g on average, which was maintained at this level for a follow-up of longer than 2 years but was still larger than normal hearts, suggesting that the LVOTO is not the only driver of hypertrophy and fibrosis that leads to cardiomegaly in HCM. A later study of 66 oHCM patients with septal myectomy using echocardiography added measurements of strain (57). This study showed that after myectomy, longitudinal strain decreased at the myectomy site, increased in the lateral segments, but remained unchanged globally, with normalization of ventricular twist.

In order to understand the differences in remodeling after afterload removal in myocardium with intrinsic myocardial abnormality vs. that with presumably normal intact intracellular pathways, it is interesting to consider the structural and functional recovery after myectomy for oHCM and aortic valve replacement (AVR) for aortic valve stenosis, an extrinsic cause of hypertrophy (58). A small prospective study of 10 patients with oHCM and 10 patients with severe aortic stenosis (AS) were examined with echocardiography, CMR, and exercise testing. After AVR, patients experienced decrease on average of mean transvalvular gradient from 49 to 11 mmHg, with decrease in global LV and LA dimensions as well as lateral wall thickening. Global longitudinal strain improved, and exercise capacity improved, with a trend toward improvement in pVO_2. In oHCM patients with myectomy, LA dimension decreased after myectomy and LV mass/septal thickness as expected, though there was no change in LV dimension specifically. Global

longitudinal strain did not improve in oHCM after myectomy, though there was some improvement in exercise capacity but no improvement in pVO_2. LGE as expected was unchanged after the procedure in either cohort. Comparing these two cohorts, the main comparable effect was that left atrial (LA) volume decreased in both implying improved diastolic function, but oHCM did not recover any strain metrics implying little functional myocardial improvement in the oHCM hearts with remodeling and intrinsic myocardial abnormalities due to the aberrant genetics likely driving that disease.

Myosin modulator mechanisms and clinical applications

Altogether, it may be that reverse remodeling and improved myocardial function cannot be achieved in HCM by conventional medical therapy or surgical means due to the intrinsic defect of the myocardium itself resulting from the genetic mutation causing HCM. While many pathological mechanisms may be initiated by the various HCM mutations, studies of thick filament mutations in myosin in particular identified hypercontractility and upregulation of crossbridge cycling as a potential drug target (59–62). No suitable agents were available until recently with the discovery mavacamten (MYK-461), a first in class myosin blocker with specificity to cardiac β myosin (63), and a second agent aficamten (64) which is under investigation (NCT04219826).

Biochemical studies demonstrated that mavacamten was able to decrease myosin ATPase activity in a dose-dependent fashion and furthermore decrease maximal tension generation in demembranated cardiac muscle without a change in calcium sensitivity (65). Initially mavacamten was suspected to have an effect on myosin crossbridge cycling by inhibiting release of phosphate from myosin and decreasing the number of actin-binding heads transitioning from weakly to strongly bound state (63) which altogether would decrease force generation. However, ultimately, mavacamten was found to act through a novel mechanism on stabilizing myosin the interacting heads motif (IHM) and locking myosin in the super relaxed state (SRX), thereby completely removing myosin from the cross-bridge cycle itself (66–68). At the tissue level, mavacamten has potent effects on diastole in addition to systole, showing improvement in relaxation, decrease in stiffness, and augmentation of Frank-Starling mechanism in human engineered heart tissue (69). In a seminal study of multiple mouse models of HCM with classic myosin heavy chain (MYH6) mutations (R403Q, R719W, and R453C), mavacamten was shown to decrease fractioning shortening *in vivo* in young and old mice (65). It further prevented hypertrophic remodeling of mouse hearts when given prior to establishment of hypertrophy in young mice. Mechanistically, treated animals also demonstrated normalization of transcriptional pathways that regulate hypertrophy, fibrosis, and energy utilization. However, the effect of reverse remodeling was ameliorated in older mice with established hypertrophy. Altogether, based on this evidence, it was likely that mavacamten could target the pathophysiology of HCM by decreasing myosin availability (31), improving patient outcomes, though it was unclear if this would also have an effect on beneficial cardiac remodeling in the long-term.

Mavacamten was tested in a phase 3 prospective randomized clinical trial (RCT) vs. placebo (8) in which 251 adult patients with symptomatic oHCM were included with LVOTO of >50 mmHg at rest, with Valsalva, or with exercise, preserved LVEF, and NYHA class II-III, with a primary endpoint of improvement in pVO_2 with at least one NYHA class improvement, or a 3.0 mL/kg per min or greater increase in pVO_2 with no worsening of NYHA class (EXPLORER-HCM). Primary endpoint was met in 45% of patients compared to 22% of patients on placebo. Importantly, there was a large mean reduction of almost 50 mmHg in post-exercise LVOT gradient which translated to improvement in pVO_2 of almost 1.4 mL/kg per min on average and further improvement in subjective symptoms as measured by scales such as KCCQ-CSS. Mavacamten had a good safety profile with 97% completion through 30 weeks and no increase in overall adverse events compared to the placebo during the trial. Notably, six patients on mavacamten had transient decrease in LVEF of <50% not attributed to other causes, though not associated with clinical adverse outcomes. After discontinuation temporarily for three of these patients, the LVEF recovered, and the study was completed. In the other three patients, LVEF was noted to be decreased to around 48% at the end of the study though notably recovered after mavacamten washed out. Therefore, the response of some individuals with lowered EF necessitates long-term monitoring and possible dose adjustments. Longer-term safety profiles are being currently explored (NCT03723655). Furthermore, in a second RCT (VALOR-HCM), in patients who met clinical criteria for SRT and were referred to SRT, there was a 60% reduction in meeting clinical criteria for SRT or proceeding with SRT in those treated with mavacamten compared to placebo at 4 months (70). Mavacamten was approved by the FDA in 2022 for the patient population included in EXPLORER-HCM, specifically patients with oHCM with NYHAII-III with a LVOT gradient >50 mmHg at rest. An initial phase 2 trial (MAVERICK-HCM) has established good safety and tolerability as well as improvement in cardiac biomarkers of mavacamten in patients with nHCM though and long term effects in a randomized clinical trial are pending further study at this time (38).

Remodeling potential of myosin modulators in obstructive HCM

While effective in relieving symptoms and effect of obstructive HCM through this proximate myosin-targeted mechanism that reduced hypercontractility, LVOTO gradient, and effective afterload on ventricular cardiomyocytes, mavacamten and similar drugs in development may also lead to positive remodeling in human hearts as suggested in animal work. An echocardiographic study on all patients in EXPLORER-HCM ($n = 251$) analyzing changes in key echocardiographic parameters in symptomatic patients with oHCM over 30 weeks recently demonstrated improvements in markers of oHCM (71). There was an increase in LV wall thickness of 1.4 mm in the placebo group over this time period while those treated maintained the same wall thickness. Interestingly, there was resolution of systolic anterior motion (SAM) of the mitral valve in patients with SAM in almost 81% of patients treated with mavacamten. Despite relatively small changes in structure in the echocardiographic study, there was significant and striking effects on LV diastolic function with improvement in septal e′ of 0.7 cm/s, septal E/e′ of −3.5, lateral E/e′ of −3.8, and decrease in left atrial volume index (LAVI) of −7.5 mL/m^2. A sub-study using CMR imaging explored the effect on structure and function in 35 patients in greater detail (72). The study observed that there was a decrease in LV mass index by median 15.8 g/m^2, max LV wall thickness by median 2.4 mm, and LA volume index by median 10.3 g/m^2. At the same time, there was no change in fibrosis markers as evidenced by no significant change in LGE over this time period of 30 weeks though there was little fibrosis in most of the patients at baseline. Interestingly, there was a significant decrease in LVEF by a median 6.4% overall in the HCM group vs. the placebo group of 3.9%; however, none of these had a LVEF <50% since all began at an elevated baseline of hyperdynamic function. Overall, these findings while early in mavacamten suggest favorable reverse remodeling which correlated with the overall improvement cardiac function in patients treated with mavacamten. LV hypertrophic thinning in patients living out the natural history of their condition is frequently associated with increased collagen replacement and increased myocardial fibrosis. Reassuringly, there was no change in fibrosis as evidenced by LGE seen in this study. Notably, studies of remodeling have not been completed in patients with nHCM and remodeling remains an important and intriguing aspect of the studies as nHCM which can be considered a type of heart failure with preserved ejection fraction (HFpEF) has even more limited treatment options than oHCM.

As seen and hypothesized in prior studies, some of the longer-term changes in cardiac remodeling may require a long study period, though it is encouraging mavacamten has demonstrated favorable changes using a pharmacological therapy that has only been seen in surgical myectomy previously. As seen previously, a profound question of utility of mavacamten in the time course of disease remains to be answered, and it may be that early treatment prior to substantial remodeling may also result in prevention of adverse cardiac remodeling in individuals with HCM though a careful analysis of safety and benefits must be undertaken. Indeed, prior work indicates the majority of HCM remodeling occurs in early adulthood and late teen years, perhaps overall interacting and driven with other hormonal changes in the body at that time that drive overall maturation and growth. It may be possible that targeted treatment during an early period could prevent further HCM changes and may not necessarily necessitate indefinite treatment which would be indeed of utmost desirability for patients. However, such targeting may require further advances in genotype-phenotype associations and early screening programs as it is not altogether feasible at this time to predict which patients even with familial mutations will necessarily develop clinically relevant HCM.

Conclusions

In this review, we survey mechanisms of novel pharmacological therapies for HCM and their clinical trial evidence and compare their potential for inducing remodeling of the myocardium compared to previous therapies. We find evidence both mechanistically and from clinical trials that induction of reverse remodeling is possible and likely beneficial. While more research is needed, therapies like myosin modulators can induce beneficial cardiac remodeling and possibly prevent further adverse remodeling of hypertrophic hearts. However, important questions about long-term treatment and appropriate time frame specifically earlier therapy remain to be answered.

Author contributions

LS and YS contributed to the conception, writing, and editing of this manuscript. All authors contributed to the article and approved the submitted version.

Funding

YS was supported by NIH R01 HL157216, the American Heart Association National Clinical and Population Research Awards, the American Heart Association Career Development Award, Korea Institute of Oriental Medicine, Feldstein Medical Foundation, Columbia University Irving Medical Center Irving Institute for Clinical and Translational Research Precision Medicine Pilot Award, and Columbia University Irving Medical

Center Marjorie and Lewis Katz Cardiovascular Research Prize. The funding organizations did not have any role in the study design, collection, analysis, or interpretation of data, in writing of the manuscript, or in the decision to submit the article for publication. The researchers were independent from the funding organizations.

Conflict of interest

The authors declare that the research was conducted in the absence of any commercial or financial relationships that could be construed as a potential conflict of interest.

Publisher's note

References

1. Marian AJ, Braunwald E. Hypertrophic cardiomyopathy. *Circ Res.* (2017) 121:749–70. doi: 10.1161/CIRCRESAHA.117.311059

2. Geisterfer-Lowrance AA, Kass S, Tanigawa G, Vosberg HP, McKenna W, Seidman CE, et al. A molecular basis for familial hypertrophic cardiomyopathy: a beta cardiac myosin heavy chain gene missense mutation. *Cell.* (1990) 62:999–1006. doi: 10.1016/0092-8674(90)90274-I

3. Redwood CS, Moolman-Smook JC, Watkins H. Properties of mutant contractile proteins that cause hypertrophic cardiomyopathy. *Cardiovasc Res.* (1999) 44:20–36. doi: 10.1016/S0008-6363(99)00213-8

4. Cohn R, Thakar K, Lowe A, Ladha FA, Pettinato AM, Romano R, et al. A contraction stress model of hypertrophic cardiomyopathy due to sarcomere mutations. *Stem Cell Reports.* (2019) 12:71–83. doi: 10.1016/j.stemcr.2018.11.015

5. Spudich JA, Aksel T, Bartholomew SR, Nag S, Kawana M, Yu EC, et al. Effects of hypertrophic and dilated cardiomyopathy mutations on power output by human β-cardiac myosin. *J Exp Biol.* (2016) 219:161–7. doi: 10.1242/jeb.125930

6. Witjas-Paalberends ER, Ferrara C, Scellini B, Piroddi N, Montag J, Tesi C, et al. Faster cross-bridge detachment and increased tension cost in human hypertrophic cardiomyopathy with the R403Q MYH7 mutation. *J Physiol.* (2014) 592:274571. doi: 10.1113/jphysiol.2014.274571

7. Bai F, Wang L, Kawai M. A study of tropomyosin's role in cardiac function and disease using thin-filament reconstituted myocardium. *J Muscle Res Cell Motil.* (2013) 34:295–310. doi: 10.1007/s10974-013-9343-z

8. Olivotto I, Oreziak A, Barriales-Villa R, Abraham TP, Masri A, Garcia-Pavia P, et al. Mavacamten for treatment of symptomatic obstructive hypertrophic cardiomyopathy (EXPLORER-HCM): a randomised, double-blind, placebo-controlled, phase 3 trial. *Lancet.* (2020) 396:759–69. doi: 10.1016/S0140-6736(20)31792-X

9. Maron BJ, Maron MS, Semsarian C. Genetics of hypertrophic cardiomyopathy after 20 years. *J Am Coll Cardiol.* (2012) 60:705–15. doi: 10.1016/j.jacc.2012.02.068

10. Hebl VB, Miranda WR, Ong KC, Hodge DO, Bos JM, Gentile F, et al. The natural history of nonobstructive hypertrophic cardiomyopathy. *Mayo Clin Proc.* (2016) 91:279–87. doi: 10.1016/j.mayocp.2016.01.002

11. Marstrand P, Han L, Day SM, Olivotto I, Ashley EA, Michels M, et al. Hypertrophic cardiomyopathy with left ventricular systolic dysfunction: insights from the SHaRe registry. *Circulation.* (2020) 141:1371–83. doi: 10.1161/CIRCULATIONAHA.119.044366

12. Neubauer S, Kolm P, Ho CY, Kwong RY, Desai MY, Dolman SF, et al. Distinct Subgroups in Hypertrophic Cardiomyopathy in the NHLBI HCM Registry. *J Am Coll Cardiol.* (2019) 74:2333–45. doi: 10.1016/j.jacc.2019.08.1057

13. Harper AR, Goel A, Grace C, Thomson KL, Petersen SE, Xu X, et al. Common genetic variants and modifiable risk factors underpin hypertrophic cardiomyopathy susceptibility and expressivity. *Nat Genet.* (2021) 58:135–42. doi: 10.1038/s41588-020-00764-0

14. Tadros R, Francis C, Xu X, Vermeer AMC, Harper AR, Huurman R, et al. Shared genetic pathways contribute to risk of hypertrophic and dilated cardiomyopathies with opposite directions of effect. *Nat Genet.* (2021) 28:128–34. doi: 10.1038/s41588-020-00762-2

15. Ferrantini C, Coppini R, Pioner JM, Gentile F, Tosi B, Mazzoni L, et al. Pathogenesis of hypertrophic cardiomyopathy is mutation rather than disease specific: a comparison of the cardiac troponin T E163R and R92Q mouse models. *J Am Heart Assoc.* (2017) 6:5407. doi: 10.1161/JAHA.116.005407

16. Sequeira V, Wijnker PJM, Nijenkamp LLAM, Kuster DWD, Najafi A, Witjas-Paalberends ER, et al. Perturbed length-dependent activation in human hypertrophic cardiomyopathy with missense sarcomeric gene mutations. *Circ Res.* (2013) 112:1491–505. doi: 10.1161/CIRCRESAHA.111.300436

17. Ashrafian H, Redwood C, Blair E, Watkins H. Hypertrophic cardiomyopathy:a paradigm for myocardial energy depletion. *Trends Genet.* (2003) 19:263–8. doi: 10.1016/S0168-9525(03)00081-7

18. Ujfalusi Z, Vera CD, Mijailovich SM, Svicevic M, Yu EC, Kawana M, et al. Dilated cardiomyopathy myosin mutants have reduced force-generating capacity. *J Biol Chem.* (2018) 293:9017–29. doi: 10.1074/jbc.RA118.001938

19. Van Der Velden J, Witjas-Paalberends ER, Stienen GJM, Dos Remedios C, Ten Cate FJ, Ho CY, et al. Increased energy utilization for force generation in human familial hypertrophic cardiomyopathy caused by sarcomere gene mutations. *Eur Hear J.* (2013) 34:P4192. doi: 10.1093/eurheartj/eht309.P4192

20. Coppini R, Ho CY, Ashley E, Day S, Ferrantini C, Girolami F, et al. Clinical phenotype and outcome of hypertrophic cardiomyopathy associated with thin-filament gene mutations. *J Am Coll Cardiol.* (2014) 64:2589–600. doi: 10.1016/j.jacc.2014.09.059

21. Van Dijk SJ, Paalberends ER, Najafi A, Michels M, Sadayappan S, Carrier L, et al. Contractile dysfunction irrespective of the mutant protein in human hypertrophic cardiomyopathy with normal systolic function. *Circ Heart Fail.* (2012) 5:36–46. doi: 10.1161/CIRCHEARTFAILURE.111.963702

22. Crilley JG, Boehm EA, Blair E, Rajagopalan B, Blamire AM, Styles P, et al. Hypertrophic cardiomyopathy due to sarcomeric gene mutations is characterized by impaired energy metabolism irrespective of the degree of hypertrophy. *J Am Coll Cardiol.* (2003) 41:1776–82. doi: 10.1016/S0735-1097(02)03009-7

23. Witjas-Paalberends ER, Güclü A, Germans T, Knaapen P, Harms HJ, Vermeer AMC, et al. Gene-specific increase in the energetic cost of contraction in hypertrophic cardiomyopathy caused by thick filament mutations. *Cardiovasc Res.* (2014) 103:248–57. doi: 10.1093/cvr/cvu127

24. Ferrantini C, Belus A, Piroddi N, Scellini B, Tesi C, Poggesi C. Mechanical and energetic consequences of HCM-causing mutations. *J Cardiovasc Transl Res.* (2009) 2:441–5. doi: 10.1007/s12265-009-9131-8

25. Lopes LR, Elliott PM. A straightforward guide to the sarcomeric basis of cardiomyopathies. *Heart.* (2014) 100:1916–23. doi: 10.1136/heartjnl-2014-305645

26. Fraysse B, Weinberger F, Bardswell SC, Cuello F, Vignier N, Geertz B, et al. Increased myofilament Ca2+ sensitivity and diastolic dysfunction as early consequences of Mybpc3 mutation in heterozygous knock-in mice. *J Mol Cell Cardiol.* (2012) 52:1299–307. doi: 10.1016/j.yjmcc.2012.03.009

27. Eschenhagen T, Carrier L. Cardiomyopathy phenotypes in human-induced pluripotent stem cell-derived cardiomyocytes—a systematic review. *Pflügers Arch Eur J Physiol.* (2019) 471:755–68. doi: 10.1007/s00424-018-2214-0

28. Sewanan LR, Campbell SGSG. Modelling sarcomeric cardiomyopathies with human cardiomyocytes derived from induced pluripotent stem cells. *J Physiol.* (2020) 598:2909–22. doi: 10.1113/JP276753

29. Sewanan LR, Schwan J, Kluger J, Park J, Jacoby DLDL, Qyang Y, et al. Extracellular matrix from hypertrophic myocardium provokes impaired twitch dynamics in healthy cardiomyocytes. *JACC Basic to Transl Sci.* (2019) 4:495–505. doi: 10.1016/j.jacbts.2019.03.004

30. Wu H, Yang H, Rhee J-W, Zhang JZ, Lam CK, Sallam K, et al. Modelling diastolic dysfunction in induced pluripotent stem cell-derived cardiomyocytes from hypertrophic cardiomyopathy patients. *Eur Heart J.* (2019) 40:3685–95. doi: 10.1093/eurheartj/ehz326

31. Yotti R, Seidman CE, Seidman JG. Advances in the genetic basis and pathogenesis of sarcomere cardiomyopathies. *Annu Rev Genomics Hum Genet.* (2019) 20:129–53. doi: 10.1146/annurev-genom-083118-015306

32. Mosqueira D, Smith JGW, Bhagwan JR, Denning C. Modeling hypertrophic cardiomyopathy: mechanistic insights and pharmacological intervention. *Trends Mol Med.* (2019) 25:775–90. doi: 10.1016/j.molmed.2019.06.005

33. Birket MJJ, Ribeiro MCC, Kosmidis G, Ward D, Leitoguinho ARR, van de Pol V, et al. Contractile defect caused by mutation in MYBPC3 revealed under conditions optimized for human PSC-cardiomyocyte function. *Cell Rep.* (2015) 13:733–45. doi: 10.1016/j.celrep.2015.09.025

34. Ormerod JOM, Frenneaux MP, Sherrid MV. Myocardial energy depletion and dynamic systolic dysfunction in hypertrophic cardiomyopathy. *Nat Rev Cardiol.* (2016) 13:677–87. doi: 10.1038/nrcardio.2016.98

35. Riaz M, Park J, Sewanan LR, Ren Y, Schwan J, Das SK, et al. Muscle LIM protein force-sensing mediates sarcomeric biomechanical signaling in human familial hypertrophic cardiomyopathy. *Circulation.* (2022) 145:1238–53. doi: 10.1161/CIRCULATIONAHA.121.056265

36. Sewanan LR, Park J, Rynkiewicz MJ, Racca AW, Papoutsidakis N, Schwan J, et al. Loss of crossbridge inhibition drives pathological cardiac hypertrophy in patients harboring the tpm1 e192k mutation. *J Gen Physiol.* (2021) 153:2640. doi: 10.1085/jgp.202012640

37. Shimada YJ, Raita Y, Liang LW, Maurer MS, Hasegawa K, Fifer MA, et al. Comprehensive proteomics profiling reveals circulating biomarkers of hypertrophic cardiomyopathy. *Circ Hear Fail.* (2021) 14:e007849. doi: 10.1161/CIRCHEARTFAILURE.120.007849

38. Ho CY, Mealiffe ME, Bach RG, Bhattacharya M, Choudhury L, Edelberg JM, et al. Evaluation of mavacamten in symptomatic patients with nonobstructive hypertrophic cardiomyopathy. *J Am Coll Cardiol.* (2020) 75:2649–60. doi: 10.1016/j.jacc.2020.03.064

39. Vander RAS, Liu C, Morck MM, Kooiker KB, Jung G, Song D, et al. Hypertrophic cardiomyopathy β-cardiac myosin mutation (P710R) leads to hypercontractility by disrupting super relaxed state. *Proc Natl Acad Sci U S A.* (2021) 118:e2025030118. doi: 10.1073/pnas.2025030118

40. Clippinger SR, Cloonan PE, Wang W, Greenberg L, Stump WT, Angsutararux P, et al. Mechanical dysfunction of the sarcomere induced by a pathogenic mutation in troponin T drives cellular adaptation. *J Gen Physiol.* (2021) 153:2787. doi: 10.1085/jgp.202012787

41. Wilkins BJ, Dai YS, Bueno OF, Parsons SA, Xu J, Plank DM, et al. Calcineurin/NFAT coupling participates in pathological, but not physiological, cardiac hypertrophy. *Circ Res.* (2004) 94:110–8. doi: 10.1161/01.RES.0000109415.17511.18

42. McMullen JR, Jennings GL. Differences between pathological and physiological cardiac hypertrophy: novel therapeutic strategies to treat heart failure. *Clin Exp Pharmacol Physiol.* (2007) 34:255–62. doi: 10.1111/j.1440-1681.2007.04585.x

43. Musumeci B, Tini G, Russo D, Sclafani M, Cava F, Tropea A, et al. Left ventricular remodeling in hypertrophic cardiomyopathy: an overview of current knowledge. *J Clin Med.* (2021) 10:1547. doi: 10.3390/jcm10081547

44. Olivotto I, Cecchi F, Poggesi C, Yacoub MH. Patterns of disease progression in hypertrophic cardiomyopathy: an individualized approach to clinical staging. *Circ Heart Fail.* (2012) 5:535–46. doi: 10.1161/CIRCHEARTFAILURE.112.967026

45. Spirito P, Maron BJ. Absence of progression of left ventricular hypertrophy in adult patients with hypertrophic cardiomyopathy. *J Am Coll Cardiol.* (1987) 9:1013–7. doi: 10.1016/S0735-1097(87)80301-7

46. Harris KM, Spirito P, Maron MS, Zenovich AG, Formisano F, Lesser JR, et al. Prevalence, clinical profile, and significance of left ventricular remodeling in the end-stage phase of hypertrophic cardiomyopathy. *Circulation.* (2006) 114:216–25. doi: 10.1161/CIRCULATIONAHA.105.583500

47. Sen-Chowdhry S, Jacoby D, Moon JC, McKenna WJ. Update on hypertrophic cardiomyopathy and a guide to the guidelines. *Nat Rev Cardiol.* (2016) 13:651–75. doi: 10.1038/nrcardio.2016.140

48. Dybro AM, Rasmussen TB, Nielsen RR, Andersen MJ, Jensen MK, Poulsen SH. Randomized trial of metoprolol in patients with obstructive hypertrophic cardiomyopathy. *J Am Coll Cardiol.* (2021) 78:2505–17. doi: 10.1016/j.jacc.2021.07.065

49. Khachfe HH, Salhab HA, Fares MY, Khachfe HM. Current state of hypertrophic cardiomyopathy clinical trials. *Glob Heart.* (2019) 14:317–25. doi: 10.1016/j.gheart.2019.07.005

50. Olivotto I, Camici PG, Merlini PA, Rapezzi C, Patten M, Climent V, et al. Efficacy of ranolazine in patients with symptomatic hypertrophic cardiomyopathy: the RESTYLE-HCM randomized, double-blind, placebo-controlled study. *Circ Heart Fail.* (2018) 11:e004124. doi: 10.1161/CIRCHEARTFAILURE.117.004124

51. Murphy SP, Ibrahim NE, Januzzi JL. Heart failure with reduced ejection fraction: a review. *JAMA.* (2020) 324:488–504. doi: 10.1001/jama.2020.10262

52. Shimada YJ, Passeri JJ, Baggish AL, O'Callaghan C, Lowry PA, Yannekis G, et al. Effects of losartan on left ventricular hypertrophy and fibrosis in patients with nonobstructive hypertrophic cardiomyopathy. *JACC Heart Fail.* (2013) 1:480–7. doi: 10.1016/j.jchf.2013.09.001

53. Maron MS, Chan RH, Kapur NK, Jaffe IZ, McGraw AP, Kerur R, et al. Effect of spironolactone on myocardial fibrosis and other clinical variables in patients with hypertrophic cardiomyopathy. *Am J Med.* (2018) 131:837–41. doi: 10.1016/j.amjmed.2018.02.025

54. Ho CY, Day SM, Axelsson A, Russell MW, Zahka K, Lever HM, et al. Valsartan in early-stage hypertrophic cardiomyopathy: a randomized phase 2 trial. *Nat Med.* (2021) 27:1818–24. doi: 10.1038/s41591-021-01505-4

55. Ommen SR, Mital S, Burke MA, Day SM, Deswal A, Elliott P, et al. 2020 AHA/ACC guideline for the diagnosis and treatment of patients with hypertrophic cardiomyopathy. *Circulation.* (2020) 142:558–631. doi: 10.1161/CIR.0000000000000938

56. Deb SJ, Schaff H V, Dearani JA, Nishimura RA, Ommen SR. Septal myectomy results in regression of left ventricular hypertrophy in patients with hypertrophic obstructive cardiomyopathy. *Ann Thorac Surg.* (2004) 78:2118–22. doi: 10.1016/j.athoracsur.2004.05.063

57. Moravsky G, Bruchal-Garbicz B, Jamorski M, Ralph-Edwards A, Gruner C, Williams L, et al. Myocardial mechanical remodeling after septal myectomy for severe obstructive hypertrophic cardiomyopathy. *J Am Soc Echocardiogr.* (2013) 26:893–900. doi: 10.1016/j.echo.2013.05.012

58. Parbhudayal RY, Güçlü A, Zweerink A, Biesbroek PS, Croisille P, Clarysse P, et al. Myocardial adaptation after surgical therapy differs for aortic valve stenosis and hypertrophic obstructive cardiomyopathy. *Int J Cardiovasc Imaging.* (2019) 35:1089–100. doi: 10.1007/s10554-019-01563-3

59. Sewanan LR, Jacoby DL. Novel myosin-based therapies in hypertrophic cardiomyopathy. *Curr Treat Options Cardiovasc Med.* (2021) 23:1–12. doi: 10.1007/s11936-021-00921-6

60. Barrick SK, Greenberg MJ. Cardiac myosin contraction and mechanotransduction in health and disease. *J Biol Chem.* (2021) 297:101297. doi: 10.1016/j.jbc.2021.101297

61. Toepfer CN, Garfinkel AC, Venturini G, Wakimoto H, Repetti G, Alamo L, et al. Myosin sequestration regulates sarcomere function, cardiomyocyte energetics, and metabolism, informing the pathogenesis of hypertrophic cardiomyopathy. *Circulation.* (2020) 141:828–42. doi: 10.1161/CIRCULATIONAHA.119.042339

62. Zampieri M, Berteotti M, Ferrantini C, Tassetti L, Gabriele M, Tomberli B, et al. Pathophysiology and treatment of hypertrophic cardiomyopathy: new perspectives. *Curr Heart Fail Rep.* (2021) 18:169–79. doi: 10.1007/s11897-021-00523-0

63. Kawas RF, Anderson RL, Bartholomew Ingle SR, Song Y, Sran AS, Rodriguez HM, et al. small-molecule modulator of cardiac myosin acts on multiple stages of the myosin chemomechanical cycle. *J Biol Chem.* (2017) 292:16571–7. doi: 10.1074/jbc.M117.776815

64. Chuang C, Collibee S, Ashcraft L, Wang W, Vander Wal M, Wang X, et al. Discovery of aficamten (CK-274), a next-generation cardiac myosin inhibitor for the treatment of hypertrophic cardiomyopathy. *J Med Chem.* (2021) 64:14142–52. doi: 10.1021/acs.jmedchem.1c01290

65. Green EM, Wakimoto H, Anderson RL, Evanchik MJ, Gorham JM, Harrison BC, et al. A small-molecule inhibitor of sarcomere contractility suppresses hypertrophic cardiomyopathy in mice. *Science.* (2016) 351:617–21. doi: 10.1126/science.aad3456

66. Rohde JA, Roopnarine O, Thomas DD, Muretta JM. Mavacamten stabilizes an autoinhibited state of two-headed cardiac myosin. *Proc Natl Acad Sci U S A.* (2018) 115:E7486–94. doi: 10.1073/pnas.1720342115

67. Spudich JA. The myosin mesa and a possible unifying hypothesis for the molecular basis of human hypertrophic cardiomyopathy. *Biochem Soc Trans.* (2015) 43:64–72. doi: 10.1042/BST20140324

68. Ait-Mou Y, Hsu K, Farman GP, Kumar M, Greaser ML, Irving TC, et al. Titin strain contributes to the frank-starling law of the heart by structural rearrangements of both thin- and thick-filament proteins. *Proc Natl Acad Sci U S A.* (2016) 113:2306–11. doi: 10.1073/pnas.1516732113

69. Sewanan LR, Shen S, Campbell SG. Mavacamten preserved length-dependent contractility and improved diastolic function in human engineered heart tissue. *Am J Physiol Circ Physiol.* (2021) 320:H1112–3. doi: 10.1016/S0735-1097(21)01895-7

70. Milind Y, Desai MM, Anjali Owens M, Jeffrey B, Geske M, Kathy Wolski M, et al. Myosin inhibition in patients with obstructive hypertrophic cardiomyopathy referred for septal reduction therapy. *J Am Coll Cardiol.* (2022) 80:95–108. doi: 10.1016/j.jacc.2022.04.048

71. Hegde SM, Lester SJ, Solomon SD, Michels M, Elliott PM, Nagueh SF, et al. Effect of mavacamten on echocardiographic features in symptomatic patients with obstructive hypertrophic cardiomyopathy. *J Am Coll Cardiol.* (2021) 78:2518–32. doi: 10.1016/j.jacc.2021.09.1381

72. Saberi S, Cardim N, Yamani MH, Schulz-Menger J, Li W, Florea V, et al. Mavacamten favorably impacts cardiac structure in obstructive hypertrophic cardiomyopathy: EXPLORER-HCM CMR substudy analysis. *Circulation.* (2021) 143:606–8. doi: 10.1161/CIRCULATIONAHA.120.052359

frontiers | Frontiers in Cardiovascular Medicine

TYPE Original Research
PUBLISHED 11 January 2023
DOI 10.3389/fcvm.2022.1044443

OPEN ACCESS

EDITED BY
Vittorio Palmieri,
Azienda Ospedaliera dei Colli, Italy

REVIEWED BY
Maria Teresa Vietri,
Seconda Università degli Studi di Napoli, Italy
Lingfang Zhuang,
Shanghai Jiao Tong University, China
Xiang Ma,
First Affiliated Hospital of Xinjiang Medical University, China

*CORRESPONDENCE
Heshui Yu
hs_yu08@163.com
Xuebin Fu
xfu@luriechildrens.org

†These authors have contributed equally to this work

SPECIALTY SECTION
This article was submitted to Heart Failure and Transplantation, a section of the journal Frontiers in Cardiovascular Medicine

RECEIVED 14 September 2022
ACCEPTED 22 December 2022
PUBLISHED 11 January 2023

CITATION
Zhang L, Lin Y, Wang K, Han L, Zhang X, Gao X, Li Z, Zhang H, Zhou J, Yu H and Fu X (2023) Multiple-model machine learning identifies potential functional genes in dilated cardiomyopathy. *Front. Cardiovasc. Med.* 9:1044443. doi: 10.3389/fcvm.2022.1044443

Multiple-model machine learning identifies potential functional genes in dilated cardiomyopathy

Lin Zhang[1†], Yexiang Lin[2†], Kaiyue Wang[1], Lifeng Han[1], Xue Zhang[1], Xiumei Gao[1], Zheng Li[1], Houliang Zhang[3], Jiashun Zhou[3], Heshui Yu[1*] and Xuebin Fu[4,5*]

[1]State Key Laboratory of Component-Based Chinese Medicine, Tianjin University of Traditional Chinese Medicine, Tianjin, China, [2]Biomedical Engineering, Imperial College London, London, United Kingdom, [3]Tianjin Jinghai District Hospital, Tianjin, China, [4]Department of Cardiovascular-Thoracic Surgery, Northwestern University Feinberg School of Medicine, Chicago, IL, United States, [5]Department of Pediatrics, Ann & Robert H. Lurie Children's Hospital of Chicago, Chicago, IL, United States

Introduction: Machine learning (ML) has gained intensive popularity in various fields, such as disease diagnosis in healthcare. However, it has limitation for single algorithm to explore the diagnosing value of dilated cardiomyopathy (DCM). We aim to develop a novel overall normalized sum weight of multiple-model MLs to assess the diagnosing value in DCM.

Methods: Gene expression data were selected from previously published databases (six sets of eligible microarrays, 386 samples) with eligible criteria. Two sets of microarrays were used as training; the others were studied in the testing sets (ratio 5:1). Totally, we identified 20 differently expressed genes (DEGs) between DCM and control individuals (7 upregulated and 13 down-regulated).

Results: We developed six classification ML methods to identify potential candidate genes based on their overall weights. Three genes, serine proteinase inhibitor A3 (*SERPINA3*), frizzled-related proteins (FRPs) 3 (*FRZB*), and ficolin 3 (*FCN3*) were finally identified as the receiver operating characteristic (ROC). Interestingly, we found all three genes correlated considerably with plasma cells. Importantly, not only in training sets but also testing sets, the areas under the curve (AUCs) for *SERPINA3*, *FRZB*, and *FCN3* were greater than 0.88. The ROC of *SERPINA3* was significantly high (0.940 in training and 0.918 in testing sets), indicating it is a potentially functional gene in DCM. Especially, the plasma levels in DCM patients of SERPINA3, FCN, and FRZB were significant compared with healthy control.

Discussion: SERPINA3, FRZB, and FCN3 might be potential diagnosis targets for DCM,Further verification work could be implemented.

KEYWORDS

diagnosis value, dilated cardiomyopathy, machine learning, *SERPINA3*, *FRZB*, *FCN3*

1. Introduction

Machine learning (ML), composed of various intricate algorithms, is recently commonly applied to explore potential biomarkers (e.g., lipidome, metabolome, and transcriptome) and prognosis (1, 2), especially in variable filtration (3–5). For example, MLs can recognize patterns better representing the individual risk compared to classical surgical risk scores (6). ML includes various types, such as support vector machine (SVM) (7, 8), random forest (RF) (9), decision tree (DT) (10–12), and so on. Different ML has its specialty and shortcoming. For example, least absolute shrinkage and selection operator (LASSO) processed a precision matrix of Gaussian variables using an $\ell 1$-penalty (13) until small values to zero but eliminated too many variables. For SVM, separated hyperplanes allow for correct partitioning and maximize geometric spacing but may be worse in a small sample size (14) compared with other MLs (15). Different ML algorithms possess both characteristics and limitations which cannot be ignored, especially in the choice of variables. Many researchers (16–18) only focus on single or two MLs which might ignore their potential shortcomings. In our previous research (19), five MLs show different weights even with the same genes. So just intersecting the top N genes may unconsciously delete some dominant genes (20–23). And ignoring the weights of genes may result in an imbalance of filtration (19, 24).

Dilated cardiomyopathy (DCM), not only the primary myocardial disease but also the dominant trigger in chronic heart failure (HF) (25), manifests clinically in systolic heart insufficiency and dilatation of the left ventricle (26, 27). Although there are already clinical diagnosis criteria for DCM, by the time the clinical diagnosis is clear, most of the patient's underlying condition is poor (27). Though drugs (e.g., ivabradine) for HF are used to treat DCM and improve the prognosis in the short term (28), the long-term prognosis remains poor (29). Therefore, early diagnosis with identifying markers of DCM is necessary. Previous studies had indicated the diagnosis value of genes (30, 31) (e.g., TBX20 or Gab1) in DCM but with few microarrays (32), which means a small sample size and non-universality. Thus, developing a predictive model for DCM genetic diagnosis with multiple microarrays is necessary.

In this study, we identified potential transcriptomic information regarding DCM diagnosis with the overall weights in MLs of multiple microarrays. Furthermore, we further developed an immune correlation analysis between diagnosis genes and immune cells. Finally, DCM patients and healthy control were recruited for validation of related proteins of genes. The process of the following analysis (**Figure 1**) was shown in the flow chart.

2. Materials and methods

2.1. Data acquisition

We derived the transcriptome information of DCM from Gene Expression Omnibus (GEO). According to the following criteria, the primary data were derived with the keyword of "DCM": (1) inclusion criteria (i) sample of the left ventricle with a diagnosis of DCM patients; (ii) transcriptome; (iii) primary data was free and accessible. (2) exclusion criteria (i) suspected carcinoma, ischemic cardiomyopathy, heart valve disease, and other diseases; (ii) intervention(s) in DCM patients.

2.2. Data processing

Firstly, the *sva* R package (version 3.36) was applied to eliminate branch effects and quantile normalization with the specific function of *ComBat*. Secondly, we divide all microarrays into training or testing sets with a ratio of 5:1 (33). Briefly, the training set for developing the potential diagnosis value, and the testing for verifying the results. Thirdly, we identify the differentially expressed genes (DEGs). The functional analysis of DEGs was applied through the Kyoto Encyclopedia of Genes and Genomes Gene Set Enrichment Analysis (KEGG-GSEA), Gene Ontology (GO), and Disease Ontology (DO) enrichment based on three packages, *DOSE* (version 3.22.1), *clusterProfiler* (version 4.4.4), and *enrichplot* (version 1.16.2). The GO consist of three parts, molecular function (MF), biological process (BP), and cellular components (CCs). Moreover, six MLs algorithms were applied to the classification model and filtered the candidate diagnosis genes. As for the testing group, we identify the diagnosis value of potential candidate genes. Lastly, the immune correlation between the above genes was developed.

2.3. Searching for DEGs

The R package, *limma* (version 3.52.4), was adopted to average the same gene expression with the function of *avereps* and then identify the DEGs. After quantile normalization, primary data sets were transformed into log2. *P*-value was adjusted to the false discovery rate based on *Benjamini and Hochberg* method. Two thresholds were set, the absolute value of fold change ($|\log FC| > 1$, and the false discovery rate < 0.001. With the DEGs, the heatmap and volcano plot were applied with the *pheatmap* (version 1.0.12) and *ggplot2* (version 3.3.6).

2.4. Classification models with six MLs

Based on the above DEGs, we further developed classification models with six MLs algorithms, SVM, LASSO,

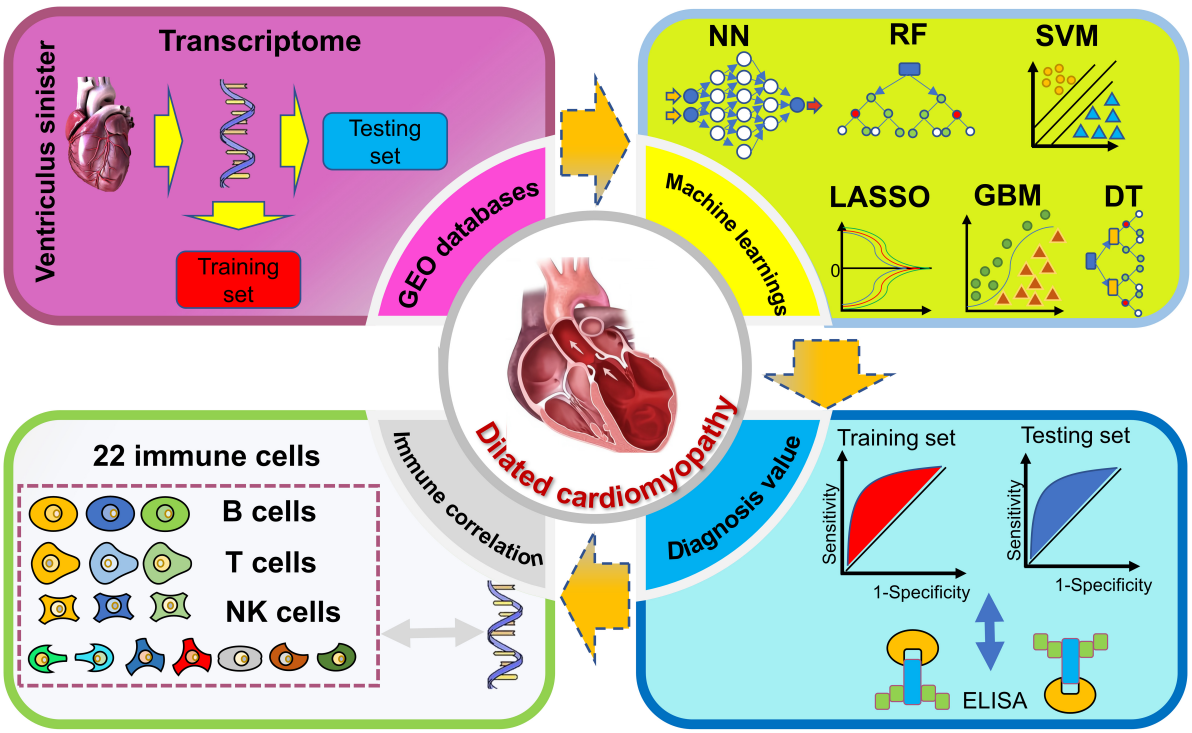

FIGURE 1
Flow chart of this study.

RF, gradient boosting machine (GBM), DT, and neural network (NN) to assess the classification value. Briefly, we constructed the six MLs classification models with optimized parameters in the training sets, and the testing was adopted for the validation of the six MLs. All ML models are cross-validated 10-fold to ensure stability. The accuracy value was adopted to estimate the value for six MLs and greater accuracy indicates the better classification value of the model.

The first ML (LASSO) was developed with the *glmnet* (version 4.1-4) R package. The function *cv.glmnet* was applied to optimize the value of lambda. For basic parameters, the following settings were the scale of lambda between 0 and 2,000 with one step size, the family of "binomial," and the type measure of "class." With the min lambda, the function *glmnet* was applied to the LASSO model in training sets with alpha (equal to 1) and a family of "binomial."

The second ML (SVM) was adopted with *e1071* R package (version 1.7-11). The function *tune.svm* was utilized to optimize the settings parameter. For basic parameters, the following settings were the kernel of "linear," and the cost between 1 and 20. With the best number of support vectors, the classification model was built.

The third ML (DT) was finished with two R packages, *rpart* (version 4.1.16) and *rpart.plot* (version 3.1.1). The *rpart* function was applied to the model with the method of "class," cp value of 0.00001.

The fourth ML (RF) was adopted with *randomForest* (version 4.7-1.1). In *randomForest*, the *tuneRF* was served to optimize 500 trees and 1 step size. With the optimal trees for min error rate, the classification model of training sets was accomplished.

The fifth ML (NN) was developed with *neuralnet* R package (version 1.44.2). In *neuralnet*, the *neuralnet* was served with five layers (containing an input layer, an output layer, and three hidden layers), the *err.fct* of "sse," and the output of linear.

The last ML, GBM, was different from the above five algorithms with more steps and prone to making. The GMB was accomplished with *h2o* (version 3.38.0.1). Only JAVA operating environment that the *h2o* can process the classification model. Thereby, we had to timely download and installed java development kit (JDK). Necessary for running memory with *h2o.init* in GBM and we adjusted the model memory of GBM to 16G. Due to the h2o data type being indispensable for GBM, we transform the data format with *as.h2o* in both the training set and testing set. Finally, *h2o.gbm* was applied to tune the parameters and model (we set the distribution of "bernoulli," 200 trees, 0.001 for a learning rate, 0.9 for a sample rate).

Importantly, based on the above weights of six MLs for DEGs, we calculated the normalized six MLs weights of DEGs as the function in R: $Overall\ weights = \frac{abs(LASSO)}{abs(LASSOmax)} + \frac{abs(SVM)}{abs(SVMmax)} + \frac{abs(RF)}{abs(RFmax)} + \frac{abs(DT)}{abs(DTmax)} + \frac{abs(GBM)}{abs(GBMmax)} +$

$\frac{abs(NN)}{abs(NNmax)}$. For example, if the weight of glyceraldehyde-3-phosphate dehydrogenase (*GAPDH*) in six MLs was 15, −11, 10, −1, 160, and −4. And the max weights of absolute value in the above model were 30, 44, 40, 4, 320, and 8, respectively. The overall weight of *GAPDH* was |15| /30 + |−11| /44 + |10| /40 + |−1| /4 + |160| /320 + |−4| /8 = 2.25. Then, we filter the candidate genes for ROC (*pROC*, version 1.18.0) and immune correlation (*CIBERSORT* function) with overall weights > 1. Area under the curve (AUC) was calculated to judge the diagnosis value between control and DCM individuals.

2.5. Access to clinical samples

The trial complied with the Declaration of Helsinki and was approved by the Ethics Committees of the participating hospitals. All DCM patients and healthy volunteers provided written informed consent from September 20, 2022 to October 31, 2022. Ethics Committee/Institutional Review Board: Ethics Review Committee Jinghai District Hospital, Plan 11. Diary number: JHYYLL-2022-0307.

Briefly, according to the Chinese guidance (27), the inclusion criteria of DCM contain three parts, (1) left ventricular end-diastolic diameter > 5.0 cm (women) or > 5.5 cm (men); (2) left ventricular ejection fraction < 45%, left ventricular fractional shortening < 25%; (3) no other heart-related diseases and >20 years old. Blood samples were collected in ethylene diamine tetraacetic acid (EDTA)-containing tubes after a 10-h overnight fast and centrifuged at 4°C, 3,000 *g* for 10 min, then plasma was stored at −80°C. All the plasma levels of SERPINA3, FCN3, and FRZB were measured by ELISA kits (SERPINA3 Human ELISA Kit, Abcam, Cambridge, UK; Hycult Biotechnology, Uden, The Netherlands; R&D Systems, Minneapolis, MN, USA, respectively).

2.6. Statistical analysis

All the statistical analyses were processed by R software (version 4.1.1). CIBERSORT was adopted for immune correlation analysis. We estimate the immune correlates of 22 immune cells and visualization in the *corrplot* R package (version 0.92). For continuous variables, the independent Student's *t*-test was adopted if the variables met Gaussian distribution, if not, the Wilcoxon test was used. A two-sided *p*-value < 0.05 was considered to be significant.

3. Results

3.1. Incorporation of microarrays

Among six microarrays (**Table 1**) (386 sample sizes) were finally obtained, including GSE5406, GSE57338, GSE1145, GSE1869, GSE3585, and GSE42955. According to the random ratio of 5:1, the training set was integrated with two microarrays (168 DCM and 152 healthy control), including GSE5406 and GSE57338. At the same time, the testing set was integrated with four (39 DCM and 27 control), composed of GSE1145, GSE1869, GSE3585, and GSE42955.

3.2. Searching for DEGs

Among 20 DEGs with biological significance (**Supplementary Table 1**) from 12,937 RNAs were identified in the training sets. Compared to the healthy control, 13 genes down-regulated (SERPINA3, PLA2G2A, IL1RL1, CD163, SERPINE1, FCN3, CYP4B1, LYVE1, S100A8, SLCO4A1, MYOT, ANKRD2, and VSIG4) and 7 genes up-regulated (MXRA5, FRZB, HBB, LUM, SFRP4, NPPA, and ASPN) in the DCM individuals (**Figure 2**).

3.3. Functional enrichment analysis

Based on the above DEGs, we identified 21 GSEA terms (**Supplementary Table 2**) and show the top 5 (**Figures 3A, B**), 102 GO terms (**Supplementary Table 3**) and show the top 4 (**Figure 3C**), 68 DO terms (**Supplementary Table 4**) and show the top 10 (**Figure 3D**). Among GSEA-KEGG enrichments, the top 3 presented significance in Type I diabetes mellitus, graft versus host disease, and allograft rejection. Regarding the GO terms in BP, the top 3 presented significant enrichments in the cellular zinc ion homeostasis, positive regulation of inflammatory response, and zinc ion homeostasis. In terms of DO, the top 3 diseases presented were atherosclerosis, arteriosclerotic cardiovascular disease, and arteriosclerosis.

3.4. Six MLs algorithms for classification model and candidate genes

Six classification models of MLs were successfully established (**Figure 4**), and we calculated the accuracy (**Table 2**) of both training sets and testing sets. In LASSO (**Figure 4A**), we filtered nine candidate genes. Disappointed, LASSO's accuracy of the two sets were only 52.5 and 59.09%. In SVM, 19 genes were identified (**Figure 4B**), and the accuracies of the two sets were unstable, 90.94 and 51.52%. In RF (**Figure 4C**), the error rate of the classification model decreases as the number of trees increases, until 234 trees the error rate is minimized and smoothed. Surprisingly, the accuracy of the two sets was 100%. In DT (**Figure 4D**), thresholds of 7.2 in SERPINA3 can discriminate the health and DCM, but the accuracies of the two sets were also unstable like SVM, 93.75

TABLE 1 Basic information on the six microarrays.

ID	Public time	Institution	Country
GSE5406	September 04, 2006	University of Pennsylvania School of Medicine	USA
GSE57338	January 01, 2015	Perelman School of Medicine at the University of Pennsylvania	USA
GSE1145	March 24, 2004	Harvard University	USA
GSE1869	October 26, 2004	Johns Hopkins Medical Institutions	USA
GSE3585	August 01, 2006	German Cancer Research Center and National Center of Tumor Diseases	Germany
GSE42955	October 17, 2013	Health Research Institute of the Hospital La Fe	Spain

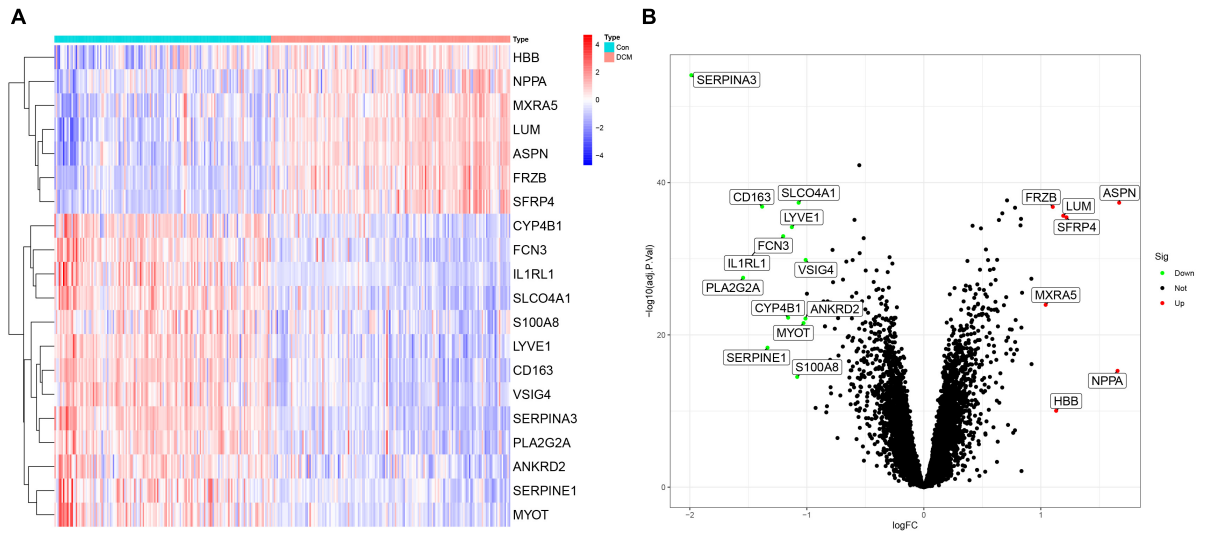

FIGURE 2
The heatmap and volcano plot of 20 differently expressed genes (DEGs) in dilated cardiomyopathy (DCM) and healthy. **(A)** The heatmap of 20 DEGs; **(B)** the volcano plot of 20 DEGs.

and 53.03%. In GBM (Figure 4E), we developed six folds models to explore the candidate genes, but the accuracies of the two sets were also unstable, 96.03 and 53.03%. In NN (Figure 4F), enough in three hidden layers to discriminate the health and DCM, and the accuracies of both sets were 100%. Among all those models, the most important genes with the primary weights were identified (Supplementary Table 5). In the six MLs, both the RF and NN show the optimal and stable classification value. The accuracy of both MLs was 100%. Furthermore, the summation (Table 3) of normalized weights (dividing the absolute value by max weights) was calculated to screen the diagnosis genes. And nine genes (*SERPINA3*, *CD163*, *FCN3*, *LYVE1*, *SLCO4A1*, *LUM*, *FRZB*, *PLA2G2A*, and *SFRP4*) talent showing themselves with overall weights > 1 (Table 3).

Based on the summed normalized weights > 1, nine candidates genes were chosen for diagnosis in DCM and healthy individuals. Next, we validate the nine candidate genes in the testing set, and except for *SLCO4A1*, the other eight show significance (Figure 5).

3.5. Evaluation of the diagnosis value

Eight genes (just mentioned above) were taken into the ROC curve (Supplementary Figures 1, 2). AUC values of *SERPINA3*, *FCN3*, *LUM*, *FRZB*, *PLA2G2A*, and *SFRP4* were higher than 0.8 in both two sets. Moreover, three genes *SERPINA3*, *FCN3*, and *FRZB* were higher than 0.88 (Figure 6) in the training sets and even >0.9 in the testing sets. Especially, *SERPINA3* was higher than 0.9 in both sets. In a word, three genes, *SERPINA3*, *FCN3*, and *FRZB* may be the potential diagnosis genes compared with DCM and healthy control.

3.6. Immune correlation

The immune correlation between signal genes and 22 immune cells was applied to all 386 samples of six microarrays (Supplementary Figure 3). *SERPINA3* (Figure 7A) shows significant correlations in Monocytes, T cells CD8, and Plasma cells. Regarding *FRZB* (Figure 7B), the T cells CD4 memory

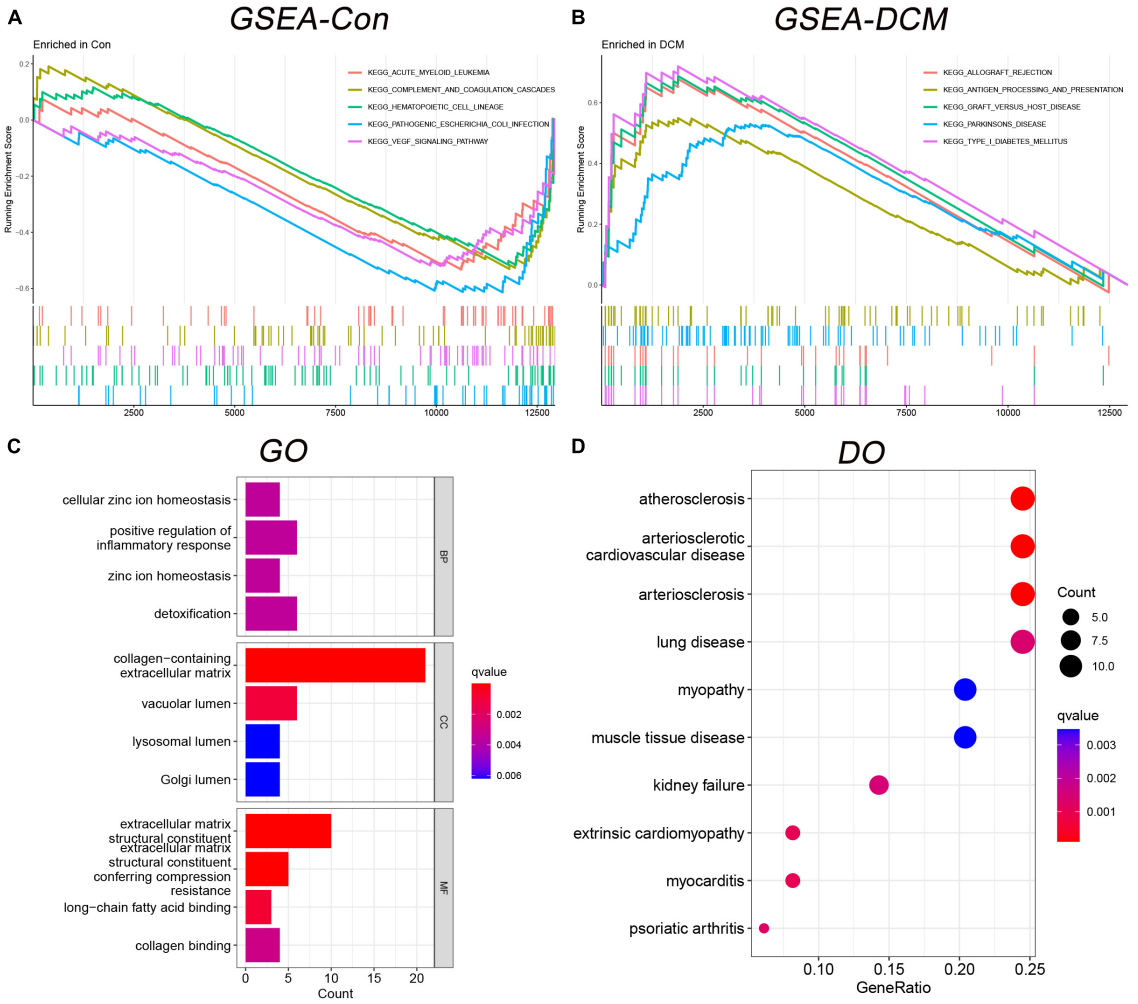

FIGURE 3
Functional enrichment analysis in gene set enrichment analysis-kyoto encyclopedia of genes and genomes (GSEA-KEGG), gene ontology (GO), and disease ontology (DO). **(A)** The GSEA-KEGG enrichment in control; **(B)** the GSEA-KEGG enrichment in DCM; **(C)** the GO enrichment term; and **(D)** the DO enrichment term.

resting, plasma cells, monocytes, and T cells regulatory (Tregs) show significant correlations. In *FCN3* (Figure 7C), the mast cells activated, macrophages M0, and plasma cells show significant correlations. These three genes show a typical significant immune cell, plasma cells. All three genes were correlated with plasma cells.

3.7. Differences in plasma proteins

Finally, 24 individuals (12 healthy controls and 12 DCM patients) were recruited. We measured the plasma levels (Figure 8) of SERPINA3, FRZB, and FCN3. The plasma levels of SERPINA3 in DCM patients (397.17 ± 49.22 μg/ml) were higher ($P < 0.001$) than in healthy individuals (221.25 ± 14.15 μg/ml). Similarly, the plasma levels of FRZB in DCM patients (2,042.75 ± 292.62 pg/ml) were higher ($P < 0.001$) than in healthy individuals (784.58 ± 55.85 pg/ml). In FCN3, the plasma levels in DCM (13.67 ± 2.69 μg/ml) were lower than in the healthy control (20.92 ± 1.38 μg/ml). More importantly, all of the protein levels of these three genes were significant in DCMs compared with healthy controls.

4. Discussion

To our knowledge, this is the first work with normalized overall weights to filter candidate genes in DCM. Three genes, *SERPINA3*, *FRZB*, and *FCN3* show the AUC values in the training set (0.940, 0.889, and 0.887, respectively) and testing set (0.918, 0.911, and 0.901, respectively). In plasma

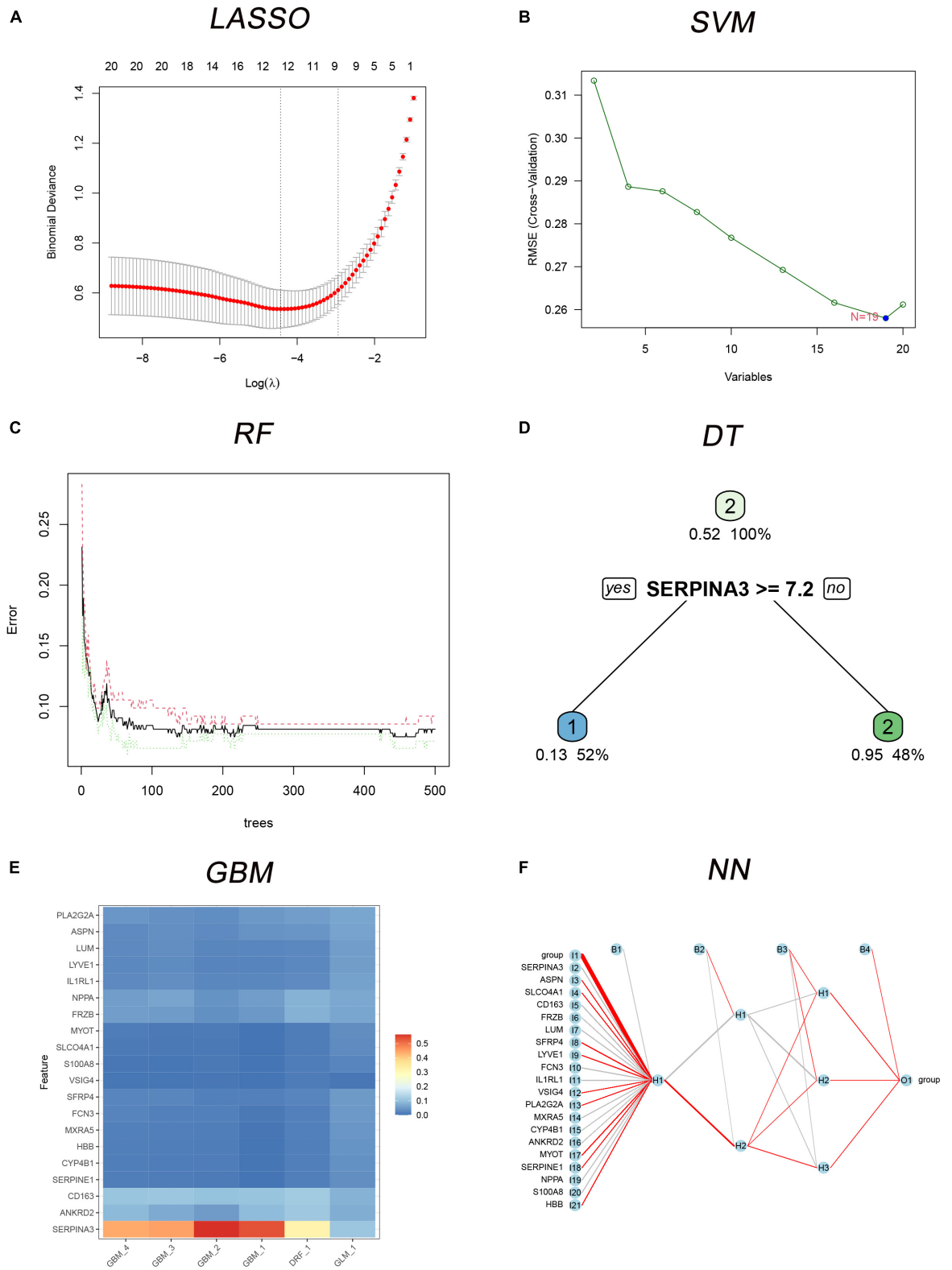

FIGURE 4
The six MLs classification models built with 20 differently expressed genes (DEGs). **(A)** Least absolute shrinkage and selection operator (LASSO) for 9 candidate genes; **(B)** support vector machine (SVM) for 19 candidates DEGs; **(C)** the error rate of the random forest (RF) classification model with increasing trees; **(D)** the decision tree (DT) for classification of control and dilated cardiomyopathy (DCM) individuals; **(E)** multiple gradient boosting machine (GBM) classification models of control and DCM individuals; **(F)** neural network (NN) for classification of control and DCM individuals.

TABLE 2 The accuracy of six classification machine learnings (MLs) in the training and testing sets.

MLs	Training set (%)	Testing set (%)
SVM	90.94	51.52
LASSO	52.5	59.09
RF	100	100
NN	100	100
GBM	96.03	53.03
DT	93.75	53.03

protein, SERPINA3, FRZB, and FCN3 in DCM were significant compared with the control.

MLs have been extensively performed in four types of analysis, filtration of variables, classification, congression, and cluster. In bioinformatics, many studies take only one or two MLs, such as WGCNA (34), LASSO, and SVM. Nevertheless, a single ML might ignore the dominant variables. In our work (**Table 1**), the *FCN3* will be missed if just take the intersection of LASSO and SVM like the previous study (35). Various MLs showed their advantages. For instance, SVM and NN show their talents in the diagnosis of pigmented skin lesions (36). And in the pre-operative prediction of postsurgical mortality (37), GBM was the most MLs compared with DT, RF, and SVM. In our work, both RF and NN show their talent discrimination value in both training and testing sets with an accuracy of 100%. The normalized weights may be different even in the same variable (**Table 1**) in various MLs. So our work takes the sum of the normalized weights of different MLs into the following diagnosis value. Three tRNA, *SERPINA3*, *FRZB*, and *FCN3*, were filtered with a potential diagnosis of DCM. Furthermore, our method finds two potential diagnosis genes (FRZB and FCN3) in DCM that have never been reported before. Compared with previous studies, *SERPIAN3* presented the diagnosis value (38) in HF, and this work expanded its scale into DCM with the same point as Asakura and Kitakaze (39). Furthermore, Yang et al. (40) emphasizes the therapeutic value of *FRZB*, and our study expands its treatment potential to diagnosis value. Regarding *FCN3*, though studies pay attention to the diagnosis value for HF (41), no study reports the diagnosis value for DCM to our knowledge.

Serine proteinase inhibitor A3 (*SERPINA3*), also known as alpha-1 antichymotrypsin, has been shown to promote the development of cancer (42) and cardiac remodeling in patients with HF. In HF, though Delrue et al. (43) had confirmed that SERPINA3 is still an independent predictor of all-cause mortality, studies have paid little attention to the effect of pharmacological treatment of DCM. Spironolactone (44–47) dominates an important treated role in DCM. The

TABLE 3 The summed normalized weights of 20 differently expressed genes (DEGs) in six classifications machine learnings (MLs).

Genes	LASSO	RF	NN	GBM	DT	SVM	Sum (weights)
SERPINA3	1	1	0.73	1	1	1	5.73
CD163	0	0.37	1	0.19	0.81	0.08	2.45
FCN3	0	0.32	0.91	0.01	0.73	0.08	2.05
LYVE1	0.07	0.41	0.51	0.03	0.72	0.16	1.91
SLCO4A1	0	0.41	0.22	0.14	0.77	0.08	1.61
LUM	0.31	0.28	0.65	0.02	0	0.07	1.33
FRZB	0.18	0.35	0.25	0.09	0	0.27	1.13
PLA2G2A	0	0.21	0.1	0.02	0.73	0.04	1.09
SFRP4	0	0.15	0.83	0.02	0	0.06	1.06
NPPA	0.11	0.18	0.36	0.06	0	0.1	0.8
MYOT	0	0.11	0.64	0.01	0	0.03	0.79
ASPN	0.09	0.27	0.27	0.02	0	0.08	0.74
ANKRD2	0.27	0.18	0.09	0.07	0	0.1	0.7
MXRA5	0	0.07	0.46	0	0	0.02	0.55
HBB	0.1	0.11	0.3	0.02	0	0.03	0.55
IL1RL1	0	0.29	0.08	0.01	0	0.07	0.46
S100A8	0	0.07	0.34	0	0	0.04	0.46
CYP4B1	0.06	0.16	0.11	0.02	0	0.05	0.39
VSIG4	0	0.16	0.05	0	0	0.02	0.24
SERPINE1	0	0.08	0.08	0	0	0.02	0.18

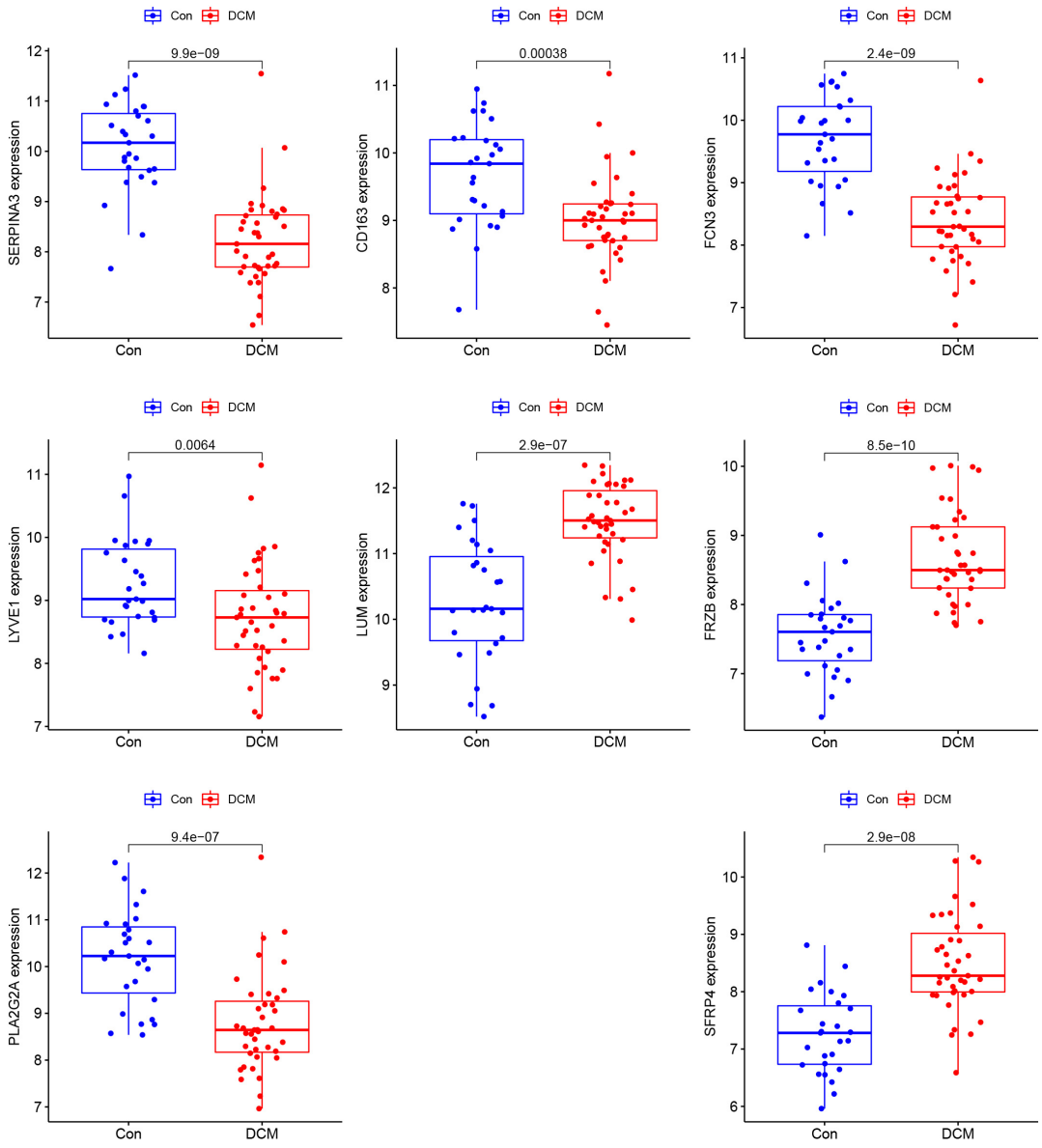

FIGURE 5
The comparison of the 8 genes between dilated cardiomyopathy (DCM) and healthy in testing sets.

previous study identified that spironolactone and lisinopril can downregulate SERPINA3 and treat mice with Duchenne muscular dystrophy, which suggests that SERPINA3 may be related to the salt corticosteroid receptor (48). Another study (49) came to a similar conclusion, *SERPINA3* was both upregulated *in vivo* (mice of mineralocorticoid receptor cardiac upregulation) and *in vitro* (H9C2 cells with aldosterone 24 h). The above studies indicated that the up-regulated of *SERPINA3* might be correlated with the mineralocorticoid receptor. However, few studies pay attention to DCM to our knowledge. And this work emphasizes the important role of *SERPINA3* in DCM.

FRZB, sFRP3 also named, is one of a frizzled-related proteins (FRPs) family (the other three were *sFRP-1*, *sFRP-2*, and *sFRP-4*). The *sFRP-3* and 4, can modulate apoptosis susceptibility in ventricular myocytes (50). However, though a previous study indicated that FRP contributed to the pathogenesis of DCM by down-regulated Wnt/β-catenin signaling pathway (51), no description of which of the four subtypes is associated. In DCM children (52), the serum circulating sFRP1 will trigger ventricular remodeling and cardiomyocyte fibrosis. And *sFRP-1* knockout mice (53) indicated an abnormal cardiac structure present with increasing age. And the *sFRP2* can prevent the conversion of inflammatory precursor components and the

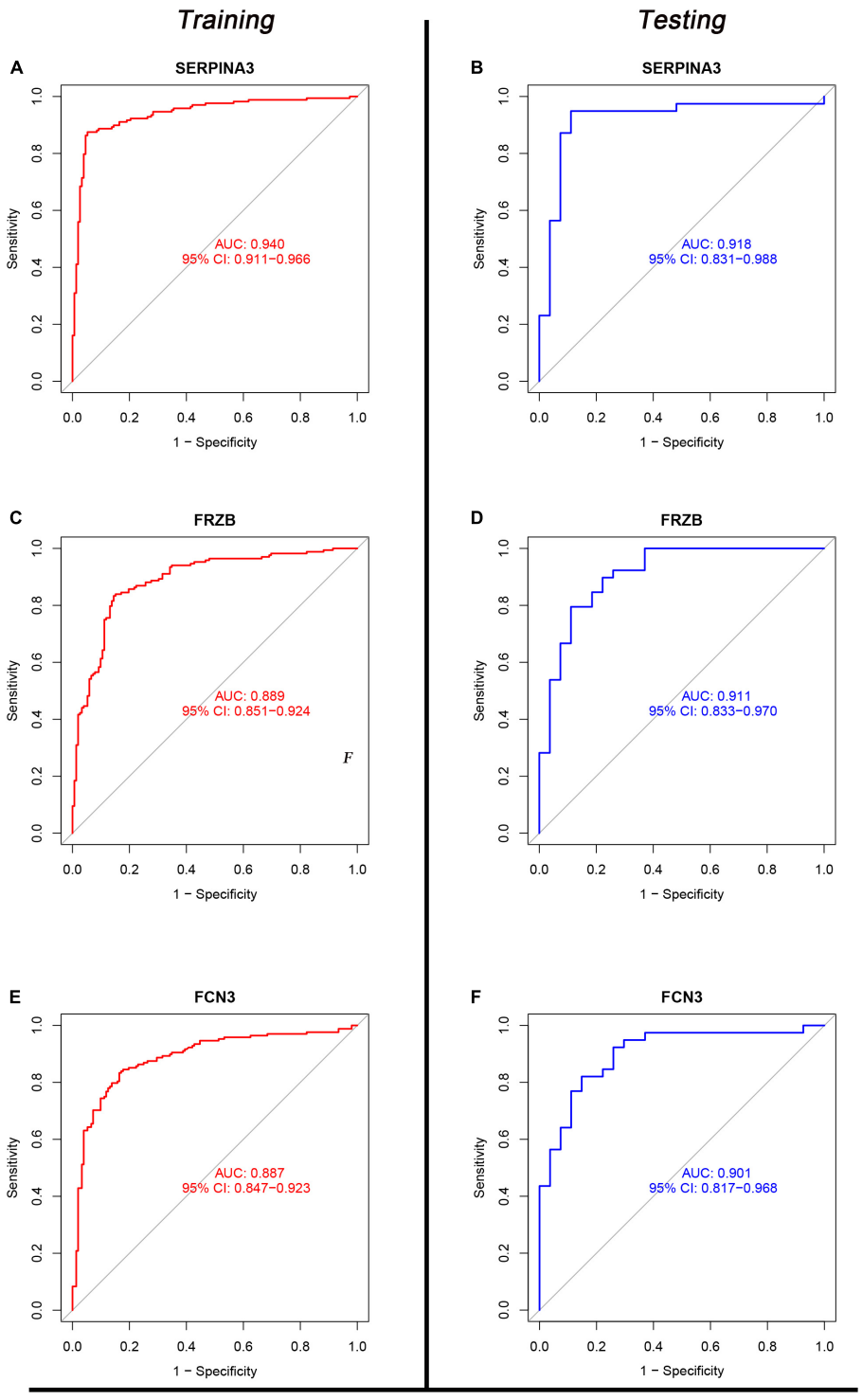

FIGURE 6
The receiver operating characteristic (ROC) of SERPINA3, FRZB, and FCN3 between the control and dilated cardiomyopathy (DCM) groups. **(A,C,E)** The ROC of SERPINA3, FRZB, and FCN3 in the Training set; **(B,D,F)** the ROC of SERPINA3, FRZB, and FCN3 in the testing set.

transformation of cardiomyocytes to pathogenic myofibroblasts (54) in DCM. However, no studies emphasized the function of FRZB in DCM, especially in plasma circulation. And our work first reported the diagnosis value of RZB in DCM. Furthermore, this work identified the significant upregulation of the circulation of FRZB protein in DCM.

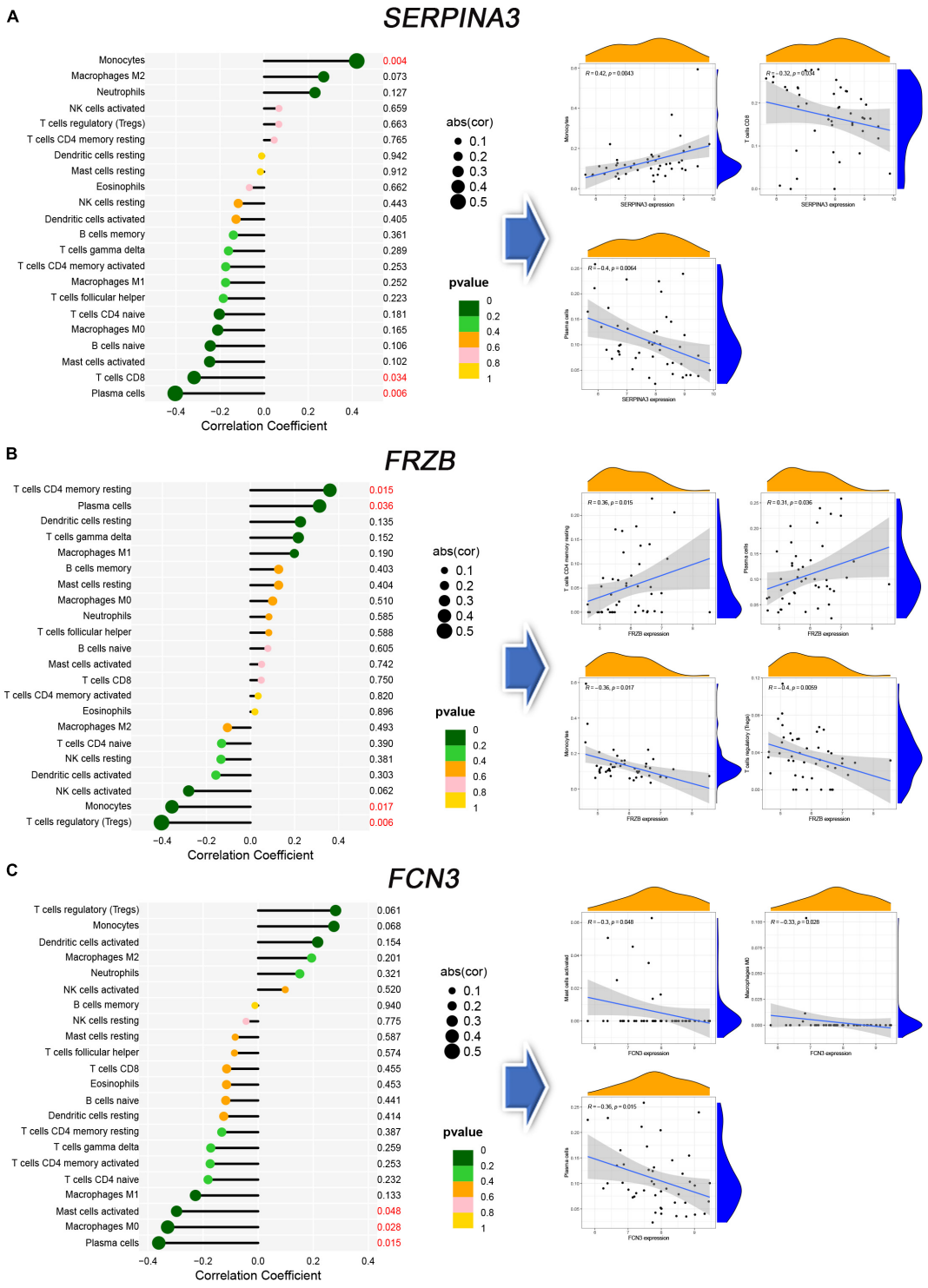

FIGURE 7
The immune correlation between diagnosis genes and immune cells. **(A–C)** The lollipop map and linear regression map in SERPINA3, FRAB, and FCN3.

FCN3, ficolin 3, was the most effective activator of the lectin pathway of complement (55) and more focus in rheumatic heart disease (56, 57). The *FCN3* is inversely associated with the severity of HF (58). Furthermore, lower *FCN3* is associated with the severity and outcome of HF (59). In congenital heart disease (60), the protein of FCN3 may prolong bleeding time and

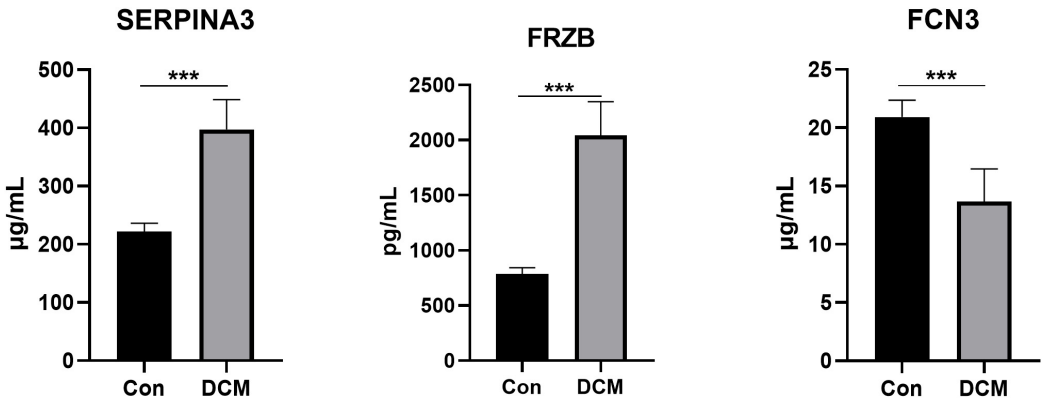

FIGURE 8
The plasma levels of SERPINA3, FRZB, and FCN3 in dilated cardiomyopathy (DCM) patients and healthy controls. ***Mean $P < 0.001$.

increase susceptibility to lung infection in the Fallot. However, few studies contribute to DCM. And our work first reported the diagnosis value of FCN3 in DCM. Furthermore, this work identified the significant downregulation of the circulation FCN3 protein in DCM.

Some limitations exist in our work. At first, inadequate validation is a common limitation in bioinformatics research. To decrease inadequate validation, three methods were taken, increase the sample size, developed the testing sets, and add little sample size clinical validation. However, additional studies should be conducted to validate, including but not limited to large sample size clinical trials or animal experiments for reliable verification of our predicted results. Secondly, MLs models exists some inevitable limitations, such as black box phenomenon (61), especially in NN (62) which contains various layers (e.g., an input layer, an output layer, and several hidden layers). Finally, few clinical features can be obtained, such as the age (63) or race (64) of the patient, which might trigger the bias of the result. In summary, further subgroup analyses are expected to assess more valuable conclusions in future works.

5. Conclusion

The overall weights methods for the filtration of genes in six MLs were developed, and we successfully found validation of three diagnosis genes, *SERPINA3*, *FRZB*, and *FCN3*. Further verification work could be implemented.

Data availability statement

The datasets presented in this study can be found in online repositories. The names of the repository/repositories and accession number(s) can be found below: https://www.ncbi.nlm.nih.gov/geo/query/acc.cgi?acc=GSE5406; https://www.ncbi.nlm.nih.gov/geo/query/acc.cgi?acc=GSE57338; https://www.ncbi.nlm.nih.gov/geo/query/acc.cgi?acc=GSE1145; https://www.ncbi.nlm.nih.gov/geo/query/acc.cgi?acc=GSE1869; https://www.ncbi.nlm.nih.gov/geo/query/acc.cgi?acc=GSE3585; and https://www.ncbi.nlm.nih.gov/geo/query/acc.cgi?acc=GSE42955.

Ethics statement

The studies involving human participants were reviewed and approved by Ethics Review Committee Jinghai District Hospital. The patients/participants provided their written informed consent to participate in this study.

Author contributions

LZ and YL: conceptualization, investigation, and data curation. LZ and KW: methodology. LZ: software and writing—original draft preparation. YL, KW, LZ, LH, HY, XF, XG, and JZ: validation. KW: writing—review and editing. ZL, HY, and XF: supervision. HZ and LH: project administration. HY: funding acquisition. All authors contributed to the article and approved the submitted version.

Funding

We are grateful for the foundation of the Science and Technology Program of Tianjin (No. 22ZYJDSS00100).

Acknowledgments

We thank for the support from the Tianjin University of Traditional Chinese Medicine.

Conflict of interest

The authors declare that the research was conducted in the absence of any commercial or financial relationships that could be construed as a potential conflict of interest.

Publisher's note

All claims expressed in this article are solely those of the authors and do not necessarily represent those of their affiliated organizations, or those of the publisher, the editors and the reviewers. Any product that may be evaluated in this article, or claim that may be made by its manufacturer, is not guaranteed or endorsed by the publisher.

Supplementary material

The Supplementary Material for this article can be found online at: https://www.frontiersin.org/articles/10.3389/fcvm.2022.1044443/full#supplementary-material

References

1. Elmarakeby H, Hwang J, Arafeh R, Crowdis J, Gang S, Liu D, et al. Biologically informed deep neural network for prostate cancer discovery. *Nature.* (2021) 598:348–52. doi: 10.1038/s41586-021-03922-4

2. Frazer J, Notin P, Dias M, Gomez A, Min J, Brock K, et al. Disease variant prediction with deep generative models of evolutionary data. *Nature.* (2021) 599:91–5. doi: 10.1038/s41586-021-04043-8

3. Cawley G, Talbot N. Gene selection in cancer classification using sparse logistic regression with bayesian regularization. *Bioinformatics.* (2006) 22:2348–55. doi: 10.1093/bioinformatics/btl386

4. Han L, van Hemert J, Baldock R. Automatically identifying and annotating mouse embryo gene expression patterns. *Bioinformatics.* (2011) 27:1101–7. doi: 10.1093/bioinformatics/btr105

5. Kouyos R, von Wyl V, Hinkley T, Petropoulos C, Haddad M, Whitcomb J, et al. Assessing predicted Hiv-1 replicative capacity in a clinical setting. *PLoS Pathog.* (2011) 7:e1002321. doi: 10.1371/journal.ppat.1002321

6. Montisci A, Palmieri V, Vietri M, Sala S, Maiello C, Donatelli F, et al. Big data in cardiac surgery: real world and perspectives. *J Cardiothorac Surg.* (2022) 17:277. doi: 10.1186/s13019-022-02025-z

7. Vo Ngoc L, Huang C, Cassidy C, Medrano C, Kadonaga J. Identification of the human Dpr core promoter element using machine learning. *Nature.* (2020) 585:459–63. doi: 10.1038/s41586-020-2689-7

8. Yan J, Qiu Y, Ribeiro Dos Santos A, Yin Y, Li Y, Vinckier N, et al. Systematic analysis of binding of transcription factors to noncoding variants. *Nature.* (2021) 591:147–51. doi: 10.1038/s41586-021-03211-0

9. Dutta A, Goldman T, Keating J, Burke E, Williamson N, Dirmeier R, et al. Machine learning predicts biogeochemistry from microbial community structure in a complex model system. *Microbiol Spectr.* (2022) 10:e0190921. doi: 10.1128/spectrum.01909-21

10. Bouraffa T, Yan L, Feng Z, Xiao B, Wu Q, Xia Y. Context-aware correlation filter learning toward peak strength for visual tracking. *IEEE Trans Cybern.* (2021) 51:5105–15. doi: 10.1109/tcyb.2019.2935347

11. Wen J, Wang G, Xie X, Lin G, Yang H, Luo K, et al. Prognostic value of a four-mirna signature in patients with lymph node positive locoregional esophageal squamous cell carcinoma undergoing complete surgical resection. *Ann Surg.* (2021) 273:523–31. doi: 10.1097/sla.0000000000003369

12. Koga S, Zhou X, Dickson D. Machine learning-based decision tree classifier for the diagnosis of progressive supranuclear palsy and corticobasal degeneration. *Neuropathol Appl Neurobiol.* (2021) 47:931–41. doi: 10.1111/nan.12710

13. Wysocki A, Rhemtulla M. On penalty parameter selection for estimating network models. *Multivariate Behav Res.* (2021) 56:288–302. doi: 10.1080/00273171.2019.1672516

14. Crabtree N, Moore J, Bowyer J, George N. Multi-class computational evolution: development, Benchmark evaluation and application to Rna-Seq biomarker discovery. *Biodata Min.* (2017) 10:13. doi: 10.1186/s13040-017-0134-8

15. Li C, Wang J, Ge L, Zhou Y, Zhou S. Optimization of sample construction based on Ndvi for cultivated land quality prediction. *Int J Environ Res Public Health.* (2022) 19:7781. doi: 10.3390/ijerph19137781

16. Zhao S, Dong X, Shen W, Ye Z, Xiang R. Machine learning-based classification of diffuse large B-Cell lymphoma patients by eight gene expression profiles. *Cancer Med.* (2016) 5:837–52. doi: 10.1002/cam4.650

17. He Y, Ma J, Ye XA. Support vector machine classifier for the prediction of osteosarcoma metastasis with high accuracy. *Int J Mol Med.* (2017) 40:1357–64. doi: 10.3892/ijmm.2017.3126

18. Li C, Zeng X, Yu H, Gu Y, Zhang W. Identification of hub genes with diagnostic values in pancreatic cancer by bioinformatics analyses and supervised learning methods. *World J Surg Oncol.* (2018) 16:223. doi: 10.1186/s12957-018-1519-y

19. Zhang L, Mao R, Lau C, Chung W, Chan J, Liang F, et al. Identification of useful genes from multiple microarrays for ulcerative colitis diagnosis based on machine learning methods. *Sci Rep.* (2022) 12:9962. doi: 10.1038/s41598-022-14048-6

20. Liu Z, Li H, Pan S. Discovery and validation of key biomarkers based on immune infiltrates in Alzheimer's disease. *Front Genet.* (2021) 12:658323. doi: 10.3389/fgene.2021.658323

21. Lu M, Qiu S, Jiang X, Wen D, Zhang R, Liu Z. Development and validation of epigenetic modification-related signals for the diagnosis and prognosis of hepatocellular carcinoma. *Front Oncol.* (2021) 11:649093. doi: 10.3389/fonc.2021.649093

22. Yao Y, Zhao J, Zhou X, Hu J, Wang Y. Potential role of a three-gene signature in predicting diagnosis in patients with myocardial infarction. *Bioengineered.* (2021) 12:2734–49. doi: 10.1080/21655979.2021.1938498

23. Yu J, Zhu M, Lv M, Wu X, Zhang X, Zhang Y, et al. Characterization of a five-microrna signature as a prognostic biomarker for esophageal squamous cell carcinoma. *Sci Rep.* (2019) 9:19847. doi: 10.1038/s41598-019-56367-1

24. Wang K, Zhang L, Li L, Wang Y, Zhong X, Hou C, et al. Identification of drug-induced liver injury biomarkers from multiple microarrays based on machine learning and bioinformatics analysis. *Int J Mol Sci.* (2022) 23:11945. doi: 10.3390/ijms231911945

25. McDonagh T, Metra M, Adamo M, Gardner R, Baumbach A, Böhm M, et al. 2021 Esc guidelines for the diagnosis and treatment of acute and chronic heart failure. *Eur Heart J.* (2021) 42:3599–726. doi: 10.1093/eurheartj/ehab368

26. Heidenreich P, Bozkurt B, Aguilar D, Allen L, Byun J, Colvin M, et al. 2022 Aha/Acc/Hfsa guideline for the management of heart failure: a report of the American College of Cardiology/American Heart Association joint committee on clinical practice guidelines. *Circulation.* (2022) 145:e895–1032. doi: 10.1161/cir.0000000000001063

27. Writing Group For Practice Guidelines For Diagnosis and Treatment Of Genetic Diseases Medical Genetics Branch Of Chinese Medical Association, Sun J, Han S, Hu J, Jiang C, Wang Q, et al. [Clinical practice guidelines for hereditary cardiomyopathy]. *Zhonghua Yi Xue Yi Chuan Xue Za Zhi.* (2020) 37:300–7. doi: 10.3760/cma.j.issn.1003-9406.2020.03.013

28. Abdel-Salam Z, Rayan M, Saleh A, Abdel-Barr M, Hussain M, Nammas W. I(F) current inhibitor ivabradine in patients with idiopathic dilated cardiomyopathy: impact on the exercise tolerance and quality of life. *Cardiol J.* (2015) 22:227–32. doi: 10.5603/CJ.a2014.0057

29. Nakano S, Miyamoto S, Movsesian M, Nelson P, Stauffer B, Sucharov C. Age-related differences in phosphodiesterase activity and effects of chronic phosphodiesterase inhibition in idiopathic dilated cardiomyopathy. *Circ Heart Fail.* (2015) 8:57–63. doi: 10.1161/circheartfailure.114.001218

30. Zhao C, Bing S, Song H, Wang J, Xu W, Jiang J, et al. Tbx20 loss-of-function mutation associated with familial dilated cardiomyopathy. *Clin Chem Lab Med.* (2016) 54:325–32. doi: 10.1515/cclm-2015-0328

31. Zhao J, Yin M, Deng H, Jin F, Xu S, Lu Y, et al. Cardiac Gab1 deletion leads to dilated cardiomyopathy associated with mitochondrial damage and cardiomyocyte apoptosis. *Cell Death Differ.* (2016) 23:695–706. doi: 10.1038/cdd.2015.143

32. Zhou L, Liu C, Zou Y, Chen Z. Development and verification of the nomogram for dilated cardiomyopathy gene diagnosis. *Sci Rep.* (2022) 12:8908. doi: 10.1038/s41598-022-13135-y

33. Wang Y, Guan Q, Lao I, Wang L, Wu Y, Li D, et al. Using deep convolutional neural networks for multi-classification of thyroid tumor by histopathology: a large-scale pilot study. *Ann Transl Med.* (2019) 7:468. doi: 10.21037/atm.2019.08.54

34. Radulescu E, Jaffe A, Straub R, Chen Q, Shin J, Hyde T, et al. Identification and prioritization of gene sets associated with schizophrenia risk by co-expression network analysis in human brain. *Mol Psychiatry.* (2020) 25:791–804. doi: 10.1038/s41380-018-0304-1

35. Choi B, Bair E, Lee J. Nearest shrunken centroids via alternative genewise shrinkages. *PLoS One.* (2017) 12:e0171068. doi: 10.1371/journal.pone.0171068

36. Dreiseitl S, Ohno-Machado L, Kittler H, Vinterbo S, Billhardt H, Binder MA. Comparison of machine learning methods for the diagnosis of pigmented skin lesions. *J Biomed Inform.* (2001) 34:28–36. doi: 10.1006/jbin.2001.1004

37. Chiew C, Liu N, Wong T, Sim Y, Abdullah H. Utilizing machine learning methods for preoperative prediction of postsurgical mortality and intensive care unit admission. *Ann Surg.* (2020) 272:1133–9. doi: 10.1097/sla.0000000000003297

38. Dang H, Ye Y, Zhao X, Zeng Y. Identification of candidate genes in ischemic cardiomyopathy by gene expression omnibus database. *BMC Cardiovasc Disord.* (2020) 20:320. doi: 10.1186/s12872-020-01596-w

39. Asakura M, Kitakaze M. Global gene expression profiling in the failing myocardium. *Circ J.* (2009) 73:1568–76. doi: 10.1253/circj.cj-09-0465

40. Yang Y, Liu P, Teng R, Liu F, Zhang C, Lu X, et al. Integrative bioinformatics analysis of potential therapeutic targets and immune infiltration characteristics in dilated cardiomyopathy. *Ann Transl Med.* (2022) 10:348. doi: 10.21037/atm-22-732

41. Li D, Lin H, Li L. Multiple feature selection strategies identified novel cardiac gene expression signature for heart failure. *Front Physiol.* (2020) 11:604241. doi: 10.3389/fphys.2020.604241

42. Meijers W, Maglione M, Bakker S, Oberhuber R, Kieneker L, de Jong S, et al. Heart failure stimulates tumor growth by circulating factors. *Circulation.* (2018) 138:678–91. doi: 10.1161/circulationaha.117.030816

43. Delrue L, Vanderheyden M, Beles M, Paolisso P, Di Gioia G, Dierckx R, et al. Circulating Serpina3 improves prognostic stratification in patients with a de novo or worsened heart failure. *ESC Heart Fail.* (2021) 8:4780–90. doi: 10.1002/ehf2.13659

44. Bell S, Adkisson D, Lawson M, Wang L, Ooi H, Sawyer D, et al. Antifailure therapy including spironolactone improves left ventricular energy supply-demand relations in nonischemic dilated cardiomyopathy. *J Am Heart Assoc.* (2014) 3:e000883. doi: 10.1161/jaha.114.000883

45. Nakagawa H, Oberwinkler H, Nikolaev V, Gaßner B, Umbenhauer S, Wagner H, et al. Atrial natriuretic peptide locally counteracts the deleterious effects of cardiomyocyte mineralocorticoid receptor activation. *Circ Heart Fail.* (2014) 7:814–21. doi: 10.1161/circheartfailure.113.000885

46. Verma A, Wulffhart Z, Lakkireddy D, Khaykin Y, Kaplan A, Sarak B, et al. Incidence of left ventricular function improvement after primary prevention Icd implantation for non-ischaemic dilated cardiomyopathy: a multicentre experience. *Heart.* (2010) 96:510–5. doi: 10.1136/hrt.2009.178061

47. Wang Y, Xu Y, Zou R, Wu L, Liu P, Yang H, et al. Effect of levocarnitine on the therapeutic efficacy of conventional therapy in children with dilated cardiomyopathy: results of a randomized trial in 29 children. *Paediatr Drugs.* (2018) 20:285–90. doi: 10.1007/s40272-018-0284-2

48. Chadwick J, Hauck J, Lowe J, Shaw J, Guttridge D, Gomez-Sanchez C, et al. Mineralocorticoid receptors are present in skeletal muscle and represent a potential therapeutic target. *FASEB J.* (2015) 29:4544–54. doi: 10.1096/fj.15-276782

49. Latouche C, Sainte-Marie Y, Steenman M, Castro Chaves P, Naray-Fejes-Toth A, Fejes-Toth G, et al. Molecular signature of mineralocorticoid receptor signaling in cardiomyocytes: from cultured cells to mouse heart. *Endocrinology.* (2010) 151:4467–76. doi: 10.1210/en.2010-0237

50. Schumann H, Holtz J, Zerkowski H, Hatzfeld M. Expression of secreted frizzled related proteins 3 and 4 in human ventricular myocardium correlates with apoptosis related gene expression. *Cardiovasc Res.* (2000) 45:720–8. doi: 10.1016/s0008-6363(99)00376-4

51. Le Dour C, Macquart C, Sera F, Homma S, Bonne G, Morrow J, et al. Decreased Wnt/B-catenin signalling contributes to the pathogenesis of dilated cardiomyopathy caused by mutations in the Lamin a/C gene. *Hum Mol Genet.* (2017) 26:333–43. doi: 10.1093/hmg/ddw389

52. Jeffrey D, Pires Da Silva J, Garcia A, Jiang X, Karimpour-Fard A, Toni L, et al. Serum circulating proteins from pediatric patients with dilated cardiomyopathy cause pathologic remodeling and cardiomyocyte stiffness. *JCI Insight.* (2021) 6:e148637. doi: 10.1172/jci.insight.148637

53. Sklepkiewicz P, Shiomi T, Kaur R, Sun J, Kwon S, Mercer B, et al. Loss of secreted frizzled-related protein-1 leads to deterioration of cardiac function in mice and plays a role in human cardiomyopathy. *Circ Heart Fail.* (2015) 8:362–72. doi: 10.1161/circheartfailure.114.001274

54. Blyszczuk P, Müller-Edenborn B, Valenta T, Osto E, Stellato M, Behnke S, et al. Transforming growth factor-B-dependent Wnt secretion controls myofibroblast formation and myocardial fibrosis progression in experimental autoimmune myocarditis. *Eur Heart J.* (2017) 38:1413–25. doi: 10.1093/eurheartj/ehw116

55. Michalski M, Świerzko A, Pągowska-Klimek I, Niemir Z, Mazerant K, Domżalska-Popadiuk I, et al. Primary ficolin-3 deficiency–is it associated with increased susceptibility to infections? *Immunobiology.* (2015) 220:711–3. doi: 10.1016/j.imbio.2015.01.003

56. Beltrame M, Catarino S, Goeldner I, Boldt A, de Messias-Reason I. The lectin pathway of complement and rheumatic heart disease. *Front Pediatr.* (2014) 2:148. doi: 10.3389/fped.2014.00148

57. Elshamaa M, Hamza H, El Rahman N, Emam S, Elghoroury E, Farid T, et al. Association of Ficolin-2 (Fcn2) functional polymorphisms and protein levels with rheumatic fever and rheumatic heart disease: relationship with cardiac function. *Arch Med Sci Atheroscler Dis.* (2018) 3:e142–55. doi: 10.5114/amsad.2018.80999

58. Li H, Zhang F, Zhang D, Tian X. Changes of serum ficolin-3 and C5b-9 in patients with heart failure. *Pak J Med Sci.* (2021) 37:1860–4. doi: 10.12669/pjms.37.7.4151

59. Prohászka Z, Munthe-Fog L, Ueland T, Gombos T, Yndestad A, Förhécz Z, et al. Association of Ficolin-3 with severity and outcome of chronic heart failure. *PLoS One.* (2013) 8:e60976. doi: 10.1371/journal.pone.0060976

60. Xuan C, Gao G, Yang Q, Wang X, Liu Z, Liu X, et al. Proteomic study reveals plasma protein changes in congenital heart diseases. *Ann Thorac Surg.* (2014) 97:1414–9. doi: 10.1016/j.athoracsur.2013.11.069

61. Regazzoni F, Chapelle D, Moireau P. Combining data assimilation and machine learning to build data-driven models for unknown long time dynamics-applications in cardiovascular modeling. *Int J Numer Method Biomed Eng.* (2021) 37:e3471. doi: 10.1002/cnm.3471

62. Peng J, Ran Z, Shen J. Seasonal variation in onset and relapse of Ibd and a model to predict the frequency of onset, relapse, and severity of Ibd based on artificial neural network. *Int J Colorectal Dis.* (2015) 30:1267–73. doi: 10.1007/s00384-015-2250-6

63. Kalkan I, Dağli U, Oztaş E, Tunç B, Ulker A. Comparison of demographic and clinical characteristics of patients with early Vs. adult Vs. late onset ulcerative colitis. *Eur J Intern Med.* (2013) 24:273–7. doi: 10.1016/j.ejim.2012.12.014

64. Jiang L, Xia B, Li J, Ye M, Deng C, Ding Y, et al. Risk factors for ulcerative colitis in a Chinese population: an age-matched and sex-matched case-control study. *J Clin Gastroenterol.* (2007) 41:280–4. doi: 10.1097/01.mcg.0000225644.75651.f1

frontiers | Frontiers in Cardiovascular Medicine

TYPE Mini Review
PUBLISHED 19 January 2023
DOI 10.3389/fcvm.2023.1114459

OPEN ACCESS

EDITED BY
John Lynn Jefferies,
The University of Tennessee Health Science Center (UTHSC), United States

REVIEWED BY
Andrew A. Gibb,
Temple University, United States
Emma Louise Robinson,
University of Colorado, United States
Kyung Chan Park,
University of Oxford, United Kingdom

*CORRESPONDENCE
Jiayi Pei
j.pei-2@umcutrecht.nl

SPECIALTY SECTION
This article was submitted to Cardiovascular Genetics and Systems Medicine, a section of the journal Frontiers in Cardiovascular Medicine

RECEIVED 02 December 2022
ACCEPTED 03 January 2023
PUBLISHED 19 January 2023

CITATION
Gaar-Humphreys KR, van den Brink A, Wekking M, Asselbergs FW, van Steenbeek FG, Harakalova M and Pei J (2023) Targeting lipid metabolism as a new therapeutic strategy for inherited cardiomyopathies.
Front. Cardiovasc. Med. 10:1114459.
doi: 10.3389/fcvm.2023.1114459

Targeting lipid metabolism as a new therapeutic strategy for inherited cardiomyopathies

Karen R. Gaar-Humphreys[1,2], Alyssa van den Brink[1,2], Mark Wekking[1,2], Folkert W. Asselbergs[3,4], Frank G. van Steenbeek[1,2,5], Magdalena Harakalova[1,2,6] and Jiayi Pei[1,2,6]*

[1]Division Heart and Lungs, Department of Cardiology, Circulatory Health Research Center, University Medical Center Utrecht, Utrecht University, Utrecht, Netherlands, [2]Regenerative Medicine Center Utrecht, University Medical Center Utrecht, Utrecht, Netherlands, [3]Department of Cardiology, Amsterdam University Medical Centers, University of Amsterdam, Amsterdam, Netherlands, [4]Health Data Research United Kingdom and Institute of Health Informatics, University College London, London, United Kingdom, [5]Department of Clinical Sciences, Faculty of Veterinary Medicine, Utrecht University, Utrecht, Netherlands, [6]Netherlands Heart Institute, Utrecht, Netherlands

Inherited cardiomyopathies caused by pathological genetic variants include multiple subtypes of heart disease. Advances in next-generation sequencing (NGS) techniques have allowed for the identification of numerous genetic variants as pathological variants. However, the disease penetrance varies among mutated genes. Some can be associated with more than one disease subtype, leading to a complex genotype-phenotype relationship in inherited cardiomyopathies. Previous studies have demonstrated disrupted metabolism in inherited cardiomyopathies and the importance of metabolic adaptations in disease onset and progression. In addition, genotype- and phenotype-specific metabolic alterations, especially in lipid metabolism, have been revealed. In this mini-review, we describe the metabolic changes that are associated with dilated cardiomyopathy (DCM) and hypertrophic cardiomyopathy (HCM), which account for the largest proportion of inherited cardiomyopathies. We also summarize the affected expression of genes involved in fatty acid oxidation (FAO) in DCM and HCM, highlighting the potential of PPARA-targeting drugs as FAO modulators in treating patients with inherited cardiomyopathies.

KEYWORDS

hypertrophic cardiomyopathy, dilated cardiomyopathy, genetic variants, lipid metabolism, fatty acid oxidation, transcription factor PPARA

Introduction

Inherited cardiomyopathies are diseases of the heart muscle due to pathological genetic variants. Based on the clinical presentations, they are often divided into four subtypes, namely, hypertrophic cardiomyopathy (HCM), dilated cardiomyopathy (DCM), arrhythmogenic cardiomyopathy (ACM), and restrictive cardiomyopathy (RCM) (1, 2). Among them, the estimated prevalence of DCM is the highest (1:250 individuals), followed by HCM (1:500 individuals) (3). Owing to the advances in next-generation sequencing (NGS) techniques, numerous genetic variants have been identified as disease-causing variants. To date, more than 60 mutated genes are associated with DCM, and they are involved in a wide range of cellular features, including the sarcomere, Z disk, cytoskeleton, sarcoplasmic reticulum and cytoplasm,

ion channels, and mitochondria (4). A subset of those mutated genes, such as *TTN*, *LMNA*, *MYH7*, and *PLN*, exhibits a stronger gene-disease relationship with DCM compared to the rest (5). Unlike the broad range of DCM-causal variants, most pathological variants in HCM affect sarcomeric genes (6). *MYH7* and *MYBPC3* are the most commonly affected genes in HCM, which account for about 70% of those variants (7). The disease penetrance varies among mutated genes, and the same mutated gene can be associated with more than one subtype (2, 8), leading to a complex genotype-phenotype relationship in inherited cardiomyopathies. Therefore, molecular insights into the affected pathways and biological processes concerning different variants and/or subtypes are needed to characterize the diseases better and provide druggable candidates for novel treatments.

Metabolic changes in inherited cardiomyopathies

The heart has a very high energy demand to fulfill its basic functions. Therefore, sufficient cardiac energy metabolism is crucial. In a healthy adult heart, over 95% of produced ATP is derived from mitochondrial oxidative phosphorylation, and this is predominantly by fatty acid oxidation (FAO) (9). However, a significant metabolic switch toward the less efficient anaerobic glycolytic metabolism occurs in failing hearts, which resembles the energy preference of the fetal heart (10, 11). The inefficiency in utilizing fatty acids results in the accumulation of lipid droplets, which subsequently lead to lipotoxicity and heart failure (12). In addition to lipid accumulation, failing hearts also exhibit impaired metabolic flexibility in switching between different energy substrates, including fatty acids, glucose, ketones, and amino acids (13). The lack of sufficient energy substrates due to prolonged fasting is, in fact, a known trigger for inherited cardiomyopathies (14). Taken together, both internal and external factors could affect cardiac performance and disease progression by disrupting metabolic homeostasis.

Cardiac tissues and plasma samples from patients carrying truncating *TTN* variants, which account for 15–20% of DCM populations, showed affected genes and metabolites involved in metabolic regulation when compared to DCM patients without *TTN* variants (15). This suggests a tight relationship between *TTN* variants and metabolic alterations. In addition, murine and human DCM hearts carrying a *PLN* variant showed suppressed mitochondrial fatty acid metabolism at mRNA and protein levels (16, 17). Suppressed metabolic genes and mitochondrial enzyme activities were also observed in 2D and 3D human induced pluripotent stem cell-derived cardiomyocytes harboring a mutated *PLN* gene (18). Multiple omics-based studies showed changes in metabolite levels, such as glutamine, lactate, and acylcarnitines, in DCM patients when compared to healthy individuals and patients with ischemic cardiomyopathy (19–21). Additionally, the metabolic changes correlated with the disease severity (19, 22). Therefore, metabolites involved in metabolic signaling, such as branched-chain amino acid metabolism, glycolysis, and glycolipid metabolism, have been proposed as potential biomarkers for DCM patients (23, 24). In line with these findings, clinical measurements using cardiac magnetic resonance imaging and positron emission tomography scanning also revealed an impaired oxidative metabolism and the subsequent energy starvation mode in DCM (12, 25). Additionally, DCM-related genetic variants, such as *LMNA* variants, show a direct influence on lipid metabolism (26). Besides the impaired fatty acid metabolism in DCM patients, individuals with FAO disorders also have a higher risk of developing DCM (27). These findings indicate a bi-directional association between DCM and impaired fatty acid metabolism. A recent study showed improved contractility and mitochondrial respiration in cardiomyocytes with various DCM-causing variants, including mutated *PLN*, *TNNT2*, *TTN*, *LMNA*, *TPM1*, and *LAMA2*, by enhancing serine metabolism (28). Serine is a non-essential amino acid and decreased serine availability has been shown to suppress mitochondrial FAO, glucose and glutamine metabolism (29), highlighting the tightly associated metabolic pathways and the promising metabolic-based treatment strategies in DCM.

High energy demand is required in HCM due to the associated hypercontractility (30). Unlike the decreased power cycle (duty ratio) and a lower force-holding capacity in DCM mutations when compared to the wildtype controls, which require much less ATP, HCM mutations exhibit an increased power cycle and a higher force-holding capacity, leading to a higher ATP usage (31). Therefore, alterations in metabolism show a profound impact on HCM pathogenesis. Additionally, in contrast to the decreased Ca^{2+} sensitivity in DCM, increased Ca^{2+} sensitivity and cytosolic adenosine diphosphate (ADP) levels are seen in HCM due to sarcomeric variants, resulting in metabolic changes (32). Increased cytosolic ADP increases the oxidation of two metabolic enzymes (NADH and NADPH), which decreases the capacity to attenuate mitochondrial reactive oxygen species (ROS) levels, as NADPH is necessary to detoxify ROS (30). Increased ROS subsequently impairs mitochondrial activation and contributes to HCM development (33). Additionally, reduced phosphocreatine (PCr)/ATP ratios in HCM, both with and without hypertrophy, indicate cardiac energetic impairments are present at an early stage of HCM (34). The switch from FAO to glucose consumption is seen in hypertrophied hearts, along with a decreased expression of CD36, a key lipid transporter (35, 36). Multiple omics-based studies comparing HCM patients to controls further revealed alterations of molecular signatures involved in a wide array of pathways suggesting fatty acid metabolism dysregulation, a reduction of acylcarnitines, and an accumulation of free fatty acids (37–39). A recent study using adult cultured rat cardiomyocytes also demonstrated that increased glucose consumption is necessary for synthesizing aspartate, which directly drives cardiomyocyte hypertrophy (40). Mouse hearts carrying mutated *MYH6*, one of the HCM-causal genes (41), showed decreased mitochondrial ATP hydrolysis (42). Additionally, a high prevalence of HCM is observed among patients with mitochondrial diseases, and several mutated mitochondrial genes are known to contribute to HCM development, such as *HADHB* (14, 43). Taken together, impaired mitochondrial lipid metabolism and the switch to glycolysis are important for HCM initiation and progression. Therefore, the potential of various metabolic compounds is currently being studied in HCM, such as perhexiline (44, 45), mavacamten (46, 47), omecamtiv mecarbil (46), and ROS scavengers (48–50). Their efficacy, however, is still to be determined.

Besides DCM and HCM, metabolic disturbances are also observed in ACM and RCM. By comparing the transcriptional landscapes between ACM and control human hearts, affected

genes were enriched for several metabolic signaling, including mitochondrial dysfunction and oxidative phosphorylation (51). By comparing the plasma metabolomes between ACM patients and healthy individuals, affected metabolites and lipids further revealed several changed metabolic pathways, including lysine degradation, tryptophan metabolism, and the beta-oxidation of fatty acids (52). A recent paper compared transcriptional changes in RCM, ischemic heart disease, and valvular heart disease to control human hearts and showed that ATP metabolic processes were enriched by altered genes in RCM but not in the other two heart diseases (53). Combined, these findings highlighted the potential benefits of restoring a balanced metabolism in inherited cardiomyopathies.

Shared and unique metabolic alterations between DCM and HCM

As a result of the recent studies indicating impaired metabolism in inherited cardiomyopathies, attention has been drawn to studying and identifying precise metabolic branches and key drivers of disease pathogenesis per subtype. In general, both DCM and HCM exhibit decreased lipid metabolism (30, 54) and increased glucose metabolism (12, 55; **Figure 1A**). Besides these two major metabolic processes, enhanced ketone body metabolism is also shown in DCM and HCM (56, 57). Interestingly, suppressed oxidative metabolism, amino acid metabolism, pentose phosphate pathway, and nucleotide metabolism are observed in DCM (58–61), whereas they are all elevated in HCM (19, 62–65). A recent study further examined the metabolic alterations in DCM and HCM hearts as compared to non-failing control hearts at the global transcriptional level and demonstrated impaired metabolic signaling of fatty acids, carbohydrates, and amino acids in both DCM and HCM hearts (66). The study also investigated the single-nucleus transcriptome in cardiomyocytes and non-myocyte cell types and showed metabolic pathways were profoundly impaired in DCM cardiomyocytes but not HCM cardiomyocytes, suggesting the disease-specific metabolic alteration. Similarly, another paper also showed HCM- or DCM-specific impaired metabolic processes (67). Disease-specific gene sets, some of which are involved in lipid metabolism, were found to be differentially changed between DCM and HCM, such as the up-regulated *APOE* and the down-regulated *GPT* in DCM, as well as the up-regulated *APOLD1* and the down-regulated *STARD13* and *PON3* in HCM. In line with these findings, we also demonstrated that *KLF15*, an important transcription factor regulating lipid metabolism (68), was significantly up-regulated in HCM hearts carrying mutated *MYBPC3* and down-regulated in DCM hearts carrying mutated *PLN* when compared to non-failing donor hearts (16, 38). Besides the transcriptional level, proteins involved in metabolic pathways, including lipid transfer and fatty acid biosynthetic process, also showed DCM- and HCM-specific changes (69). To conclude, a profoundly impaired metabolism is well-characterized in inherited cardiomyopathies. Meanwhile, DCM- and HCM-specific metabolic alterations, particularly candidate genes in lipid metabolism, have also been cataloged.

The shared and unique metabolic signaling pathways and candidate genes have opened up new avenues to identify innovative compounds and design novel treatments for inherited cardiomyopathies in general but also for specific cardiomyopathy subtypes. For instance, mavacamten, a selective inhibitor of cardiac myosin ATPase that modulates ATP turnover time, exhibited a promising and beneficial effect on HCM patients (47, 70). FAO inhibitors and lipid-lowering agents have also been studied for treating DCM patients (71). The potential of SGLT2 inhibitors, which improve mitochondrial function, is currently under investigation in treating both DCM and HCM (72–74). Yet, the need for additional drugs targeting metabolism and mitochondrial function as the precision medicine for inherited cardiomyopathies has been urged by the Translational Committee of the Heart Failure Association and the Working Group of Myocardial Function of the European Society of Cardiology (75).

FAO alteration in DCM and HCM

Given FAO is severely impaired in both DCM and HCM, yet a subset of FAO-related genes might be unique for each subset, we searched for relevant studies that presented global transcriptional profiles using either RNA sequencing or microarray in DCM or HCM cohorts. We filtered for studies that were conducted using either human tissue or cells or experiments that were validated in a human model after animal experiments. In total, 10 relevant papers published between 2015 and 2022 were compiled and included for the purpose of this meta-analysis. Next, we collected 76 established genes that are involved in fatty acid beta-oxidation from the gene ontology project (GO:0006635). *KLF15* was added to the gene set due to its role in FAO and its unique alteration directions in DCM and HCM. Strikingly, almost all of the 77 genes were significantly differentially expressed between DCM and control hearts in one included paper, confirming the profoundly affected lipid metabolism in DCM (**Figure 1B**). Interestingly, altered expression patterns for some genes, such as *IRS1* and *CPT1A*, were contrasting between DCM and HCM, suggesting the disease subtype-specific differences in the FAO impairment. Besides, *HADHA* and *HADHB*, genes coding for key enzymes in mitochondrial FAO (76), showed generally suppressed mRNA levels in DCM and HCM, whereas *ACOX1*, *ACOX2*, and *ACOX3*, genes coding for key enzymes in peroxisomal FAO (77), showed increased mRNA levels in DCM but not in HCM. This further suggests disease subtype-specific differences in subcellular organelles-related FAO impairment. It is also important to note that some FAO-related genes showed contradicting expression patterns among different DCM-based or HCM-based studies. This could be partially explained by the heterogeneous genetic variants and their mutated genes, the different disease severities of included patients, and the variable group sizes of those studies. Therefore, studies with synchronized patient cohorts and well-characterized genetic information and clinical presentations are needed to address this complex gene-disease relationship. Protein-protein interaction analysis was performed using the genes found to be differentially expressed in DCM and HCM, respectively, to further elucidate their functional networks. Among these affected genes associated with FAO, biological processes, including the regulation of FAO (GO:0031998), mitochondrial FAO (HSA-77289), and peroxisome proliferator-activated receptor (PPAR) signaling pathway (WP3942, **Figure 1C**), remained significantly enriched in both DCM and HCM. PPARs are important upstream transcription

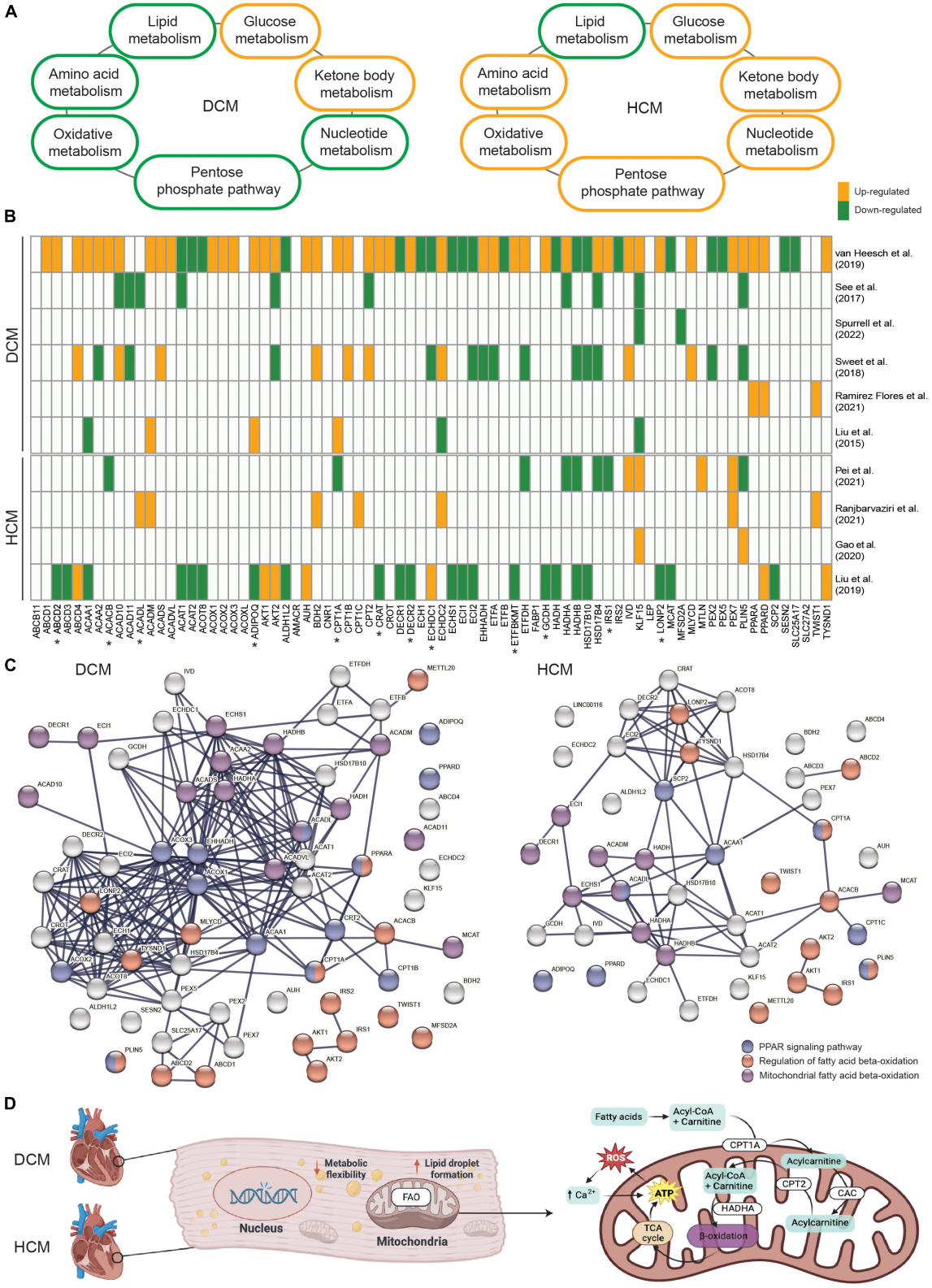

FIGURE 1

(A) An overview demonstrating the alteration direction of seven main metabolic processes in dilated cardiomyopathy (DCM) and hypertrophic cardiomyopathy (HCM). **(B)** The involvement and expression pattern of 77 protein-coding genes associated with fatty acid beta-oxidation (FAO) in DCM and HCM. Up-regulated genes in DCM or HCM vs. the controls are shown in orange, and down-regulated genes are shown in green. Genes that were either not significantly altered or not shown in the related paper were shown in white. Genes with opposite alteration directions between DCM and HCM are indicated by "*". **(C)** The enriched protein-protein interaction network in DCM and HCM, respectively. Highlighted genes involved in the regulation of FAO (red), mitochondrial-related FAO (purple), and the peroxisome proliferator-activated receptor (PPAR) signaling pathway (blue). **(D)** Schematic representation of mitochondrial FAO and its key regulators in inherited cardiomyopathies.

factors in regulating FAO and other facets of lipid metabolism and regulation (78). Notably, *PPARA* and *CPT1A* are shown in both the PPAR signaling pathway network and the regulation of FAO network. Both *ACADM* and *ACADL* overlap with the PPAR signaling pathway network and are involved with mitochondrial FAO.

PPARA-related FAO modulators as novel candidates for the treatment of inherited cardiomyopathies?

PPARA, PPARD, and PPARG are three isoforms of the peroxisome proliferator-activated receptors (PPARs), which are ligand-activated transcription factors. Since their DNA binding regions are highly similar, they show overlapping biological functions, especially in lipid metabolism (79). PPARA is a key regulator in modulating fatty acid uptake and FAO; PPARD enhances the utilization of lipids and glucose; and PPARY increases fatty acid uptake, triglyceride formation, and lipid storage (80). Notably, multiple studies from us and others have shown suppressed PPARA expressions in DCM and HCM hearts carrying different genetic variants (16, 81, 82). Additionally, the interaction between PPARA and KLF15 showed a significant impact on cardiac lipid metabolism (83).

The cardioprotective effects of ligand-activated PPARA have been reported, including the restored balance between fatty acid uptake and FAO, increased insulin sensitivity, reduced ROS production, and attenuated fibrosis formation (80, 84). Both natural ligands (i.e., omega-3 fatty acids) and synthetic ligands (i.e., fibrates), referred to as PPARA agonists (80), are commonly used to activate PPARA. Previous studies have summarized well-established PPARA agonists and those that are still in development (85–88), some of which are PPARA-specific. Several agonists, such as bezafibrate, ciprofibrate, clofibrate, and fenofibrate, have been FDA-approved for treating type 2 diabetes or dyslipidemia, and many more are under active research (80, 87). However, most research is focused on the application of fibrates as treatments for diseases such as primary biliary cholangitis, COVID-19, and non-alcoholic fatty liver disease (89–91), and limited studies have evaluated fibrates in inherited cardiomyopathies. A recent study using knockout-*Dsg2* ACM murine hearts showed that improved myocardial fibrosis was observed after the activation of PPARA by either fenofibrate treatment or adeno-associated virus injections of PPARA (92). Nevertheless, several clinical trials have investigated the effects of bezafibrate on mitochondrial disease, neutral lipid storage disease, muscle/mitochondrial FAO disorders, and Barth syndrome (93–99), which reflect impaired mitochondrial function, lipid accumulation, and heart failure as seen in cardiomyopathies. Therefore, the results obtained from these conducted trials might also shield light on its effect on inherited cardiomyopathies.

Conclusion

Metabolic homeostasis plays an important role in cardiac performance and disrupted metabolism is generally present in inherited cardiomyopathies, regardless of the pathogenic DNA variant and the phenotypes. Despite the shared metabolism alterations among different subtypes of inherited cardiomyopathies, etiology- and phenotype-specific metabolic impairments have been revealed, particularly in relation to FAO (**Figure 1D**). Those shared and unique metabolic changes provide promising candidate targets for future therapeutic strategies in treating inherited cardiomyopathies. Moreover, due to the importance of PPARA in regulating FAO and the beneficial effects of PPARA agonists observed in cardiomyocytes (100–103), studies have started to specify the pharmacological activities and cardiotoxicity of PPARA agonists (104). However, currently, there is no systematic study on the use of PPARA agonists, even FDA-approved PPARA-targeting fibrates, in patients with inherited cardiomyopathies. In conclusion, the potential of PPARA-activating drugs as FAO modulators to restore a balanced metabolism is worthy of investigation in inherited cardiomyopathies.

Author contributions

KG-H, AB, and JP wrote the manuscript. KG-H, AB, MW, JP, and MH collected and interpreted public datasets. FWA, FvS, and MH edited the text and provided the critical input. All authors contributed to the article and approved the submitted version.

Funding

This work was supported by the Leducq grant (CURE-PLaN no. 18CVD01 to JP, MH, and FWA), ZonMW Open Competition grant (CONTRACT no. 09120012010018 to KG-H, FWA, and MH), Dutch Cardiovascular Alliance (DCVA) grant (DOUBLE-DOSE no. 2020B005 to MH, FvS, and FWA), and ERA-CVD grant (SCALE no. 2019T109 to JP, FvS, and MH). FWA is supported by UCL Hospitals NIHR Biomedical Research Centre.

Conflict of interest

The authors declare that the research was conducted in the absence of any commercial or financial relationships that could be construed as a potential conflict of interest.

Publisher's note

References

1. Towbin JA. Inherited cardiomyopathies. *Circ J.* (2014) 78:2347.

2. Watkins H, Ashrafian H, Redwood C. Inherited cardiomyopathies. *N Engl J Med.* (2011) 364:1643–56.

3. McKenna WJ, Judge DP. Epidemiology of the inherited cardiomyopathies. *Nat Rev Cardiol.* (2020) 18:22–36.

4. McNally EM, Mestroni L. Dilated cardiomyopathy: genetic determinants and mechanisms. *Circ Res.* (2017) 121:731–48.

5. Jordan E, Peterson L, Ai T, Asatryan B, Bronicki L, Brown E, et al. Evidence-based assessment of genes in dilated cardiomyopathy. *Circulation.* (2021) 144:7–19.

6. Vander Roest AS, Liu C, Morck MM, Kooiker KB, Jung G, Song D, et al. Hypertrophic cardiomyopathy β-cardiac myosin mutation (P710R) leads to hypercontractility by disrupting super relaxed state. *Proc Natl Acad Sci U.S.A.* (2021) 118:e2025030118. doi: 10.1073/pnas.2025030118

7. Akhtar M, Elliott P. The genetics of hypertrophic cardiomyopathy. *Glob Cardiol Sci Pract.* (2018) 2018:36. doi: 10.21542/gcsp.2018.36

8. Cahill TJ, Ashrafian H, Watkins H. Genetic cardiomyopathies causing heart failure. *Circ Res.* (2013) 113:660–75.

9. Ferreira CR, Blau N. Clinical and biochemical footprints of inherited metabolic diseases. IV. Metabolic cardiovascular disease. *Mol Genet Metab.* (2021) 132:112–8. doi: 10.1016/j.ymgme.2020.12.290

10. Bae J, Paltzer WG, Mahmoud AI. The role of metabolism in heart failure and regeneration. *Front Cardiovasc Med.* (2021) 8:702920. doi: 10.3389/fcvm.2021.702920

11. Carvajal K, Moreno-Sánchez R. Heart metabolic disturbances in cardiovascular diseases. *Arch Med Res.* (2003) 34:89–99.

12. Dávila-Román VG, Vedala G, Herrero P, de las Fuentes L, Rogers JG, Kelly DP, et al. Altered myocardial fatty acid and glucose metabolism in idiopathic dilated cardiomyopathy. *J Am Coll Cardiol.* (2002) 40:271–7. doi: 10.1016/s0735-1097(02)01967-8

13. Karwi QG, Uddin GM, Ho KL, Lopaschuk GD. Loss of metabolic flexibility in the failing heart. *Front Cardiovasc Med.* (2018) 5:68. doi: 10.3389/fcvm.2018.00068

14. Brailova M, Clerfond G, Trésorier R, Minet-Quinard R, Durif J, Massoullié G, et al. Inherited metabolic diseases and cardiac pathology in adults: diagnosis and prevalence in a CardioMetabo study. *J Clin Med Res.* (2020) 9:694. doi: 10.3390/jcm9030694

15. Verdonschot JAJ, Hazebroek MR, Derks KWJ, Barandiarán Aizpurua A, Merken JJ, Wang P, et al. Titin cardiomyopathy leads to altered mitochondrial energetics, increased fibrosis and long-term life-threatening arrhythmias. *Eur Heart J.* (2018) 39:864–73. doi: 10.1093/eurheartj/ehx808

16. Pei J, Maas RGC, Nagyova E, Gho JMI, Blok CS, van Adrichem I, et al. Transcriptional regulation profiling reveals disrupted lipid metabolism in failing hearts with a pathogenic phospholamban mutation. *bioRxiv* [Preprint]. (2020). doi: 10.1101/2020.11.30.402792

17. Eijgenraam TR, Boogerd CJ, Stege NM, Teixeira VON, Dokter MM, Schmidt LE, et al. Protein aggregation is an early manifestation of phospholamban p.(Arg14del)–related cardiomyopathy: development of PLN-R14del–related cardiomyopathy. *Circ Heart Fail.* (2021) 14:e008532. doi: 10.1161/CIRCHEARTFAILURE.121.008532

18. Cuello F, Knaust AE, Saleem U, Loos M, Raabe J, Mosqueira D, et al. Impairment of the ER/mitochondria compartment in human cardiomyocytes with PLN p.Arg14del mutation. *EMBO Mol Med.* (2021) 13:e13074. doi: 10.15252/emmm.202013074

19. Ampong I. Metabolic and metabolomics insights into dilated cardiomyopathy. *Ann Nutr Metab.* (2022) 78:147–55. doi: 10.1159/000524722

20. Haas J, Frese KS, Sedaghat-Hamedani F, Kayvanpour E, Tappu R, Nietsch R, et al. Energy metabolites as biomarkers in ischemic and dilated cardiomyopathy. *Int J Mol Sci.* (2021) 22:1999. doi: 10.3390/ijms22041999

21. Flam E, Jang C, Murashige D, Yang Y, Morley MP, Jung S, et al. Integrated landscape of cardiac metabolism in end-stage human nonischemic dilated cardiomyopathy. *Nat Cardiovasc Res.* (2022) 1:817–29.

22. Verdonschot JAJ, Wang P, Van Bilsen M, Hazebroek MR, Merken JJ, Vanhoutte EK, et al. Metabolic profiling associates with disease severity in nonischemic dilated cardiomyopathy. *J Card Fail.* (2020) 26:212–22. doi: 10.1016/j.cardfail.2019.09.004

23. Zhao J, Yang S, Jing R, Jin H, Hu Y, Wang J, et al. Plasma metabolomic profiles differentiate patients with dilated cardiomyopathy and ischemic cardiomyopathy. *Front Cardiovasc Med.* (2020) 7:597546. doi: 10.3389/fcvm.2020.597546

24. Liu C, Li R, Liu Y, Li Z, Sun Y, Yin P, et al. Characteristics of blood metabolic profile in coronary heart disease, dilated cardiomyopathy and valvular heart disease induced heart failure. *Front Cardiovasc Med.* (2021) 7:622236. doi: 10.3389/fcvm.2020.622236

25. Bell SP, Adkisson DW, Ooi H, Sawyer DB, Lawson MA, Kronenberg MW. Impairment of subendocardial perfusion reserve and oxidative metabolism in nonischemic dilated cardiomyopathy. *J Card Fail.* (2013) 19:802–10. doi: 10.1016/j.cardfail.2013.10.010

26. Boschmann M, Engeli S, Moro C, Luedtke A, Adams F, Gorzelniak K, et al. LMNA mutations, skeletal muscle lipid metabolism, and insulin resistance. *J Clin Endocrinol Metab.* (2010) 95:1634. doi: 10.1210/jc.2009-1293

27. Merritt JL, MacLeod E, Jurecka A, Hainline B. Clinical manifestations and management of fatty acid oxidation disorders. *Rev Endocr Metab Disord.* (2020) 21:479–93.

28. Perea-Gil I, Seeger T, Bruyneel AAN, Termglinchan V, Monte E, Lim EW, et al. Serine biosynthesis as a novel therapeutic target for dilated cardiomyopathy. *Eur Heart J.* (2022) 43:3477–89.

29. Gao X, Lee K, Reid MA, Sanderson SM, Qiu C, Li S, et al. Serine availability influences mitochondrial dynamics and function through lipid metabolism. *Cell Rep.* (2018) 22:3507. doi: 10.1016/j.celrep.2018.03.017

30. van der Velden J, Tocchetti CG, Varricchi G, Bianco A, Sequeira V, Hilfiker-Kleiner D, et al. Metabolic changes in hypertrophic cardiomyopathies: scientific update from the Working Group of Myocardial Function of the European Society of Cardiology. *Cardiovasc Res.* (2018) 114:1273. doi: 10.1093/cvr/cvy147

31. Ujfalusi Z, Vera CD, Mijailovich SM, Svicevic M, Yu EC, Kawana M, et al. Dilated cardiomyopathy myosin mutants have reduced force-generating capacity. *J Biol Chem.* (2018) 293:9017.

32. Robinson P, Griffiths PJ, Watkins H, Redwood CS. Dilated and hypertrophic cardiomyopathy mutations in troponin and alpha-tropomyosin have opposing effects on the calcium affinity of cardiac thin filaments. *Circ Res.* (2007) 101:1266–73. doi: 10.1161/CIRCRESAHA.107.156380

33. Szyguła-Jurkiewicz B, Szczurek-Wasilewicz W, Osadnik T, Frycz-Kurek AM, Macioł-Skurk K, Małyszek-Tumidajewicz J, et al. Oxidative stress markers in hypertrophic cardiomyopathy. *Medicina.* (2022) 58:31. doi: 10.3390/medicina58010031

34. Crilley JG, Boehm EA, Blair E, Rajagopalan B, Blamire AM, Styles P, et al. Hypertrophic cardiomyopathy due to sarcomeric gene mutations is characterized by impaired energy metabolism irrespective of the degree of hypertrophy. *J Am Coll Cardiol.* (2003) 41:1776–82. doi: 10.1016/s0735-1097(02)03009-7

35. Magida JA, Leinwand LA. Metabolic crosstalk between the heart and liver impacts familial hypertrophic cardiomyopathy. *EMBO Mol Med.* (2014) 6:482–95. doi: 10.1002/emmm.201302852

36. Glatz JFC, Luiken JJF, Nabben M. CD36 (SR-B2) as a target to treat lipid overload-induced cardiac dysfunction. *J Lipid Atheroscler.* (2020) 9:66. doi: 10.12997/jla.2020.9.1.66

37. Ranjbarvaziri S, Kooiker KB, Ellenberger M, Fajardo G, Zhao M, Vander Roest AS, et al. Altered cardiac energetics and mitochondrial dysfunction in hypertrophic cardiomyopathy. *Circulation.* (2021) 144:1714–31.

38. Pei J, Schuldt M, Nagyova E, Gu Z, El Bouhaddani S, Yiangou L, et al. Multi-omics integration identifies key upstream regulators of pathomechanisms in hypertrophic cardiomyopathy due to truncating MYBPC3 mutations. *Clin Epigenet.* (2021) 13:61. doi: 10.1186/s13148-021-01043-3

39. Schuldt M, Pei J, Harakalova M, Dorsch LM, Schlossarek S, Mokry M, et al. Proteomic and functional studies reveal detyrosinated tubulin as treatment target in sarcomere mutation-induced hypertrophic cardiomyopathy. *Circ Heart Fail.* (2021) 14:e007022. doi: 10.1161/CIRCHEARTFAILURE.120.007022

40. Ritterhoff J, Young S, Villet O, Shao D, Neto FC, Bettcher LF, et al. Metabolic remodeling promotes cardiac hypertrophy by directing glucose to aspartate biosynthesis. *Circ Res.* (2020) 126:182–96. doi: 10.1161/CIRCRESAHA.119.315483

41. Marian AJ, Braunwald E. Hypertrophic cardiomyopathy: genetics, pathogenesis, clinical manifestations, diagnosis, and therapy. *Circ Res.* (2017) 121:749–70. doi: 10.1161/CIRCRESAHA.117.311059

42. Spindler M, Saupe KW, Christe ME, Sweeney HL, Seidman CE, Seidman JG, et al. Diastolic dysfunction and altered energetics in the alphaMHC403/+ mouse model of familial hypertrophic cardiomyopathy. *J Clin Invest.* (1998) 101:1775–83. doi: 10.1172/JCI1940

43. Chung H, Kim Y, Park C-H, Kim J-Y, Min P-K, Yoon YW, et al. Genetic relevance and determinants of mitral leaflet size in hypertrophic cardiomyopathy. *Cardiovasc Ultrasound.* (2019) 17:21. doi: 10.1186/s12947-019-0171-1

44. Abozguia K, Elliott P, McKenna W, Phan TT, Nallur-Shivu G, Ahmed I, et al. Metabolic modulator perhexiline corrects energy deficiency and improves exercise capacity in symptomatic hypertrophic cardiomyopathy. *Circulation.* (2010) 122:1562–9. doi: 10.1161/CIRCULATIONAHA.109.934059

45. Gehmlich K, Dodd MS, Allwood JW, Kelly M, Bellahcene M, Lad HV, et al. Changes in the cardiac metabolome caused by perhexiline treatment in a mouse model of hypertrophic cardiomyopathy. *Mol Biosyst.* (2015) 11:564–73. doi: 10.1039/c4mb00594e

46. Kampourakis T, Zhang X, Sun Y-B, Irving M. Omecamtiv mercabil and blebbistatin modulate cardiac contractility by perturbing the regulatory state of the myosin filament. *J Physiol.* (2018) 596:31–46. doi: 10.1113/JP275050

47. Olivotto I, Oreziak A, Barriales-Villa R, Abraham TP, Masri A, Garcia-Pavia P, et al. Mavacamten for treatment of symptomatic obstructive hypertrophic cardiomyopathy (EXPLORER-HCM): a randomised, double-blind, placebo-controlled, phase 3 trial. *Lancet.* (2020) 396:759–69. doi: 10.1016/S0140-6736(20)31792-X

48. Marian AJ, Senthil V, Chen SN, Lombardi R. Antifibrotic effects of antioxidant N-acetylcysteine in a mouse model of human hypertrophic cardiomyopathy mutation. *J Am Coll Cardiol.* (2006) 47:827–34. doi: 10.1016/j.jacc.2005.10.041

49. Lombardi R, Rodriguez G, Chen SN, Ripplinger CM, Li W, Chen J, et al. Resolution of established cardiac hypertrophy and fibrosis and prevention of systolic dysfunction in a transgenic rabbit model of human cardiomyopathy through thiol-sensitive mechanisms. *Circulation.* (2009) 119:1398–407. doi: 10.1161/CIRCULATIONAHA.108.790501

50. Wilder T, Ryba DM, Wieczorek DF, Wolska BM, Solaro RJ. N-acetylcysteine reverses diastolic dysfunction and hypertrophy in familial hypertrophic cardiomyopathy. *Am J Physiol Heart Circ Physiol.* (2015) 309:H1720–30. doi: 10.1152/ajpheart.00339.2015

51. Hall CL, Gurha P, Sabater-Molina M, Asimaki A, Futema M, Lovering RC, et al. RNA sequencing-based transcriptome profiling of cardiac tissue implicates novel putative disease mechanisms in FLNC-associated arrhythmogenic cardiomyopathy. *Int J Cardiol.* (2020) 302:124–30. doi: 10.1016/j.ijcard.2019.12.002

52. Volani C, Rainer J, Hernandes VV, Meraviglia V, Pramstaller PP, Smárason SV, et al. Metabolic signature of arrhythmogenic cardiomyopathy. *Metabolites.* (2021) 11:195. doi: 10.3390/metabo11040195

53. Zhu M, Zhang C, Zhang Z, Liao X, Ren D, Li R, et al. Changes in transcriptomic landscape in human end-stage heart failure with distinct etiology. *iScience.* (2022) 25:103935. doi: 10.1016/j.isci.2022.103935

54. Lopaschuk GD, Ussher JR, Folmes CDL, Jaswal JS, Stanley WC. Myocardial fatty acid metabolism in health and disease. *Physiol Rev.* (2010) 90:207–58. doi: 10.1152/physrev.00015.2009

55. Tran DH, Wang ZV. Glucose metabolism in cardiac hypertrophy and heart failure. *J Am Heart Assoc.* (2019) 8:e012673. doi: 10.1161/JAHA.119.012673

56. Schugar RC, Moll AR, André d'Avignon D, Weinheimer CJ, Kovacs A, Crawford PA. Cardiomyocyte-specific deficiency of ketone body metabolism promotes accelerated pathological remodeling. *Mol Metab.* (2014) 3:754. doi: 10.1016/j.molmet.2014.07.010

57. Selvaraj S, Kelly DP, Margulies KB. Implications of altered ketone metabolism and therapeutic ketosis in heart failure. *Circulation.* (2020) 141:1800–12. doi: 10.1161/CIRCULATIONAHA.119.045033

58. Naya M, Tamaki N. Imaging of myocardial oxidative metabolism in heart failure. *Curr Cardiovasc Imaging Rep.* (2014) 7:9244. doi: 10.1007/s12410-013-9244-y

59. Uddin GM, Zhang L, Shah S, Fukushima A, Wagg CS, Gopal K, et al. Impaired branched chain amino acid oxidation contributes to cardiac insulin resistance in heart failure. *Cardiovasc Diabetol.* (2019) 18:86. doi: 10.1186/s12933-019-0892-3

60. Dörner A, Schulze K, Rauch U, Schultheiss HP. Adenine nucleotide translocator in dilated cardiomyopathy: pathophysiological alterations in expression and function. *Mol Cell Biochem.* (1997) 174:261–9.

61. Kolwicz SC Jr, Tian R. Glucose metabolism and cardiac hypertrophy. *Cardiovasc Res.* (2011) 90:194.

62. Tuunanen H, Kuusisto J, Toikka J, Jääskeläinen P, Marjamäki P, Peuhkurinen K, et al. Myocardial perfusion, oxidative metabolism, and free fatty acid uptake in patients with hypertrophic cardiomyopathy attributable to the Asp175Asn mutation in the α-tropomyosin gene: a positron emission tomography study. *J Nucl Cardiol.* (2007) 14:354–65. doi: 10.1016/j.nuclcard.2006.12.329

63. Previs MJ, O'Leary TS, Morley MP, Palmer BM, LeWinter M, Yob JM, et al. Defects in the proteome and metabolome in human hypertrophic cardiomyopathy. *Circ Heart Fail.* (2022) 15:e009521.

64. Rossi A, Olivares J, Aussedat J, Ray A. Increased uracil nucleotide metabolism during the induction of cardiac hypertrophy by β-stimulation in rats. *Basic Res Cardiol.* (1980) 75:139–42. doi: 10.1007/BF02001405

65. West JA, Beqqali A, Ament Z, Elliott P, Pinto YM, Arbustini E, et al. A targeted metabolomics assay for cardiac metabolism and demonstration using a mouse model of dilated cardiomyopathy. *Metabolomics.* (2016) 12:1–18. doi: 10.1007/s11306-016-0956-2

66. Chaffin M, Papangeli I, Simonson B, Akkad A-D, Hill MC, Arduini A, et al. Single-nucleus profiling of human dilated and hypertrophic cardiomyopathy. *Nature.* (2022) 608:174–80.

67. Quttainah M, Raveendran VV, Saleh S, Parhar R, Aljoufan M, Moorjani N, et al. Transcriptomal insights of heart failure from normality to recovery. *Biomolecules.* (2022) 12:731. doi: 10.3390/biom12050731

68. Prosdocimo DA, Anand P, Liao X, Zhu H, Shelkay S, Artero-Calderon P, et al. Kruppel-like factor 15 is a critical regulator of cardiac lipid metabolism. *J Biol Chem.* (2014) 289:5914.

69. Ghose S, Varshney S, Adlakha K, Bhat A, Naushin S, Seth S, et al. Quantitative proteomics study reveals differential proteomic signature in dilated, restrictive, and hypertrophic cardiomyopathies. *J Proteins Proteomics.* (2019) 10:33–44.

70. Edelberg JM, Sehnert AJ, Mealiffe ME, del Rio CL, McDowell R. The impact of mavacamten on the pathophysiology of hypertrophic cardiomyopathy: a narrative review. *Am J Cardiovasc Drugs.* (2022) 22:497–510. doi: 10.1007/s40256-022-00532-x

71. Taegtmeyer H. Cardiac metabolism as a target for the treatment of heart failure. *Circulation.* (2004) 110:894–6.

72. Li N, Zhou H. SGLT2 inhibitors: a novel player in the treatment and prevention of diabetic cardiomyopathy. *Drug Des Devel Ther.* (2020) 14:4775. doi: 10.2147/DDDT.S269514

73. Paneni F, Costantino S, Hamdani N. Regression of left ventricular hypertrophy with SGLT2 inhibitors. *Eur Heart J.* (2020) 41:3433–6.

74. Dyck JRB, Sossalla S, Hamdani N, Coronel R, Weber NC, Light PE, et al. Cardiac mechanisms of the beneficial effects of SGLT2 inhibitors in heart failure: evidence for potential off-target effects. *J Mol Cell Cardiol.* (2022) 167:17–31.

75. de Boer RA, Heymans S, Backs J, Carrier L, Coats AJS, Dimmeler S, et al. Targeted therapies in genetic dilated and hypertrophic cardiomyopathies: from molecular mechanisms to therapeutic targets. A position paper from the Heart Failure Association (HFA) and the Working Group on Myocardial Function of the European Society of Cardiology (ESC). *Eur J Heart Fail.* (2022) 24:406. doi: 10.1002/ejhf.2414

76. Sekine Y, Yamamoto K, Kurata M, Honda A, Onishi I, Kinowaki Y, et al. HADHB, a fatty acid beta-oxidation enzyme, is a potential prognostic predictor in malignant lymphoma. *Pathology.* (2022) 54:286–93. doi: 10.1016/j.pathol.2021.06.119

77. Van Veldhoven PP. Biochemistry and genetics of inherited disorders of peroxisomal fatty acid metabolism. *J Lipid Res.* (2010) 51:2863.

78. Wagner N, Wagner KD. The role of PPARs in disease. *Cells.* (2020) 9:2367. doi: 10.3390/cells9112367

79. Ricote M, Glass CK. PPARs and molecular mechanisms of transrepression. *Biochim Biophys Acta.* (2007) 1771:926.

80. Montaigne D, Butruille L, Staels B. PPAR control of metabolism and cardiovascular functions. *Nat Rev Cardiol.* (2021) 18:809–23. doi: 10.1038/s41569-021-00569-6

81. Schupp M, Kintscher U, Fielitz J, Thomas J, Pregla R, Hetzer R, et al. Cardiac PPARα expression in patients with dilated cardiomyopathy. *Eur J Heart Fail.* (2006) 8:290–4. doi: 10.1016/j.ejheart.2005.09.003

82. Burke MA, Chang S, Wakimoto H, Gorham JM, Conner DA, Christodoulou DC, et al. Molecular profiling of dilated cardiomyopathy that progresses to heart failure. *JCI Insight.* (2016) 1:e86898. doi: 10.1172/jci.insight.86898

83. Prosdocimo DA, John JE, Zhang L, Efraim ES, Zhang R, Liao X, et al. KLF15 and PPARα cooperate to regulate cardiomyocyte lipid gene expression and oxidation. *PPAR Res.* (2015) 2015:201625. doi: 10.1155/2015/201625

84. Khuchua Z, Glukhov AI, Strauss AW, Javadov S. Elucidating the beneficial role of PPAR agonists in cardiac diseases. *Int J Mol Sci.* (2018) 19:3464. doi: 10.3390/ijms19113464

85. Takada I, Makishima M. Peroxisome proliferator-activated receptor agonists and antagonists: a patent review (2014-present). *Expert Opin Ther Pat.* (2020) 30:1–13. doi: 10.1080/13543776.2020.1703952

86. Grygiel-Górniak B. Peroxisome proliferator-activated receptors and their ligands: nutritional and clinical implications–a review. *Nutr J.* (2014) 13:17. doi: 10.1186/1475-2891-13-17

87. Hong F, Xu P, Zhai Y. The opportunities and challenges of peroxisome proliferator-activated receptors ligands in clinical drug discovery and development. *Int J Mol Sci.* (2018) 19:2189. doi: 10.3390/ijms19082189

88. Cheng HS, Tan WR, Low ZS, Marvalim C, Lee JYH, Tan NS. Exploration and development of PPAR modulators in health and disease: an update of clinical evidence. *Int J Mol Sci.* (2019) 20:5055. doi: 10.3390/ijms20205055

89. Chung SW, Lee JH, Kim MA, Leem G, Kim SW, Chang Y, et al. Additional fibrate treatment in UDCA-refractory PBC patients. *Liver Int.* (2019) 39:1776–85. doi: 10.1111/liv.14165

90. Talasaz AH, Sadeghipour P, Aghakouchakzadeh M, Dreyfus I, Kakavand H, Ariannejad H, et al. Investigating lipid-modulating agents for prevention or treatment of COVID-19: JACC state-of-the-art review. *J Am Coll Cardiol.* (2021) 78:1635–54. doi: 10.1016/j.jacc.2021.08.021

91. Yoo J, Jeong I-K, Ahn KJ, Chung HY, Hwang Y-C. Fenofibrate, a PPARα agonist, reduces hepatic fat accumulation through the upregulation of TFEB-mediated lipophagy. *Metabolism.* (2021) 120:154798. doi: 10.1016/j.metabol.2021.154798

92. Qiu Z, Zhao Y, Tao T, Guo W, Liu R, Huang J, et al. Activation of PPARα ameliorates cardiac fibrosis in Dsg2-deficient arrhythmogenic cardiomyopathy. *Cells.* (2022) 11:3184. doi: 10.3390/cells11203184

93. Steele H, Gomez-Duran A, Pyle A, Hopton S, Newman J, Stefanetti RJ, et al. Metabolic effects of bezafibrate in mitochondrial disease. *EMBO Mol Med.* (2020) 12:e11589.

94. Garcia MA, Rojas JA, Millán SP, Flórez AA. Neutral lipid storage disease with myopathy and dropped head syndrome. Report of a new variant susceptible of treatment with late diagnosis. *J Clin Neurosci.* (2018) 58:207–9. doi: 10.1016/j.jocn.2018.10.046

95. Ørngreen MC, Madsen KL, Preisler N, Andersen G, Vissing J, Laforêt P. Bezafibrate in skeletal muscle fatty acid oxidation disorders: a randomized clinical trial. *Neurology.* (2014) 82:607–13. doi: 10.1212/WNL.0000000000000118

96. Yamada K, Taketani T. Management and diagnosis of mitochondrial fatty acid oxidation disorders: focus on very-long-chain acyl-CoA dehydrogenase deficiency. *J Hum Genet.* (2019) 64:73–85. doi: 10.1038/s10038-018-0527-7

97. Suyama T, Shimura M, Fushimi T, Kuranobu N, Ichimoto K, Matsunaga A, et al. Efficacy of bezafibrate in two patients with mitochondrial trifunctional protein deficiency. *Mol Genet Metab Rep.* (2020) 24:100610. doi: 10.1016/j.ymgmr.2020.100610

98. Bonnefont JP, Bastin J, Laforêt P, Aubey F, Mogenet A, Romano S, et al. Long-term follow-up of bezafibrate treatment in patients with the myopathic form of carnitine palmitoyltransferase 2 deficiency. *Clin Pharmacol Ther.* (2010) 88:101–8. doi: 10.1038/clpt.2010.55

99. Thompson R, Jefferies J, Wang S, Pu WT, Takemoto C, Hornby B, et al. Current and future treatment approaches for Barth syndrome. *J Inherit Metab Dis.* (2022) 45:17–28. doi: 10.1002/jimd.12453

100. Sharifpanah F, Wartenberg M, Hannig M, Piper HM, Sauer H. Peroxisome proliferator-activated receptor alpha agonists enhance cardiomyogenesis of mouse ES cells by utilization of a reactive oxygen species-dependent mechanism. *Stem Cells.* (2008) 26:64–71. doi: 10.1634/stemcells.2007-0532

101. Kar D, Bandyopadhyay A. Targeting peroxisome proliferator activated receptor α (PPAR α) for the prevention of mitochondrial impairment and hypertrophy in cardiomyocytes. *Cell Physiol Biochem.* (2018) 49:245–59. doi: 10.1159/000492875

102. Jen HL, Liu PL, Chen YH, Yin WH, Chen JW, Lin SJ. Peroxisome proliferator-activated receptor α reduces endothelin-1-caused cardiomyocyte hypertrophy by inhibiting nuclear factor- κ B and adiponectin. *Mediators Inflamm.* (2016) 2016:5609121. doi: 10.1155/2016/5609121

103. Huang Q, Huang J, Zeng Z, Luo J, Liu P, Chen S, et al. Effects of ERK1/2/PPARα/SCAD signal pathways on cardiomyocyte hypertrophy induced by insulin-like growth factor 1 and phenylephrine. *Life Sci.* (2015) 124:41–9. doi: 10.1016/j.lfs.2015.01.015

104. Xi Y, Zhang Y, Zhu S, Luo Y, Xu P, Huang Z. PPAR-mediated toxicology and applied pharmacology. *Cells.* (2020) 9:352. doi: 10.3390/cells9020352

frontiers | Frontiers in Cardiovascular Medicine

TYPE Original Research
PUBLISHED 21 April 2023
DOI 10.3389/fcvm.2023.1129349

OPEN ACCESS

EDITED BY
John Lynn Jefferies,
University of Tennessee Health Science Center (UTHSC), United States

REVIEWED BY
Zhou Yafeng,
Suzhou Dushu Lake Hospital, China
Yeliz Demir,
Ardahan University, Türkiye

*CORRESPONDENCE
Gavin Y. Oudit
✉ gavin.oudit@ualberta.ca

SPECIALTY SECTION
This article was submitted to General Cardiovascular Medicine, a section of the journal Frontiers in Cardiovascular Medicine

RECEIVED 21 December 2022
ACCEPTED 28 March 2023
PUBLISHED 21 April 2023

CITATION
Zhabyeyev P, Sadasivan C, Shah S, Wang F and Oudit GY (2023) Amlodipine rescues advanced iron overload cardiomyopathy in hemojuvelin knockout murine model: Clinical implications. Front. Cardiovasc. Med. 10:1129349. doi: 10.3389/fcvm.2023.1129349

Amlodipine rescues advanced iron overload cardiomyopathy in hemojuvelin knockout murine model: Clinical implications

Pavel Zhabyeyev[1,2], Chandu Sadasivan[1,2], Saumya Shah[1,2], Faqi Wang[1] and Gavin Y. Oudit[1,2]*

[1]Division of Cardiology, Department of Medicine, University of Alberta, Edmonton, AB, Canada, [2]Mazankowski Alberta Heart Institute, University of Alberta, Edmonton, AB, Canada

Background: Iron overload cardiomyopathy (IOC) is a major co-morbidity of genetic hemochromatosis and secondary iron overload with limited therapeutic options. We aim to investigate mechanisms of rescue action of amlodipine in the murine model of iron overload, characterize changes in human cardiac tissue due to IOC, and compare them to the changes in the animal model of IOC.
Methods and results: As an animal model, we used male hemojuvelin knockout (HJVKO) mice, which lacked hemojuvelin (a co-receptor protein for hepcidin expression). The mice were fed a high-iron diet from 4 weeks to 1 year of age. As a rescue, iron-fed mice received the Ca^{2+} channel blocker, amlodipine, from 9 to 12 months. Iron overload resulted in systolic and diastolic dysfunctions and changes in the cardiac tissue similar to the changes in the explanted human heart with IOC. An IOC patient (β-thalassemia) with left-ventricular ejection fraction (LVEF) 25% underwent heart transplantation. The murine model and the explanted heart showed intra-myocyte iron deposition, fibrosis, hypertrophy, oxidative stress, remodeling of Ca^{2+} cycling proteins, and metabolic kinases typical of heart failure. Single-myocyte contractility and Ca^{2+} release were diminished in the murine model. The amlodipine-treated group exhibited normalization of cellular function and reversed fibrosis, hypertrophy, oxidative stress, and metabolic remodeling. We also report a clinical case of primary hemochromatosis successfully treated with amlodipine.
Conclusions: The aged HJVKO murine model on the iron-rich diet reproduced many features of the human case of IOC. The use of amlodipine in the murine model and clinical case reversed IOC remodeling, demonstrating that amlodipine is effective adjuvant therapy for IOC.

KEYWORDS
iron overload, cardiomyopathy, hemochromatosis, calcium channel blockers, hemojuvelin

1. Introduction

Iron is an essential trace element that plays a crucial role in oxygen transport, oxidative phosphorylation, and the production of reactive oxygen species (ROS) (1, 2). Iron homeostasis is achieved by a concerted action of multiple proteins, whose actions converge on the SMAD signaling pathway controlling the expression of the *Hamp* gene encoding a suppressor of iron uptake, hepcidin (2–5). The two major regulatory proteins involved in the control of hepcidin expression are human hemochromatosis protein (HFE protein) and hemojuvelin (HJV) (4, 5). Mutations in these genes lead to primary hemochromatosis (iron overload) (6). Mutations in the *Hfe* gene are the most prevalent, constituting approximately

90% of adult hemochromatosis phenotypes in white populations of European descent (4–8). Mutations in *Hjv* (*Hfe2*) gene are considerably less frequent but lead to juvenile hemochromatosis with a high degree of iron overload and overt cardiac phenotype (7, 9). Secondary hemochromatosis primarily arises as a side effect of frequent blood transfusions used to treat congenital anemias (2, 10) and intravenous iron supplementation in hemodialysis (11). In the case of primary hemochromatosis, the current approach to treatment is an early screening of susceptible populations, so early interventions (dietary management and phlebotomy) can be used to control iron levels (4, 6). Secondary hemochromatosis is managed by chelation therapy to reduce iron cardiotoxicity (6, 12). Combining chelation therapy with antioxidants was also suggested [for review, see Wongjaikam, Kumfu (13)].

Another route for improving chelation therapy is to combine iron chelators with L-type Ca^{2+} channel blockers. Ca^{2+} channels aid iron cardiotoxicity by providing a major entry route for Fe^{2+} ions into cardiomyocytes (14–16). Clinical trials to investigate the effectiveness of Ca^{2+} channel blockers as an adjunct therapy to iron chelators have been started (17, 18), and one has been completed (19). Based on subgroup analyses, the AmloThal clinical trial (NCT01395199) concluded that amlodipine combined with chelation therapy reduced cardiac iron more effectively than chelation therapy alone (19). In light of these findings, mechanistic studies on the animal models are important to elucidate the mechanism of action of amlodipine in the settings of iron overload. Amlodipine is a dihydropyridine Ca^{2+} channel blocker mainly used to treat hypertension (20). Besides channel-blocking, the compound has antioxidant (21) and inhibitory activity on several enzymes at concentrations above 5 µmol/L (22, 23). The typical plasma concentration of amlodipine in patients is 10–20 nmol/L (24, 25), and in the mouse model of iron overload is about 650 nmol/L (15).

In this study, we report two cases of hemochromatosis (primary and secondary) managed by the L-type Ca^{2+} channel blocker (amlodipine) and compare them to the animal model of iron overload treated with amlodipine. In the case of secondary hemochromatosis, we obtained explanted tissue samples of the heart with iron overload cardiomyopathy (IOC). We compared these samples with non-failing controls to identify IOC-related changes. Then, we compared these changes to the analogous changes in the animal model of iron overload. As the animal model of iron overload, we used a 12-month hemojuvelin knockout ($Hjv^{-/-}$) on a high-iron diet. That model has a more severe and pronounced phenotype resembling human IOC more closely than wild-type mice on a high-iron diet (26, 27). We also investigated the ability of amlodipine (i) to lower cardiac iron and (ii) to reverse maladaptive cardiac remodeling by introducing amlodipine at the age of 9 months (after 8 months of an iron diet).

2. Materials and methods

2.1. Experimental animal protocols

Male $Hjv^{-/-}$ (HJVKO) mice (kindly provided by Dr. Nancy C. Andrews, Duke University) were bred in-house at the University of Alberta Health Sciences Laboratory Animal Services facility. All experiments were performed in accordance with the University of Alberta institutional guidelines, which conformed to guidelines published by the Canadian Council on Animal Care and the Guide for the Care and Use of Laboratory Animals published by the US National Institutes of Health (revised 2011). We performed advanced iron overload protocol by feeding 4 weeks old HJVKO mice with the high iron diet (28) (Prolab®RHM 3000 with iron 380 ppm) until they were 1 year old. At 9 months, the amlodipine group received amlodipine in drinking water (95 mg/L) for 3 months. The vehicle group comprised male HJVKO mice receiving a regular diet without treatment.

2.2. Case of human primary overload cardiomyopathy

This patient was consented with written informed consent as part of the Heart Function and Cardiomyopathy Clinic registry, which is approved by the Ethics Committee at the University of Alberta (Pro00077124). Data for this patient's case was obtained through an electronic chart review.

2.3. Human explanted hearts

The study was approved by the Ethics Committee at the University of Alberta, and all patients provided written informed consents in accordance with the Declaration of Helsinki (2008) of the World Medical Association. Left ventricular tissue was harvested from explanted human failing hearts and donor non-failing human hearts *via* HELP (Human Explanted Heart Program) at the Mazankowski Alberta Heart Institute and the HOPE (Human Organ Procurement and Exchange) program at the University of Alberta Hospital. The harvested hearts were preserved in cold cardioplegia solution, and collected samples were snap-frozen in liquid nitrogen within 15 min of explantation and stored at −80°C.

2.4. Tissue iron levels

Samples (20 mg) of frozen tissue from LV were subjected to inductively coupled plasma resonance mass spectrometry to quantify iron levels at the Trace Metals Laboratory, London, Western Ontario. The samples were analyzed in triplicates, and the average values were used (15, 26).

2.5. Scanning electron microscopy

Images were obtained on Hitachi S5500 SEM. Energy-dispersive X-ray spectra were acquired using Oxford INCA Energy in STEM mode with a 1.5 nm probe.

2.6. Echocardiography

Transthoracic echocardiography was performed at 1 year of iron overload phenotype mice with the Vevo 2100 high-resolution imaging system equipped with a 30-MHz transducer using 1.5%–2% isoflurane (26, 29).

2.7. Hemodynamics

Mice were anesthetized with 1.5% isoflurane, and the right common carotid artery was cannulated. 1.4F Scisense catheter (Scisense Inc.) was advanced through the aortic valve and placed into the LV chamber. Pressure-volume loops were recorded *via* TCP-500 amplifier (Scisense Inc.) and analyzed offline using LabScribe 2 software (IWorks Inc.) as described previously (26, 29).

2.8. Measurement of single-myocyte excitability, contractility, and Ca^{2+} transients

Myocytes were enzymatically isolated as described previously (30) without blebbistatin to preserve contractility. After isolation, myocytes were kept in the perfusion buffer solution (pH 7.4). An aliquot of isolated cardiomyocytes was transferred to a bath atop of an inverted microscope to measure excitability, contractility, or Ca^{2+} transients (loaded with FURA-2AM). The measurements were done in myocytes superfused with Tyrode's solution (1.2 mM Ca^{2+}) at 35–36°C and paced with field stimulation at 1 Hz as previously described (26, 30, 31). Action potentials were recorded in the whole-cell ruptured-patch configuration with K^+ pipette solution (31).

2.9. In-vivo electrocardiographic (ECG) recording

Mice were placed under isoflurane anesthesia (1.5%–2%) on a heated pad (body temperature maintained at 37°C, measured by the rectal probe). ECG leads were placed in Lead I configuration. The signal was digitized using acquisition interface ACQ-7700 (Data Science International, USA) with P3 Plus software (ver. 5.0, Data Science International, USA).

2.10. Histology

The excised hearts from anesthetized mice were arrested in diastole using saline with 15 mM KCl, fixed in 10% buffered formalin, and embedded in paraffin. Thin sections (5 µm) were stained with Prussian blue, picro-sirius red (PSR), Masson trichrome, or wheat germ agglutinin (WGA) stain as described previously (26, 32). Iron depositions were visualized as blue depositions using a bright field view. Myocardial fibrosis was evaluated by quantifying PSR stained sections, and myocyte cross-sectional area (MCSA) was assessed from WGA staining using an Olympus IX81 microscope. Image analysis was done using MetaMorph software (26, 32).

2.11. Immunofluorescence

Immunofluorescence was performed on formalin-fixed paraffin-embedded heart sections (5 µm). Briefly, the sections were deparaffinized, followed by antigen retrieval and blocked with blocking buffer (1% BSA in 1X PBS) for 1 h. Similarly, OCT-embedded sections were fixed with 4% paraformaldehyde for 20 min and rehydrated in PBS for 30 min. Then, sections were incubated overnight in a humidified chamber at 4°C with primary antibody against rat anti-mouse neutrophil (Serotec), rat anti-mouse F4/80 (Serotec), mouse anti-nitrotyrosine (Santa Cruz), mouse anti-4-HNE (Abcam). Finally, sections were incubated with different fluorophore-conjugated secondary antibodies (Invitrogen USA), as described previously (26, 32).

2.12. Measurement of lipid peroxidation and glutathione levels

The levels of malondialdehyde (MDA), an indicator of lipid peroxidation, were measured in myocardial tissue (100–150 mg) by using a commercially available kit (Bioxytech, MDA-586TM assay, Oxis International Inc., Foster City, CA). Myocardial reduced (GSH) and oxidized glutathione (GSSG) levels were measured as described previously (26, 33).

2.13. Taqman real-time PCR

mRNA expression levels were evaluated using TaqMan real-time PCR. Total RNA was extracted from flash-frozen LV tissue using the TRIzol RNA extraction method. RNA (1 µg) was subjected to reverse transcription to synthesize cDNA. Samples were loaded in triplicate, and the data were analyzed by Roche's Light cycler® 480 system.

2.14. Bulk RNA sequencing

Transcriptome sequencing, including sample preparation, library construction, and Illumina sequencing, were carried out by Novogene Corporation Inc. (California, USA). The reported methods below were modified based on the standard procedures provided by Novogene. Total RNAs from left ventricles (4 hearts/group) were extracted. The pathway analysis was performed using iDEP.94 http://bioinformatics.sdstate.edu/idep94/ (34).

2.15. Western blot analysis

Western blot analysis was performed on flash-frozen LV tissue samples as previously described (26, 32). Briefly, we extracted

protein from LV tissues and performed immunoblotting for various proteins using the following primary antibodies: SERCA2a, NCX1 (Thermo Fisher Scientific), PLN-P^{Ser16}, total PLN (Badrilla Ltd), Akt-P^{Ser473}, Akt-P^{Thr308}, total Akt (Cell Signaling), AMPK-P^{Thr172} and total AMPK (Cell Signaling) and subsequently incubated with HRP conjugated secondary antibodies respectively.

2.16. Statistical analysis

All data are presented as mean ± SEM. The explanted heart was assessed using the one-sample *t*-test. In the case of multiple group comparisons, differences were evaluated by one-way ANOVA followed by Tukey's post-test. Statistical analysis was performed using Origin 2020 software (OriginLab).

3. Results

3.1. Amlodipine reduces cardiac iron levels but not hepatic iron levels

HJVKO mice were fed a high-iron diet to achieve iron overload as mice aged to 12 months. In the rescue group, amlodipine was introduced at 9 months (**Figure 1A**). Prussian blue histological staining showed a marked increase in iron deposition in groups receiving the high-iron diet (**Figure 1B**). Direct measurement of iron levels with inductively-coupled plasma mass spectrometry showed that the iron-fed group had markedly elevated iron levels and the amlodipine group had significantly reduced iron levels (**Figure 1C**). At the cellular level, iron deposition occurred as sub-micrometer particles (**Figure 1D**). The composition of the deposits was confirmed using energy-dispersive X-ray spectra, which showed a characteristic Fe peak at 6.4 keV (**Figure 1D**). In contrast to the heart, liver iron levels were increased at 12 months in both iron-fed groups (placebo and amlodipine; see **Figures 1E, F**). These results demonstrate that amlodipine reduces the iron load in the heart but not in the liver.

3.2. Amlodipine improves systolic and diastolic function

3.2.1. Echocardiography

Advanced iron overload led to a significant reduction of systolic function, and this reduction was rescued by treating iron-fed mice with amlodipine (**Figure 2A**). In response to iron overload, the systolic function was substantially reduced (reductions in fractional shortening, FS, and ejection fraction, EF; **Figure 2B**), and this reduction was accompanied by LV hypertrophy (increase in LV posterior wall thickness, LV PWT; **Figure 2B**) and LV dilation (increase in LV end-diastolic dimensions, LV EDD; **Figure 3B**). Amlodipine treated group showed normalization of systolic function and LV dilation (normalization of FS, EF, and LV EDD; **Figure 2B**). Noticeable change toward normalization of hypertrophic status in the amlodipine group did not achieve significance ($p = 0.096$; LV PWT, **Figure 3B**). Mitral and tissue Doppler measurements showed that diastolic function markedly deteriorated in response to iron overload (**Figure 2C**). Iron overload resulted in impaired cardiac relaxation as evident from (i) an increase in isovolumic relaxation time (IVRT), (ii) an increase in deceleration time (DT), and (iii) a decrease in the ratio of annular velocities (E'/A') (**Figure 2D**). These functional changes were also accompanied by left-atrial (LA) dilation (**Figure 2D**). The amlodipine-treated group exhibited normalization of all diastolic parameters but one (IVRT) (**Figure 2D**). In short, iron overload diminished both systolic and diastolic function, whereas amlodipine was able to rescue most of these developments.

3.2.2. Hemodynamics (pressure-volume loop analysis)

Assessment of cardiac function using pressure-volume loop technique showed that (i) iron overload resulted in dilation (increase in LV end-diastolic volume, LV EDV; **Table 1**), (ii) systolic dysfunction (reductions in ejection fraction, EF; pre-load adjusted contractility, dP/dt_{max}/EDV; and end-systolic pressure-volume relationship, ESPVR; **Table 1**), and (iii) diastolic dysfunction [elevated LV end-diastolic pressure, LVEDP; and larger isovolumic relaxation time constant, τ (Glantz); but increase in end-diastolic pressure-volume relation, EDPVR, was not statistically significant; **Table 1**]. The amlodipine-treated group had (i) normalized cardiac volume (LVEDV; **Table 1**), (ii) normalized systolic function (normal and nearly-normal values for EF, dP/dt_{max}/EDV, and ESPVR), and (iii) partial normalization of diastolic function (some reduction in LVEDP (not significant), normalization of isovolumic relaxation, τ (Glantz), and statistically insignificant reduction in EDPVR). In the case of pressure-volume loops, the results were similar to echocardiography: dilation, systolic and diastolic dysfunctions in the iron group, and quasi-normal cardiac function in the amlodipine-treated group).

3.3. Amlodipine reverses hypertrophic cardiac remodeling

Iron accumulation led to elevated expression levels of heart failure markers (natriuretic peptides, ANF and BNP, and myosin heavy chain β, β-MHC) in the iron group. In contrast, the amlodipine-treated group exhibited overall normalization of expression of heart failure markers (**Figure 3A**). In addition, the morphometric index of hypertrophy, LV mass adjusted by tibia length (LV/TL), was increased in the iron group but normalized in the amlodipine-treated group treated with amlodipine (**Figure 3B**). At the cellular level, measurement of length (L) and width (W) of isolated cardiomyocytes demonstrated that myocytes were elongated (increased L:W ratio) in the iron group and had an L:W ratio close to normal in the amlodipine-treated

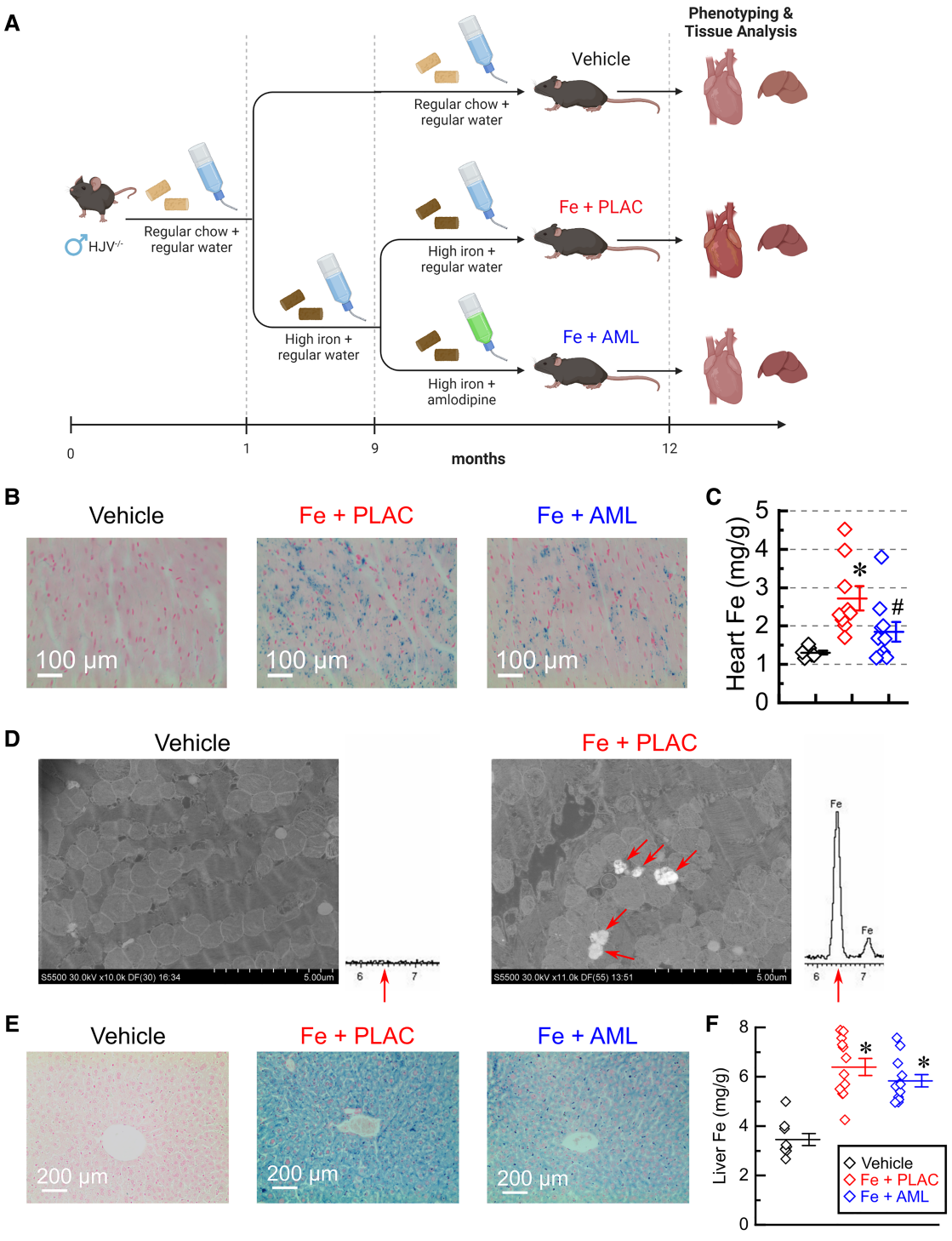

FIGURE 1
Amlodipine reduces cardiac iron levels. (**A**) The schematic of the study design (created with BioRender.com). (**B**) Representative images of Prussian blue staining. (**C**) Total myocardial iron levels (per dry weight; $n = 7–10$ per group) measured by inductively-coupled plasma mass spectrometry. (**D**) Representative scanning electron microscopy images (iron deposits marked by red arrows) and energy-dispersive X-ray spectra for vehicle and iron groups. Spectrum from the iron group, but not from the vehicle group, has a characteristic Fe peak at 6.4 keV (red arrow). (**E**) Representative images of Prussian Blue staining of liver sections. (**F**) Quantification of iron levels in the liver by inductive plasma mass-spectrometry ($n = 10–14$ per group). ppm = parts per million; $^{*}p < 0.05$ compared with the vehicle group. $^{\#}p < 0.05$ compared with the Iron (Fe) group.

group (Figure 3C). Assessment of hypertrophy at the tissue level using WGA staining (Figure 3D) revealed increased MCSA in the iron group and substantially reduced myocyte area in the amlodipine-treated group. The data suggest that iron overload leads to eccentric-hypertrophy remodeling, and amlodipine treatment reversed a significant part of hypertrophic remodeling.

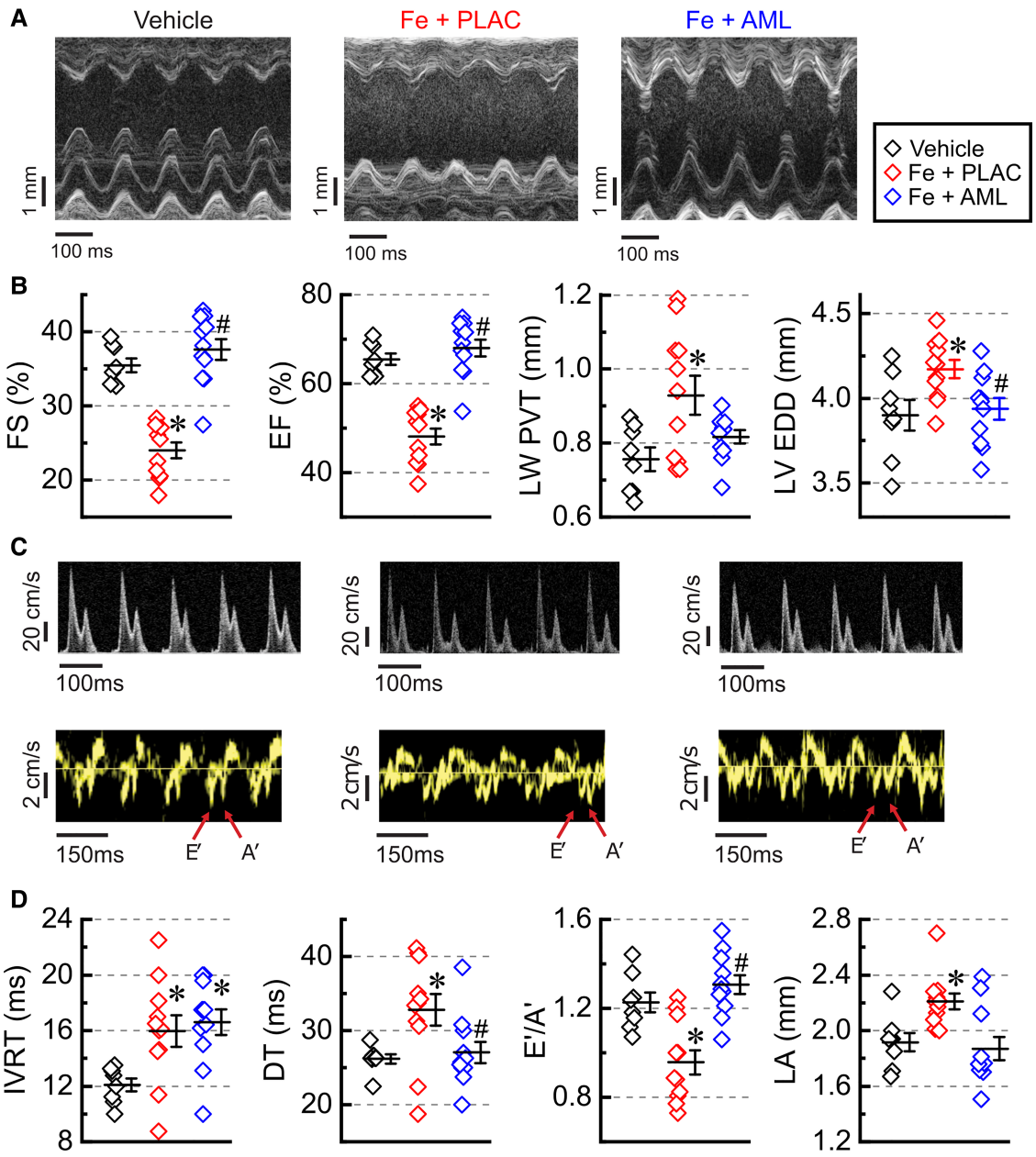

FIGURE 2
Amlodipine improves systolic and diastolic function. (**A**) Representative M-mode images. (**B**) Quantification of systolic function: fractional shortening (FS), ejection fraction (EF), left ventricular posterior wall thickness (LV PWT), and left ventricular end-diastolic dimensions (LV EDD). (**C**) Representative Doppler (top row) and Tissue Doppler (bottom row) images. (**D**) Quantification of diastolic function: isovolumic relaxation time (IVRT), deceleration time (DT), E prime (*E*′) to A prime (*A*′) ratio (*E*′/*A*′) of Tissue Doppler velocities, and left atrial dimensions (LA). $n = 8–11$ per group. $^{*}p < 0.05$ compared with the control group; $^{\#}p < 0.05$ compared with the iron group.

3.4. Amlodipine reduces cardiac fibrosis

Cardiac fibrosis was assessed using Mason's trichrome (Figure 3E) and PSR (Figure 3F) staining. The quantification of PSR staining (Figure 3G) showed a marked increase in interstitial fibrosis in iron-overloaded hearts and a considerable reduction of fibrosis in the hearts from the amlodipine-treated group. Expression levels of pro-fibrotic markers (pro-collagen Iα1 and IIIα1) followed a similar pattern: upregulation in the iron overload group and normalization in the amlodipine-treated group (Figure 3H).

3.5. Amlodipine normalizes single-myocyte contractility and Ca^{2+} cycling

3.5.1. Excitability

Measurements of electrical activity (action potentials) in the isolated cardiac myocytes showed no significant change in the major parameters of action potential: the maximal slope of depolarization ($\dot{V}_{max}$) and action potential duration (APDs corresponding to repolarization levels of 20%, 50%, and 90%; Figures 4A, B) suggesting that iron and amlodipine effects on

10.3389/fcvm.2023.1129349

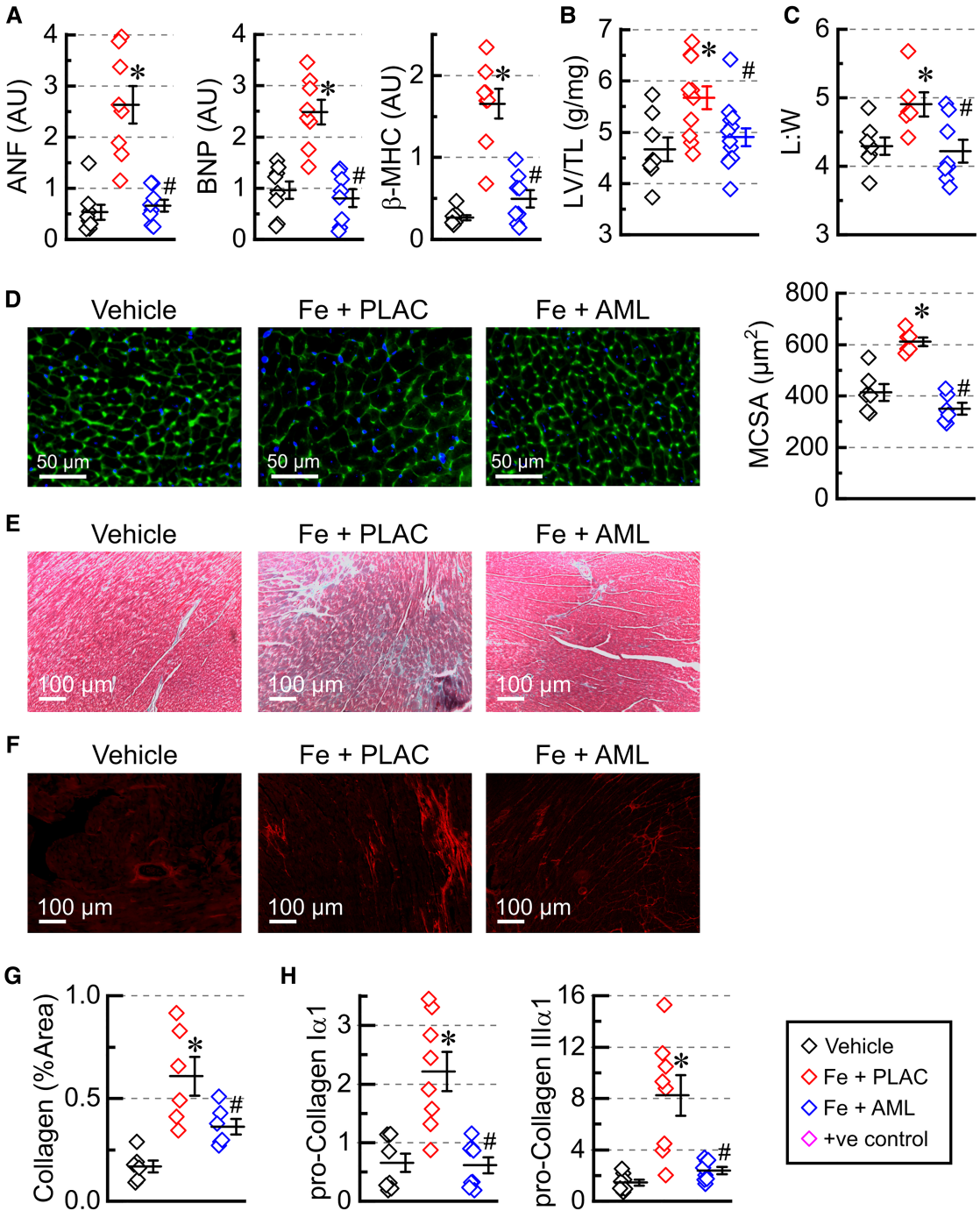

FIGURE 3
Amlodipine reverses hypertrophic cardiac remodeling. (**A**) Expression levels of heart failure markers: atrial natriuretic factor (ANF), brain natriuretic peptide (BNP), and myosin heavy chain β isoform (β-MHC) (n = 8 per group). (**B**) Morphometric index of cardiac hypertrophy (left ventricular weight (LV) adjusted by tibia length (TL); n = 8–13). (**C**) Morphometric index of cellular hypertrophy: length to width ratio (L:W) for isolated myocytes (6–8 hearts per group 50–150 myocytes per heart). (**D**) Representative images of wheat germ agglutinin (WGA) staining and myocytes cross-sectional area (MCSA) measured from WGA staining images (6 hearts per group, 4 sections per heart). (**E**) Representative images of Mason's trichrome staining. (**F**) Representative images of picrosirius-red (PSR) staining and quantification of PSR stained sections (**G**); 6 hearts per group; 4 sections per heart. (**H**) Expression levels of pro-collagens (n = 8 hearts per group). *$p < 0.05$ compared with the control group; $^{\#}p < 0.05$ compared with the iron group.

contractility were driven primarily *via* changes in Ca^{2+} cycling. The lack of the effect of iron and amlodipine on cardiac electrical activity was corroborated by electrocardiographic measurements. The Lead I electrocardiogram in anesthetized mice revealed no substantial differences in ECG parameters between the groups (Figures 4C, D).

TABLE 1 Echocardiographic and hemodynamic (pressure-volume loop) assessment.

	HJVKO Placebo	HJVKO Iron	HJVKO-Iron-CCB
n	8	12	8
HR (bpm)	418 ± 8	491 ± 10*	388 ± 11#
LVEDP (mmHg)	2.94 ± 0.52	12.62 ± 2.13*	8.60 ± 1.90
LVESP (mmHg)	120 ± 4.39	135 ± 3.84*	117.3 ± 4.58#
LVEDV(μl)	29.5 ± 2.2	43.85 ± 4.0*	30.2 ± 4.2#
LVESV (μl)	6.45 ± 0.9	20.26 ± 4.77*	4.77 ± 2.24#
SV(μl)	23.07 ± 1.62	23.59 ± 2.28	25.47 ± 2.9
EF (%)	79.55 ± 1.79	59.20 ± 6.74*	85.81 ± 4.6#
dP/dt_{max}/EDV (mmHg/s/μl)	343.2 ± 23	204.5 ± 27.2*	299 ± 25.3#
ESPVR (mmHg/μl)	5.58 ± 0.6	3.19 ± 0.5*	5.85 ± 1.7#
τ (Glantz) (ms)	12.3 ± 0.7	21.13 ± 2.4*	14.3 ± 0.2#
EDPVR (mmHg/μl)	0.117 ± 0.017	0.135 ± 0.016	0.105 ± 0.025

HR, heart rate; LVEDP, end diastolic pressure; LVESP, end systolic pressure; LVEDV, end diastolic volume; LVESV, end systolic volume; SV, stroke volume; EF, ejection fraction; dP/dt_{max}/EDV, Starling's contractile index; ESPVR, end-systolic pressure-volume relationship; Tau (τ), LV relaxation time constant; EDPVR, end-diastolic pressure-volume relationship.
*$p < 0.05$ compared with the placebo; #$p < 0.05$ compared with the iron group.

3.5.2. Contractility

Single-myocyte contractility was inhibited in the myocytes isolated from iron-overloaded hearts (Figure 5A). Both contractility (FS and maximal velocity of contraction, $-dL/dt$) and relaxation (maximal velocity of relaxation, $+dL/dt$) were diminished in the iron group (Figure 5A). Conversely, the amlodipine-treated group showed normalization of both contractility and relaxation parameters (Figure 5A).

3.5.3. Ca^{2+} cycling

The amplitude of Ca^{2+} transients (A_{Ca}) was inhibited in the iron-overload group and normalized in the amlodipine-treated group (Figure 5B). To investigate what underlines changes in Ca^{2+} transients, we assessed levels and phosphorylation state of three major proteins that control the time constant and amplitude of Ca^{2+} transient: Na^+–Ca^{2+} exchanger (NCX1), sarco-endoplasmic reticulum Ca^{2+}-ATPase (SERCa2), and phospholamban (PLN) (Figure 5C). NCX1 levels were markedly elevated in the iron-overload group and mostly normalized in the amlodipine-treated group (Figure 5D). SERCa2 levels were lowered in the iron-overload group, but roughly normalized in the amlodipine-treated group (Figure 5D), which is consistent with the normalization of Ca^{2+} transient amplitude (A_{Ca}) (Figure 5B). PLN phosphorylation was decreased in the iron group and was normalized in the amlodipine-treated groups (Figure 5D).

3.6. Amlodipine normalizes oxidative stress and metabolic signaling

The state of the intrinsic antioxidant system was assessed by measuring the concentration of GSH and GSSG. Consistent with a heightened degree of oxidative stress, the iron group had low GSH and high GSSG concentrations (Figure 6A); on the other hand, the amlodipine-treated group had a close-to-normal pattern of GSH-GSSG distribution (high GSH with low GSSG) (Figure 6A). MDA was elevated in the iron group but largely normalized levels in the amlodipine-treated group, corroborating GSH-GSSG results that oxidative stress was elevated in the iron group and was at near-normal levels in the amlodipine-treated hearts (Figure 6A). Assessment of metabolic signaling showed that iron overload was associated with (i) decreased Akt phosphorylation at both Thr308 (Akt-T308) and Ser473 (Akt-S473) and (ii) increased AMPK phosphorylation (Thr172) (Figure 6B). In contrast, the amlodipine-treated group had near-normal phosphorylation levels at all three sites (Figure 6B), suggesting that the amlodipine treatment normalizes pathological metabolic signaling in cardiac tissue.

Iron overload alters the expression of multiple genes involved in cardiac muscle contraction and the citrate cycle. We used bulk RNA sequencing to assess broad changes in expression levels (Data Supplement and Supplementary Figure S1) and found two important pathways being affected: cardiac muscle contraction and citrate cycle. In both pathways, iron overload led to an overall reduction in the expression levels (cardiac muscle contraction pathway Figure 7A and citrate cycle Figure 7B). Amlodipine therapy partially normalized the changes in myocardial gene expression in response to iron overload (Figures 7A, B).

3.7. Adverse remodeling in an explanted human heart with IOC

A 16-year-old girl with β-thalassemia major was admitted with refractory heart failure (HF). Echocardiogram showed dilation with bi-ventricular systolic and diastolic dysfunction with LVEF of 25%. The pre-transplant iron panel showed elevated serum iron (31 μmol/L; normal: 9.0–30 μmol/L), severely high transferrin iron saturation (94%; normal: 25%–35%) and low hemoglobin (94 g/L; normal: 120–160 g/L). Pre-transplant cardiac MRI indicated severe iron overload. With proper consent, samples were collected from the explanted heart for further comparison to non-failing control heart samples obtained from HOPE.

Prussian blue staining showed widespread myocardial iron deposition in the IOC heart but no detectable staining in the non-failing control hearts (Figure 8A). The IOC heart had marked fibrosis, as evident from trichrome staining (Figure 8B) and PSR staining (Figure 8C), in association with marked hypertrophy judging by the increase in MCSA (Figure 8D). Scanning electron microscopy revealed micron-sized iron deposits in the IOC heart but not in non-failing control (Figure 8E), with spectral analysis showing a marked increase of characteristic Fe peak at 6.4 keV (Figure 8F). Assessment of key proteins involved in Ca^{2+} cycling showed a reduction in the levels of SERCA2 and a compensatory increase in the levels of NCX1 (Figure 8G). Iron overload was also associated with metabolic remodeling, as evidenced by increased phosphorylation ratios of Akt^{Thr308} and AMPK (Figure 8H). Assessment of oxidative stress status showed a marked increase in MDA (Figure 8I), reduction in GSH, increase in GSSG, and lower

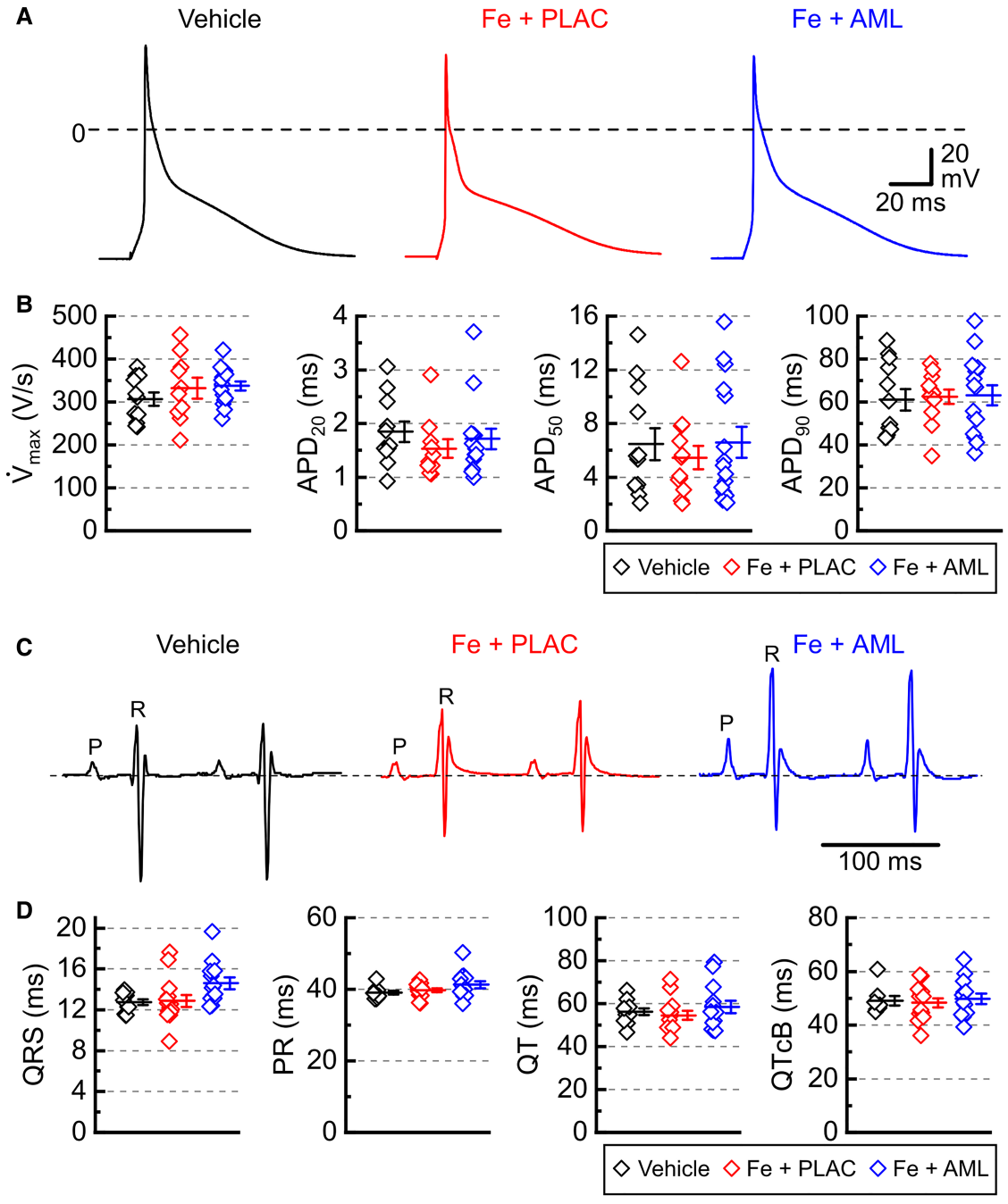

FIGURE 4
Cardiac electrical activity in murine iron overload. (**A**) Representative action potentials for the vehicle, iron with placebo (Fe + PLAC), and iron with amlodipine (Fe + AML) groups (left to right). (**B**) Maximal rate of rise of action potential ($\dot{V}_{max}$) and action potential durations for 20, 50, and 90% of repolarization (APD_{20}, APD_{50}, and APD_{90}, respectively); 3 hearts /group; 4–6 cells /heart. (**C**) Representative electrocardiograms for the vehicle, iron with placebo (Fe + PLAC), and iron with amlodipine (Fe + AML) groups. (**D**) Durations of QRS, PR, QT, and QT Bazett corrected (QTcB) intervals (n = 11–14 per group).

GSH/GSSG ratio (**Figure 8J**). In this clinical case, IOC exhibited iron deposition (including intracellular micrometer-size particles), fibrosis, hypertrophy, remodeling of Ca^{2+} cycling, metabolic remodeling, and a heightened degree of oxidative stress compared to non-failing control hearts. One-year post-cardiac transplant, this patient is on chelators (deferiprone and deferoxamine) and L-type Ca^{2+} channel blocker (amlodipine), has no signs of heart failure, and is followed up regularly. Cardiac MRI showed no evidence of myocardial (T2* = 45.5 ms) or hepatic (T2* = 17.5 ms) iron overload and normal bi-ventricular size and function, with LVEF of 66% and normal right ventricular ejection fraction of 63%.

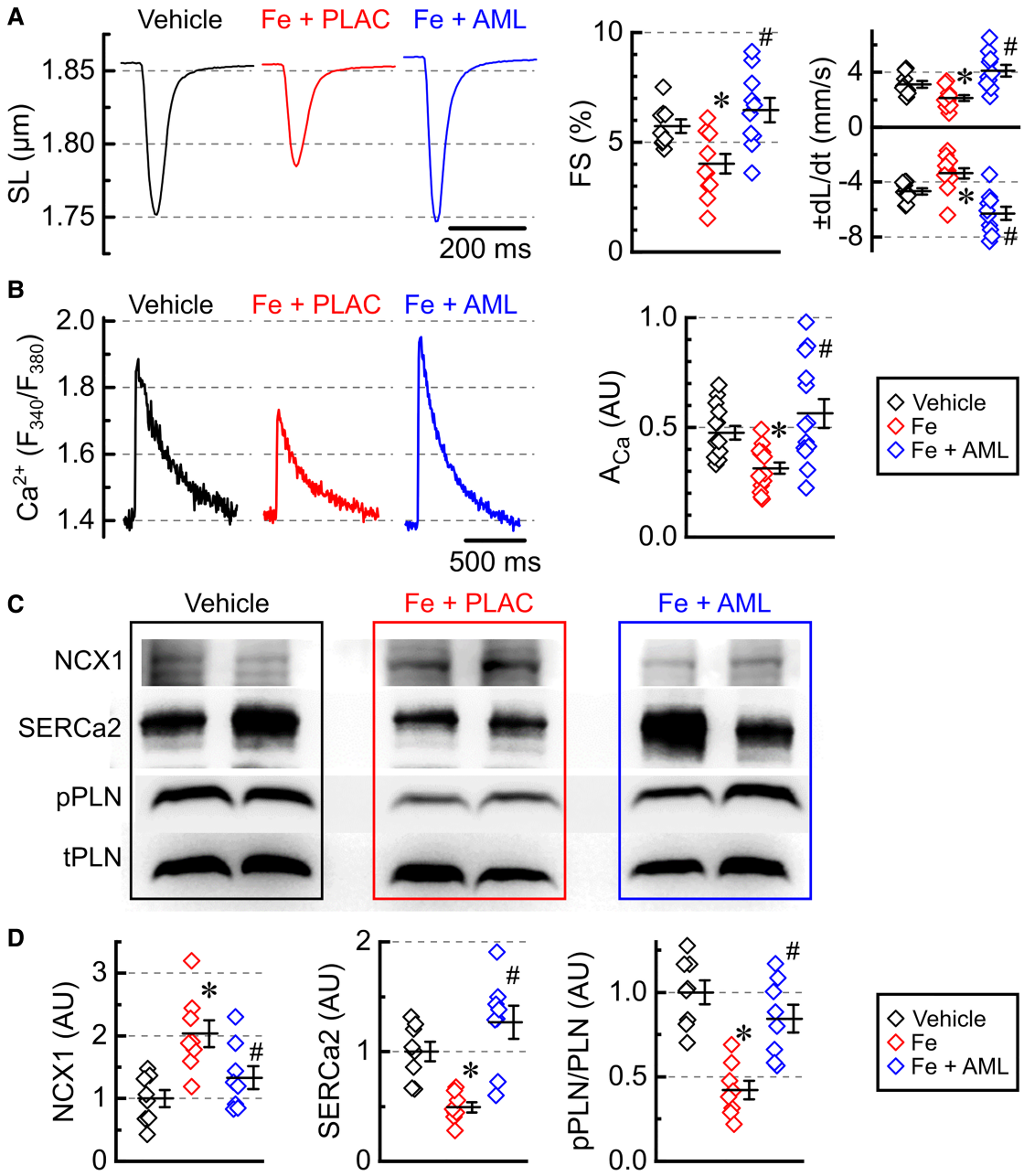

FIGURE 5
Amlodipine normalizes single-myocyte contractility and Ca^{2+} cycling. (**A**) Averaged recording of sarcomeric length (SL), fractional shortening (FS), contractility (*–dL/dt*), and relaxation (*+dL/dt*) (2 hearts per group 4–6 cells per heart). (**B**) Averaged recording of Ca^{2+} release transients plotted as the ratio of FURA-2 fluorescence (F_{380}/F_{340}) and Ca^{2+} release amplitudes (A_{Ca}). (**C**) Representative western blots for Na^{+}–Ca^{2+} exchanger (NCX1), sarcoplasmic reticulum Ca^{2+} ATPase (SERCa2), Ser16-phosphorylated phospholamban (pPLN), and total phospholamban (tPLN). (**D**) Protein levels for NCX1 and SERCa2 and phosphorylation ratio for phospholamban (pPLN/tPLN), quantified from western blots ($n = 8$ hearts per group). $^{*}p < 0.05$ compared with the control group; $^{\#}p < 0.05$ compared with the iron group.

3.8. Amlodipine rescues a patient with IOC due to primary hemochromatosis

A 69-year-old man with a history of primary hemochromatosis (PH) (C282Y/H63D compound heterozygote) and myelodysplastic syndrome (MDS) presented with IOC leading to HF and conduction abnormalities. He reported fatigue, shortness of breath, paroxysmal nocturnal dyspnea, and bilateral leg swelling [New York Heart Association (NYHA) Class III]. Blood work demonstrated anemia (hemoglobin = 87 g/L), elevated serum ferritin (1,230 µg/L), and elevated B-type natriuretic peptide (1,224 ng/L). Electrocardiogram showed abnormal conduction delays with underlying atrial flutter (**Figure 9A**). Cardiac magnetic resonance imaging (CMR) demonstrated dilated left ventricle with moderately reduced systolic function (LVEF = 40%). Cardiac T2 mapping showed evidence of moderate

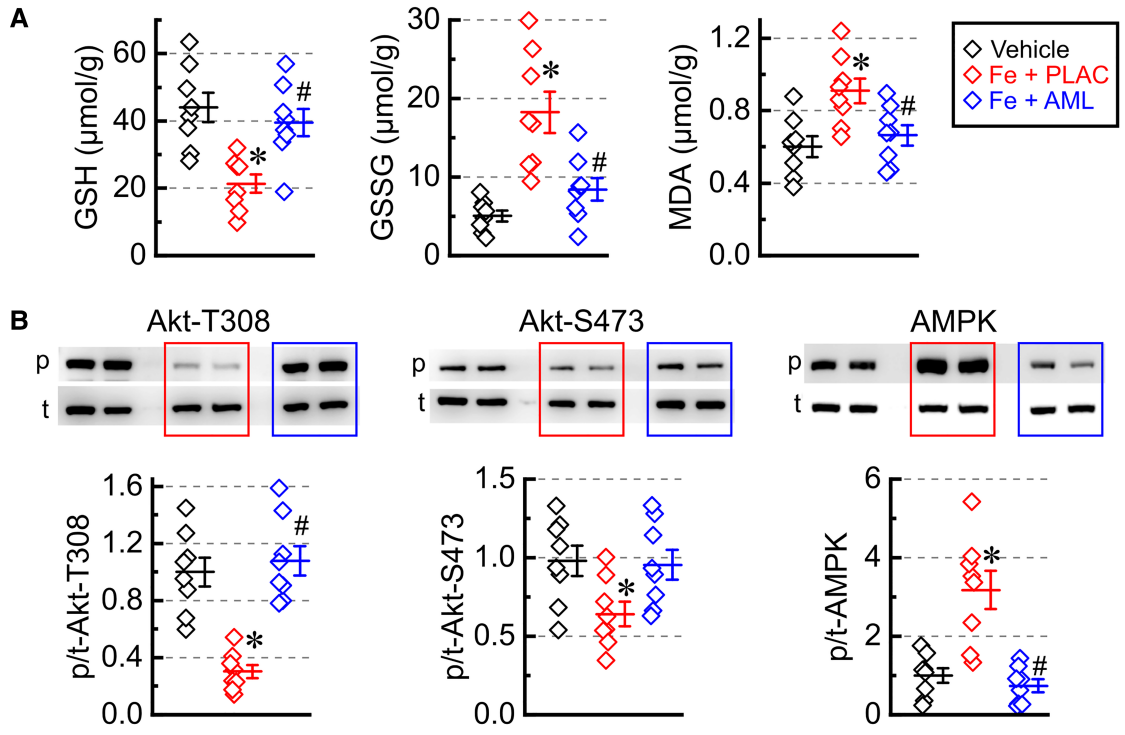

FIGURE 6
Amlodipine normalizes oxidative stresses and metabolic signaling. (**A**) Concentrations of reduced glutathione (GSH), oxidized glutathione (GSSG), and malondialdehyde (MDA) ($n = 8$ per group). (**B**) Phosphorylation levels (p/t) for Akt [Thr308 phosphorylation site (Akt-T308, p), Ser473 phosphorylation site (Akt-S473, p), and total Akt (t)] as well as AMP-activated protein kinase [AMPK; Thr172 phosphorylation site (p) and total (t)]. $^{*}p < 0.05$ compared with the control group; $^{\#}p < 0.05$ compared with the iron group.

myocardial iron loading (T2* 12–13 ms) and hepatic iron overload (T2* 2 ms) (**Figure 9B**). Medical therapies were initiated to manage this patient's IOC and subsequent HF. Given this patient's concurrent MDS and PH, therapeutic phlebotomy was not feasible. Oral iron chelation therapy was undertaken with increasing doses of deferasirox; however, iron saturation remained elevated at 70%. Despite improvements, this patient still expressed marked limitations in physical activities (NYHA class III). He was started on amlodipine 2.5 mg orally daily in addition to iron chelation and was titrated to the maximum dose of 10 mg daily. During follow-up 2 years after adding amlodipine, the patient reported marked improvement in HF symptoms (NYHA class I). Comparing initial CMR imaging to 24 months demonstrated improvement in LVEF and RVEF from 40% to 66% and 41% to 64%, respectively, with normalized ventricular volumes and mass. Myocardial T2* improved from 12.5 ms to 30 ms, indicating a marked reduction in myocardial iron loading (**Figure 9C**).

4. Discussion

Iron homeostasis is essential to maintain cardiac function, and dysfunction of iron metabolism has been implicated in various cardiovascular diseases (35–38). IOC is a major cause of heart failure in patients with hemochromatosis (iron overload) (12, 39–41). Phlebotomy and chelation therapy are the two main approaches to treating and managing iron overload (4, 6, 12, 39–41). However, phlebotomy cannot be used in patients with significant anemia, malignancy, or hemodynamic instability, and chelation therapy has an inherent risk of toxicity (4, 40, 41). Chelation therapies lower overall systemic iron, and amlodipine complements that by hindering the entry of Fe^{2+} *via* L-type Ca^{2+} channels, which are abundant in the heart. Therefore, using amlodipine as an adjunct therapy can improve the effectiveness of chelation therapy (19), creating an opportunity to lower cardiac iron levels faster and with a lower dosage of chelating agents, potentially improving the safety of the therapy.

4.1. Characterization of IOC in the explanted human heart and the animal model

Hemojuvelin-deficient mice on an iron-rich diet are an established IOC model that exhibits both systolic and diastolic dysfunction (26, 27). Iron levels obtained in the hearts of the animal model (2.7 mg/g dry weight) were approaching myocardial iron levels (3.5–9.2 mg/g dry weight) reported in patients with IOC and associated heart failure. The presented animal model replicated many crucial changes that develop during IOC in patients. We observed deterioration of cardiac

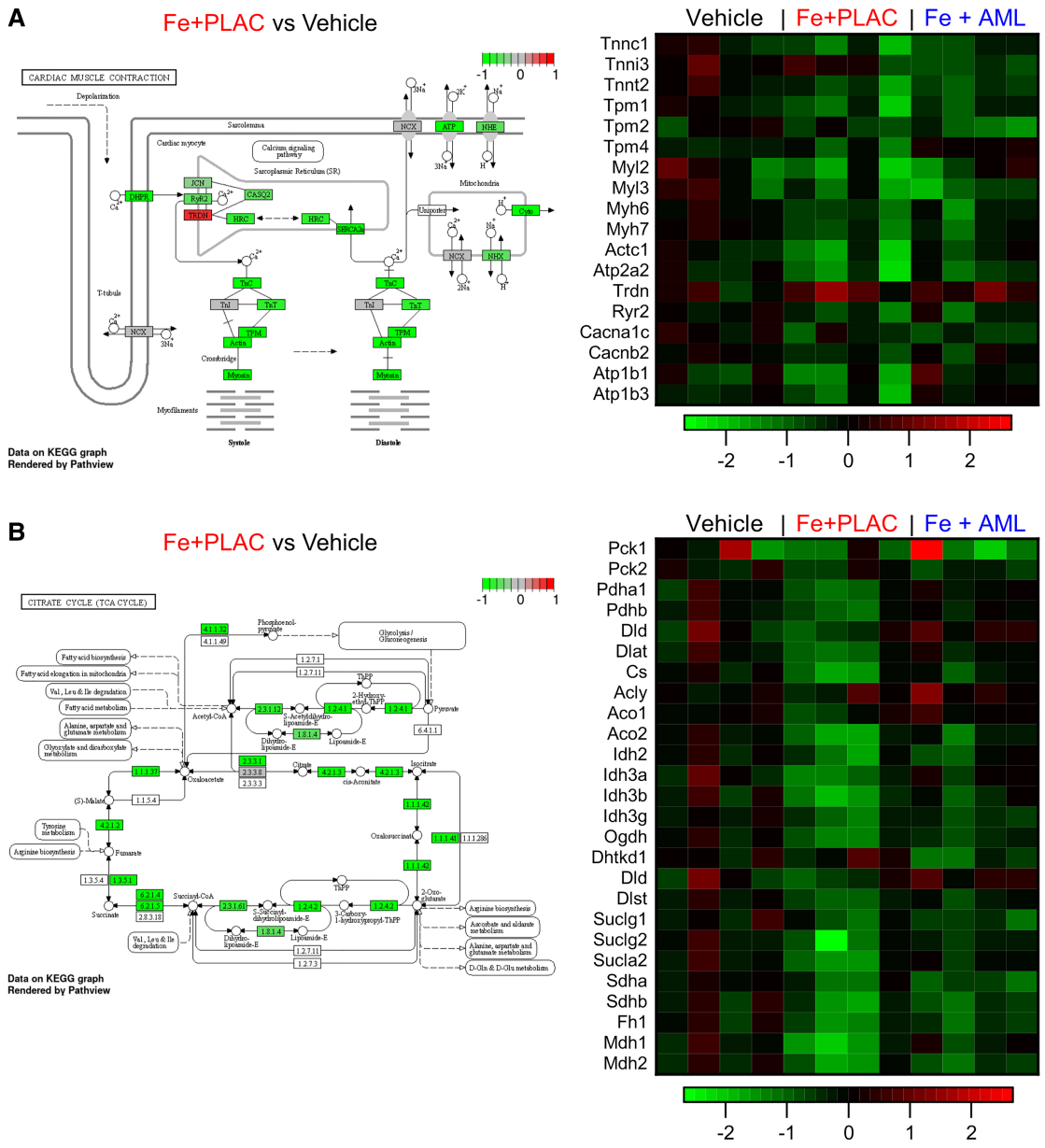

FIGURE 7
Iron overload reduces RNA expression of proteins in the cardiac muscle contraction pathway and citrate cycle. (A) Relative expression changes in cardiac muscle pathway and heat map of relative expression changes of selected RNA from cardiac muscle pathway. (B) Relative expression changes in citrate cycle and heat map of relative expression changes of selected RNA from citrate cycle.

function and micron-sized iron particles in cardiac tissue both in the explanted human heart with IOC and in the mouse model. In the case of the explanted heart, the heart failure was very severe (LVEF = 25%), whereas mice on the iron-rich diet had moderate cardiomyopathy (LVEF = 48%). Despite these few differences, both the explanted heart and the mouse model had fibrosis, hypertrophy, remodeling of Ca^{2+} cycling (decrease in SERCa2 levels accompanied by a compensatory increase in NCX levels), metabolic remodeling (inhibition of Akt activity coupled with upregulation of AMPK activity), and oxidative stress (increased MDA levels and low GSH/GSSG ratio). Accumulation of Fe^{2+} inside the cardiac cells is known to lead to the excessive production of ROS and trigger cell death due to ferroptosis (42), resulting in heart failure (35). In this animal model of IOC, we observed no changes in cardiac excitability but impaired cardiac cellular contractility and relaxation. The diminished contractility was associated with the reduction in Ca^{2+} release suggesting that changes in Ca^{2+} cycling underly reduced cardiac contractility.

4.2. Rescuing IOC with amlodipine in the animal model

As an L-type Ca^{2+} channel blocker, amlodipine can reduce the entry of non-transferrin-bound iron (Fe^{2+}) *via* L-type Ca^{2+} channels, resulting in lower levels of cardiac iron and reduced

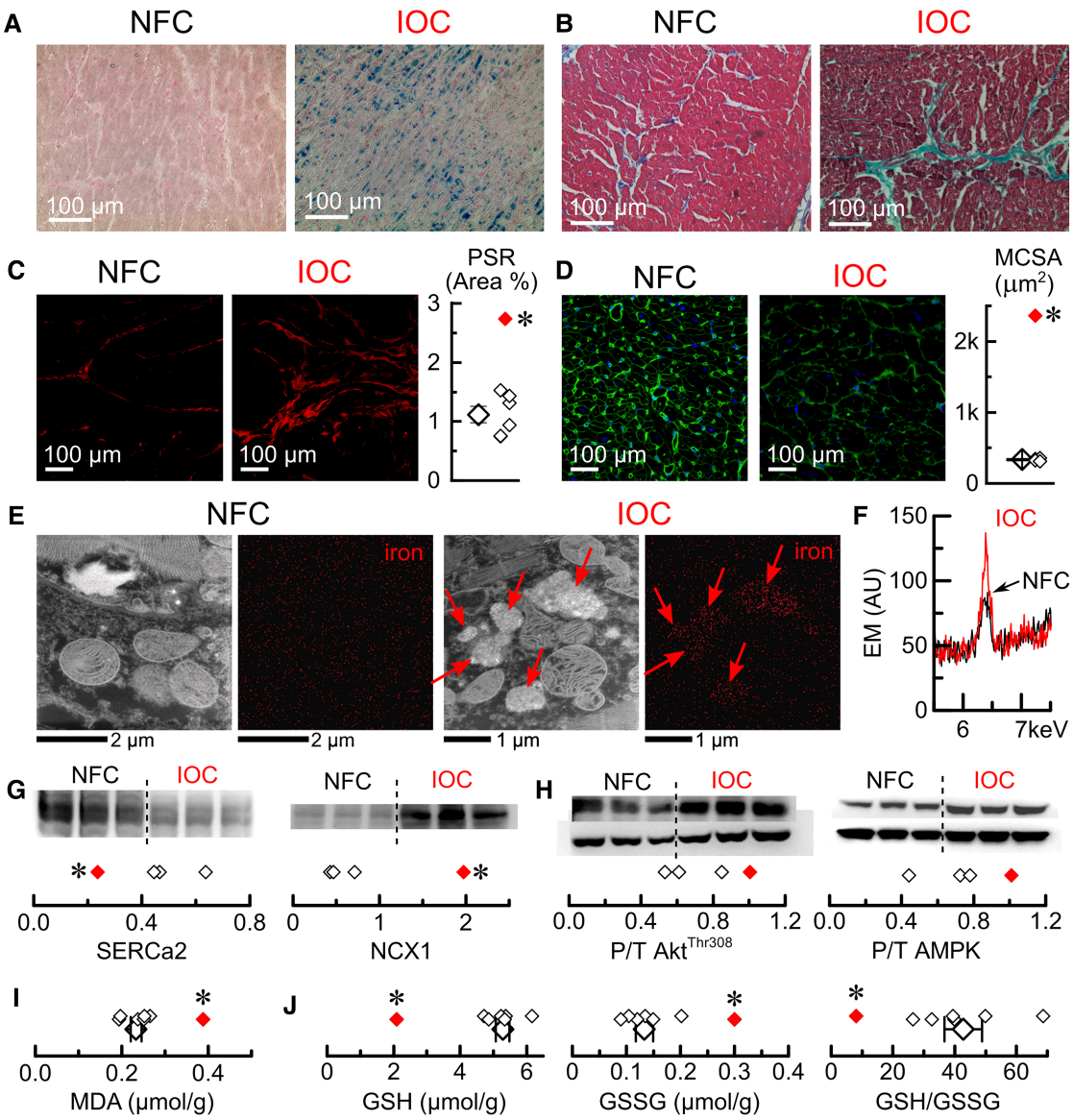

FIGURE 8
Characterization of the explanted human heart with IOC. (A) Representative images of Prussian blue staining. (B) Representative images of Mason's trichrome staining. (C) Representative images of picrosirius-red (PSR) staining and quantification of PSR stained sections. (D) Representative images of wheat germ agglutinin (WGA) staining and myocytes cross-sectional area (MCSA) measured from WGA staining images. (E) Representative scanning-electron microscopy images for control and iron (Fe) groups (iron deposits marked by red arrows). (F) Superimposed energy-dispersive X-ray spectra for non-failing controls (Ctl, black) and iron overload cardiomyopathy (IOC, red), showing the characteristic Fe peak at 6.4 keV. (G) Western blots and their quantifications (3 non-failing controls vs. an average of IOC) for sarcoplasmic reticulum Ca^{2+} ATPase (SERCa2) and Na^{+}–Ca^{2+} exchanger (NCX1). (H) Western blots and their quantifications (3 non-failing controls vs. an average of IOC) for phosphorylation levels of Akt (Thr308 phosphorylation site, Akt^{Thr308}) and AMP-activated protein kinase (Thr172 phosphorylation site, AMPK). (I) Malondialdehyde (MDA) concentration. (J) Reduced glutathione (GSH), oxidized glutathione (GSSG) concentrations, and GSH/GSSG ratio; open symbols—non-failing controls, filled symbol—explanted heart with IOC; *$p < 0.05$ compared with the non-failing controls.

oxidative stress in cardiac tissue. Mitigated damage from oxidative stress will contribute to the normalization of expression of Ca^{2+} cycling proteins and collagens, leading to the reversion of fibrosis and normalization of Ca^{2+} cycling, which translates to the normalization of systolic and diastolic dysfunctions at the whole-heart level. Besides being a channel blocker, amlodipine has been shown to have highly efficient antioxidant properties due to high lipophilicity and the ability to quench free radical formation (21). Antioxidants have been shown to mitigate damage associated with iron toxicity. For example, resveratrol (26, 27), thrombopoetin (43), and ebselen (44) have been shown to protect the heart in the settings of iron overload in mouse models. In our study, amlodipine demonstrated properties that can also be attributed to antioxidant activity (normalization of GSH, GSSG, and MDA levels).

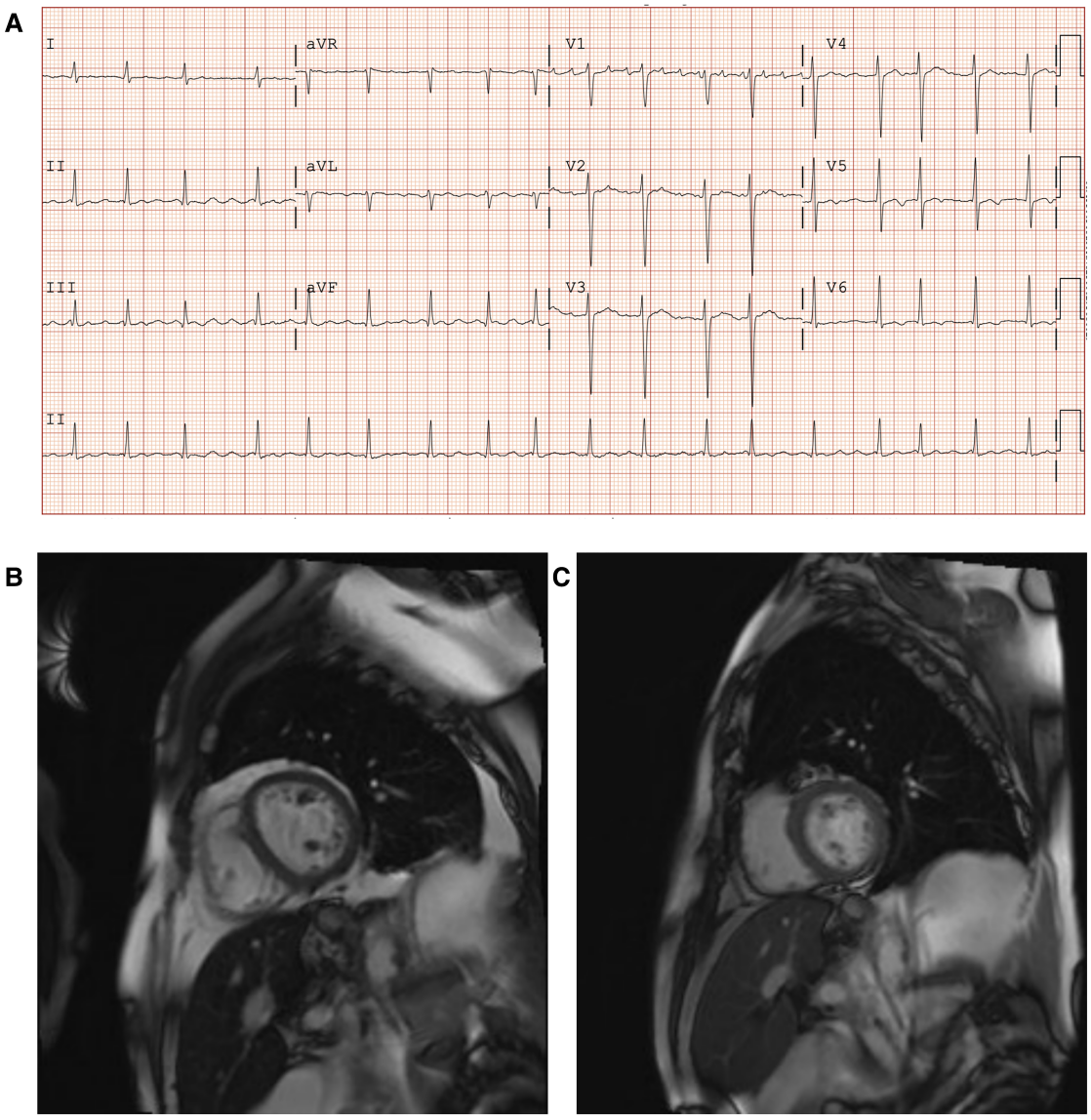

FIGURE 9
Patient with primary hemochromatosis and IOC treated with amlodipine. (**A**) Twelve-lead electrocardiogram at initial clinic visit demonstrating irregular conduction with an atrial flutter at 105 beats per minute and non-specific lateral t-wave inversion. (**B**) Cardiac magnetic resonance imaging (CMR) with T2 mapping at baseline (October 2019), prior to initiation of amlodipine to iron chelation therapy. T2 mapping showed moderate iron loading of the myocardium (T2* 12–13 ms), and hepatic iron overload was also noted (T2* 2 ms). (**C**) CMR with T2 mapping after iron chelation therapy with adjunctive amlodipine (12 months after baseline CMR, October 2020). Improvement of myocardial T2* to 26 ms, indicating the absence of myocardial iron loading and hepatic T2* improved to 5 ms, indicating mild hepatic iron loading.

4.3. Amlodipine as a treatment for IOC

In the reported case of primary hemochromatosis and IOC, the myelodysplastic syndrome prevented therapeutic phlebotomy. Iron chelation alone (deferasirox) was insufficient to reduce the burden of cardiac iron overload. However, adjunctive amlodipine therapy provided objective improvement in cardiac iron overload on imaging and symptomatic improvement in functional status for this patient. Despite randomized clinical trials demonstrating that amlodipine did not exhibit favorable clinical effects for the treatment of chronic heart failure (45, 46), amlodipine therapy could be used as adjunctive therapy in cases of iron overload, as seen in our patient's case and recent randomized clinical trials of amlodipine in patients with iron overload (17, 19). Therefore, any beneficial action from reducing iron deposition in the heart may also be reinforced by the antioxidant properties of amlodipine, suggesting that amlodipine is a good option for an adjuvant agent in chelation therapy.

5. Conclusions

We used a genetic model of primary hemochromatosis, human explanted heart tissue with iron overload and a patient with

primary hemochromatosis to reveal convergent pathways of iron-mediated injury and heart disease. IOC had a similar pathogenic profile (iron accumulation pattern, histological changes, regulatory protein alterations and ROS status) in the animal model and the explanted human heart. Amlodipine was shown to rescue IOC in the animal model and the reported clinical case of primary hemochromatosis. Amlodipine's ability to suppress Fe^{2+} entry and effectively quench the free radical formation and oxidative damage makes it an effective agent to improve the effectiveness of chelation therapy. The clinical significance of our findings supports the use of amlodipine as an adjuvant therapy in patients with IOC.

Data availability statement

The datasets presented in this study can be found in online repositories. The names of the repository/repositories and accession number(s) can be found below: https://www.ncbi.nlm.nih.gov/sra/PRJNA922223.

Ethics statement

The studies involving human participants were reviewed and approved by HREB Biomedical, University of Alberta (Pro00077124). Written informed consent to participate in this study was provided by the participants' legal guardian/next of kin. The animal study was reviewed and approved by ACUC Health Sciences, University of Alberta, Canada.

Author contributions

PZ performed animal experiments and data collection. CS and SS collected clinical data. SS collected explanted heart samples. FW performed histological studies and molecular analysis. PZ, CS, SS, and GO were responsible for data analysis and manuscript writing. All authors contributed to the article and approved the submitted version.

Funding

Heart and Stroke Foundation (Canada), Alberta Innovates-Health Solutions (Alberta, Canada), Canadian Institutes of Health Research (Canada).

Acknowledgments

We thank the National Institute of Nanotechnology (NINT) (University of Alberta, Canada) for technical help in acquiring electron microscopy images and spectra.

Conflict of interest

The authors declare that the research was conducted in the absence of any commercial or financial relationships that could be construed as a potential conflict of interest. The handling editor [JLJ] declared a past co-authorship with the author [GO].

Publisher's note

Supplementary material

The Supplementary Material for this article can be found online at: https://www.frontiersin.org/articles/10.3389/fcvm.2023.1129349/full#supplementary-material.

References

1. Xu W, Barrientos T, Andrews NC. Iron and copper in mitochondrial diseases. *Cell Metab.* (2013) 17(3):319–28. doi: 10.1016/j.cmet.2013.02.004

2. Hentze MW, Muckenthaler MU, Andrews NC. Balancing acts: molecular control of mammalian iron metabolism. *Cell.* (2004) 117(3):285–97. doi: 10.1016/S0092-8674(04)00343-5

3. Zhabyeyev P, Oudit GY. Unravelling the molecular basis for cardiac iron metabolism and deficiency in heart failure. *Eur Heart J.* (2017) 38(5):373–5. doi: 10.1093/eurheartj/ehw386

4. Zhabyeyev P, Oudit GY. Hemochromatosis protein (HFE) knockout mice as a novel model of hemochromatosis: implications for study and management of iron-overload cardiomyopathy. *Can J Cardiol.* (2017) 33(7):835–7. doi: 10.1016/j.cjca.2017.04.013

5. Powell LW, Seckington RC, Deugnier Y. Haemochromatosis. *Lancet.* (2016) 388(10045):706–16. doi: 10.1016/S0140-6736(15)01315-X

6. Olynyk JK, Ramm GA. Hemochromatosis. *N Engl J Med.* (2022) 387(23):2159–70. doi: 10.1056/NEJMra2119758

7. Bardou-Jacquet E, Brissot P. Diagnostic evaluation of hereditary hemochromatosis (HFE and non-HFE). *Hematol Oncol Clin North Am.* (2014) 28(4):625–35; v. doi: 10.1016/j.hoc.2014.04.006

8. Barton JC, Edwards CQ, Acton RT. HFE gene: structure, function, mutations, and associated iron abnormalities. *Gene.* (2015) 574(2):179–92. doi: 10.1016/j.gene.2015.10.009

9. Roetto A, Papanikolaou G, Politou M, Alberti F, Girelli D, Christakis J, et al. Mutant antimicrobial peptide hepcidin is associated with severe juvenile hemochromatosis. *Nat Genet.* (2003) 33(1):21–2. doi: 10.1038/ng1053

10. Farmakis D, Triposkiadis F, Lekakis J, Parissis J. Heart failure in haemoglobinopathies: pathophysiology, clinical phenotypes, and management. *Eur J Heart Fail.* (2017) 19(4):479–89. doi: 10.1002/ejhf.708

11. Rostoker G, Vaziri ND, Fishbane S. Iatrogenic iron overload in dialysis patients at the beginning of the 21st century. *Drugs*. (2016) 76(7):741–57. doi: 10.1007/s40265-016-0569-0

12. Pennell DJ, Udelson JE, Arai AE, Bozkurt B, Cohen AR, Galanello R, et al. Cardiovascular function and treatment in beta-thalassemia major: a consensus statement from the American heart association. *Circulation*. (2013) 128(3):281–308. doi: 10.1161/CIR.0b013e31829b2be6

13. Wongjaikam S, Kumfu S, Chattipakorn SC, Fucharoen S, Chattipakorn N. Current and future treatment strategies for iron overload cardiomyopathy. *Eur J Pharmacol*. (2015) 765:86–93. doi: 10.1016/j.ejphar.2015.08.017

14. Tanaka H, Shigenobu K. Efonidipine hydrochloride: a dual blocker of L- and T-type Ca^{2+} channels. *Cardiovasc Drug Rev*. (2002) 20(1):81–92. doi: 10.1111/j.1527-3466.2002.tb00084.x

15. Oudit GY, Sun H, Trivieri MG, Koch SE, Dawood F, Ackerley C, et al. L-type Ca^{2+} channels provide a major pathway for iron entry into cardiomyocytes in iron-overload cardiomyopathy. *Nat Med*. (2003) 9(9):1187–94. doi: 10.1038/nm920

16. Kumfu S, Chattipakorn SC, Fucharoen S, Chattipakorn N. Dual T-type and L-type calcium channel blocker exerts beneficial effects in attenuating cardiovascular dysfunction in iron-overloaded thalassaemic mice. *Exp Physiol*. (2016) 101(4):521–39. doi: 10.1113/EP085517

17. Fernandes JL, Sampaio EF, Fertrin K, Coelho OR, Loggetto S, Piga A, et al. Amlodipine reduces cardiac iron overload in patients with thalassemia major: a pilot trial. *Am J Med*. (2013) 126(9):834–7. doi: 10.1016/j.amjmed.2013.05.002

18. Shakoor A, Zahoor M, Sadaf A, Alvi N, Fadoo Z, Rizvi A, et al. Effect of L-type calcium channel blocker (amlodipine) on myocardial iron deposition in patients with thalassaemia with moderate-to-severe myocardial iron deposition: protocol for a randomised, controlled trial. *BMJ Open*. (2014) 4(12):e005360. doi: 10.1136/bmjopen-2014-005360

19. Fernandes JL, Loggetto SR, Verissimo MP, Fertrin KY, Baldanzi GR, Fioravante LA, et al. A randomized trial of amlodipine in addition to standard chelation therapy in patients with thalassemia major. *Blood*. (2016) 128(12):1555–61. doi: 10.1182/blood-2016-06-721183

20. Officers A, Coordinators for the ACRGTA, Lipid-Lowering Treatment to Prevent Heart Attack T. Major outcomes in high-risk hypertensive patients randomized to angiotensin-converting enzyme inhibitor or calcium channel blocker vs diuretic: the antihypertensive and lipid-lowering treatment to prevent heart attack trial (ALLHAT). *JAMA*. (2002) 288(23):2981–97. doi: 10.1001/jama.288.23.2981

21. Mason RP, Walter MF, Trumbore MW, Olmstead EG, Mason PE. Membrane antioxidant effects of the charged dihydropyridine calcium antagonist amlodipine. *J Mol Cell Cardiol*. (1999) 31(1):275–81. doi: 10.1006/jmcc.1998.0867

22. Turkes C, Demir Y, Beydemir S. Anti-diabetic properties of calcium channel blockers: inhibition effects on aldose reductase enzyme activity. *Appl Biochem Biotechnol*. (2019) 189(1):318–29. doi: 10.1007/s12010-019-03009-x

23. Turkes C, Demir Y, Beydemir S. Calcium channel blockers: molecular docking and inhibition studies on carbonic anhydrase I and II isoenzymes. *J Biomol Struct Dyn*. (2021) 39(5):1672–80. doi: 10.1080/07391102.2020.1736631

24. Setiawati E, Yunaidi DA, Handayani LR, Harinanto G, Santoso ID, Deniati SH. Comparative bioavailability cf two amlodipine formulation in healthy volunteers. *Arzneimittelforschung*. (2007) 57(7):467–71. PMID 17803060.

25. Wang T, Wang Y, Lin S, Fang L, Lou S, Zhao D, et al. Evaluation of pharmacokinetics and safety with bioequivalence of amlodipine in healthy Chinese volunteers: bioequivalence study findings. *J Clin Lab Anal*. (2020) 34(6):e23228. doi: 10.1002/jcla.23228

26. Das SK, Wang W, Zhabyeyev P, Basu R, McLean B, Fan D, et al. Iron-overload injury and cardiomyopathy in acquired and genetic models is attenuated by resveratrol therapy. *Sci Rep*. (2015) 5:18132. doi: 10.1038/srep18132

27. Das SK, Zhabyeyev P, Basu R, Patel VB, Dyck JRB, Kassiri Z, et al. Advanced iron-overload cardiomyopathy in a genetic murine model is rescued by resveratrol therapy. *Biosci Rep*. (2018) 38(1):BSR20171302. doi: 10.1042/BSR20171302

28. Huang FW, Pinkus JL, Pinkus GS, Fleming MD, Andrews NC. A mouse model of juvenile hemochromatosis. *J Clin Invest*. (2005) 115(8):2187–91. doi: 10.1172/JCI25049

29. Patel VB, Wang Z, Fan D, Zhabyeyev P, Basu R, Das SK, et al. Loss of p47phox subunit enhances susceptibility to biomechanical stress and heart failure because of dysregulation of cortactin and actin filaments. *Circ Res*. (2013) 112(12):1542–56. doi: 10.1161/CIRCRESAHA.111.300299

30. McLean BA, Zhabyeyev P, Patel VB, Basu R, Parajuli N, DesAulniers J, et al. PI3Kα is essential for the recovery from cre/tamoxifen cardiotoxicity and in myocardial insulin signalling but is not required for normal myocardial contractility in the adult heart. *Cardiovasc Res*. (2015) 105(3):292–303. doi: 10.1093/cvr/cvv016

31. Zhabyeyev P, McLean B, Chen X, Vanhaesebroeck B, Oudit GY. Inhibition of PI3Kinase-alpha is pro-arrhythmic and associated with enhanced late Na(+) current, contractility, and Ca(2+) release in murine hearts. *J Mol Cell Cardiol*. (2019) 132:98–109. doi: 10.1016/j.yjmcc.2019.05.008

32. Parajuli N, Patel VB, Wang W, Basu R, Oudit GY. Loss of NOX2 (gp91phox) prevents oxidative stress and progression to advanced heart failure. *Clin Sci*. (2014) 127(5):331–40. doi: 10.1042/CS20130787

33. Das SK, DesAulniers J, Dyck JR, Kassiri Z, Oudit GY. Resveratrol mediates therapeutic hepatic effects in acquired and genetic murine models of iron-overload. *Liver Int*. (2016) 36(2):246–57. doi: 10.1111/liv.12893

34. Ge SX, Son EW, Yao R. iDEP: an integrated web application for differential expression and pathway analysis of RNA-seq data. *BMC Bioinform*. (2018) 19(1):534. doi: 10.1186/s12859-018-2486-6

35. Fang X, Ardehali H, Min J, Wang F. The molecular and metabolic landscape of iron and ferroptosis in cardiovascular disease. *Nat Rev Cardiol*. (2023) 20(1):7–23. doi: 10.1038/s41569-022-00735-4

36. Teng T, Kong CY, Huang R, Ma ZG, Hu C, Zhang X, et al. Mapping current research and identifying hotspots of ferroptosis in cardiovascular diseases. *Front Cardiovasc Med*. (2022) 9:1046377. doi: 10.3389/fcvm.2022.1046377

37. Zhang H, Jamieson KL, Grenier J, Nikhanj A, Tang Z, Wang F, et al. Myocardial iron deficiency and mitochondrial dysfunction in advanced heart failure in humans. *J Am Heart Assoc*. (2022) 11(11):e022853. doi: 10.1161/JAHA.121.022853

38. Das SK, Patel VB, Basu R, Wang W, DesAulniers J, Kassiri Z, et al. Females are protected from iron-overload cardiomyopathy independent of iron metabolism: key role of oxidative stress. *J Am Heart Assoc*. (2017) 6(1):e003456. doi: 10.1161/JAHA.116.003456

39. Allen KJ, Gurrin LC, Constantine CC, Osborne NJ, Delatycki MB, Nicoll AJ, et al. Iron-overload-related disease in HFE hereditary hemochromatosis. *N Engl J Med*. (2008) 358(3):221–30. doi: 10.1056/NEJMoa073286

40. Murphy CJ, Oudit GY. Iron-overload cardiomyopathy: pathophysiology, diagnosis, and treatment. *J Card Fail*. (2010) 16(11):888–900. doi: 10.1016/j.cardfail.2010.05.009

41. Gujja P, Rosing DR, Tripodi DJ, Shizukuda Y. Iron overload cardiomyopathy: better understanding of an increasing disorder. *J Am Coll Cardiol*. (2010) 56(13):1001–12. doi: 10.1016/j.jacc.2010.03.083

42. Dixon SJ, Lemberg KM, Lamprecht MR, Skouta R, Zaitsev EM, Gleason CE, et al. Ferroptosis: an iron-dependent form of nonapoptotic cell death. *Cell*. (2012) 149(5):1060–72. doi: 10.1016/j.cell.2012.03.042

43. Chan S, Chan GC, Ye J, Lian Q, Chen J, Yang M. Thrombopoietin protects cardiomyocytes from iron-overload induced oxidative stress and mitochondrial injury. *Cell Physiol Biochem*. (2015) 36(5):2063–71. doi: 10.1159/000430173

44. Davis MT, Bartfay WJ. Ebselen decreases oxygen free radical production and iron concentrations in the hearts of chronically iron-overloaded mice. *Biol Res Nurs*. (2004) 6(1):37–45. doi: 10.1177/1099800403261350

45. Packer M, O'Connor CM, Ghali JK, Pressler ML, Carson PE, Belkin RN, et al. Effect of amlodipine on morbidity and mortality in severe chronic heart failure. Prospective randomized amlodipine survival evaluation study group. *N Engl J Med*. (1996) 335(15):1107–14. doi: 10.1056/NEJM199610103351504

46. Packer M, Carson P, Elkayam U, Konstam MA, Moe G, O'Connor C, et al. Effect of amlodipine on the survival of patients with severe chronic heart failure due to a nonischemic cardiomyopathy: results of the PRAISE-2 study (prospective randomized amlodipine survival evaluation 2). *JACC Heart Fail*. (2013) 1(4):308–14. doi: 10.1016/j.jchf.2013.04.004

frontiers | Frontiers in Cardiovascular Medicine

TYPE Review
PUBLISHED 22 May 2023
DOI 10.3389/fcvm.2023.1116925

OPEN ACCESS

EDITED BY
John Lynn Jefferies,
University of Tennessee Health Science Center (UTHSC), United States

REVIEWED BY
Paul Cheng,
Stanford Healthcare, United States
Roddy Walsh,
Academic Medical Center, Netherlands
Elena V. Zaklyazminskaya,
Russian National Research Center of Surgery named after B.V. Petrovsky, Russia

*CORRESPONDENCE
Emmanouil Tampakakis
✉ etampak1@jhmi.edu

†These authors have contributed equally to this work

RECEIVED 06 December 2022
ACCEPTED 04 May 2023
PUBLISHED 22 May 2023

CITATION
Htet M, Lei S, Bajpayi S, Zoitou A, Chamakioti M and Tampakakis E (2023) The role of noncoding genetic variants in cardiomyopathy. Front. Cardiovasc. Med. 10:1116925. doi: 10.3389/fcvm.2023.1116925

The role of noncoding genetic variants in cardiomyopathy

Myo Htet[1†], Shunyao Lei[2†], Sheetal Bajpayi[1], Asimina Zoitou[2], Myrsini Chamakioti[3] and Emmanouil Tampakakis[1,2,4*]

[1]Department of Medicine, Division of Cardiology, Johns Hopkins University, Baltimore, MD, United States, [2]Department of Biomedical Engineering, Johns Hopkins University, Baltimore, MD, United States, [3]School of Medicine, University of Patras, Patra, Greece, [4]Department of Genetic Medicine, Johns Hopkins University, Baltimore, MD, United States

Cardiomyopathies remain one of the leading causes of morbidity and mortality worldwide. Environmental risk factors and genetic predisposition account for most cardiomyopathy cases. As with all complex diseases, there are significant challenges in the interpretation of the molecular mechanisms underlying cardiomyopathy-associated genetic variants. Given the technical improvements and reduced costs of DNA sequence technologies, an increasing number of patients are now undergoing genetic testing, resulting in a continuously expanding list of novel mutations. However, many patients carry noncoding genetic variants, and although emerging evidence supports their contribution to cardiac disease, their role in cardiomyopathies remains largely understudied. In this review, we summarize published studies reporting on the association of different types of noncoding variants with various types of cardiomyopathies. We focus on variants within transcriptional enhancers, promoters, intronic sites, and untranslated regions that are likely associated with cardiac disease. Given the broad nature of this topic, we provide an overview of studies that are relatively recent and have sufficient evidence to support a significant degree of causality. We believe that more research with additional validation of noncoding genetic variants will provide further mechanistic insights on the development of cardiac disease, and noncoding variants will be increasingly incorporated in future genetic screening tests.

KEYWORDS

cardiomyopathy, noncoding variants, enhancers, promoters, untranslated regions, intronic variants

Introduction

Cardiomyopathies are disorders of the myocardium caused by genetic and environmental factors that eventually result in impaired cardiac function and heart failure (15). Depending on the specific effects in the function and morphology of the heart, and the isolated presence of arrhythmias, cardiomyopathies are divided into dilated, hypertrophic, restrictive, and arrhythmogenic (22). Dilated cardiomyopathy (DCM) is the most common cardiomyopathy affecting 1 in 250 individuals, followed by hypertrophic cardiomyopathy (HCM), which affects 1 in 500, and arrhythmogenic cardiomyopathy (ACM) encountered 1 in 5,000, while the prevalence of restrictive cardiomyopathy is even less common (40). About 30%–50% of cardiomyopathies are heritable, and the different types can have variable phenotypes, prognosis and causal mutations (16, 40, 70, 72, 81). HCM is primarily a disease of the sarcomere, as in up to 60% of patients, a pathogenic or likely pathogenic variant is detected in sarcomeric genes (22, 37). Beta-myosin heavy chain (*MYH7*) and myosin binding protein C3 (*MYBPC3*) are the most frequently affected genes, encoding for proteins of the thick sarcomeric filaments, and patients tend to exhibit disease onset in their forties. Other

commonly affected genes in the thin filaments of the sarcomere are cardiac Troponin I (*TNNI3*) and cardiac Troponin T (*TNNT2*) (37). In contrast to HCM, the causative genes in DCM are functionally diverse. Titin (*TTN*) mutations represent 12%–25% of DCM patients and Lamin (*LMNA*) genetic variants represent the second most common mutations in DCM patients (40). Other genes that are associated with DCM are *MYH7*, *TNNT2*, Tropomyosin 1 (*TPM1),* Desmoplakin (*DSP*), RNA binding motif protein 20 (*RBM20*), and sodium voltage-gated channel alpha subunit 5 (*SCN5A*) (57). In arrhythmogenic cardiomyopathy (ACM), most pathogenic variants are in genes encoding desmosomal proteins such as Plakoglobin (*JUP*) (13, 41), *DSP* (48), Plakophilin-2 (*PKP2*), Desmoglein-2 (*DSG2*) and Desmocollin-2 (*DSC2*) (4, 51, 67). Finally, inherited restrictive cardiomyopathies are caused by mutations in sarcomeric genes such as cardiac troponin I, and less commonly by mutations in Desmin (*DES*) and Filamin C (*FLNC*) (7). It is worth noting that although cardiomyopathies are classified based on phenotypes manifested in the general population, the pathogenic mechanisms and phenotypic features among the various types of cardiomyopathies can overlap to a significant degree.

With the advancement of next generation sequencing and genome wide association studies (GWAS), our understanding of the genetic basis of cardiomyopathies has significantly improved. Multiple GWAS have identified susceptibility loci and variants associated with different types of cardiomyopathies (3, 23, 42, 68, 75). Most rare disease causal variants have been found within the coding region of the genome (81). For example, *TTN* coding variants usually lead to gene truncations and are viewed as the leading genetic causes in DCM patients (25). Contrarily, *MYBPC3* truncating and *MYH7* missense variants are the most pathogenic HCM mutations detected in next generation sequencing research studies (23). Although definitive causative genetic mutations have been identified for familial cardiomyopathies, in over half of the cases targeted genetic screening tests do not identify a contributing variant. This is because most of the current clinical genetic screening tests and earlier research studies relied heavily on whole exome sequencing (WES) or targeted sequencing of coding regions (45, 53, 54). Another explanation regarding the lack of focus in noncoding variants is that even in large meta-analyses, the power of variant detection is limited by variant frequency and penetrance, and lack of systemic interpretation. However, recent evidence from whole genome sequencing (WGS) supports a strong association between genetic variants within noncoding regions and cardiomyopathies (75). Also, emerging evidence corroborates the role of noncoding regulatory regions, where disruption of transcription factor binding sites within enhancers or promoters can alter the 3D chromatin structure and reduce target gene expression, which can be critical for disease (9, 34, 62, 64, 69, 74). Similarly, based on other studies variants within intronic or untranslated regions (UTRs) could also be involved in the pathogenesis of cardiomyopathies (6, 18, 19, 82). Furthermore, according to ClinVar, a significant percentage of non-coding variants in splice sites (~60%) and UTRs (~5%), are classified as pathogenic or likely pathogenic (www.ncbi.nlm.nih.gov/clinvar). In this review we will provide an overview of the role of noncoding genetic variants and their association with cardiomyopathies. We will specifically focus on variants within promoter, enhancer, untranslated, splice and intronic regions (**Figure 1**), where there is sufficient evidence to support a strong association with cardiac disease.

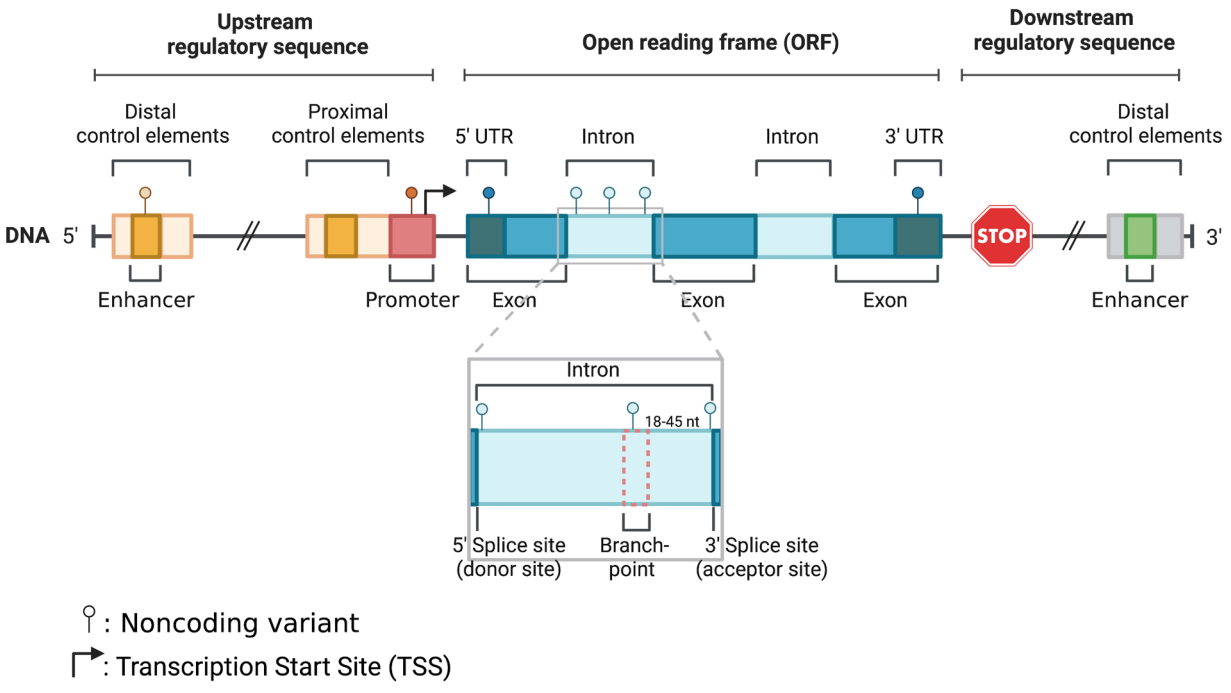

FIGURE 1
Schematic illustration of noncoding parts in the eukaryotic genome: enhancer, promoter, 5′ UTR, intron, and 3′ UTR.

Cardiomyopathy-associated genetic variants in enhancer and promoter regions

GWAS in heart failure patients have described a strong link with noncoding variants within transcriptional enhancer regions (3, 27, 38, 50, 60, 78) (**Table 1**). Enhancers are cis-regulatory DNA elements of the noncoding genome that recruit transcription factors to the promoter of target genes for temporal and tissue specific transcription regulation (10, 21, 76). Enhancers play key roles during growth and development, and many studies have shown that disease-associated variants are found within enhancers (52, 56, 74). Furthermore, thousands of cardiac specific enhancers have been described, and it is hypothesized that enhancers may have critical roles in cardiac diseases (1, 14, 24). This was also elegantly illustrated in a recent GWAS, where several regulatory variants in the promoter and enhancer regions were linked to cardiomyopathy (33).

Dilated cardiomyopathy

A study by Gacita et al. demonstrated a potential association between a variant upstream of the *MYH7* enhancer (rs875908) and DCM (20). Genetic deletion of this region in human induced pluripotent stem cell-derived cardiomyocytes (hiPSC-CMs) reduced *MYH7* expression and increased the alpha to beta myosin heavy chain ratio. It is predicted that this region is bound by the transcription factors GATA4 and T-box transcription factor 5 (TBX5) and that this variant likely disrupts the TBX5 binding motif. Interestingly, data from the US Northwestern biobank revealed that the same variant is associated with cardiac function in patients with heart failure. The authors also identified more than 1,700 putative enhancer variants in genes important for cardiac function such as *TNNT2*, Natriuretic peptide A (*NPPA*), Gap junction protein alpha 5 (*GJA5*) and Myocyte enhancer factor 2A (*MEF2A*) etc. (20). Recently, a study led by Vadgama and colleagues analyzed WGS data of 143 parent-offspring trios from the Genomics England 100,000 Genomes project, and found novel noncoding *de novo* variants in enhancer and promoter regions associated with cardiomyopathy (73). Furthermore, this study reported on a DCM patient who harbored a variant within an enhancer region which was predicted to regulate multiple genes such as Utrophin (*UTRN*), Syntaxin 11 (*STX11*), and Splicing factor 3B subunit 5 (*SF3B5*). Indeed, animal studies have shown that *UTRN* deficient mice develop DCM (12). Curiously, another DCM patient from the same cohort harbored a variant in an enhancer region that regulates multiple genes such as Unc-13 homolog D (*UNC13D*), WW domain binding protein 2 (*WBP2*), SAP30 binding protein (*SAP30BP*) and Tripartite motif containing 65 (*TRIM65*). Importantly, this enhancer region interacts with the distal promoter region of Transmembrane protein 94 (*TMEM94*), and biallelic *TMEM94* truncating mutation is associated with congenital heart defects (65).

Hypertrophic cardiomyopathy

In the study by Vadgama et al. one HCM patient was reported to carry a variant within the enhancer of the junctophilin-2 gene (*JPH2*) (73). Junctophilin-2 is a major structural protein in cardiomyocytes, where it also plays a critical role in calcium handling. Heart failure is commonly associated with downregulation of *JPH2,* and mutations in *JPH2* can result in HCM (55, 65, 77). Thus, it is possible that disrupted *JPH2* can alter cytoplasmic calcium signaling leading to cardiomyopathy.

Arrhythmogenic cardiomyopathy

ACM was linked with a variant within the enhancer of G protein coupled receptor kinase 2 (*GRK2*) and Ras homology family

TABLE 1 Variants in enhancer and overlapping promoter regions of genes associated with different types of cardiomyopathies.

Disease	Genomic position (GRCh38)	Enhancer	Promoter overlap	Promoter interaction	Validation method	Proposed pathogenic mechanism	Reference
DCM	Chr14:23438399 (rs875908 C > G)	*MYH7*	–	–	Functional: *in vitro;* phenotype correlation: biobank data	Disrupted TBX-5 binding to *MYH7* enhancer	(20)
DCM	Chr6:144216524C > A	*UTRN, STX11, SF3B5*	–	–	Case-control analysis; functional: computational tools	Disrupted *UTRN* enhancer function	(12, 73)
DCM	Ch17:75784788 T > C	*UNC13D, WBP2, SAP30BP* and *TRIM65*	*H3-3B, MIR4738* and *UNK*	*TRIM56* and *TMEM94*	Trio analysis	Disrupted interaction with *TMEM94* promoter	(65, 73)
HCM	Chr20:44116250A > G	*JPH2*	–	–	Case-control study	Disrupted *JPH2* enhancer function and altered intracellular Ca^{2+} signaling	(73)
ACM	Chr11:67317729C > T	*GRK2* and *RHOD*	*RAD9A*	–	Trio analysis	Gain of function of *GRK2* enhancer leading to increased *GRK2* kinase activity	(73)
ACM	Chr18:31497935 (-317G > A)		*DSG2*	–	Case-control study, pedigree analysis; functional: *in vitro*	Reduced AP-1 binding to *DSG2* promoter	(11)

DCM, dilated cardiomyopathy; HCM, hypertrophic cardiomyopathy; ACM, arrhythmogenic cardiomyopathy.

member D (*RHOD*) (73). Furthermore, it was shown that this enhancer region overlaps with the promoter of RAD9 checkpoint clamp component A (*RAD9A*). Importantly, GRK2 expression is upregulated in heart failure and GRK2 inhibition improves cardiac remodeling (59). Recently, a rare noncoding variant (DSG2-317G > A) in the *DSG2* promoter, was also associated with ACM. This heterozygous variant segregated in two daughters of the proband and experimental validation showed a disrupted binding site for the transcription factor AP-1 (11).

Cardiomyopathy-associated genetic variants in untranslated regions

5′ and 3′ UTRs are key mediators of post-transcriptional gene regulation. They impact mRNA processing, localization and stability (30, 44, 61). They also regulate downstream translation through elements including upstream open reading frames (ORFs), internal ribosome entry sites (IRES), m7G cap, polyadenylation signals, microRNA binding sites and secondary structures (26, 30, 39, 44). With WGS and the advancement of global RNA structure probing *in vivo* (46), an increasing number of UTR variants have been discovered and studied for their association with diseases (32, 63, 80) (**Table 2**). In addition, several UTR variants appear to increase the risk for disease because of differential microRNA binding affinity to altered alleles and subsequent changes in gene expression regulation (47, 66). Interestingly, more than 45,000 microRNA binding sites in 3′ UTRs of human genes had been discovered by 2009 (17), and these regulate nearly half of the transcriptome (58).

Dilated cardiomyopathy

In a study of 159 DCM patients and 215 control subjects, Zhou et al. showed an association of DCM with TATC and CAA insertion/deletion polymorphisms in 3′ UTR of Reticulon 4 (*RTN4*) gene (82). The gene codes for NOGO isoforms that have been previously linked with heart failure. (TATC)2 allele and (TATC)2/(TATC)2 genotypes were reported to be associated with an increased risk for DCM. However, there are still limited insights on the functional role of this mutation as it could not be matched with any known 3′ UTR functional motifs. In the Han Chinese population, a 3′ UTR variant in the *TBX5* gene, increased the risk for congenital heart disease such as atrial and ventricular septal defects by nearly two-fold (79). The mutant allele has increased binding affinity to microRNAs-9 and 30a which decreases *TBX5* expression.

CTG repeat expansion in the 3′ UTR of the myotonic dystrophy protein kinase (*DMPK*) gene has been linked to myotonic dystrophy type 1, a neuromuscular disease that can cause cardiac conduction disorders and cardiomyopathy (8). Transcription of this expansion results in CUG repeats that fold into hairpin loops, and sequestration of the nuclear protein muscleblind like (*MBNL*) and heterogeneous nuclear riboprotein 1 (*hnRNPH1*) splicing regulators leading to aberrant alternative splicing of numerous pre-mRNAs (35).

Arrhythmogenic cardiomyopathy

Through targeted genomic DNA sequencing in a small cohort in ACM patients, Beffagna et al. described two mutations in the 5′ and 3′ UTR regions of the transforming growth factor-beta3 (*TGFβ3*) gene (6). They reported a 5′UTR variant (c.−36G > A) in all clinically affected individuals of the family and in 3 asymptomatic relatives. *TGFβ3* has 11 upstream open reading frames (uORFs). ATG at position -142 translates to a truncated 88 amino acid peptide that has been shown to inhibit the translation of full length *TGFβ3* (2). It was also hypothesized that the 5′UTR variant may result in loss of function of the inhibitory truncated peptide isoform leading to increased *TGFβ* signaling and fibrosis. The disease mechanism for the 3′ UTR mutation found in one patient with ACM, has not been well studied (6).

Cardiomyopathy-associated genetic variants at deep intronic sites

Deep intronic variants are defined as those located more than 20 bp away from exons, and function to introduce aberrant splicing, distort transcription regulatory motifs, alter non-coding RNA activities, etc. (31). The identification and interpretation of these variants remains challenging due to the large size of introns and lack of consensus sequences (**Table 3**).

Hypertrophic cardiomyopathy

Variants found in deep intronic regions of Vinculin (*VCL*) and protein kinase AMP-activated non-catalytic subunit gamma 2

TABLE 2 Variants in 5′ and 3′ UTR of genes that are associated with different types of cardiomyopathies.

Disease	Variant location	Gene regulated	Validation method	Proposed pathogenic mechanism	Reference
DCM	(TATC)2 and (TATC)2/(CAA)2 in 3′ UTR	*RTN4*	Case-control study;	TATC insertion and altered Nogo isoform expression	(82)
DCM	3′ UTR (rs6489956 C > T)	*TBX5*	Case-control study; functional: *in vitro* and *in vivo*	Increased miR9 and miR30a mediated downregulation of *TBX5*	(79)
ACM	5′ UTR (rs770828281 −36G > A)	*TGFβ3*	Case control study; functional: *in vitro*	Loss of auto-inhibitory truncated *TGFβ3* isoform	(6)
ACM	3′ UTR (1723C→T)	*TGFβ3*	Case control study; functional: *in vitro*	Unknown, likely involved altered miRNA mediated regulation	(6)

DCM, dilated cardiomyopathy; ACM, arrhythmogenic cardiomyopathy.

TABLE 3 Deep-intronic variants related to different cardiomyopathies and their proposed pathogenic mechanism.

Disease	Genomic position	Affected gene	Validation method	Proposed pathogenic mechanism	Reference
HCM	c.499+367T > C	*VCL*	Pedigree analysis; functional: computational tools	Disruption of transcriptional motif bindings	(43)
HCM	c.1234−317T > G	*PRKAG2*	Pedigree analysis; functional: computational tools	Disruption of transcriptional motif bindings	(43)
HCM	c.1224−52G > A, c.1224−80G > A, c.1224−21A > G, c.906−36G > A, c.1898−23A > G, c.1090+453C > T, c.1091−575A > C, c.1928−569G > T, c.3331−26T > G	*MYBPC3*	Pedigree analysis; functional: *in vitro*, computational tools	Cryptic splice site, branchpoint disruption and intron retention, leading to haploinsufficiency	(5, 28, 36, 71)

All variants listed according to their reported sequence. HCM, hypertrophic cardiomyopathy; ACM, arrhythmogenic cardiomyopathy.

(*PRKAG2*) were associated with HCM (43). In this study, both *VCL* (c.499 + 367T > C) and *PRKAG2* variants (c.1234−317T > G) are predicted to be deleterious based on computational algorithms, and have a higher prevalence in patients with cardiomyopathy compared to the general population. Additionally, it has been demonstrated through pedigree analysis that the splice site mutation in *MYBPC3* needs to co-exist with the *VCL* variant for disease manifestation. Moreover, these deep intronic variants appear to be enriched in binding sites for specific transcription factors such as FOS, JUN and EP300, and thus they may disturb the transcriptional regulation of cardiomyocytes.

As predicted by comprehensive computational analyses (SpliceAI - prediction tool for cryptic sites, and LabBranchoR - prediction tool for branch point at the splice site (49), the study found *MYBPC3* harbors four splicing-site variants (three in intron 13: c.1224−52G > A, c.1224−80G > A, and c.1224−21A > G; one in intron 9: c.906−36G > A) which result in cryptic splice sites, while one variant (c.1898v23A > G) is likely disrupting a branchpoint in intron 19 and results in nonsense mediated decay-led haploinsufficiency in HCM patients (36). Moreover, an earlier report in two South Asian HCM cohorts revealed a rare pathogenic intronic *MYBPC3* variant (c.1224−52G > A) where the mutation introduces a cryptic splice acceptor site in intron 13 and 50 nucleotide inclusion, which led to altered reading frame and premature termination codon at position 438 (p.Ser408fs*31) (23). Furthermore, a different study in a French HCM patient cohort suggested that deep intronic pathogenic *MYBPC3* variants account for about 6% of HCM highlighting the need for routine *MYBPC3* intronic NGS (29). Moreover, WGS and transcriptomic analysis identified three other *MYBPC3* deep intronic variants (c.1090 + 453C > T, c.1091−575A > C, c.1928−569G > T) in HCM patients (5, 28). RNA analyses were performed to confirm aberrant splicing through the inclusion of cryptic exons in cardiomyocytes from patient-derived induced pluripotent stem cells (iPSC-CMs) and in a myectomy sample from one affected relative of the proband (c.1928−569G > T only). In addition, the role of one *MYBPC3* intronic variant (c.3331−26T > G) was found to account for a genotype-negative proband in a family with a history of HCM (71). This variant segregates with two diseased descendants of the proband and it was found in unrelated HCM patients. Through splicing assays using minigene and patient's blood, the authors confirmed that the variant leads to the retention of intron 30 and thus protein haploinsufficiency.

Conclusions

Over the last two decades, numerous novel genetic variants have been linked with different types of cardiomyopathies. However, with more information comes greater responsibility, and given the variable penetrance of genetic mutations and lack of in-depth validation studies, attributing causality to most genetic variants has been challenging. Unsurprisingly, this becomes even more complicated when assessing noncoding genetic variants. Nevertheless, analysis of noncoding variants has witnessed tremendous advancements in sequencing techniques and the booming of artificial intelligence. The transition of common methodologies from traditional WES and pedigree analysis to more advanced sequencing incorporated with *in silico* studies and prediction algorithms, fuels the discovery of *de novo* noncoding variants with a potential disease-causing or modifying role in cardiomyopathies. In this review, we provided an overview of the progress in uncovering noncoding variants and their potential pathogenic mechanisms linked with different cardiomyopathies. Given the accumulation of more genetic information and computational tools, the role of some noncoding variants in key genes can be explored further leading to a better understanding of cardiomyopathy mechanisms. Additionally, it is now more obvious that further validation of noncoding genetic variants is missing. Both *in silico* analyses and prediction tools are limited by the population base of rare cardiomyopathies and the oversimplification of disease mechanisms, which result in discrepancies and inaccurate classifications. This supports the development and optimization of more research protocols such as standardized high-throughput *in vitro* testing platforms. Moreover, patient-derived iPSCs serve as an invaluable tool in studying or modeling disease mechanisms and thus could be exploited to functionally annotate and validate the causal roles of certain noncoding variants. In addition, the rapidly evolving field of gene editing with CRISPR technologies, would further accelerate the deeper interrogation of non-coding genetic variants.

Protein coding genes comprise only a small percentage of the entire human genome and frequently their mutations cannot fully

account for the observed clinical phenotypes. Noncoding genetic variants have been previously overlooked and it is gradually becoming more obvious that they have more meaningful contributions to cardiac diseases. Therefore, incorporating noncoding variants in genetic screening and demonstrating a potential association with clinical prognosis is foreseeable and could be established as part of personalized medicine in the near future.

Author contributions

MH and SL: supervised, outlined and wrote the manuscript. SB, AZ and MC: wrote parts of the manuscript. ET: supervised and wrote the manuscript. All authors contributed to the article and approved the submitted version.

Funding

The present work is supported by NHLBI (HL-145135), AHA (CDA34660077), W.W. Smith Charitable Trust, the Magic that Matters Fund, The Johns Hopkins University Catalyst Award, and MSCRF (2023-MSCRFL-5984).

Conflict of interest

The authors declare that the research was conducted in the absence of any commercial or financial relationships that could be construed as a potential conflict of interest.

Publisher's note

References

1. Anene-Nzelu CG, Lee MCJ, Tan WLW, Dashi A, Foo RSY. Genomic enhancers in cardiac development and disease. *Nat Rev Cardiol*. (2022) 19(1):7–25. doi: 10.1038/s41569-021-00597-2

2. Arrick BA, Lee AL, Grendell RL, Derynck R. Inhibition of translation of transforming growth factor-beta 3 mRNA by its 5′ untranslated region. *Mol Cell Biol*. (1991) 11(9):4306–13. doi: 10.1128/mcb.11.9.4306-4313.1991

3. Arvanitis M, Tampakakis E, Zhang Y, Wang W, Auton A, Dutta D, et al. Genome-wide association and multi-omic analyses reveal ACTN2 as a gene linked to heart failure. *Nat Commun*. (2020) 11(1):1122. doi: 10.1038/s41467-020-14843-7

4. Awad MM, Dalal D, Cho E, Amat-Alarcon N, James C, Tichnell C, et al. DSG2 Mutations contribute to arrhythmogenic right ventricular dysplasia/cardiomyopathy. *Am J Hum Genet*. (2006) 79(1):136–42. doi: 10.1086/504393

5. Bagnall RD, Ingles J, Dinger ME, Cowley MJ, Ross SB, Minoche AE, et al. Whole genome sequencing improves outcomes of genetic testing in patients with hypertrophic cardiomyopathy. *J Am Coll Cardiol*. (2018) 72(4):419–29. doi: 10.1016/j.jacc.2018.04.078

6. Beffagna G, Occhi G, Nava A, Vitiello L, Ditadi A, Basso C, et al. Regulatory mutations in transforming growth factor-beta3 gene cause arrhythmogenic right ventricular cardiomyopathy type 1. *Cardiovasc Res*. (2005) 65(2):366–73. doi: 10.1016/j.cardiores.2004.10.005

7. Brodehl A, Gerull B. Genetic insights into primary restrictive cardiomyopathy. *J Clin Med*. (2022) 11(8):1–25. doi: 10.3390/jcm11082094

8. Brook JD, McCurrach ME, Harley HG, Buckler AJ, Church D, Aburatani H, et al. Molecular basis of myotonic dystrophy: expansion of a trinucleotide (CTG) repeat at the 3′ end of a transcript encoding a protein kinase family member. *Cell*. (1992) 68(4):799–808. doi: 10.1016/0092-8674(92)90154-5

9. Bruneau BG, Nemer G, Schmitt JP, Charron F, Robitaille L, Caron S, et al. A murine model of Holt-Oram syndrome defines roles of the T-box transcription factor Tbx5 in cardiogenesis and disease. *Cell*. (2001) 106(6):709–21. doi: 10.1016/s0092-8674(01)00493-7

10. Catarino RR, Stark A. Assessing sufficiency and necessity of enhancer activities for gene expression and the mechanisms of transcription activation. *Genes Dev*. (2018) 32(3-4):202–23. doi: 10.1101/gad.310367.117

11. Christensen AH, Andersen CB, Wassilew K, Svendsen JH, Bundgaard H, Brand SM, et al. Rare non-coding desmoglein-2 variant contributes to arrhythmogenic right ventricular cardiomyopathy. *J Mol Cell Cardiol*. (2019) 131:164–70. doi: 10.1016/j.yjmcc.2019.04.029

12. Chun JL, O'Brien R, Berry SE. Cardiac dysfunction and pathology in the dystrophin and utrophin-deficient mouse during development of dilated cardiomyopathy. *Neuromuscul Disord*. (2012) 22(4):368–79. doi: 10.1016/j.nmd.2011.07.003

13. Coonar AS, Protonotarios N, Tsatsopoulou A, Needham EW, Houlston RS, Cliff S, et al. Gene for arrhythmogenic right ventricular cardiomyopathy with diffuse nonepidermolytic palmoplantar keratoderma and woolly hair (Naxos disease) maps to 17q21. *Circulation*. (1998) 97(20):2049–58. doi: 10.1161/01.cir.97.20.2049

14. Dickel DE, Barozzi I, Zhu Y, Fukuda-Yuzawa Y, Osterwalder M, Mannion BJ, et al. Genome-wide compendium and functional assessment of in vivo heart enhancers. *Nat Commun*. (2016) 7:12923. doi: 10.1038/ncomms12923

15. Elliott P, Andersson B, Arbustini E, Bilinska Z, Cecchi F, Charron P, et al. Classification of the cardiomyopathies: a position statement from the European society of cardiology working group on myocardial and pericardial diseases. *Eur Heart J*. (2008) 29(2):270–6. doi: 10.1093/eurheartj/ehm342

16. Elliott PM. Classification of cardiomyopathies: evolution or revolution? *J Am Coll Cardiol*. (2013) 62(22):2073–4. doi: 10.1016/j.jacc.2013.10.008

17. Friedman RC, Farh KK, Burge CB, Bartel DP. Most mammalian mRNAs are conserved targets of microRNAs. *Genome Res*. (2009) 19(1):92–105. doi: 10.1101/gr.082701.108

18. Friedrich FW, Dilanian G, Khattar P, Juhr D, Gueneau L, Charron P, et al. A novel genetic variant in the transcription factor Islet-1 exerts gain of function on myocyte enhancer factor 2C promoter activity. *Eur J Heart Fail*. (2013) 15(3):267–76. doi: 10.1093/eurjhf/hfs178

19. Frisso G, Detta N, Coppola P, Mazzaccara C, Pricolo MR, D'Onofrio A, et al. Functional studies and in silico analyses to evaluate non-coding variants in inherited cardiomyopathies. *Int J Mol Sci*. (2016) 17(11):1–13. doi: 10.3390/ijms17111883

20. Gacita AM, Fullenkamp DE, Ohiri J, Pottinger T, Puckelwartz MJ, Nobrega MA, et al. Genetic variation in enhancers modifies cardiomyopathy gene expression and progression. *Circulation*. (2021) 143(13):1302–16. doi: 10.1161/circulationaha.120.050432

21. Gao T, Qian J. Enhanceratlas 2.0: an updated resource with enhancer annotation in 586 tissue/cell types across nine species. *Nucleic Acids Res*. (2020) 48(D1):D58–D64. doi: 10.1093/nar/gkz980

22. Goldman L, Schafer A. *Goldman-Cecil Medicine* (2019).

23. Harper AR, Bowman M, Hayesmoore JBG, Sage H, Salatino S, Blair E, et al. Reevaluation of the south Asian MYBPC3(Δ25 bp) intronic deletion in hypertrophic cardiomyopathy. *Circ Genom Precis Med*. (2020) 13(3):e002783. doi: 10.1161/circgen.119.002783

24. He A, Kong SW, Ma Q, Pu WT. Co-occupancy by multiple cardiac transcription factors identifies transcriptional enhancers active in heart. *Proc Natl Acad Sci U S A*. (2011) 108(14):5632–7. doi: 10.1073/pnas.1016959108

25. Herman DS, Lam L, Taylor MR, Wang L, Teekakirikul P, Christodoulou D, et al. Truncations of titin causing dilated cardiomyopathy. *N Engl J Med*. (2012) 366(7):619–28. doi: 10.1056/NEJMoa1110186

26. Hinnebusch AG, Ivanov IP, Sonenberg N. Translational control by 5′-untranslated regions of eukaryotic mRNAs. *Science*. (2016) 352(6292):1413–6. doi: 10.1126/science.aad9868

27. Hnisz D, Abraham BJ, Lee TI, Lau A, Saint-André V, Sigova AA, et al. Super-enhancers in the control of cell identity and disease. *Cell*. (2013) 155(4):934–47. doi: 10.1016/j.cell.2013.09.053

28. Holliday M, Singer ES, Ross SB, Lim S, Lal S, Ingles J, et al. Transcriptome sequencing of patients with hypertrophic cardiomyopathy reveals novel splice-altering variants in MYBPC3. *Circ Genom Precis Med*. (2021) 14(2):e003202. doi: 10.1161/circgen.120.003202

29. Janin A, Chanavat V, Rollat-Farnier PA, Bardel C, Nguyen K, Chevalier P, et al. Whole MYBPC3 NGS sequencing as a molecular strategy to improve the efficiency of molecular diagnosis of patients with hypertrophic cardiomyopathy. *Hum Mutat*. (2020) 41(2):465–75. doi: 10.1002/humu.23944

30. Jia L, Mao Y, Ji Q, Dersh D, Yewdell JW, Qian SB. Decoding mRNA translatability and stability from the 5′ UTR. *Nat Struct Mol Biol*. (2020) 27 (9):814–21. doi: 10.1038/s41594-020-0465-x

31. Jung H, Lee KS, Choi JK. Comprehensive characterisation of intronic mis-splicing mutations in human cancers. *Oncogene*. (2021) 40(7):1347–61. doi: 10.1038/s41388-020-01614-3

32. Lee DSM, Park J, Kromer A, Baras A, Rader DJ, Ritchie MD, et al. Disrupting upstream translation in mRNAs is associated with human disease. *Nat Commun*. (2021) 12(1):1515. doi: 10.1038/s41467-021-21812-1

33. Lesurf R, Said A, Akinrinade O, Breckpot J, Delfosse K, Liu T, et al. Whole genome sequencing delineates regulatory, copy number, and cryptic splice variants in early onset cardiomyopathy. *NPJ Genom Med*. (2022) 7(1):18. doi: 10.1038/s41525-022-00288-y

34. Liu CF, Abnousi A, Bazeley P, Ni Y, Morley M, Moravec CS, et al. Global analysis of histone modifications and long-range chromatin interactions revealed the differential cistrome changes and novel transcriptional players in human dilated cardiomyopathy. *J Mol Cell Cardiol*. (2020) 145:30–42. doi: 10.1016/j.yjmcc.2020.06.001

35. Llamusí B, Artero R. Molecular effects of the CTG repeats in mutant dystrophia myotonica protein kinase gene. *Curr Genomics*. (2008) 9(8):509–16. doi: 10.2174/138920208786847944

36. Lopes LR, Barbosa P, Torrado M, Quinn E, Merino A, Ochoa JP, et al. Cryptic splice-altering variants in MYBPC3 are a prevalent cause of hypertrophic cardiomyopathy. *Circ Genom Precis Med*. (2020) 13(3):e002905. doi: 10.1161/circgen.120.002905

37. Marian AJ. Clinical interpretation and management of genetic variants. *JACC Basic Transl Sci*. (2020) 5(10):1029–42. doi: 10.1016/j.jacbts.2020.05.013

38. May D, Blow MJ, Kaplan T, McCulley DJ, Jensen BC, Akiyama JA, et al. Large-scale discovery of enhancers from human heart tissue. *Nat Genet*. (2011) 44(1):89–93. doi: 10.1038/ng.1006

39. Mazumder B, Seshadri V, Fox PL. Translational control by the 3′-UTR: the ends specify the means. *Trends Biochem Sci*. (2003) 28(2):91–8. doi: 10.1016/s0968-0004(03)00002-1

40. McKenna WJ, Judge DP. Epidemiology of the inherited cardiomyopathies. *Nat Rev Cardiol*. (2021) 18(1):22–36. doi: 10.1038/s41569-020-0428-2

41. McKoy G, Protonotarios N, Crosby A, Tsatsopoulou A, Anastasakis A, Coonar A, et al. Identification of a deletion in plakoglobin in arrhythmogenic right ventricular cardiomyopathy with palmoplantar keratoderma and woolly hair (Naxos disease). *Lancet*. (2000) 355(9221):2119–24. doi: 10.1016/s0140-6736(00)02379-5

42. Meder B, Rühle F, Weis T, Homuth G, Keller A, Franke J, et al. A genome-wide association study identifies 6p21 as novel risk locus for dilated cardiomyopathy. *Eur Heart J*. (2014) 35(16):1069–77. doi: 10.1093/eurheartj/eht251

43. Mendes de Almeida R, Tavares J, Martins S, Carvalho T, Enguita FJ, Brito D, et al. Whole gene sequencing identifies deep-intronic variants with potential functional impact in patients with hypertrophic cardiomyopathy. *PLoS One*. (2017) 12(8):e0182946. doi: 10.1371/journal.pone.0182946

44. Mignone F., Gissi C., Liuni S., Pesole G. (2002). Untranslated regions of mRNAs. *Genome Biol*, 3(3), Reviews0004. doi: 10.1186/gb-2002-3-3-reviews0004

45. Minoche AE, Horvat C, Johnson R, Gayevskiy V, Morton SU, Drew AP, et al. Genome sequencing as a first-line genetic test in familial dilated cardiomyopathy. *Genet Med*. (2019) 21(3):650–62. doi: 10.1038/s41436-018-0084-7

46. Mortimer SA, Kidwell MA, Doudna JA. Insights into RNA structure and function from genome-wide studies. *Nat Rev Genet*. (2014) 15(7):469–79. doi: 10.1038/nrg3681

47. Moszyńska A, Gebert M, Collawn JF, Bartoszewski R. SNPs in microRNA target sites and their potential role in human disease. *Open Biol*. (2017) 7(4):1–13. doi: 10.1098/rsob.170019

48. Norgett EE, Hatsell SJ, Carvajal-Huerta L, Cabezas JC, Common J, Purkis PE, et al. Recessive mutation in desmoplakin disrupts desmoplakin-intermediate filament interactions and causes dilated cardiomyopathy, woolly hair and keratoderma. *Hum Mol Genet*. (2000) 9(18):2761–6. doi: 10.1093/hmg/9.18.2761

49. Paggi JM, Bejerano G. A sequence-based, deep learning model accurately predicts RNA splicing branchpoints. *Rna*. (2018) 24(12):1647–58. doi: 10.1261/rna.066290.118

50. Parker SC, Stitzel ML, Taylor DL, Orozco JM, Erdos MR, Akiyama JA, et al. Chromatin stretch enhancer states drive cell-specific gene regulation and harbor human disease risk variants. *Proc Natl Acad Sci U S A*. (2013) 110(44):17921–6. doi: 10.1073/pnas.1317023110

51. Pilichou K, Nava A, Basso C, Beffagna G, Bauce B, Lorenzon A, et al. Mutations in desmoglein-2 gene are associated with arrhythmogenic right ventricular cardiomyopathy. *Circulation*. (2006) 113(9):1171–9. doi: 10.1161/circulationaha.105.583674

52. Plank JL, Dean A. Enhancer function: mechanistic and genome-wide insights come together. *Mol Cell*. (2014) 55(1):5–14. doi: 10.1016/j.molcel.2014.06.015

53. Pua CJ, Bhalshankar J, Miao K, Walsh R, John S, Lim SQ, et al. Development of a comprehensive sequencing assay for inherited cardiac condition genes. *J Cardiovasc Transl Res*. (2016) 9(1):3–11. doi: 10.1007/s12265-016-9673-5

54. Pugh TJ, Kelly MA, Gowrisankar S, Hynes E, Seidman MA, Baxter SM, et al. The landscape of genetic variation in dilated cardiomyopathy as surveyed by clinical DNA sequencing. *Genet Med*. (2014) 16(8):601–8. doi: 10.1038/gim.2013.204

55. Reynolds JO, Quick AP, Wang Q, Beavers DL, Philippen LE, Showell J, et al. Junctophilin-2 gene therapy rescues heart failure by normalizing RyR2-mediated Ca (2+) release. *Int J Cardiol*. (2016) 225:371–80. doi: 10.1016/j.ijcard.2016.10.021

56. Rickels R, Shilatifard A. Enhancer logic and mechanics in development and disease. *Trends Cell Biol*. (2018) 28(8):608–30. doi: 10.1016/j.tcb.2018.04.003

57. Rosenbaum AN, Agre KE, Pereira NL. Genetics of dilated cardiomyopathy: practical implications for heart failure management. *Nat Rev Cardiol*. (2020) 17 (5):286–97. doi: 10.1038/s41569-019-0284-0

58. Salman OF, El-Rayess HM, Abi Khalil C, Nemer G, Refaat MM. Inherited cardiomyopathies and the role of mutations in non-coding regions of the genome. *Front Cardiovasc Med*. (2018) 5:77. doi: 10.3389/fcvm.2018.00077

59. Schlegel P, Reinkober J, Meinhardt E, Tscheschner H, Gao E, Schumacher SM, et al. G protein-coupled receptor kinase 2 promotes cardiac hypertrophy. *PLoS One*. (2017) 12(7):e0182110. doi: 10.1371/journal.pone.0182110

60. Schunkert H, König IR, Kathiresan S, Reilly MP, Assimes TL, Holm H, et al. Large-scale association analysis identifies 13 new susceptibility loci for coronary artery disease. *Nat Genet*. (2011) 43(4):333–8. doi: 10.1038/ng.784

61. Singer RH. RNA Zipcodes for cytoplasmic addresses. *Curr Biol*. (1993) 3 (10):719–21. doi: 10.1016/0960-9822(93)90079-4

62. Smemo S, Campos LC, Moskowitz IP, Krieger JE, Pereira AC, Nobrega MA. Regulatory variation in a TBX5 enhancer leads to isolated congenital heart disease. *Hum Mol Genet*. (2012) 21(14):3255–63. doi: 10.1093/hmg/dds165

63. Soukarieh O, Meguerditchian C, Proust C, Aïssi D, Eyries M, Goyenvalle A, et al. Common and rare 5′UTR variants altering upstream open Reading frames in cardiovascular genomics. *Front Cardiovasc Med*. (2022) 9:841032. doi: 10.3389/fcvm.2022.841032

64. Spurrell CH, Barozzi I, Kosicki M, Mannion BJ, Blow MJ, Fukuda-Yuzawa Y, et al. Genome-wide fetalization of enhancer architecture in heart disease. *Cell Rep*. (2022) 40(12):111400. doi: 10.1016/j.celrep.2022.111400

65. Stephen J, Maddirevula S, Nampoothiri S, Burke JD, Herzog M, Shukla A, et al. Bi-allelic TMEM94 truncating variants are associated with neurodevelopmental delay, congenital heart defects, and distinct facial dysmorphism. *Am J Hum Genet*. (2018) 103(6):948–67. doi: 10.1016/j.ajhg.2018.11.001

66. Steri M, Idda ML, Whalen MB, Orrù V. Genetic variants in mRNA untranslated regions. *Wiley Interdiscip Rev RNA*. (2018) 9(4):e1474. doi: 10.1002/wrna.1474

67. Syrris P, Ward D, Evans A, Asimaki A, Gandjbakhch E, Sen-Chowdhry S, et al. Arrhythmogenic right ventricular dysplasia/cardiomyopathy associated with mutations in the desmosomal gene desmocollin-2. *Am J Hum Genet*. (2006) 79 (5):978–84. doi: 10.1086/509122

68. Tadros R, Francis C, Xu X, Vermeer AMC, Harper AR, Huurman R, et al. Shared genetic pathways contribute to risk of hypertrophic and dilated cardiomyopathies with opposite directions of effect. *Nat Genet*. (2021) 53 (2):128–34. doi: 10.1038/s41588-020-00762-2

69. Tan WLW, Anene-Nzelu CG, Wong E, Lee CJM, Tan HS, Tang SJ, et al. Epigenomes of human hearts reveal new genetic variants relevant for cardiac disease and phenotype. *Circ Res*. (2020) 127(6):761–77. doi: 10.1161/circresaha.120.317254

70. Tobita T, Nomura S, Fujita T, Morita H, Asano Y, Onoue K, et al. Genetic basis of cardiomyopathy and the genotypes involved in prognosis and left ventricular reverse remodeling. *Sci Rep*. (2018) 8(1):1998. doi: 10.1038/s41598-018-20114-9

71. Torrado M, Maneiro E, Lamounier Junior A, Fernández-Burriel M, Sánchez Giralt S, Martínez-Carapeto A, et al. Identification of an elusive spliceogenic MYBPC3 variant in an otherwise genotype-negative hypertrophic cardiomyopathy pedigree. *Sci Rep*. (2022) 12(1):7284. doi: 10.1038/s41598-022-11159-y

72. Towbin JA. Inherited cardiomyopathies. *Circ J*. (2014) 78(10):2347–56. doi: 10.1253/circj.cj-14-0893

73. Vadgama N, Ameen M, Sundaram L, Gaddam S, Gifford C, Nasir J, et al. De novo and inherited variants in coding and regulatory regions in genetic cardiomyopathies. *Hum Genomics*. (2022) 16(1):55. doi: 10.1186/s40246-022-00420-0

74. van den Boogaard M, Wong LY, Tessadori F, Bakker ML, Dreizehnter LK, Wakker V, et al. Genetic variation in T-box binding element functionally affects SCN5A/SCN10A enhancer. *J Clin Invest*. (2012) 122(7):2519–30. doi: 10.1172/jci62613

75. Villar D, Frost S, Deloukas P, Tinker A. The contribution of non-coding regulatory elements to cardiovascular disease. *Open Biol*. (2020) 10(7):200088. doi: 10.1098/rsob.200088

76. Visel A, Rubin EM, Pennacchio LA. Genomic views of distant-acting enhancers. *Nature*. (2009) 461(7261):199–205. doi: 10.1038/nature08451

77. Walsh R, Offerhaus JA, Tadros R, Bezzina CR. Minor hypertrophic cardiomyopathy genes, major insights into the genetics of cardiomyopathies. *Nat Rev Cardiol*. (2022) 19(3):151–67. doi: 10.1038/s41569-021-00608-2

78. Wamstad JA, Wang X, Demuren OO, Boyer LA. Distal enhancers: new insights into heart development and disease. *Trends Cell Biol*. (2014) 24(5):294–302. doi: 10.1016/j.tcb.2013.10.008

79. Wang F, Liu D, Zhang RR, Yu LW, Zhao JY, Yang XY, et al. A TBX5 3′UTR variant increases the risk of congenital heart disease in the Han Chinese population. *Cell Discov*. (2017) 3:17026. doi: 10.1038/celldisc.2017.26

80. Whiffin N, Karczewski KJ, Zhang X, Chothani S, Smith MJ, Evans DG, et al. Characterising the loss-of-function impact of 5′ untranslated region variants in 15,708 individuals. *Nat Commun*. (2020) 11(1):2523. doi: 10.1038/s41467-019-10717-9

81. Yamada T, Nomura S. Recent findings related to cardiomyopathy and genetics. *Int J Mol Sci*. (2021) 22:22. doi: 10.3390/ijms222212522

82. Zhou B, Rao L, Li Y, Gao L, Li C, Chen Y, et al. The association between dilated cardiomyopathy and RTN4 3′UTR insertion/deletion polymorphisms. *Clin Chim Acta*. (2009) 400(1–2):21–4. doi: 10.1016/j.cca.2008.09.028

frontiers | Frontiers in Cardiovascular Medicine

TYPE Case Report
PUBLISHED 23 May 2023
DOI 10.3389/fcvm.2023.1150657

OPEN ACCESS

EDITED BY
Hilary Vernon,
Johns Hopkins Medicine, United States

REVIEWED BY
Angeliki Asimaki,
St George's, University of London, United Kingdom
Andreas Brodehl,
Heart and Diabetes Center North Rhine-Westphalia, Germany

*CORRESPONDENCE
Yimin Hua
✉ Nathan_hua@163.com
Hongyu Duan
✉ 495429978@qq.com
Yifei Li
✉ liyfwcsh@scu.edu.cn

†These authors have contributed equally to this work

RECEIVED 24 January 2023
ACCEPTED 03 May 2023
PUBLISHED 23 May 2023

CITATION
Liu X, Zhang Y, Li W, Zhang Q, Zhou L, Hua Y, Duan H and Li Y (2023) Misdiagnosed myocarditis in arrhythmogenic cardiomyopathy induced by a homozygous variant of *DSG2*: a case report.
Front. Cardiovasc. Med. 10:1150657.
doi: 10.3389/fcvm.2023.1150657

Misdiagnosed myocarditis in arrhythmogenic cardiomyopathy induced by a homozygous variant of *DSG2*: a case report

Xuwei Liu[1†], Yue Zhang[1†], Wenjuan Li[1,2†], Qian Zhang[1], Letao Zhou[1], Yimin Hua[1*], Hongyu Duan[1*] and Yifei Li[1*]

[1]Key Laboratory of Birth Defects and Related Diseases of Women and Children of MOE, Department of Pediatrics, West China Second University Hospital, Sichuan University, Chengdu, China, [2]Department of Nursing, West China Second University Hospital, Sichuan University, Chengdu, China

Background: Arrhythmogenic cardiomyopathy (ACM) is an inherited cardiomyopathy that is rarely diagnosed in infants or young children. However, some significant homozygous or compound heterozygous variants contribute to more severe clinical manifestations. In addition, inflammation of the myocardium and ventricular arrhythmia might lead to misdiagnosis with myocarditis. Here, we describe an 8-year-old patient who had been misdiagnosed with myocarditis. Timely genetic sequencing helped to identify this case as ACM induced by a homozygous variant of *DSG2*.

Case presentation: The proband of this case was an 8-year-old boy who initially presented with chest pain with an increased level of cardiac Troponin I. In addition, the electrocardiogram revealed multiple premature ventricular beats. Cardiac magnetic resonance revealed myocardial edema in the lateral ventricular wall and apex, indicating localized injuries of the myocardium. The patient was primarily suspected to have acute coronary syndrome or viral myocarditis. Whole-exome sequencing confirmed that the proband had a homozygous variation, c.1592T > G, of the *DSG2* gene. This mutation site was regulated by DNA modification, which induced amino acid sequence changes, protein structure effects, and splice site changes. According to MutationTaster and PolyPhen-2 analyses, the variant was considered a disease-causing mutation. Next, we used SWISS-MODEL to illustrate the mutation site of p.F531C. The ensemble variance of p.F531C indicated the free energy changes after the amino acid change.

Conclusion: In summary, we reported a rare pediatric case initially presenting as myocarditis that transitioned into ACM during follow-up. A homozygous genetic variant of DSG2 was inherited in the proband. This study expanded the clinical feature spectrum of DSG2-associated ACM at an early age. Additionally, the presentation of this case emphasized the difference between homozygous and heterozygous variants of desmosomal genes in disease progression. Genetic sequencing screening could be helpful in distinguishing unexplained myocarditis in children.

KEYWORDS

DSG2, ACM, myocarditis, genetic sequencing, case report

1. Introduction

Arrhythmogenic right ventricular cardiomyopathy (ARVC, OMIM:#610476) is an inherited heart muscle disease characterized by the loss of the ventricular myocardium and fibrofatty replacement, which predisposes patients to fatal ventricular arrhythmias and sudden cardiac death (SCD) (1, 2). A genetic etiology has been identified for most inherited cardiovascular diseases, especially cardiomyopathies, with the rapid development of sequencing techniques. Regarding the molecular mechanism, ARVC has been identified as being related to pathogenetic variants in desmosomes and adherens junctions, which are critical for establishing cell–cell junctions and maintaining intercellular communication (3, 4). Thus, the disease group ACM should be considered to define the broader spectrum of the phenotypic expressions of the disease (4). From a molecular perspective, multiple genes encoding desmosomal proteins, such as plakophilin-2 (*PKP2*), desmoplakin (*DSP*), *DSG2*, desmocollin (*DSC2*), and plakoglobin (*JUP*), account for 50% of patients with ACM in different cohorts (5, 6). However, there are other genetic (non-desmosomal) and non-genetic causes of the disease. The non-desmosomal genes include *DES*, *LMNA*, *SCN5A*, *PLN*, *TMEM43*, and *TGFB3*, which are not involved in the molecular formation of desmosomes and participate in several types of ARVC origins (2). The inclusion of sarcomere-, ion transporter-, and cytokine-related genes would increase the percentage of patients positive for molecular characterization. However, the incomplete dominance and variable expressiveness of certain variants suggest that environmental factors play an important role. Initially, ARVC was considered to mainly cause right ventricular lesions and impair the function of the right ventricle. However, with the development of sequencing analysis and clinical imaging screening techniques, such as cardiac magnetic resonance (CMR), it has been found that biventricular or even left ventricular dysfunction is the dominant phenotype in ARVC, especially for *DSP* and *DSG2* mutations (2).

Large-sample studies have shown that individuals with more than one mutation may have poorer clinical outcomes, with a fivefold increased risk of developing left ventricular dysfunction and heart failure compared with patients with a single mutation (6). Recently, several types of ACM, especially those involving the left-dominant and biventricular forms, presented atypical and diverse phenotypes. Studies have demonstrated a spectrum of biventricular and left-dominant forms that could be misdiagnosed as myocarditis, unexplained myocardial injuries, or even acute coronary syndrome (ACS). Furthermore, case reports have identified patients who were erroneously diagnosed with myocarditis instead of ARVC, or vice versa, highlighting the clinical and diagnostic overlap (7, 8). There is increasing evidence that underlying genetic abnormalities associated with cardiomyopathy may predispose patients to myocarditis or other myocardial injuries (9). Brodehl et al. (10) demonstrated that genetic mouse models of ACM can exhibit early inflammation between 2 and 3.5 weeks of age. Herein, we report a rare case that initially presented as myocarditis. However, we failed to identify any lesions in his coronary arteries. Molecular genetic analysis revealed a homozygous mutation of *DSG2*, and the proband presented with ACM after a 1-year follow-up. This report expands the spectrum of the clinical presentation of ACM, especially in homozygous *DSG2* variants.

2. Case presentation

2.1. Clinical presentation and physical examination

This study was approved by the Ethics Committee of the West China Second Hospital of Sichuan University (approval number 2014–034). Informed consent was obtained from the patient's parents before performing whole-exome sequencing and for the inclusion of the patient's clinical and imaging details in subsequent publications.

The proband was an 8-year-old male admitted to our hospital for 5 days due to severe, recurrent, and persistent chest pain. Moreover, the chest pain attacks became more frequent and his pain levels worsened, which he could not tolerate. He described the acute and repeated chest pain as aching and tightness. Additionally, the patient complained of pain spreading from the chest to the shoulders, upper abdomen, and back. In the last 2 days before hospital admission, the patient suffered severe vomiting more than five times per day. When the chest attacks occurred, he experienced palpitations and slightly reduced activity tolerance. However, he denied any syncope and shortness of breath. There was no fever, cough, or indigestion.

The initial physical examination at the emergency department revealed an acute critical illness involving severe diaphoresis, dizziness, and fatigue, with the patient presenting with a pale face and feeling restless. The heart rate was approximately 75 beats per minute, and irregular premature beats were observed. His blood pressure was 91/52 mmHg. At the same time, the breathing rate slightly increased to 25 breaths per minute. This patient had a normal nutrition status, and his response to external stimulation was also normal. No trauma injuries were found on the body surface. The respiratory movements of both lungs were symmetrical; the breath sounds of both lungs were rough, no significant wet rales were heard in the bilateral lungs, and occasional wheezing sounds were heard. The apex of the heartbeat moved to the lower left, and there was a sense of lift in the precordial area. A mildly enlarged heart boundary was identified, and the rhythm was heterogeneous with premature beats. However, the heart sound was dull, and a level I–II systolic murmur was recorded. The abdomen was soft, the liver was 2 cm below the subcostal margin and 1 cm–2 cm below the xiphoid process, the texture was medium, and the spleen was not palpable subcostally. The muscle strength and tension of the four extremities were normal. The pathological signs and meningeal irritation signs were negative.

The patient suffered influenza A infection 1 year before these chest pain attacks, and myocardial injuries had been identified by an increased level of cardiac troponin I (cTnI). The

electrocardiogram (ECG) revealed multiple premature ventricular beats. After a series of myocardial protection treatments had been provided, the patient recovered and did not complain of any other cardiac-related symptoms in the year before this illness. Moreover, his parents denied any positive family history of cardiac attacks or cardiovascular, hypertension, and coronary artery diseases. The parents also denied any history of diabetes and obesity among his family members. No inherited disease had been identified in this family, including any cardiomyopathies and metabolic diseases.

2.2. Imaging and laboratory examinations

Routine blood cell tests and blood gas analyses produced results that were within a standard range. In addition, hepatic and renal function tests yielded no significant findings. However, serum cardiac troponin I (2.808 μg/L, n.v. < 0.06 μg/L) and B-type natriuretic peptide (1020.24 pg/ml, n.v. < 100 pg/ml) levels were significantly elevated, demonstrating significant myocardial injury. An ECG was performed immediately, and abnormal Q waves were observed in the II, III, aVF, V5, and V6 leads (**Figure 1A**). At the same time, Holter scanning revealed multiple ventricular premature beats and paired atrial premature beats. Thus, ACS or viral myocarditis was primarily suspected in this patient. All infection parameters, including CRP, PCT, and ESR, were in the expected range. Additionally, antibody tests of potential viruses involved in myocarditis were assessed, including cytomegalovirus, Epstein–Barr virus, adenovirus, coxsackie virus, and herpes simplex virus, such as human parvovirus B19, and no positive viral infection results were obtained. In addition, autoimmune antibodies and rheumatic tests were performed and all the related results were negative.

Echocardiography demonstrated a slight enlargement of the left ventricle (42 mm), while the left ventricular ejection fraction dropped slightly to 46% at the time he was admitted (**Figure 2A**). Holter scanning revealed multiple premature ventricular beats and atrial tachycardia, while abnormal Q waves were also identified in the II, III, aVF, and V3-V6 leads (**Figures 1B, C**). Moreover, repeated ECG examination found an ST-segment elevation among the abovementioned leads, which strongly indicated ACS. Cardiac magnetic resonance (CMR) revealed myocardial edema in the lateral ventricular wall and apex, indicating localized myocardium injuries (**Figures 2B, B'**). The area of infected myocardium was consistent with the changes in ECG presentation. In addition, CT coronary artery angiography was performed to examine the morphology of the coronary arteries (**Figures 2C–E**). The right coronary artery was infused and presented a typical structure. Angiographic images of the left coronary artery were also obtained and no significant positive result was recorded (**Figures 2F, F'**).

Therefore, a myocarditis attack was suspected, while ACS with non-obstructive coronary arteries could not be entirely excluded. Thus, myocardial protection treatment, including creatine phosphate and levocarnitine, and non-invasive mechanical ventilation were provided. Then, antibiotics were administered for potential infection treatment. Dexamethasone was administered to relieve edema of the myocardium. After 2 weeks of treatment and intensive care, the patient recovered from severe chest pain and did not report any discomfort of the heart. After that, the patient was discharged with strict follow-up.

2.3. WES technical method

Owing to the complicated symptoms and negative imaging assessments of this proband, a particular cardiomyopathy was still suspected. Therefore, whole-exome sequencing (WES) was carried out to identify any essential genetic variants. A peripheral blood sample was obtained from the patient in an ethylenediaminetetraacetic acid (EDTA) anticoagulant blood sample tube that was stored at 4°C for less than 6 h. DNA was extracted using a Blood Genome Column Medium Extraction Kit (Tiangen Biotech, Beijing, China). WES was performed using the NovaSeq 6,000 platform (Illumina, San Diego, CA, USA), and the raw data were processed using FastP to remove adapters and filter low-quality reads. Paired-end reads were aligned to the Ensembl GRCh38/hg38 reference genome using the Burrows–Wheeler Aligner. Variant annotation was performed in accordance with database-sourced minor allele frequencies (MAFs) and practical guidelines on pathogenicity issued by the American College of Medical Genetics. The annotation of MAFs was performed according to the 1,000 Genomes, dbSNP, ESP, ExAC, and Chigene inhouse MAF databases and the Provean, Sift, Polypen2_hdiv, and Polypen2_hvar databases using R software (R Foundation for Statistical Computing, Vienna, Austria). To elucidate the molecular architecture of the targeted gene, we used MutationTaster with R software to predict the pathogenicity of the targeted gene and assess the impact of the mutations on protein structure. We performed comparative modeling using SWISS-MODEL. If there was no available full-length protein crystal structure for the targeted gene, the AlphaFold protein structure database (https://alphafold.ebi.ac.uk/) tool was used to predict the protein crystal structure.

2.4. Molecular results

A homozygous missense variant in the *DSG2* gene was identified (NM_001943, c.1592T >G; p.F531C). His biological parents were allelic carriers without any clinical manifestations (**Figure 3A**), and Sanger validation was performed (**Figure 3B**). Additionally, no other cardiovascular-related variants were retrieved between the proband and his parents. Beyond the reported DSG2 variant, there were no other potential cardiomyopathic variants, and most of them were synonymous mutations. The molecular crystal structure was built in AlphaFold (AF-Q14126-F1, **Figure 3C**), while the extracellular domain protein structure was used for specific site analysis (5erd.1.A, **Figure 3E**) (11). In addition, the frequency of this mutation in the population according to database research is presented (**Figure 3D**), but only a few allele carriers were found in previous reports. This proband would be the youngest identified patient with a homozygous variant change of c.1592T >G in *DSG2*. This mutation site was regulated by DNA

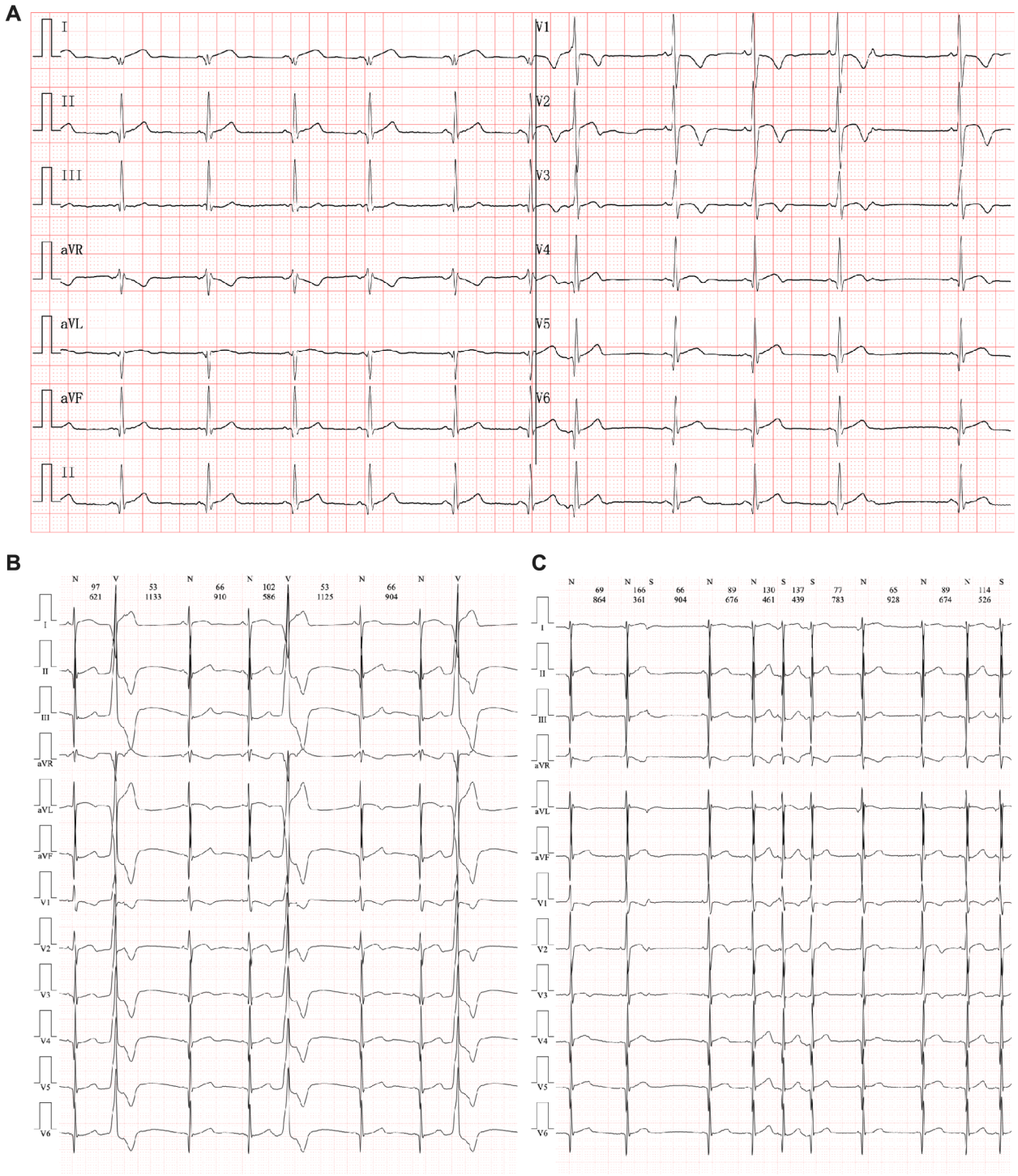

FIGURE 1
Electrocardiography manifestation in the current proband. (A) An abnormal Q wave had been found in II, III, aVF, V5, and V6 leads. (B) Multiple premature ventricular beats. (C) Paired premature atrial beats.

modification, which induced amino acid sequence changes, protein structure effects, and splice-site changes. According to MutationTaster analysis, the variant was considered a disease-causing mutation, and the probability value was 0.99. PolyPhen-2 analysis demonstrated a damaging change in this protein (1.00). The SIFT score predicted protein damage (0.001), and MutationAssessor indicated a high molecular function impact on the variant (FI score, 3.79; VC score, 4.80; and VS score 2.77). Then, we used SWISS-MODEL to illustrate the mutation site of p.F531C (**Figure 3E**) (11). The ensemble variance of p.F531C indicated free energy changes after the amino acid change (**Figure 3F**).

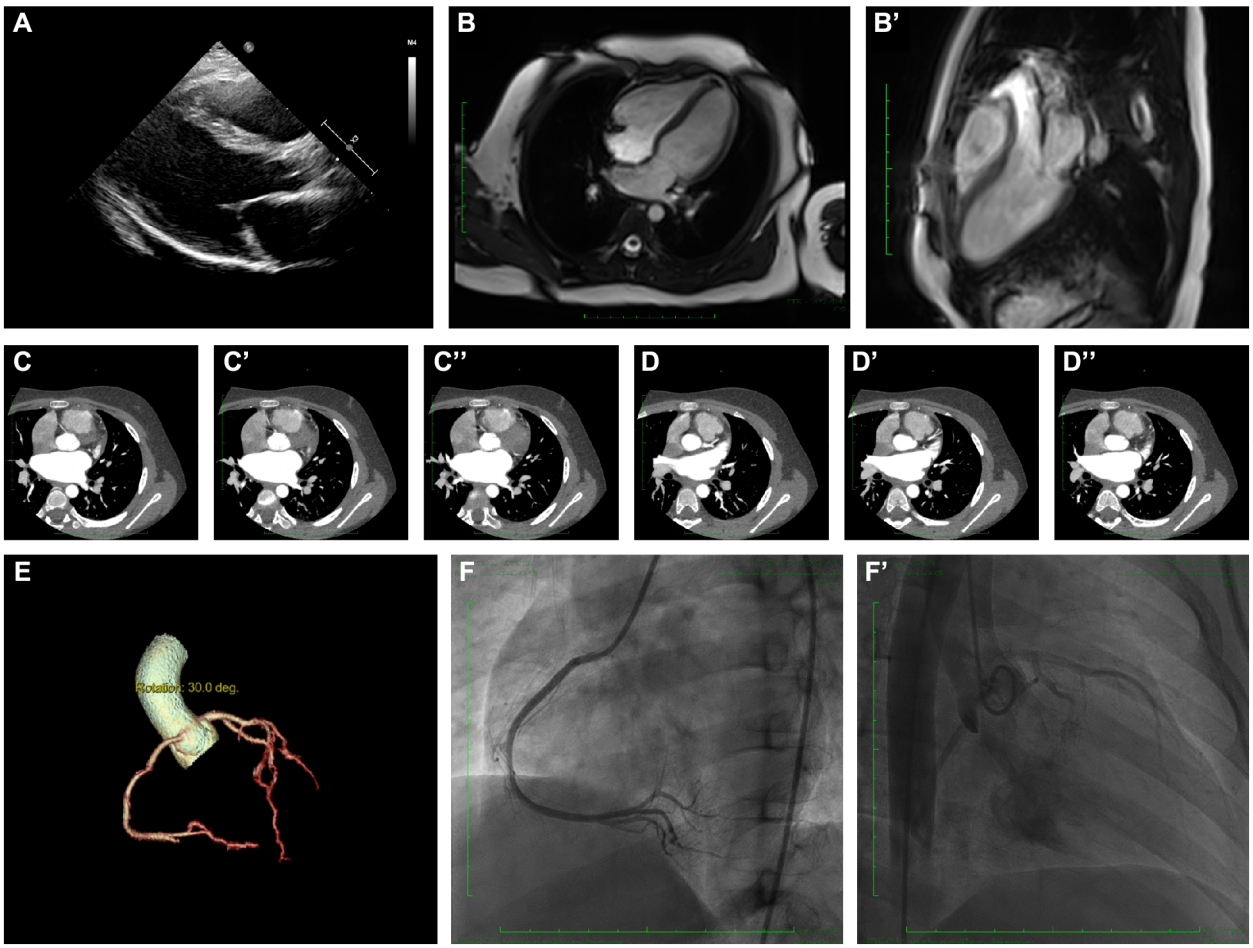

FIGURE 2
Clinical and radiographic manifestation of the current proband. (A) Echocardiography revealed a slight enlargement of the left ventricle. (B–B'). Cardiac magnetic resonance showed myocardial edema in the lateral ventricular wall and apex, indicating localized injures of the myocardium. (C–C''). CTA revealed normal right coronary artery structure. (D–D'') CTA revealed normal left coronary artery structure. (E) Coronary artery rebuilding based on CTA. (F–F') Angiographic images of the left coronary artery; no significant positive result was recorded.

2.5. Final diagnosis, treatment, and follow-Up

During follow-up, the patient presented left ventricular dysfunction (LVEF = 36%) and aggressive enlargement of the left ventricle (48 mm). ECG also identified frequent premature ventricular beats (>1,000 beats per day). Based on the molecular genetic analysis of a homozygous variant of *DSG2*, a diagnosis of arrhythmogenic cardiomyopathy was made, as no significant involvement was found in the right ventricle. After diagnosis, metoprolol and captopril were administered to the patient, who reported no further chest pain and a reduced frequency of arrhythmia. This patient was misdiagnosed as having myocarditis at his initial admission. The results indicate that this homozygous variant of *DSG2* could cause an earlier onset of an adverse cardiac event than heterozygous variants. The first attack of arrhythmogenic cardiomyopathy might result in a series of symptoms, such as ACS. Therefore, genetic screening of unexplained myocarditis is critical.

3. Discussion

ACM was once regarded as the most relevant disease in the young adult population. However, an increasing number of pediatric patients, including toddlers and infants, have been identified by advanced imaging and genetic analysis. However, the clinical characteristics and natural history of pediatric ACM are largely unknown. Furthermore, few available data or recommendations have been proposed for administration strategies of ACM in children. We described an 8-year-old child who initially presented with clinical ACS and was subsequently diagnosed with ACM during follow-up due to molecular test results. ACM is considered a rare disease that is probably underestimated due to insufficient awareness of the atypical symptoms, including myocardial injuries, ACS, and myocarditis (12). Left ventricular involvement and biventricular failure were common among homozygous *DSG2* p.F531C variant patients, even at an early age, while heterozygous variant carriers were either unaffected or mild ARVC-related symptoms only

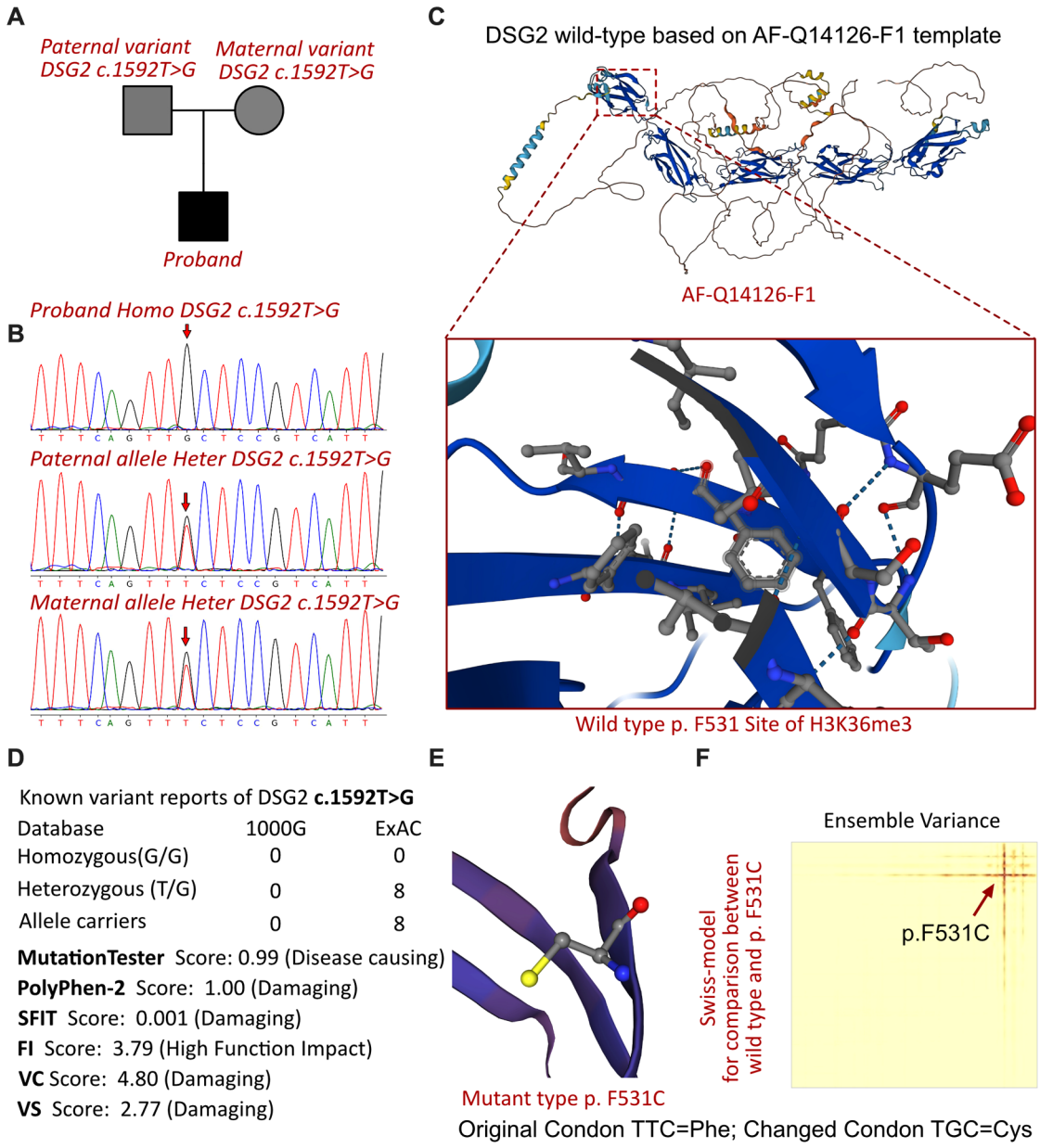

FIGURE 3
The DSG2 mutations in this family and molecular analysis. (**A**) The proband exhibited a homozygous variant of DSG2 (c.1592T >G; p.F531C). (**B**) Sanger sequencing validation. (**C**) Protein structure predicted by AlphaFold (AF-Q14126-F1). (**D**) The homozygous variant of DSG2 c.1592T >G had never been reported in 1000G and ExAC, while eight records had been retrieved from the ExAC database. Protein damage was predicted by PolyPhen-2 and SFIT. (**E**) Altered amino acid structural site of DSG2 p.F531C. (**F**) Changed free energy on the DSG2 p.F531C site.

presented in 25% of relatives (13). The changes in amino acids were predicted to impair the extracellular domain connections between cardiomyocytes. Patients with ARVC can rarely develop chest pain and ST-segment changes on an ECG, which present similarly to ACS (14). Lopez-Ayala et al. (15) identified 7 out of 195 *DSP* variant carriers who presented with acute myocarditis. The atypical clinical presentation defined as the "hot phase" often occurs in pediatric patients carrying *DSP* and *DSG2* gene mutations (7). Previous studies have suggested that pathogenic *DSP* variants might play a unique role in myocarditis in ACM (16). However, Belkaya et al. (7) demonstrated the enrichment of rare biallelic non-synonymous or splice-site variants in genes associated with inherited cardiomyopathies in a pediatric acute myocarditis cohort (12%) compared with healthy subjects (0.9%). Several specific genetic variants of ACM have been identified in patients with myocarditis-like symptoms. In addition, *DSG2* variants have been recognized as pathogenic variants involved in biventricular impairments, and these variants also contribute to an overlapping manifestation with myocarditis. Moreover, in a recent study, Boogerd et al. (17) found that *PKP2* variants also lead to biventricular dysfunction, which expanded the understanding of ARVC. Brodehl et al. demonstrated two similar cases with *DSG2* and *DSC2* variants (18, 19). This evidence indicated that several extracellular domain impairments of

desmosomes would lead to biventricular dysfunction, and it was critical to distinguish them from cardiomyopathies, as they presented a higher risk of SCD. Desmosome-related mutations have been associated with a peculiar phenotype characterized by episodes of acute myocardial injury, induced LV fibrosis, progressive systolic dysfunction, and a high incidence of ventricular arrhythmia (20). These forms are often diagnosed as acute myocarditis. Hata Yukiko et al. (21) revealed that 8 out of 10 cases with unexplained minimal inflammatory foci might be the causative gene variant of cardiomyopathy. Generally, myocarditis has been identified as reduced heart function, changes in ECG, elevated cTnI levels, and abnormal signals in cardiac MRI, according to various guidelines for distinguishing myocarditis. Unfortunately, patients with ACM can also present these clinical manifestations, and several ACM cases were misdiagnosed as myocarditis in practice. Thus, it is urgent to understand the association between different genetic variants in ACM and their overlap with myocarditis.

ACS is seldom observed in pediatric patients. Previous studies demonstrated that familial hypercholesterolemia was the most common cause of pediatric ACS (22). Davlat et al. (23) demonstrated the association of left ventricular non-compaction with ACS. Moreover, Puwanant et al. (24) presented a cohort of 200 patients with hypertrophic cardiomyopathy (HCM) suffering a higher prevalence of ACS. Therefore, it is essential to distinguish the onset of ACS as a significant symptom before the dominant phenotype of cardiomyopathies appears.

Notably, the phenotypic variation between homozygous and heterozygous variant carriers should be addressed. The study of a *DSG2* knockout murine model of ACM revealed cardiac inflammation as a critical early event leading to myocardial fibrosis (25). Modulating inflammatory signaling pathways, such as NF-κB, may be a novel therapeutic target for desmosomal-mediated cardiomyopathy, as recently demonstrated in a mouse model harboring homozygous mutations in *DSG2* (26). Compound/digenic heterozygosity has been identified in up to 25% of patients and has been reported to account for both phenotypic variability and more malignant lifetime arrhythmic outcome (dose effect) (27, 28). While the right-dominant form was typically associated with genes encoding desmosomal proteins, other (non-desmosomal) mutations have been shown to cause biventricular and left-dominant variants. DSG2 mutations have been related to biventricular variants of ACM (29, 30). As several clinical presentations caused by ACM-related genetic variants have recently been identified, the role of genetic mutations in ACM pathogenesis should not be simplified as a linear cause-effect relationship to which a particular phenotype corresponds.

4. Conclusion

In summary, we reported a rare pediatric case initially presenting as myocarditis that transitioned into ACM during follow-up. A homozygous genetic variant of *DSG2* was inherited in the proband. This study expanded the clinical feature spectrum of *DSG2*-associated ACM at an early age. Additionally, the presentation of this case emphasized the difference between homozygous and heterozygous variants of desmosomal genes in disease progression. Genetic sequencing screening can be helpful in distinguishing unexplained myocarditis or ACS in children.

Data availability statement

The original contributions presented in the study are included in the article/supplementary materials, further inquiries can be directed to the corresponding authors.

Ethics statement

The studies involving human participants were reviewed and approved by Ethics Committee of West China Second Hospital of Sichuan University (2014-034). Written informed consent to participate in this study was provided by the participants' legal guardian/next of kin. Written informed consent was obtained from the individual(s), and minor(s)' legal guardian/next of kin, for the publication of any potentially identifiable images or data included in this article.

Author contributions

LX, ZY, and LW contributed equally to this work. LX, LW, ZQ, ZL, HY, DH, and LY were the patient's physicians. LX and ZQ reviewed the literature and contributed to manuscript drafting; ZY and LY performed the mutation analysis. LX and LY conceptualized and designed the study, coordinated and supervised data collection, and critically reviewed the manuscript for important intellectual content. HY, LY, and DH were responsible for the revision of the manuscript for important intellectual content. All authors contributed to the article and approved the submitted version.

Funding

This work was supported by grants from the Technology Project of Sichuan Province of China (2021YFQ0061) and the National Natural Science Foundation of China (82270249). The funders did not participate in the design of the study, the collection, analysis, and interpretation of the data, nor the writing of the manuscript.

Conflict of interest

The authors declare that the research was conducted in the absence of any commercial or financial relationships that could be construed as a potential conflict of interest.

Publisher's note

References

1. Basso C, Thiene G, Corrado D, Angelini A, Nava A, Valente M. Arrhythmogenic right ventricular cardiomyopathy. Dysplasia, dystrophy, or myocarditis? *Circulation*. (1996) 94(5):983–91. doi: 10.1161/01.cir.94.5.983

2. Austin KM, Trembley MA, Chandler SF, Sanders SP, Saffitz JE, Abrams DJ, et al. Molecular mechanisms of arrhythmogenic cardiomyopathy. *Nat Rev Cardiol*. (2019) 16(9):519–37. doi: 10.1038/s41569-019-0200-7

3. Sen-Chowdhry S, Syrris P, Prasad SK, Hughes SE, Merrifield R, Ward D, et al. Left-dominant arrhythmogenic cardiomyopathy: an under-recognized clinical entity. *J Am Coll Cardiol*. (2008) 52(25):2175–87. doi: 10.1016/j.jacc.2008.09.019

4. Corrado D, Basso C, Judge DP. Arrhythmogenic cardiomyopathy. *Circ Res*. (2017) 121(7):784–802. doi: 10.1161/circresaha.117.309345

5. Quarta G, Muir A, Pantazis A, Syrris P, Gehmlich K, Garcia-Pavia P, et al. Familial evaluation in arrhythmogenic right ventricular cardiomyopathy: impact of genetics and revised task force criteria. *Circulation*. (2011) 123(23):2701–9. doi: 10.1161/circulationaha.110.976936

6. Bhonsale A, Groeneweg JA, James CA, Dooijes D, Tichnell C, Jongbloed JD, et al. Impact of genotype on clinical course in arrhythmogenic right ventricular dysplasia/cardiomyopathy-associated mutation carriers. *Eur Heart J*. (2015) 36(14):847–55. doi: 10.1093/eurheartj/ehu509

7. Belkaya S, Kontorovich AR, Byun M, Mulero-Navarro S, Bajolle F, Cobat A, et al. Autosomal recessive cardiomyopathy presenting as acute myocarditis. *J Am Coll Cardiol*. (2017) 69(13):1653–65. doi: 10.1016/j.jacc.2017.01.043

8. Scheel PJ 3rd, Murray B, Tichnell C, James CA, Tandri H, Calkins H, et al. Arrhythmogenic right ventricular cardiomyopathy presenting as clinical myocarditis in women. *Am J Cardiol*. (2021) 145:128–34. doi: 10.1016/j.amjcard.2020.12.090

9. Brown EE, McMilllan KN, Halushka MK, Ravekes WJ, Knight M, Crosson JE, et al. Genetic aetiologies should be considered in paediatric cases of acute heart failure presumed to be myocarditis. *Cardiol Young*. (2019) 29(7):917–21. doi: 10.1017/s1047951119001124

10. Brodehl A, Belke DD, Garnett L, Martens K, Abdelfatah N, Rodriguez M, et al. Transgenic mice overexpressing desmocollin-2 (DSC2) develop cardiomyopathy associated with myocardial inflammation and fibrotic remodeling. *PLoS One*. (2017) 12(3):e0174019. doi: 10.1371/journal.pone.0174019

11. Harrison OJ, Brasch J, Lasso G, Katsamba PS, Ahlsen G, Honig B, et al. Structural basis of adhesive binding by desmocollins and desmogleins. *Proc Natl Acad Sci U S A*. (2016) 113(26):7160–5. doi: 10.1073/pnas.1606272113

12. Lota AS, Hazebroek MR, Theotokis P, Wassall R, Salmi S, Halliday BP, et al. Genetic architecture of acute myocarditis and the overlap with inherited cardiomyopathy. *Circulation*. (2022) 146(15):1123–34. doi: 10.1161/circulationaha.121.058457

13. Chen L, Rao M, Chen X, Chen K, Ren J, Zhang N, et al. A founder homozygous DSG2 variant in east Asia results in ARVC with full penetrance and heart failure phenotype. *Int J Cardiol*. (2019) 274:263–70. doi: 10.1016/j.ijcard.2018.06.105

14. Asimaki A, Tandri H, Duffy ER, Winterfield JR, Mackey-Bojack S, Picken MM, et al. Altered desmosomal proteins in granulomatous myocarditis and potential pathogenic links to arrhythmogenic right ventricular cardiomyopathy. *Circ Arrhythm Electrophysiol*. (2011) 4(5):743–52. doi: 10.1161/circep.111.964890

15. Lopez-Ayala JM, Pastor-Quirante F, Gonzalez-Carrillo J, Lopez-Cuenca D, Sanchez-Munoz JJ, Oliva-Sandoval MJ, et al. Genetics of myocarditis in arrhythmogenic right ventricular dysplasia. *Heart Rhythm*. (2015) 12(4):766–73. doi: 10.1016/j.hrthm.2015.01.001

16. Te Riele A, James CA, Sawant AC, Bhonsale A, Groeneweg JA, Mast TP, et al. Arrhythmogenic right ventricular dysplasia/cardiomyopathy in the pediatric population: clinical characterization and comparison with adult-onset disease. *JACC Clin Electrophysiol*. (2015) 1(6):551–60. doi: 10.1016/j.jacep.2015.08.004

17. Boogerd CJ, Lacraz GPA, Vértesy Á, van Kampen SJ, Perini I, de Ruiter H, et al. Spatial transcriptomics unveils ZBTB11 as a regulator of cardiomyocyte degeneration in arrhythmogenic cardiomyopathy. *Cardiovasc Res*. (2023) 119(2):477–91. doi: 10.1093/cvr/cvac072

18. Brodehl A, Meshkov A, Myasnikov R, Kiseleva A, Kulikova O, Klauke B, et al. Hemi- and homozygous loss-of-function mutations in DSG2 (desmoglein-2) cause recessive arrhythmogenic cardiomyopathy with an early onset. *Int J Mol Sci*. (2021) 22(7):3786. doi: 10.3390/ijms22073786

19. Brodehl A, Weiss J, Debus JD, Stanasiuk C, Klauke B, Deutsch MA, et al. A homozygous DSC2 deletion associated with arrhythmogenic cardiomyopathy is caused by uniparental isodisomy. *J Mol Cell Cardiol*. (2020) 141:17–29. doi: 10.1016/j.yjmcc.2020.03.006

20. Smith ED, Lakdawala NK, Papoutsidakis N, Aubert G, Mazzanti A, McCanta AC, et al. Desmoplakin cardiomyopathy, a fibrotic and inflammatory form of cardiomyopathy distinct from typical dilated or arrhythmogenic right ventricular cardiomyopathy. *Circulation*. (2020) 141(23):1872–84. doi: 10.1161/circulationaha.119.044934

21. Hata Y, Hirono K, Yamaguchi Y, Ichida F, Oku Y, Nishida N. Minimal inflammatory foci of unknown etiology may be a tentative sign of early stage inherited cardiomyopathy. *Mod Pathol*. (2019) 32(9):1281–90. doi: 10.1038/s41379-019-0274-0

22. Wang N, Wei Y, Zhou G, Zhang Y, Song J. Acute coronary syndrome in an 8-year-old child with familial hypercholesterolemia: a case report. *J Med Case Rep*. (2022) 16(1):290. doi: 10.1186/s13256-022-03488-3

23. Davlat M, Massin M, Rodriguez Castro J, Damry N. Association of left ventricular non-compaction with acute coronary syndrome. *Acta Cardiol*. (2022) 77(5):465–6. doi: 10.1080/00015385.2021.1897258

24. Puwanant S, Trongtorsak A, Wanlapakorn C, Songsirisuk N, Ariyachaipanich A, Boonyaratavej S. Acute coronary syndrome with non-obstructive coronary arteries (ACS-NOCA) in patients with hypertrophic cardiomyopathy. *BMC Cardiovasc Disord*. (2021) 21(1):556. doi: 10.1186/s12872-021-02373-z

25. Ng KE, Delaney PJ, Thenet D, Murtough S, Webb CM, Zaman N, et al. Early inflammation precedes cardiac fibrosis and heart failure in desmoglein 2 murine model of arrhythmogenic cardiomyopathy. *Cell Tissue Res*. (2021) 386(1):79–98. doi: 10.1007/s00441-021-03488-7

26. Chelko SP, Asimaki A, Lowenthal J, Bueno-Beti C, Bedja D, Scalco A, et al. Therapeutic modulation of the immune response in arrhythmogenic cardiomyopathy. *Circulation*. (2019) 140(18):1491–505. doi: 10.1161/circulationaha.119.040676

27. Xu T, Yang Z, Vatta M, Rampazzo A, Beffagna G, Pilichou K, et al. Compound and digenic heterozygosity contributes to arrhythmogenic right ventricular cardiomyopathy. *J Am Coll Cardiol*. (2010) 55(6):587–97. doi: 10.1016/j.jacc.2009.11.020

28. Cox MG, van der Zwaag PA, van der Werf C, van der Smagt JJ, Noorman M, Bhuiyan ZA, et al. Arrhythmogenic right ventricular dysplasia/cardiomyopathy: pathogenic desmosome mutations in index-patients predict outcome of family screening: dutch arrhythmogenic right ventricular dysplasia/cardiomyopathy genotype-phenotype follow-up study. *Circulation*. (2011) 123(23):2690–700. doi: 10.1161/circulationaha.110.988287

29. Fressart V, Duthoit G, Donal E, Probst V, Deharo JC, Chevalier P, et al. Desmosomal gene analysis in arrhythmogenic right ventricular dysplasia/cardiomyopathy: spectrum of mutations and clinical impact in practice. *Europace*. (2010) 12(6):861–8. doi: 10.1093/europace/euq104

30. Wong JA, Duff HJ, Yuen T, Kolman L, Exner DV, Weeks SG, et al. Phenotypic analysis of arrhythmogenic cardiomyopathy in the hutterite population: role of electrocardiogram in identifying high-risk desmocollin-2 carriers. *J Am Heart Assoc*. (2014) 3(6):e001407. doi: 10.1161/jaha.114.001407

frontiers | Frontiers in Cardiovascular Medicine

TYPE Original Research
PUBLISHED 26 June 2023
DOI 10.3389/fcvm.2023.1223244

OPEN ACCESS

EDITED BY
Alexandre Francois Roy Stewart,
University of Ottawa, Canada

REVIEWED BY
Andreas Brodehl,
Heart and Diabetes Center North Rhine-Westphalia, Germany
Nadine Norton,
Mayo Clinic Florida, United States

*CORRESPONDENCE
Michael T. Chin
✉ mchin3@tuftsmedicalcenter.org

RECEIVED 15 May 2023
ACCEPTED 13 June 2023
PUBLISHED 26 June 2023

CITATION
Chou C, Martin GL, Perera G, Awata J, Larson A, Blanton R and Chin MT (2023) A novel αB-crystallin R123W variant drives hypertrophic cardiomyopathy by promoting maladaptive calcium-dependent signal transduction. Front. Cardiovasc. Med. 10:1223244. doi: 10.3389/fcvm.2023.1223244

A novel αB-crystallin R123W variant drives hypertrophic cardiomyopathy by promoting maladaptive calcium-dependent signal transduction

Chun Chou[1], Gregory L. Martin[2], Gayani Perera[2], Junya Awata[2], Amy Larson[2], Robert Blanton[1,2] and Michael T. Chin[1,2]*

[1]Department of Medicine, Tufts University School of Medicine, Boston, MA, United States, [2]Molecular Cardiology Research Institute, Tufts Medical Center, Boston, MA, United States

Hypertrophic cardiomyopathy (HCM) is the most common inherited cardiovascular disorder affecting 1 in 500 people in the general population. Characterized by asymmetric left ventricular hypertrophy, cardiomyocyte disarray and cardiac fibrosis, HCM is a highly complex disease with heterogenous clinical presentation, onset and complication. While mutations in sarcomere genes can account for a substantial proportion of familial cases of HCM, 40%–50% of HCM patients do not carry such sarcomere variants and the causal mutations for their diseases remain elusive. Recently, we identified a novel variant of the alpha-crystallin B chain (*CRYAB*^{R123W}) in a pair of monozygotic twins who developed concordant HCM phenotypes that manifested over a nearly identical time course. Yet, how *CRYAB*^{R123W} promotes the HCM phenotype remains unclear. Here, we generated mice carrying the *Cryab*^{R123W} knock-in allele and demonstrated that hearts from these animals exhibit increased maximal elastance at young age but reduced diastolic function with aging. Upon transverse aortic constriction, mice carrying the *Cryab*^{R123W} allele developed pathogenic left ventricular hypertrophy with substantial cardiac fibrosis and progressively decreased ejection fraction. Crossing of mice with a *Mybpc3* frame-shift model of HCM did not potentiate pathological hypertrophy in compound heterozygotes, indicating that the pathological mechanisms in the *Cryab*^{R123W} model are independent of the sarcomere. In contrast to another well-characterized *CRYAB* variant (R120G) which induced Desmin aggregation, no evidence of protein aggregation was observed in hearts expressing *CRYAB*^{R123W} despite its potent effect on driving cellular hypertrophy. Mechanistically, we uncovered an unexpected protein-protein interaction between CRYAB and calcineurin. Whereas CRYAB suppresses maladaptive calcium signaling in response to pressure-overload, the R123W mutation abolished this effect and instead drove pathologic NFAT activation. Thus, our data establish the *Cryab*^{R123W} allele as a novel genetic model of HCM and unveiled additional sarcomere-independent mechanisms of cardiac pathological hypertrophy.

KEYWORDS

hypertrophic cardiomyopathy, cardiac hypertrophy, cryab, calcineurin, NFAT, transverse aortic constriction, cardiac fibrosis

Abbreviations
HCM, Hypertrophic Cardiomyopathy; CRYAB, alpha-crystallin B chain; TAC, Transverse aortic constriction; NFAT, Nuclear factor of activated T cells; PMSF, Phenylmethylsulfonyl Fluoride.

Introduction

Hypertrophic cardiomyopathy (HCM), characterized by myocyte hypertrophy resulting in the thickening of the ventricular wall, decreased ventricular volume and diastolic dysfunction, has been recognized as the most common inherited cardiovascular disease, affecting 1 in every 500 young individuals (1). Inheritance is archetypally considered autosomal dominant with high penetrance in 50%–60% of patients (2, 3). The relatively high concordance has enabled multiple genome wide association studies to identify causal genetic mutations that underly HCM pathogenesis in large and unrelated cardiomyopathy families (4–8). Among the chromosomal loci that have been linked to HCM, the majority of mutations occur in genes encoding cardiac sarcomere proteins (8), including β-myosin heavy chain, cardiac myosin binding protein C and cardiac troponin T, which have well described roles in cardiomyocyte excitation-contraction coupling (9). While extensive studies have been conducted to elucidate the molecular mechanisms by which sarcomere protein variants cause HCM, less than 30% of patients with established diagnosis of HCM carry sarcomere gene mutations classified as or presumed to be pathogenic (10). In fact, isolated and sporadic HCM cases in which the proband does not carry any known HCM mutations may account for up to 40% of all HCM cases (11). Thus, the sarcomere-centric paradigm of HCM pathogenesis does not fully encapsulate the pathogenic mechanisms of HCM and many causal mutations for HCM still remain elusive (12).

Decades ago, a genetic linkage study identified a novel variant of the alpha-crystallin B chain (CRYAB) as a cause of HCM in a French family with myopathy in multiple organs (13). CRYAB is a member of the small heat shock binding protein (sHSBP) family and serves as a molecular chaperone with a wide spectrum of biological functions in cardiomyocytes, ranging from modulating calcium signaling (14), preventing protein aggregation (15–17), regulating autophagy (18, 19), to maintaining cellular survival (20). Intriguingly, under physiologic conditions, CRYAB in fact spontaneously organize into dimers and oligomers with little chaperone activity (21, 22). Stress signals such as elevated temperature disrupt the oligomeric complex, thereby exposing the unstructured N- and C-terminal domain, which provide the necessary chaperone function (23, 24). It thus appears that maintenance of CRYAB dimer/oligomer state under physiologic conditions may be essential in preventing inappropriate interaction with other proteins. Stabilization of CRYAB dimers is critically dependent on salt-bridges formed by arginine at position 120 and aspartic acid at position 109 on respective dimerization partners (21, 22) with non-synonymous mutations of R120 and D109 causally linked to various familial cardiomyopathies (25). In particular, substitution of R120 for glycine (hereon designated as *CRYAB*^{R120G}) was identified as a causal mutation in Desmin related myopathy characterized by intracellular accumulation of spheroid inclusion bodies consisted of Desmin (26). Consistently, CRYAB^{R120G} expression was sufficient to induce Desmin aggregation in murine cardiomyocytes and mice over-expressing CRYAB^{R120G} specifically in cardiomyocytes developed spontaneous cardiac dysfunction and succumbed to disease at 32 weeks of age (27). Cryoelectron microscopy revealed abnormal quaternary structure of CRYAB^{R120G} with an apparent molecular weight more than doubled compared to wild-type CRYAB, suggesting R120G mutation disrupts proper oligomerization of CRYAB (28). Another variant of CRYAB where D109 was mutated to glycine (hereon designated as *CRYAB*^{D109G}) has been linked to familial restrictive cardiopathy (29), with a presumed mechanism of dimer/oligomer destabilization considering the critical ionic interaction between D109 and R120. Collectively, these seminal works identified *CRYAB* as a potential hotspot for cardiomyopathy-inducing gene mutations. Recently, we reported a case of monozygotic twins who developed concordant HCM phenotypes that manifested over a nearly identical time course (30). Among the non-synonymous variants of HCM-associated genes, we identified yet another variant of CRYAB (OMIM 123590) where the arginine at amino acid 123 was substituted for tryptophan (hereon designated as *CRYAB*^{R123W}). While previously classified as a variant of unknown significance, the high concordance of diease manifestation by the pair of monozygotic twins strongly implies a causal role of *CRYAB*^{R123W} in HCM pathogenesis.

In this study, we demonstrated that CRYAB^{R123W} readily promoted cellular hypertrophy *in vitro* and mice carrying the *Cryab*^{R123W} allele spontaneously developed diastolic dysfunction with aging. Although hearts from these animals did not undergo hypertrophy at steady-state, pressure-overload by transaortic constriction (TAC) markedly induced cardiac hypertrophy and parenchymal fibrosis, associated with progressive systolic dysfunction. Mechanistically, CRYAB binds to calcineurin in co-immunoprecipitation assays, and such interaction may be critical for CRYAB-dependent suppression of maladaptive calcium signaling in response to pressure-overload. Intriguingly, the R123W mutation abolished such cardioprotective effects and instead converted CRYAB into an activator of pathologic calcium signaling.

Results

CRYAB^{R123W} enhances contractility early but impairs diastolic function with aging

To test whether the CRYAB^{R123W} variant is sufficient to drive cardiomyocyte hypertrophy, H9c2 cells derived from rat cardiomyofibroblasts were engineered to express human wild-type CRYAB (hCRYAB^{WT}) or the R123W variant (hCRYAB^{R123W}) via lentiviral transduction (**Figure 1A**). Consistently, ectopic expression of hCRYAB^{R123W} variant but not hCRYAB^{WT} resulted in substantial cellular hypertrophy (**Figures 1B,C**). To evaluate whether CRYAB^{R123W} drives HCM pathogenesis *in vivo*, we generated knock-in mice carrying the *Cryab*^{R123W} mutation using CRISPR/Cas9-mediated homology directed repair (**Figures 1D–F**). While no cardiomyocyte or cardiac hypertrophy was observed in heterozygous or homozygous mice at steady-state (**Figures 2A–C**), Emax was already increased in *Cryab*$^{R123W/R123W}$ mice and to a lesser extent in *Cryab*$^{R123W/+}$ counterparts at eight weeks of age (**Figure 2D**). Intriguingly, enhanced Emax was no longer observed in aged mice carrying the *Cryab*^{R123W} allele (**Figure 2E**). Rather,

10.3389/fcvm.2023.1223244

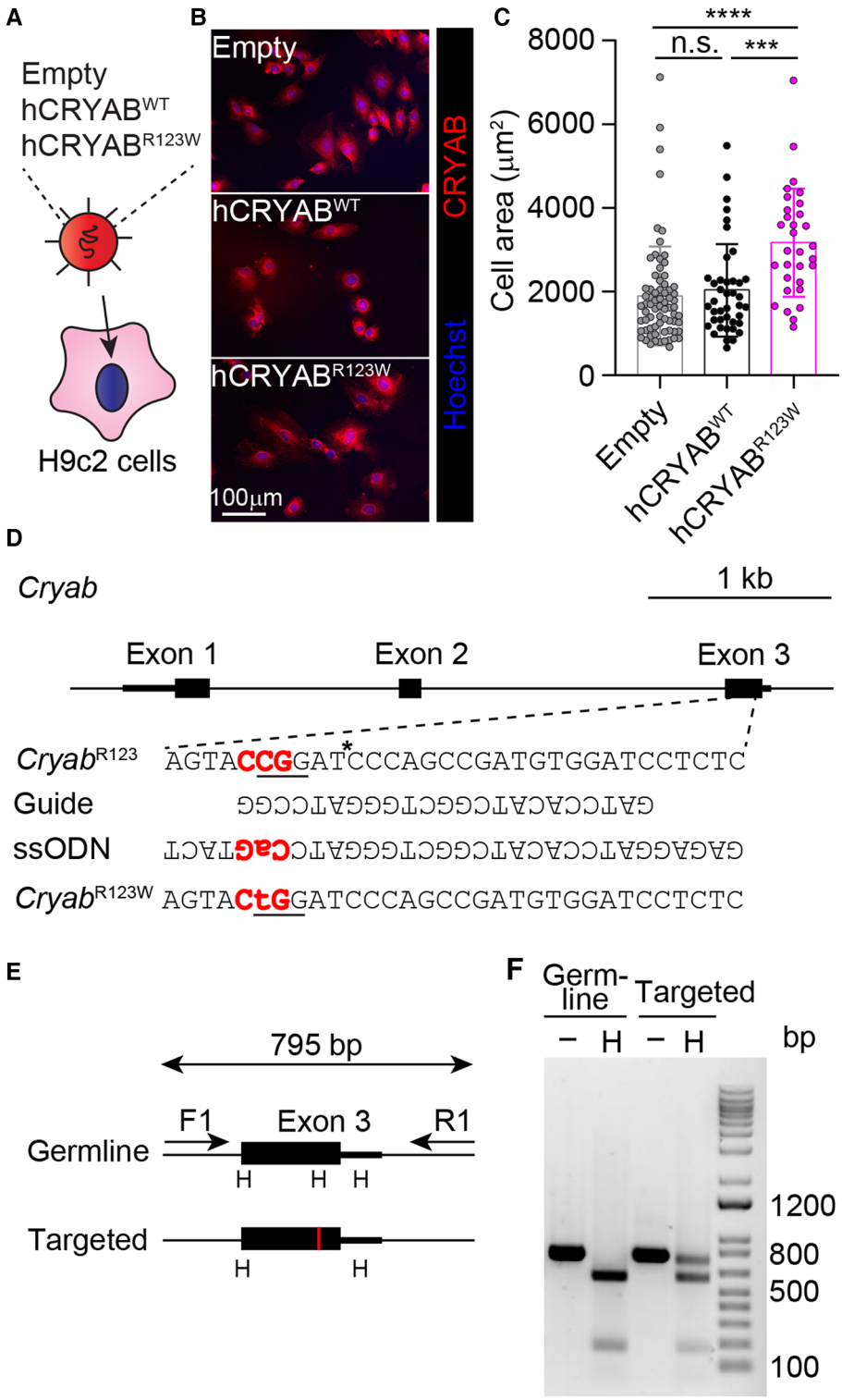

FIGURE 1
Generation of the *Cryab*^{R123W} knock-in allele. (**A**) Transduction of H9c2 cells with lentiviruses expressing the indicated constructs. (**B**) Immunofluorescence microscopic images showing CRYAB expression in H9c2 cardiomyofibroblasts transduced with empty, human wild-type CRYAB (hCRYAB^{WT})- or R123W variant (hCRYAB^{R123W})-expressing lentivirus. Data are representative of two independent experiments. (**C**) Cross-section areas of H9c2 cells transduced with indicated lentiviruses. Data are pooled from two independent experiments. (**D**) A schematic diagram showing the generation of the *Cryab*^{R123W} knock-in allele via CRISPR/Cas9-mediated homology directed repair. The trinucleotides in red denote the protospacer adjacent motif (PAM). The asterisk indicates the cleavage site by the Cas9 nuclease. The underlined trinucleotides encode the target amino acid and the desired missense mutation. (**E**) A screening strategy to identify targeted founders. PCR products of targeted allele differed from germ line configuration by a loss of HpaI (**H**) restriction enzyme site, denoted by the red vertical line. (**F**) Restriction fragment length polymorphisms analysis of germline and targeted animals. PCR fragments spanning the exon of interest before and after HpaI digestion were analyzed by agarose gel electrophoresis. Data are mean ± s.d. Kruskal-Wallis test (**C**). ***$P < 0.001$; ****$P < 0.0001$.

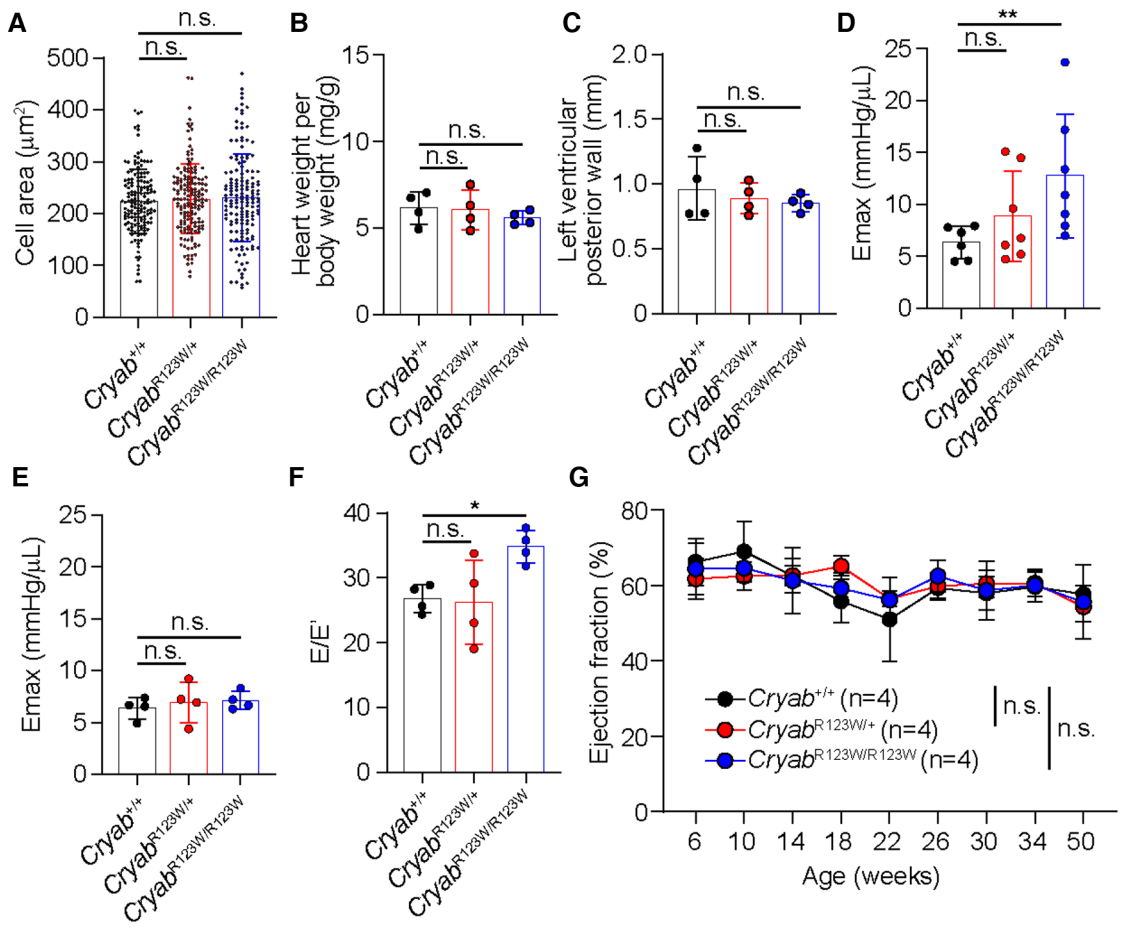

FIGURE 2
CRYAB^{R123W}-expressing mice spontaneously developed diastolic dysfunction. (**A**) Cross section areas of cardiomyocytes from *Cryab*$^{+/+}$, *Cryab*$^{R123W/+}$ and *Cryab*$^{R123W/R123W}$ mice between 8- to 12- weeks of age. Data are pooled from two independent experiments. (**B**) Normalized heart weight by body weight in *Cryab*$^{+/+}$, *Cryab*$^{R123W/+}$ or *Cryab*$^{R123W/R123W}$ mice at 8- to 12-weeks of age. Data are pooled from two independent experiments. (**C**) Left ventricular posterior wall thickness measured by echocardiogram in mice of indicated genotypes at 8- to 12-weeks of age. Data are pooled from two independent experiments. (**D**,**E**) Left ventricular maximal elastance (Emax) of hearts from *Cryab*$^{+/+}$, *Cryab*$^{R123W/+}$ or *Cryab*$^{R123W/R123W}$ mice at 8- to 10-weeks (**D**) or 50- to 52-weeks (**E**) of age derived from volume-pressure loop data during the pre-load reduction stage. Data are pooled from three independent experiments. (**F**) E/E′ of hearts from indicated genotypes at 25- to 30-weeks of age derived from transmural inflow Doppler indexes. Data are pooled from two independent experiments. (**G**) Longitudinal analysis of left ventricular ejection fraction of *Cryab*$^{+/+}$, *Cryab*$^{R123W/+}$ and *Cryab*$^{R123W/R123W}$ hearts. Data are pooled from two independent experiments. Data are mean ± s.d. Kruskal-Wallis test (**A**–**F**). Two-way ANOVA test (**G**). *$P < 0.05$; n.s., not significant.

Cryab$^{R123W/R123W}$ mice showed an increased E/E′ (Figure 2F), indicating diastolic dysfunction which is commonly seen in almost all HCM patients (31). Together, these data established CRYAB^{R123W} as a potential disease-causing variant in human HCM with its pathogenic function likely conserved between human and rodents.

CRYAB^{R123W} drives maladaptive cardiac remodeling upon pressure-overload

While the monozygotic twins carrying the heterozygous *CRYAB*^{R123W} mutation developed clinically significant HCM at a young age, no histologic or echocardiographic evidence of significant HCM was observed throughout the lifespan of mice harboring the *Cryab*^{R123W} allele at steady state (Figure 2G and data not shown). Notably, only a few genetic mouse models of HCM to date exhibited spontaneous cardiac hypertrophy and almost all were driven by mutated sarcomere genes expressed from a transgene rather than the endogenous loci (32–35). Knock-in mice for a truncated form of *Mybpc3*, one of the most commonly mutated disease-causing genes of HCM, in fact did not develop spontaneous cardiac hypertrophy. Rather, the hypertrophic phenotype was only evident upon pressure-overload by TAC (36). Indeed, both *Cryab*$^{R123W/+}$ and *Cryab*$^{R123W/R123W}$ mice underwent marked cardiac hypertrophy after TAC compared to wild-type controls (Figures 3A,B). Of note, the hypertrophic phenotype appears to be circumferential as often observed in models of pressure overload (Figures 3A,C). Asymmetric hypertrophy, which preferentially affects the interventricular septum in HCM patients is rarely reproduced in mouse models of HCM and was expectedly not observed in the *Cryab*^{R123W} model (Figure 3D).

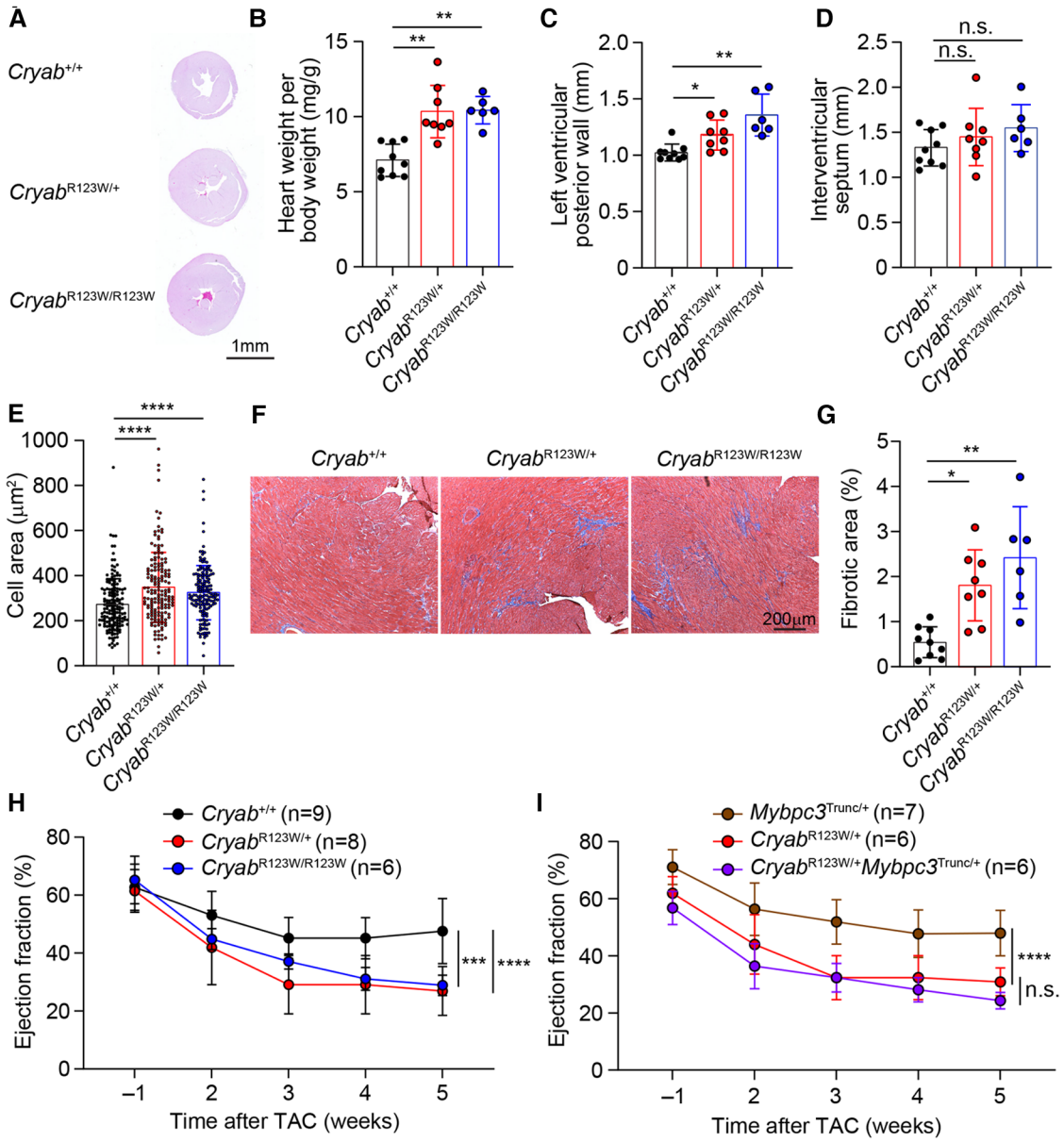

FIGURE 3
CRYAB^{R123W} drives maladaptive cardiac remodeling in response to pressure overload. (A) Hematoxylin/Eosin-stained cross-section of mid-papillary regions from *Cryab*$^{+/+}$, *Cryab*$^{R123W/+}$ or *Cryab*$^{R123W/R123W}$ hearts five weeks after TAC. Data are representative of three independent experiments. (B) Normalized heart weight by body weight in mice of indicated genotypes five weeks after TAC. Data are pooled from three independent experiments. (C,D) Statistical analysis of left ventricular posterior wall thickness and interventricular septum thickness measured by echocardiogram in mice of indicated genotypes five weeks after TAC. Data are pooled from three independent experiments. (E) Cross section areas of cardiomyocytes from mice of indicated genotypes five weeks after TAC. Data are pooled from three independent experiments. (F,G) Masson trichome stained histological sections and percentage of fibrotic areas in hearts from indicated genotypes five weeks after TAC. Data are representative (F) and pooled (G) from three independent experiments. (H) Statistical analysis of left ventricular ejection fraction of *Cryab*$^{+/+}$, *Cryab*$^{R123W/+}$ and *Cryab*$^{R123W/R123W}$ hearts one week prior to and weekly after TAC. Data are pooled from three independent experiments. (I) Left ventricular ejection fraction of *Mybpc3*$^{Trunc/+}$, *Cryab*$^{R123W/+}$ and *Cryab*$^{R123W/+}$*Mybpc3*$^{Trunc/+}$ hearts at indicated time prior to or after TAC. Data are pooled from three independent experiments. Data are mean ± s.d. Kruskal-Wallis test (B–E,G). Two-way ANOVA test (H,I). *$P < 0.05$; **$P < 0.01$; ***$P < 0.001$; ****$P < 0.0001$; n.s., not significant.

Microscopically, cardiomyocytes from mice carrying the *Cryab*^{R123W} allele underwent greater extent of cellular hypertrophy compared to wild-type counterparts (Figure 3E). Furthermore, hearts from *Cryab*$^{R123W/+}$ and *Cryab*$^{R123W/R123W}$ mice demonstrated larger areas of parenchymal fibrosis compared to control animals (Figures 3F,G). Thus, the *Cryab*^{R123W} mouse model recapitulated key features of human HCM.

Systolic dysfunction has been reported in a small proportion of patients with HCM and is associated with poor prognosis (37, 38). Intriguingly, *Cryab*^{R123W} mice progressively developed systolic dysfunction after TAC (Figure 3H). In fact, the decline in ejection fraction was markedly more severe compared to that caused by two truncation variants of MYBPC3, identified by others (36) and our lab (Supplementary Figure S1 and Figure 3I). Importantly,

systolic function was not further impaired in *Cryab*$^{R123W/+}$*Mybpc3*$^{Trunc/+}$ mice compared to *Cryab*$^{R123W/+}$ counterparts (**Figure 3I**), together suggesting that CRYAB may promote HCM through sarcomere-independent mechanisms. Notably, while *Cryab*-deficient mice also exhibited pathologic cardiac hypertrophy with systolic dysfunction upon pressure overload (14), such phenotype was not seen in *Cryab*$^{null/+}$ mice but readily evident in *Cryab*$^{R123W/+}$ animals, indicating that CRYAB^{R123W} represents a pathologic rather than loss-of-function variant. These data thus demonstrated that the CRYAB^{R123W} variant actively promotes maladaptive cardiac remodeling in response to pressure-overload.

CRYAB^{R123W} and CRYAB^{R120G} drive cardiomyopathy through distinct mechanisms

Another pathogenic CRYAB variant with substitution of amino acid arginine 120 for glycine (CRYAB^{R120G}) has been linked to familial Desmin myopathy, characterized by intrasarcoplasmic accumulation of Desmin aggregates (13). However, distinct from *Cryab*^{R123W} mice which developed cardiac hypertrophy upon pressure-overload, mice expressing the CRYAB^{R120G} variant predominantly succumbed to spontaneously developed dilated cardiomyopathy at young age (27). Despite these disparate phenotypes, the close proximity of the two mutated amino acids nevertheless raises the possibility that CRYAB^{R123W} may also induce Desmin aggregation. Intriguingly, overexpression of hCRYAB^{R123W} did not result in perinuclear aggregation of Desmin, which was otherwise robustly induced by hCRYAB^{R120G} (**Figure 4A**) (39). In fact, unlike CRYAB^{R120G}-expressing hearts (27), no protein aggregates were detected in heart tissues from *Cryab*$^{R123W/+}$ or *Cryab*$^{R123W/R123W}$ mice (**Figure 4B**). Additionally, while CRYAB^{R120G} has been shown to disrupt mitochondrial membrane potential (40, 41) such a defect was not observed in hCRYAB^{R123W}-expressing cardiomyocytes (**Figure 4C**). Thus, CRYAB^{R123W} and CRYAB^{R120G} drive cardiomyopathy through distinct mechanisms.

CRYAB interacts with calcineurin

Myriad molecular mechanisms have been implicated in HCM pathogenesis (42). In particular, enhanced calcium-dependent signaling was consistently observed in myectomized heart tissues from HCM patients regardless of whether sarcomere mutations are present (43, 44). Similarly, an increase in calcium-dependent signaling was also observed in TAC-induced pathologic cardiac hypertrophy in mice (45). Interestingly, *Cryab* expression was induced by pressure overload and its upregulation appears to be a cardio-protective adaptation that mitigates an otherwise pathologic hyperactivation of calcium signaling and the ensuing cellular hypertrophy (14). These findings thus ascribe *CRYAB* an anti-hypertrophy role in part through curbing maladaptive calcium-dependent signaling. Mechanistically, CRYAB inhibited nuclear translocation of the transcription factor NFAT (45). As one of the most abundantly expressed chaperone proteins in cardiomyocytes (46), CRYAB has been shown to interact with a wide variety of proteins (47). Yet, besides reported interactions with components of cytoskeleton (48) and effectors of apoptosis (49), whether CRYAB interacts with mediators of the calcium-dependent signaling cascade remains unclear. To this end, we performed a targeted survey of the CRYAB protein interactome focusing on key regulators of the calcium-dependent signaling cascade. Interestingly, immunoprecipitation of CRYAB revealed a robust interaction with calcineurin, but not calmodulin or NFAT (**Figure 5A** and data not shown). Reciprocally, CRYAB was also detected in a calcineurin-containing protein complex (**Figure 5B**). Thus, these findings suggest that CRYAB may dampen pathologic calcium-dependent signaling via modulation of calcineurin activity.

CRYAB^{R123W} enhances calcium-dependent signaling

To investigate whether the R123W mutation alters CRYAB's ability to suppress calcium-dependent signal transduction, control, hCRYAB^{WT}- or hCRYAB^{R123W}-expressing H9c2 cardiomyofibroblasts were transfected with a NFAT-luciferase reporter plasmid in which firefly luciferase expression is under the control of a myosin heavy chain promoter and tandem calcium-responsive enhancer elements (45). Strikingly, the hCRYAB^{R123W} variant readily induced calcium-dependent signaling even in the absence of hypertrophic stimuli (**Figure 5C**), indicating that the R123W mutation in fact converted CRYAB from a suppressor to maladaptive activator of calcium-dependent signaling. To test whether CRYAB^{R123W} also promotes calcium-dependent signaling *in vivo*, we crossed *Cryab*^{R123W} mice to a NFAT-luciferase reporter line in which transgenic firefly luciferase expression is driven by a myosin heavy chain promoter and NFAT enhancer elements (45). Consistent with published results (45), NFAT-luciferase activity in control hearts from adult mice remained minimally detected at steady state. In contrast, hearts from *Cryab*$^{R123W/R123W}$ mice exhibited enhanced NFAT-luciferase activity (**Figure 5D**). Of note, hyperactivation of calcium-dependent signaling was only observed in homozygous animals and in cardiomyofibroblast lines overexpressing CRYAB^{R123W}, suggesting that the ability of CRYAB^{R123W} to promote calcium signaling may be copy-number dependent. This dose dependency may also account for the weaker manifestation of hemodynamic changes at steady-state seen in *Cryab*$^{R123W/+}$ mice compared to *Cryab*$^{R123W/R123W}$ littermates (**Figures 2D,F**). Mechanistically, whether CRYAB^{R123W} promotes nuclear localization of NFAT by hyperactivating calcineurin remains to be tested. Nevertheless, these data demonstrated that CRYAB^{R123W} drives pathologic calcium-dependent signaling, which is normally suppressed by wild-type CRYAB in response to pressure overload.

Discussion

In this study, we generated a novel HCM mouse model carrying the *Cryab*^{R123W} allele identified in monozygotic twins

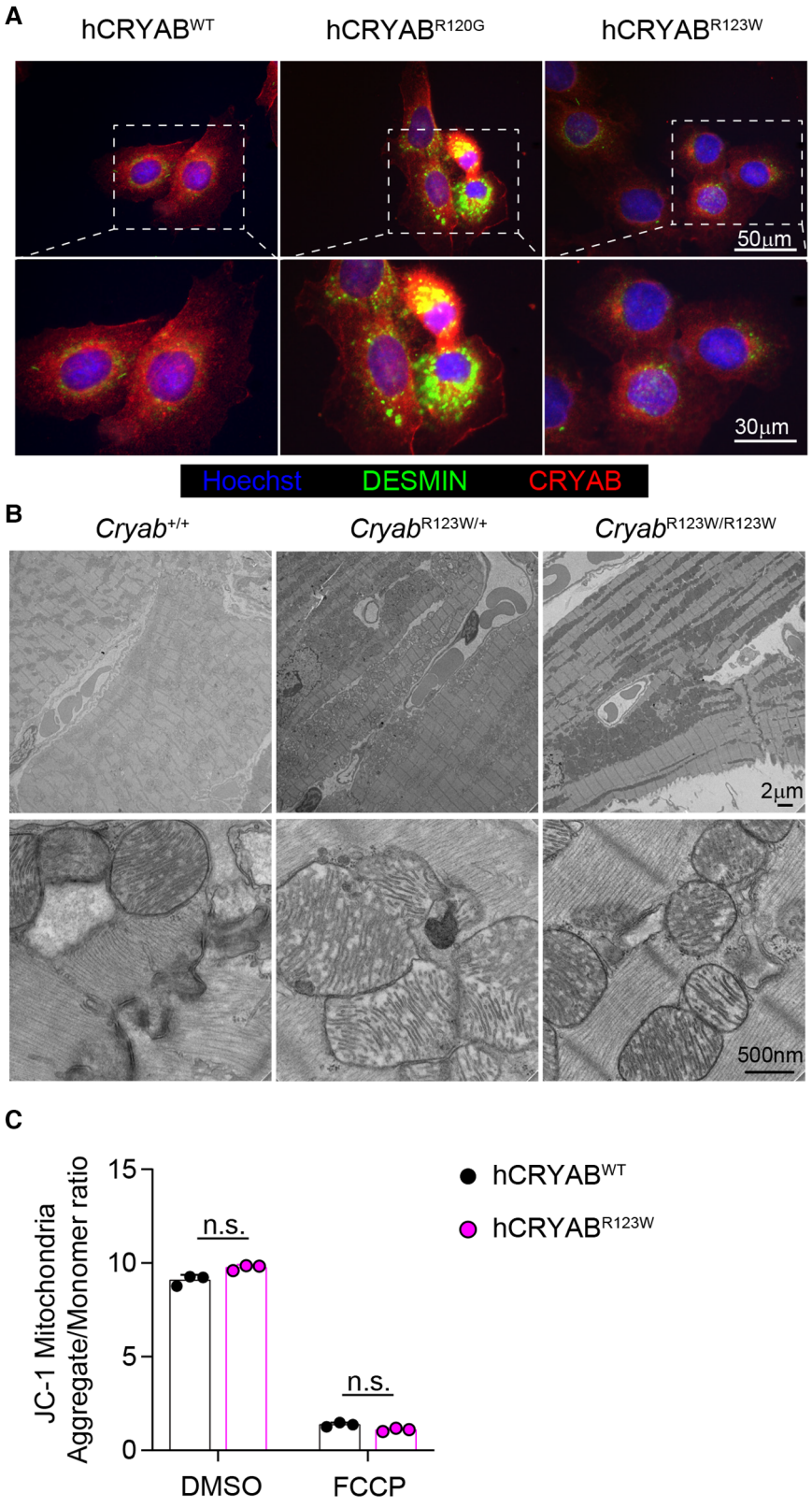

FIGURE 4
CRYAB^{R123W} does not induce protein aggregation. (**A**) Immunofluorescence microscopic images showing CRYAB and DESMIN expression in hCRYAB^{WT}-, hCRYAB^{R120G}-, and hCRYAB^{R123W}-expressing H9c2 cells. Data are representative of two independent experiments. (**B**) Electron microscopy images of heart sections from *Cryab*$^{+/+}$, *Cryab*$^{R123W/+}$ or *Cryab*$^{R123W/R123W}$ mice at six- to eight-weeks of age. (**C**) Statistical analysis of mitochondria aggregates to monomer ratio in hCRYAB^{WT}- and hCRYAB^{R123W}-expressing H9c2 cells treated with DMSO or an electron transport chain uncoupler FCCP. Data are pooled from two independent experiments. Data are mean ± s.d. Mann-Whitney test (**C**). n.s., not significant.

10.3389/fcvm.2023.1223244

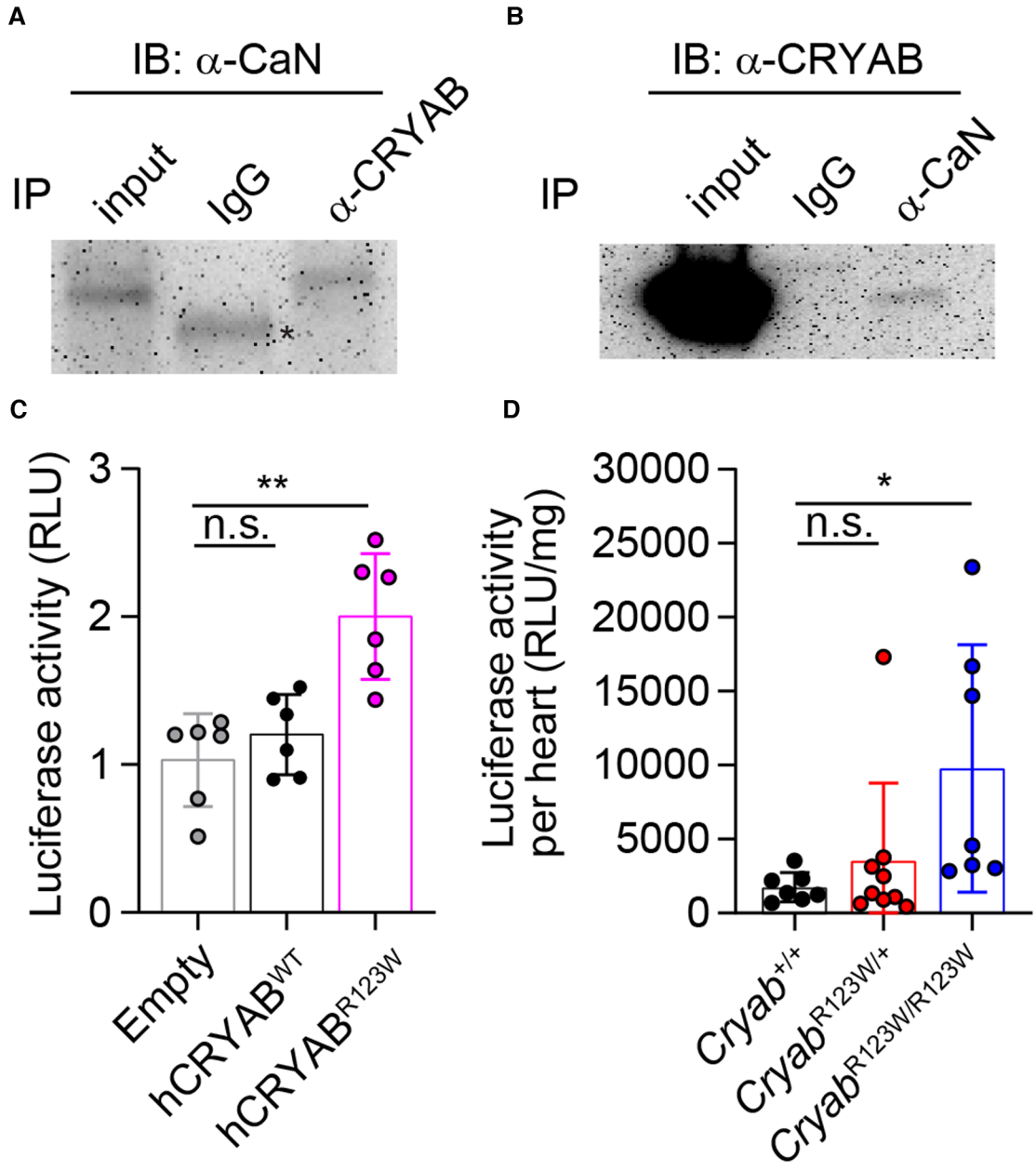

FIGURE 5
CRYAB^{R123W} promotes pathologic calcium-dependent signaling transduction. (**A**) Immunoblot analysis of anti-CRYAB immunoprecipitates (IP) and total cell lysate (input) from H9c2 cardiomyofibroblasts with an anti-Calcineurin (CaN) antibody and a peroxidase-conjugated anti-mouse IgG light chain-specific secondary antibody. Data is representative of three independent experiments. (**B**) Anti-CaN IP and input from H9c2 cardiomyofibroblasts were analyzed by immunoblot assay using an anti-CRYAB antibody and a peroxidase-conjugated anti-mouse IgG Fc-specific secondary antibody. Data are representative of two independent experiments. (**C**) Statistical analysis of NFAT-luciferase activity in empty, hCRYAB^{WT}- or hCRYAB^{R123W}-expressing H9c2 cells one day after co-transfection with a NFAT-inducible firefly luciferase expression plasmid and a constitutive expression plasmid encoding renilla luciferase. The relative luciferase unit is calculated as a ratio between firefly and renilla luciferase activity. Data are pooled from three independent experiments. (**D**) Normalized firefly luciferase activity by heart weight in steady state six- to eight-week-old *Cryab*$^{+/+}$, *Cryab*$^{R123W/+}$ or *Cryab*$^{R123W/R123W}$ mice carrying a transgene in which firefly luciferase expression is under the control of myosin heavy chain promoter and tandem NFAT enhancer elements. Data are pooled from three independent experiments. Data are mean ± s.d. Kruskal-Wallis test (**C**,**D**). *$P < 0.05$; **$P < 0.01$; n.s., not significant.

who developed concordant HCM. Mice expressing the CRYAB^{R123W} variant manifest many pathologic features of HCM: early enhanced systolic function that spontaneously degenerates into diastolic dysfunction and marked cardiac fibrosis triggered by maladaptive hypertrophy. Subsequent mechanistic studies unexpectedly uncovered calcineurin as a protein interactor of CRYAB and demonstrated that the R123W variant in fact enhances NFAT signal transduction, which is otherwise physiologically suppressed by wild-type CRYAB in response to pressure overload. Intriguingly, spontaneous HCM phenotypes were not observed in mice carrying the *Cryab*^{R123W} allele, regardless of zygosity. This is in stark contrast to the concordant

clinical manifestation of HCM in the pair of monozygotic twins heterozygous for the *CRYAB*^{R123W} allele. As the initial genetic study focused on non-synonymous variants of known HCM-associated genes (30), it is conceivable that other extremely rare variants may principally drive HCM pathogenesis, with *CRYAB*^{R123W} serving a facilitative role. Alternatively, the discrepancy in HCM phenotypes may arise from intrinsic physiologic differences between mouse and human hearts, considering that many mouse genetic models of HCM in fact do not exhibit spontaneous HCM phenotypes.

Cryab is expressed across various tissues with highest expression in lens, skeletal and cardiac muscles. While a germline *Cryab*^{R123W} knock-in allele best approximates the genetic configuration in HCM patients, whether the CRYAB^{R123W} variant exerts pathogenic effects principally in a cardiomyocyte-intrinsic manner cannot be easily discerned. Recent single cell RNA-sequencing studies unveiled global alteration in cell-cell communication networks in HCM patients (50–52), even in those where pathogenic drivers are considered to be cardiomyocyte-restricted proteins (unpublished data). Thus, future single cell transcriptomic analysis of *Cryab*^{R123W} hearts may allow identification of key cellular players implicated in this new mouse model of HCM. Conditional expression of the CRYAB^{R123W} variant in those cell types may further help elucidate the contribution of non-cardiomyocyte cellular constituents to HCM development.

Prior studies have demonstrated the critical role of CRYAB in suppressing pathologic calcium signaling induced by pressure-overload (14). Our data further suggest that such function may be mediated via protein-protein interaction between CRYAB and Calcineurin. Unexpectedly, this cardioprotective effect is transformed into a pathogenic one with a single amino acid substitution, R123W. How CRYAB and the R123W variant modulate calcineurin activity, if at all, remains unclear. A recent structural study uncovered that both R120 and R123 are located in the β7–8 sheets of the crystallin domain (53). However, whereas R120 maintains solubility of CRYAB via forming salt bridges with D109 of the dimerization partner (53), R123 does not appear to participate in such activity. It is thus perhaps not surprising that the R123W variant did not induce protein aggregation compared to its R120G counterpart. Besides providing dimerization/oligomerization interface with other crystallin-domain-containing proteins (54–56), the crystallin domain also appears to regulate the chaperone activity of the unstructured N- or C-terminal tails. A recent report demonstrated that the R120G mutation in fact alters structural dynamics of the N-terminal domain, thereby prematurely activating its chaperone function (24). Whether R123W mutation also impacts dimerization and/or alters functions of the flexible N- or C-terminal domain remains to be determined.

In addition to modulating the calcineurin-NFAT axis, *CRYAB* has been implicated in a variety of pathologic processes associated with cardiomyopathies, including autophagy (18, 19), apoptosis (20) and redox balance (41, 57). While a large array of proteins have been demonstrated as CRYAB-interactors (58, 59), a complete inventory of CRYAB interaction partners in cardiac tissues has not been done. Notably, an unbiased characterization of the protein interactome of HSBP2, another family member of the crystallin-domain containing proteins, in heart tissues uncovered many previously unknown mitochondrial binding partners involved in ATP generation and redox balance (60). Thus, future profiling of protein interaction clienteles of CRYAB and CRYAB^{R123W}, coupled with comparison of proteomics and phosphoproteomics studies between the two genotypes at steady-state and in response to pressure-overload may provide a comprehensive understanding of their functions in HCM pathogenesis.

Lastly, owing to its ability to bind multiple pro-inflammatory serum proteins from patients with various autoimmune diseases (58), the therapeutic potential of CRYAB as an anti-inflammatory agent has been extensively explored. Unexpected, administration of purified CRYAB was sufficient to mitigate inflammation in several mouse models with minimal toxicity (61–63). Conceivably, identification of a minimal calcineurin-interacting domain may thus allow development of novel therapeutic peptide for HCM patients with evidence of increased calcium signaling. This work thus supports the novel concept that precision targeting of intracellular signaling in HCM may be therapeutically important and add to the disease-specific pharmacologic armamentarium beyond myosin inhibitors.

Methods

Mice

Myh6/NFAT-luc [FVB-Tg(Myh6/NFAT-luc)1Jmol/J] reporter mice were purchased from Jackson Laboratories. The *Cryab*^{R123W} allele was generated via homology directed repair using the CRISPR/Cas9 system. Briefly, a guide RNA (GATCCACATCGGCT GGGATCCGG), single-stranded oligodeoxynucleotides (ssODN) donor template containing the CGG to TGG mutation, and mRNA encoding Cas9 were co-injected into the cytoplasm/pronucleus of single cell embryos. Chimeric founders were first screened for Cas9-mediated genomic targeting by PCR using the primer pair: Cryab-F1-GGGGCCTTTCACCACTAGACT and Cryab-R1-TTGAGCACCTTCCGGTATGAG, followed by restriction fragment length polymorphisms analysis using HpaI. PCR fragments from targeted founders were then subject to Sanger sequencing to confirm the desired CGG to TGG mutation. Generation of the *Mybpc3*^{Y838X} allele was attempted by co-injection of a guide RNA (TGCGTAGACTCGCATCTCATAGG), ssODN donor template containing the TAT to TAA mutation, and mRNA encoding Cas9 into cytoplasm/pronucleus of single cell embryos. Founders were screened by PCR using the following primer pair: Mybpc3-F1-GGTAATCCGGGTCTAGATAGCTT and Mybpc3-R2-CAGCCT GAGCTTCTTCGTGTGTA, followed by restriction fragment length polymorphisms analysis using AflII. Subsequent Sanger sequencing of all targeted founders revealed indels rather than the desired substitution, resulting in a translation termination further downstream of the expected Y838 position. The allele carrying a 10 bp deletion is heron designated as *Mybpc3*^{Trunc}. Founders with

germ-line transmission were maintained on a C57BL/6 background. All mice were handled in accordance with US National Institutes of Health standards, and all procedures were approved by the Tufts University Institutional Animal Care and Use Committee.

Cell lines

H9c2 cells were purchased from ATCC (CRL-1446) and maintained on Dulbecco's Modified Eagle Medium supplemented with 10% fetal bovine serum. To generate H9c2 cell lines expressing wild-type human CRYAB (hCRYAB^{WT}), R120G (hCRYAB^{R120G}) or R123W (hCRYAB^{R123W}) variants, DNA sequences encoding the variants were inserted to pLenti-puro vector (#39481, Addgene). H9c2 cells were spin-inoculated with 3rd generation empty or hCRYAB-expressing lentivirus, packaged as previously described (64). Transduced cells were selected and maintained on 10 μg/ml puromycin.

Transverse aortic constriction (TAC) surgery

Pressure overload was produced by constricting the transverse aorta just after the first great vessel as previously described (65). Ten- to twelve-week-old *Cryab*$^{+/+}$, *Cryab*$^{R123W/+}$ and *Cryab*$^{R123W/R123W}$ mice were subject to severe (27G needle) TAC operation and recovered for five weeks.

In vivo left ventricular hemodynamic studies

In vivo left ventricular function was assessed by pressure-volume analysis (66). Briefly, 12- to 16-week-old *Cryab*$^{+/+}$, *Cryab*$^{R123W/+}$ and *Cryab*$^{R123W/R123W}$ mice were anesthetized with 2.5% isoflurance. A 1.4-French PV catheter (SPR-839; Millar Instruments) was advanced across the aortic valve into the left ventricle. The absolute volume was calibrated, and pressure-volume data was assessed at steady state and during preload reduction. Hemodynamics were recorded and analyzed with IOX software (EMKA instruments, Falls Church, VA). Investigators were blinded to genotype during performance of hemodynamic studies and analysis of data.

Echocardiography

Echocardiography and pulse wave velocity were conducted using Doppler ultrasound (Vevo 2100, VisualSonics). Mice were anesthetized with isoflurane and placed in a recumbent position with paws in contact with pad electrodes for ECG recording on a heated platform (37°C) and maintained with ~2.0% isofluorane during the procedure to maintain heart rate of 450–550 bpm. For cardiac function, left ventricular end-diastolic and -systolic diameter as well as interventricular septum and posterior wall thickness were determined by averaging values from at least 5 cardiac cycles obtained by M-mode with the short axis view (66). Parameters for diastolic function, including E/E′ were derived from transmural inflow Doppler indexes obtained in an apical four-chamber view or the left ventricular long axis view (67). For animals subject to TAC surgery, cardiac functional parameters were assessed before TAC and weekly starting two weeks after TAC for five weeks.

Histological analysis

Whole hearts were fixed in 10% formalin, embedded in paraffin and sectioned at 5 μm thickness. Sections from mid-papillary regions of the left ventricular tissues were stained with Masson trichrome reagent for evaluation of cardiac fibrosis or hematoxylin and eosin for assessment of cardiomyocyte size as well as left ventricular wall thickness. Brightfield images were acquired using an Olympus BX40 microscope and SPOT Insight camera and software. Subsequent area measurement was performed in an ImageJ software (NIH).

Immunoprecipitation

Approximately 40 million H9c2 cells were lysed with 2 ml of non-denaturing lysis buffer (20 mM Tris-HCl pH 8.0, 137 mM NaCl, 1% Nonidet P-40, 2 mM EDTA) in the presence of a protease inhibitor cocktail (G6521, Promega) and phenylmethylsulfonyl fluoride (PMSF) at 50 μg/ml at 4°C on a rotator for 20 min, followed by centrifugation at 12,000 rpm for 10 min. A 40 μl sample of clarified lysate was taken as input. Equal amount of lysate was added to four tubes containing 20 μl of Dynabeads protein G (10003D, ThermoFisher Scientific) and lysis buffer was added to a total of 1 ml, followed by incubation with 1 μg of anti-Cryab (ab76467, Abcam) antibody, anti-calcineurin A antibody (2,614, Cell signaling), or rabbit IgG (2,729, Cell Signaling) on a rotator at 4°C for 16 h. After unbound protein was removed, protein G beads were washed three times with wash buffer (10 mM Tris-HCl pH 7.4, 1 mM EDTA, 1 mM EGTA, 150 mM NaCl, 1% Triton X-100) in the presence of protease inhibitor cocktail and PMSF at 4°C. After final wash, the protein G beads were resuspended in 20 μl of 1x Laemmli Sample Buffer and boiled for 5 min. Immunoprecipitated proteins were resolved by SDS-PAGE and analyzed by immunoblotting. The following primary antibodies were used for immunoblot assay: anti-Cryab (ab13496, Abcam) and anti-Calcineurin (55,6350, BD Biosciences). The following secondary antibodies were used: horse radish peroxidase-conjugated goat anti-mouse IgG light chain specific (115-035-174, Jackson Immunoresearch) and horse radish peroxidase-conjugated goat anti-mouse IgG Fc (A16084, ThermoFisher Scientific).

Immunofluorescence microscopy

H9c2 cells expressing human wild-type CRYAB or CRYAB variants were plated in coverslip containing 24-well plates at a density of 10^4 cells per well. The following day, culture medium

was removed, and cells were fixed with 4% paraformaldehyde (Electron Microscopy Sciences) at room temperature for 10 min, followed by permeabilization with 0.1% Triton X-100 in blocking buffer (1% bovine serum albumin in phosphate buffered saline) for 15 min. The following primary antibodies were used: anti-CRYAB (ab76467, Abcam) and anti-DESMIN (ab32362, Abcam). The following secondary antibodies were used: Alexa Fluor 488-conjugated goat anti-rabbit IgG (A-11008, ThermoFisher Scientific) and Alexa Fluor 594-conjugated goat anti-mouse IgG (A-11005, ThermoFisher Scientific). Cells were stained with Hoechst (H3570, ThermoFisher Scientific) before mounting. Immunofluorescent images were acquired using a Nikon A1R confocal microscope. Subsequent color balancing, overlaying, and area measurements were performed in an ImageJ software (NIH).

Electron microscopy

Samples were fixed overnight in a mixture of 1.25% formaldehyde, 2.5% glutaraldehyde, and 0.03% picric acid in 0.1 M sodium cacodylate buffer, pH 7.4. The fixed tissues were washed with 0.1M sodium cacodylate buffer and post-fixed with 1% osmium tetroxide/1.5% potassium ferrocyanide (in H2O) for 2 h. Samples were then washed in a maleate buffer and post fixed in 1% uranyl acetate in maleate buffer for 1 h. Tissues were then rinsed in ddH20 and dehydrated through a series of ethanol [50%, 70%, 95%, (2×)100%] for 15 min per solution. Dehydrated tissues were put in propylene oxide for five minutes before they were infiltrated in epon mixed 1:1 with propylene oxide overnight at 4°C. Samples were polymerized in a 60°C oven in epon resin for 48 h. They were then sectioned into 80 nm thin sections and imaged on a JEOL 1200EX Transmission Electron Microscope.

Luciferase reporter assay

To assess NFAT transcriptional activity *in vitro*, a mixture of 9X NFAT-alpha-MHC-Luc (51,941, Addgene) and pRL-TK (E2241, Promega) plasmids at a ratio of 3:1 was transfected into H9c2 cell lines expressing human wild-type CRYAB or CRYAB variants plated at 2000 cells per well in a 96-well plate (165,305, ThermoFisher Scientific) using Lipofectamine Transfection Reagent (18,324,012, ThermoFisher Scientific) according to the manufacturer's instruction. One day after transfection, firefly and renilla luciferase activities were assessed using the Dual-Glo Luciferase Assay System (E2920, Promega) and a plate reader (PR3100 Microplate reader, Bio-Rad). For evaluation of NFAT transcriptional activity ex vivo, whole hearts from six- to eight-week-old $Cryab^{+/+}$ Myh6/NFAT-luc, $Cryab^{R123W/+}$ Myh6/NFAT-luc and $Cryab^{R123W/R123W}$ Myh6/NFAT-luc were dissected into 1–2 mm pieces and lysed in 1 ml of Luciferase Cell Culture Lysis Reagent (E1531, Promega) using a dounce homogenizer, followed by centrifugation at 12,000 g for 5 min. Equal amount of clarified lysate and luciferase assay buffer (E1500, Promega) were mixed in a 96-well plate and firefly luciferase activity was immediately measured by a plate reader.

Mitochondrial membrane potential assay

Mitochondrial membrane potential in human CRYAB variants-expressing H9c2 cell lines was assessed using a JC-1 assay kit (ab113850, Abcam) according to the manufacturer's instructions.

Statistical analysis

All statistical measurements are displayed as mean ± S.D. *P*-values were calculated with a Mann-Whitney test for two-group comparisons, by Kruskal-Wallis test for multiple-group comparisons, or by two-way ANOVA for multi-group comparisons over a time course using Prims 8 software.

Data availability statement

The original contributions presented in the study are included in the article/**Supplementary Material**, further inquiries can be directed to the corresponding author.

Ethics statement

The animal study was reviewed and approved by Tufts University Institutional Animal Care and Use Committee.

Author contributions

Conceptualization, MC; methodology, CC, MC, GM, and RB; software, CC, GP, AL, and JA; validation, CC and GP; formal analysis, CC, RB, and MC; investigation, CC and AL; resources, MC and RB; data curation, CC, GP, and RB; writing—original draft preparation, CC; writing—review and editing, MC and CC; visualization, CC; supervision, MC; project administration, MC and CC; funding acquisition, MC. All authors have read and agreed to the published version of the manuscript.

Acknowledgments

We thank Barry Maron, Ethan Rowin and Marty Maron for useful discussions on the role of $CRYAB^{R123W}$ in HCM.

Conflict of interest

The authors declare that the research was conducted in the absence of any commercial or financial relationships that could be construed as a potential conflict of interest.

Publisher's note

All claims expressed in this article are solely those of the authors and do not necessarily represent those of their affiliated organizations, or those of the publisher, the editors and the reviewers. Any product that may be evaluated in this article, or claim that may be made by its manufacturer, is not guaranteed or endorsed by the publisher.

Supplementary material

The Supplementary Material for this article can be found online at: https://www.frontiersin.org/articles/10.3389/fcvm.2023.1223244/full#supplementary-material

References

1. Maron BJ. Hypertrophic cardiomyopathy: a systematic review. *JAMA*. (2002) 287:1308–20. doi: 10.1001/jama.287.10.1308

2. Marian AJ, Roberts R. The molecular genetic basis for hypertrophic cardiomyopathy. *J Mol Cell Cardiol*. (2001) 33:655–70. doi: 10.1006/jmcc.2001.1340

3. Marian AJ. Modifier genes for hypertrophic cardiomyopathy. *Curr Opin Cardiol*. (2002) 17:242–52. doi: 10.1097/00001573-200205000-00006

4. Geisterfer-Lowrance AA, Kass S, Tanigawa G, Vosberg HP, Mckenna W, Seidman CE, et al. A molecular basis for familial hypertrophic cardiomyopathy: a beta cardiac myosin heavy chain gene missense mutation. *Cell*. (1990) 62:999–1006. doi: 10.1016/0092-8674(90)90274-I

5. Watkins H, Macrae C, Thierfelder L, Chou YH, Frenneaux M, Mckenna W, et al. A disease locus for familial hypertrophic cardiomyopathy maps to chromosome 1q3. *Nat Genet*. (1993) 3:333–7. doi: 10.1038/ng0493-333

6. Thierfelder L, Watkins H, Macrae C, Lamas R, Mckenna W, Vosberg HP, et al. Alpha-tropomyosin and cardiac troponin T mutations cause familial hypertrophic cardiomyopathy: a disease of the sarcomere. *Cell*. (1994) 77:701–12. doi: 10.1016/0092-8674(94)90054-X

7. Seidman CE, Seidman JG. Identifying sarcomere gene mutations in hypertrophic cardiomyopathy: a personal history. *Circ Res*. (2011) 108:743–50. doi: 10.1161/CIRCRESAHA.110.223834

8. Watkins H, Ashrafian H, Redwood C. Inherited cardiomyopathies. *N Engl J Med*. (2011) 364:1643–56. doi: 10.1056/NEJMra0902923

9. Maron BJ, Maron MS. Hypertrophic cardiomyopathy. *Lancet*. (2013) 381:242–55. doi: 10.1016/S0140-6736(12)60397-3

10. Maron BJ, Maron MS, Maron BA, Loscalzo J. Moving beyond the sarcomere to explain heterogeneity in hypertrophic cardiomyopathy: JACC review topic of the week. *J Am Coll Cardiol*. (2019) 73:1978–86. doi: 10.1016/j.jacc.2019.01.061

11. Ingles J, Burns C, Bagnall RD, Lam L, Yeates L, Sarina T, et al. Nonfamilial hypertrophic cardiomyopathy: prevalence, natural history, and clinical implications. *Circ Cardiovasc Genet*. (2017) 10. doi: 10.1161/CIRCGENETICS.116.001620

12. Gerull B, Klaassen S, Brodehl A. The genetic landscape of cardiomyopathies. *Genetic Causes of Cardiac Disease*. (2019):45–91. doi: 10.1007/978-3-030-27371-2_2

13. Vicart P, Caron A, Guicheney P, Li Z, Prevost MC, Faure A, et al. A missense mutation in the alphaB-crystallin chaperone gene causes a desmin-related myopathy. *Nat Genet*. (1998) 20:92–5. doi: 10.1038/1765

14. Kumarapeli AR, Su H, Huang W, Tang M, Zheng H, Horak KM, et al. Alpha B-crystallin suppresses pressure overload cardiac hypertrophy. *Circ Res*. (2008) 103:1473–82. doi: 10.1161/CIRCRESAHA.108.180117

15. Bennardini F, Wrzosek A, Chiesi M. Alpha B-crystallin in cardiac tissue. Association with actin and desmin filaments. *Circ Res*. (1992) 71:288–94. doi: 10.1161/01.RES.71.2.288

16. Nicholl ID, Quinlan RA. Chaperone activity of alpha-crystallins modulates intermediate filament assembly. *EMBO J*. (1994) 13:945–53. doi: 10.1002/j.1460-2075.1994.tb06339.x

17. Wang K, Spector A. alpha-crystallin stabilizes actin filaments and prevents cytochalasin-induced depolymerization in a phosphorylation-dependent manner. *Eur J Biochem*. (1996) 242:56–66. doi: 10.1111/j.1432-1033.1996.0056r.x

18. Tannous P, Zhu H, Johnstone JL, Shelton JM, Rajasekaran NS, Benjamin IJ, et al. Autophagy is an adaptive response in desmin-related cardiomyopathy. *Proc Natl Acad Sci U S A*. (2008) 105:9745–50. doi: 10.1073/pnas.0706802105

19. Bhuiyan MS, Pattison JS, Osinska H, James J, Gulick J, Mclendon PM, et al. Enhanced autophagy ameliorates cardiac proteinopathy. *J Clin Invest*. (2013) 123:5284–97. doi: 10.1172/JCI70877

20. Mitra A, Basak T, Datta K, Naskar S, Sengupta S, Sarkar S. Role of alpha-crystallin B as a regulatory switch in modulating cardiomyocyte apoptosis by mitochondria or endoplasmic reticulum during cardiac hypertrophy and myocardial infarction. *Cell Death Dis*. (2013) 4:e582. doi: 10.1038/cddis.2013.114

21. Bagneris C, Bateman OA, Naylor CE, Cronin N, Boelens WC, Keep NH, et al. Crystal structures of alpha-crystallin domain dimers of alphaB-crystallin and Hsp20. *J Mol Biol*. (2009) 392:1242–52. doi: 10.1016/j.jmb.2009.07.069

22. Laganowsky A, Benesch JL, Landau M, Ding L, Sawaya MR, Cascio D, et al. Crystal structures of truncated alphaA and alphaB crystallins reveal structural mechanisms of polydispersity important for eye lens function. *Protein Sci*. (2010) 19:1031–43. doi: 10.1002/pro.380

23. Mchaourab HS, Godar JA, Stewart PL. Structure and mechanism of protein stability sensors: chaperone activity of small heat shock proteins. *Biochemistry*. (2009) 48:3828–37. doi: 10.1021/bi900212j

24. Woods CN, Ulmer LD, Janowska MK, Stone NL, James EI, Guttman M, et al. HSPB5 disease-associated mutations have long-range effects on structure and dynamics through networks of quasi-ordered interactions. *bioRxiv*. (2022) 2022.2005.2030.493970.

25. Sacconi S, Feasson L, Antoine JC, Pecheux C, Bernard R, Cobo AM, et al. A novel CRYAB mutation resulting in multisystemic disease. *Neuromuscul Disord*. (2012) 22:66–72. doi: 10.1016/j.nmd.2011.07.004

26. Van Spaendonck-Zwarts KY, Van Hessem L, Jongbloed JD, De Walle HE, Capetanaki Y, Van Der Kooi AJ, et al. Desmin-related myopathy. *Clin Genet*. (2011) 80:354–66. doi: 10.1111/j.1399-0004.2010.01512.x

27. Wang X, Osinska H, Klevitsky R, Gerdes AM, Nieman M, Lorenz J, et al. Expression of R120G-alphaB-crystallin causes aberrant desmin and alphaB-crystallin aggregation and cardiomyopathy in mice. *Circ Res*. (2001) 89:84–91. doi: 10.1161/hh1301.092688

28. Bova MP, Yaron O, Huang Q, Ding L, Haley DA, Stewart PL, et al. Mutation R120G in alphaB-crystallin, which is linked to a desmin-related myopathy, results in an irregular structure and defective chaperone-like function. *Proc Natl Acad Sci U S A*. (1999) 96:6137–42. doi: 10.1073/pnas.96.11.6137

29. Brodehl A, Gaertner-Rommel A, Klauke B, Grewe SA, Schirmer I, Peterschroder A, et al. The novel alphaB-crystallin (CRYAB) mutation p.D109G causes restrictive cardiomyopathy. *Hum Mutat*. (2017) 38:947–52. doi: 10.1002/humu.23248

30. Maron BJ, Rowin EJ, Arkun K, Rastegar H, Larson AM, Maron MS, et al. Adult monozygotic twins with hypertrophic cardiomyopathy and identical disease expression and clinical course. *Am J Cardiol*. (2020) 127:135–8. doi: 10.1016/j.amjcard.2020.04.020

31. Rakowski H, Carasso S. Quantifying diastolic function in hypertrophic cardiomyopathy: the ongoing search for the holy grail. *Circulation*. (2007) 116:2662–5. doi: 10.1161/CIRCULATIONAHA.107.742395

32. Vikstrom KL, Factor SM, Leinwand LA. Mice expressing mutant myosin heavy chains are a model for familial hypertrophic cardiomyopathy. *Mol Med*. (1996) 2:556–67. doi: 10.1007/BF03401640

33. Ertz-Berger BR, He H, Dowell C, Factor SM, Haim TE, Nunez S, et al. Changes in the chemical and dynamic properties of cardiac troponin T cause discrete cardiomyopathies in transgenic mice. *Proc Natl Acad Sci U S A*. (2005) 102:18219–24. doi: 10.1073/pnas.0509181102

34. Lowey S, Lesko LM, Rovner AS, Hodges AR, White SL, Low RB, et al. Functional effects of the hypertrophic cardiomyopathy R403Q mutation are different in an alpha- or beta-myosin heavy chain backbone. *J Biol Chem*. (2008) 283:20579–89. doi: 10.1074/jbc.M800554200

35. Vakrou S, Fukunaga R, Foster DB, Sorensen L, Liu Y, Guan Y, et al. Allele-specific differences in transcriptome, miRNome, and mitochondrial function in two

hypertrophic cardiomyopathy mouse models. *JCI Insight*. (2018) 3. doi: 10.1172/jci.insight.94493

36. Barefield D, Kumar M, Gorham J, Seidman JG, Seidman CE, De Tombe PP, et al. Haploinsufficiency of MYBPC3 exacerbates the development of hypertrophic cardiomyopathy in heterozygous mice. *J Mol Cell Cardiol*. (2015) 79:234–43. doi: 10.1016/j.yjmcc.2014.11.018

37. Marstrand P, Han L, Day SM, Olivotto I, Ashley EA, Michels M, et al. Hypertrophic cardiomyopathy with left ventricular systolic dysfunction: insights from the SHaRe registry. *Circulation*. (2020) 141:1371–83. doi: 10.1161/CIRCULATIONAHA.119.044366

38. Beltrami M, Bartolini S, Pastore MC, Milli M, Cameli M. Relationship between measures of left ventricular systolic and diastolic dysfunction and clinical and biomarker status in patients with hypertrophic cardiomyopathy. *Arch Cardiovasc Dis*. (2022) 115:598–609. doi: 10.1016/j.acvd.2022.07.002

39. Sanbe A, Osinska H, Saffitz JE, Glabe CG, Kayed R, Maloyan A, et al. Desmin-related cardiomyopathy in transgenic mice: a cardiac amyloidosis. *Proc Natl Acad Sci U S A*. (2004) 101:10132–6. doi: 10.1073/pnas.0401900101

40. Maloyan A, Sanbe A, Osinska H, Westfall M, Robinson D, Imahashi K, et al. Mitochondrial dysfunction and apoptosis underlie the pathogenic process in alpha-B-crystallin desmin-related cardiomyopathy. *Circulation*. (2005) 112:3451–61. doi: 10.1161/CIRCULATIONAHA.105.572552

41. Alam S, Abdullah CS, Aishwarya R, Morshed M, Nitu SS, Miriyala S, et al. Dysfunctional mitochondrial dynamic and oxidative phosphorylation precedes cardiac dysfunction in R120G-alphaB-crystallin-induced desmin-related cardiomyopathy. *J Am Heart Assoc*. (2020) 9:e017195. doi: 10.1161/JAHA.120.017195

42. Chou C, Chin MT. Pathogenic mechanisms of hypertrophic cardiomyopathy beyond sarcomere dysfunction. *Int J Mol Sci*. (2021) 22:8933–46. doi: 10.3390/ijms22168933

43. Helms AS, Alvarado FJ, Yob J, Tang VT, Pagani F, Russell MW, et al. Genotype-dependent and -independent calcium signaling dysregulation in human hypertrophic cardiomyopathy. *Circulation*. (2016) 134:1738–48. doi: 10.1161/CIRCULATIONAHA.115.020086

44. Coppini R, Ferrantini C, Mugelli A, Poggesi C, Cerbai E. Altered Ca(2+) and Na(+) homeostasis in human hypertrophic cardiomyopathy: implications for arrhythmogenesis. *Front Physiol*. (2018) 9:1391. doi: 10.3389/fphys.2018.01391

45. Wilkins BJ, Dai YS, Bueno OF, Parsons SA, Xu J, Plank DM, et al. Calcineurin/NFAT coupling participates in pathological, but not physiological, cardiac hypertrophy. *Circ Res*. (2004) 94:110–8. doi: 10.1161/01.RES.0000109415.17511.18

46. Golenhofen N, Ness W, Koob R, Htun P, Schaper W, Drenckhahn D. Ischemia-induced phosphorylation and translocation of stress protein alpha B-crystallin to Z lines of myocardium. *Am J Physiol*. (1998) 274:H1457–64. doi: 10.1152/ajpheart.1998.274.5.H1457

47. Maksimiuk M, Sobiborowicz A, Tuzimek A, Deptala A, Czerw A, Badowska-Kozakiewicz AM. alphaB-crystallin as a promising target in pathological conditions—a review. *Ann Agric Environ Med*. (2020) 27:326–34. doi: 10.26444/aaem/111759

48. Head MW, Hurwitz L, Kegel K, Goldman JE. AlphaB-crystallin regulates intermediate filament organization in situ. *Neuroreport*. (2000) 11:361–5. doi: 10.1097/00001756-200002070-00028

49. Chis R, Sharma P, Bousette N, Miyake T, Wilson A, Backx PH, et al. alpha-Crystallin B prevents apoptosis after H2O2 exposure in mouse neonatal cardiomyocytes. *Am J Physiol Heart Circ Physiol*. (2012) 303:H967–78. doi: 10.1152/ajpheart.00040.2012

50. Codden CJ, Chin MT. Common and distinctive intercellular communication patterns in human obstructive and nonobstructive hypertrophic cardiomyopathy. *Int J Mol Sci*. (2022) 23:946–68. doi: 10.3390/ijms23020946

51. Codden CJ, Larson A, Awata J, Perera G, Chin MT. Single nucleus RNA-sequencing reveals altered intercellular communication and dendritic cell activation in nonobstructive hypertrophic cardiomyopathy. *Cardiol Cardiovasc Med*. (2022) 6:398–415. doi: 10.26502/fccm.92920277

52. Larson A, Codden CJ, Huggins GS, Rastegar H, Chen FY, Maron BJ, et al. Altered intercellular communication and extracellular matrix signaling as a potential disease mechanism in human hypertrophic cardiomyopathy. *Sci Rep*. (2022) 12:5211. doi: 10.1038/s41598-022-08561-x

53. Shatov VM, Muranova LK, Zamotina MA, Sluchanko NN, Gusev NB. alpha-crystallin domains of five human small heat shock proteins (sHsps) differ in dimer stabilities and ability to incorporate themselves into oligomers of full-length sHsps. *Int J Mol Sci*. (2023) 24:1085–102. doi: 10.3390/ijms24021085

54. Baranova EV, Weeks SD, Beelen S, Bukach OV, Gusev NB, Strelkov SV. Three-dimensional structure of alpha-crystallin domain dimers of human small heat shock proteins HSPB1 and HSPB6. *J Mol Biol*. (2011) 411:110–22. doi: 10.1016/j.jmb.2011.05.024

55. Delbecq SP, Jehle S, Klevit R. Binding determinants of the small heat shock protein, alphaB-crystallin: recognition of the "IxI" motif. *EMBO J*. (2012) 31:4587–94. doi: 10.1038/emboj.2012.318

56. Janowska MK, Baughman HER, Woods CN, Klevit RE. Mechanisms of small heat shock proteins. *Cold Spring Harb Perspect Biol*. (2019) 11. doi: 10.1101/cshperspect.a034025

57. Rajasekaran NS, Connell P, Christians ES, Yan LJ, Taylor RP, Orosz A, et al. Human alpha B-crystallin mutation causes oxido-reductive stress and protein aggregation cardiomyopathy in mice. *Cell*. (2007) 130:427–39. doi: 10.1016/j.cell.2007.06.044

58. Rothbard JB, Kurnellas MP, Brownell S, Adams CM, Su L, Axtell RC, et al. Therapeutic effects of systemic administration of chaperone alphaB-crystallin associated with binding proinflammatory plasma proteins. *J Biol Chem*. (2012) 287:9708–21. doi: 10.1074/jbc.M111.337691

59. Xu W, Guo Y, Huang Z, Zhao H, Zhou M, Huang Y, et al. Small heat shock protein CRYAB inhibits intestinal mucosal inflammatory responses and protects barrier integrity through suppressing IKKbeta activity. *Mucosal Immunol*. (2019) 12:1291–303. doi: 10.1038/s41385-019-0198-5

60. Grose JH, Langston K, Wang X, Squires S, Mustafi SB, Hayes W, et al. Characterization of the cardiac overexpression of HSPB2 reveals mitochondrial and myogenic roles supported by a cardiac HspB2 interactome. *PLoS One*. (2015) 10:e0133994. doi: 10.1371/journal.pone.0133994

61. Arac A, Brownell SE, Rothbard JB, Chen C, Ko RM, Pereira MP, et al. Systemic augmentation of alphaB-crystallin provides therapeutic benefit twelve hours post-stroke onset via immune modulation. *Proc Natl Acad Sci U S A*. (2011) 108:13287–92. doi: 10.1073/pnas.1107368108

62. Pangratz-Fuehrer S, Kaur K, Ousman SS, Steinman L, Liao YJ. Functional rescue of experimental ischemic optic neuropathy with alphaB-crystallin. *Eye (Lond)*. (2011) 25:809–17. doi: 10.1038/eye.2011.42

63. Velotta JB, Kimura N, Chang SH, Chung J, Itoh S, Rothbard J, et al. alphaB-crystallin improves murine cardiac function and attenuates apoptosis in human endothelial cells exposed to ischemia-reperfusion. *Ann Thorac Surg*. (2011) 91:1907–13. doi: 10.1016/j.athoracsur.2011.02.072

64. Dull T, Zufferey R, Kelly M, Mandel RJ, Nguyen M, Trono D, et al. A third-generation lentivirus vector with a conditional packaging system. *J Virol*. (1998) 72:8463–71. doi: 10.1128/JVI.72.11.8463-8471.1998

65. Richards DA, Aronovitz MJ, Calamaras TD, Tam K, Martin GL, Liu P, et al. Distinct phenotypes induced by three degrees of transverse aortic constriction in mice. *Sci Rep*. (2019) 9:5844. doi: 10.1038/s41598-019-42209-7

66. Blanton RM, Takimoto E, Lane AM, Aronovitz M, Piotrowski R, Karas RH, et al. Protein kinase g ialpha inhibits pressure overload-induced cardiac remodeling and is required for the cardioprotective effect of sildenafil in vivo. *J Am Heart Assoc*. (2012) 1:e003731. doi: 10.1161/JAHA.112.003731

67. Gao S, Ho D, Vatner DE, Vatner SF. Echocardiography in mice. *Curr Protoc Mouse Biol*. (2011) 1:71–83. doi: 10.1002/9780470942390.mo100130

frontiers | Frontiers in Cardiovascular Medicine

TYPE Review
PUBLISHED 17 July 2023
DOI 10.3389/fcvm.2023.1176828

OPEN ACCESS

EDITED BY
Michael T. Chin,
Tufts Medical Center, United States

REVIEWED BY
Paolo Versacci,
Sapienza University of Rome, Italy
Jirko Kühnisch,
Charité University Medicine Berlin, Germany

*CORRESPONDENCE
Sangita Choudhury
✉ sangita.choudhury@childrens.harvard.edu

RECEIVED 28 February 2023
ACCEPTED 20 June 2023
PUBLISHED 17 July 2023

CITATION
Hilal N, Chen Z, Chen MH and Choudhury S (2023) RASopathies and cardiac manifestations. Front. Cardiovasc. Med. 10:1176828. doi: 10.3389/fcvm.2023.1176828

RASopathies and cardiac manifestations

Nazia Hilal[1,2,3], Zi Chen[2,4], Ming Hui Chen[2,5] and Sangita Choudhury[1,2,3]*

[1]Division of Genetics and Genomics, Department of Pediatrics, Boston Children's Hospital, Boston, MA, United States, [2]Harvard Medical School, Boston, MA, United States, [3]Broad Institute of Harvard and MIT, Cambridge, MA, United States, [4]Department of Surgery, Brigham, and Women's Hospital, Boston, MA, United States, [5]Department of Cardiology, Boston Children's Hospital, Boston, MA, United States

As binary switches, RAS proteins switch to an ON/OFF state during signaling and are on a leash under normal conditions. However, in RAS-related diseases such as cancer and RASopathies, mutations in the genes that regulate RAS signaling or the RAS itself permanently activate the RAS protein. The structural basis of this switch is well understood; however, the exact mechanisms by which RAS proteins are regulated are less clear. RAS/MAPK syndromes are multisystem developmental disorders caused by germline mutations in genes associated with the RAS/mitogen-activated protein kinase pathway, impacting 1 in 1,000–2,500 children. These include a variety of disorders such as Noonan syndrome (NS) and NS-related disorders (NSRD), such as cardio facio cutaneous (CFC) syndrome, Costello syndrome (CS), and NS with multiple lentigines (NSML, also known as LEOPARD syndrome). A frequent manifestation of cardiomyopathy (CM) and hypertrophic cardiomyopathy associated with RASopathies suggest that RASopathies could be a potential causative factor for CM. However, the current supporting evidence is sporadic and unclear. RASopathy-patients also display a broad spectrum of congenital heart disease (CHD). More than 15 genes encode components of the RAS/MAPK signaling pathway that are essential for the cell cycle and play regulatory roles in proliferation, differentiation, growth, and metabolism. These genes are linked to the molecular genetic pathogenesis of these syndromes. However, genetic heterogeneity for a given syndrome on the one hand and alleles for multiple syndromes on the other make classification difficult in diagnosing RAS/MAPK-related diseases. Although there is some genetic homogeneity in most RASopathies, several RASopathies are allelic diseases. This allelism points to the role of critical signaling nodes and sheds light on the overlap between these related syndromes. Even though considerable progress has been made in understanding the pathophysiology of RASopathy with the identification of causal mutations and the functional analysis of their pathophysiological consequences, there are still unidentified causal genes for many patients diagnosed with RASopathies.

KEYWORDS

rasopathy, cardiac abnormalities, congenital heart disease, hypertrophic cardiomyopathy, ras/MAPK

Introduction

Rat Sarcoma Virus, a highly conserved protein, belongs to a class of proteins called small GTPase. The three most widely studied RAS genes in humans are HRAS, KRAS, and NRAS, named after the Harvey Rat sarcoma virus, Kirsten Rat sarcoma virus, and NRAS, for its initial identification in neuroblastoma cells. Since the identification of the RAS protein in 1982, extensive studies have been conducted to identify the RAS-associated pathway and

its involvement in human disease. RASopathies refer to multisystem disorders caused by gene mutations that belong to the RAS/MAPK (Mitogen-activated protein kinase) signaling pathway. RAS can be either "switched on" or activated by incoming signals through growth factors binding to receptor tyrosine kinases (RTKs), G-protein-coupled receptors, cytokine receptors, and extracellular matrix receptors, or activated by mutations in RAS genes, which can lead to the production of permanently activated RAS proteins and can cause unintended and overactive signaling inside the cell, even in the absence of incoming signals. The mitogen-activated protein kinase (MAPK) pathway is one of RAS's critical downstream signaling cascades. Activated RAS leads to the phosphorylation of Raf, leading to the activation of the MAPK kinases MEK1 and/or MEK2; these, in turn, phosphorylate and activate ERK1 and/or ERK2. ERK1 and ERK2 are the ultimate effectors which exert their function on many downstream molecules in the cytoplasm and nucleus (**Figure 1**). RASopathy disorders include wide range of disorders such as neurofibromatosis type 1, Noonan syndrome, Noonan syndrome with multiple lentigines, Costello syndrome, cardio-facio-cutaneous syndrome, and Legius syndrome (1, 2), exhibiting multi-organ dysfunction, including craniofacial dysmorphology, cardiac malformation, cutaneous, musculoskeletal, and ocular abnormalities, neurocognitive impairment, hypotonia and increased cancer risk (1–3). In **Table 1**, we summarize the critical and cardiac-specific features as well as all other RASopathy-associated malformations. This review will discuss only the cardiac manifestation in RASopathies associated with Noonan syndrome and Neurofibromatosis type 1 (NF1). RASopathy-related heart defects include congenital heart disease (CHD), hypertrophic cardiomyopathy (HCM) as well as dilated cardiomyopathy (DCM).

Noonan syndrome and cardiac manifestation

Noonan syndrome (NS1, OMIM 163950), caused by mutation and activation of the genes involved in the RAS-MAPK pathway, including *PTPN11, SOS1, KRAS, NRAS, RAF1, BRAF, RIT1, and LZTR1*, is a common developmental disorder with an autosomal dominant inheritance. The incidence is 1:1,000–2,500 live births. Many patients with NS1 indicate cardiovascular abnormalities, most commonly in the form of congenital heart diseases, such as pulmonary valve stenosis, septal defects, left-sided lesions, and complex forms with multiple anomalies. The most common congenital heart disease (CHD) involves pulmonary valve stenosis in 50%–60% of patients, and a small portion (6%–10%) indicates an atrial septal defect. The other CHDs, such as ventricular septal defect,

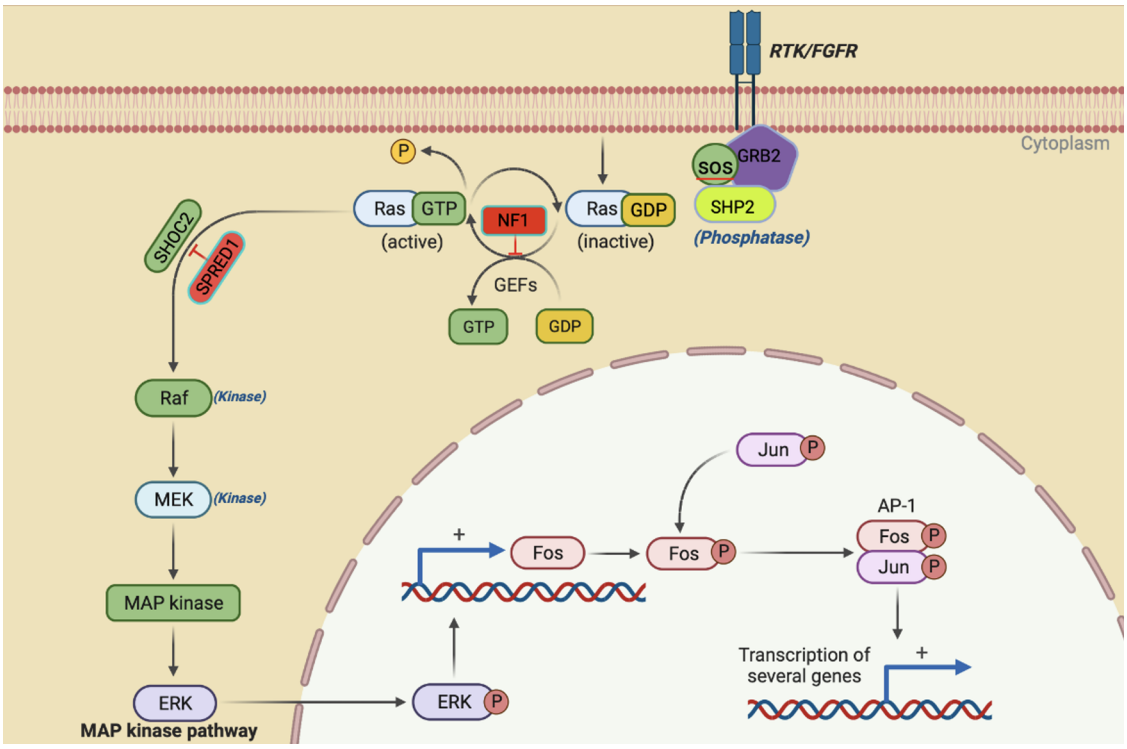

FIGURE 1
The activation of RAS/ERK occurs when cell survival signals bind to receptor tyrosine kinases (RTK). Once the RTK intracellular domain is phosphorylated following this binding, it triggers a sequence of events that ultimately results in the activation of RAS. NF1 and SPRED 1 act as negative effectors of the pathway. The activation of RAS recruits and activates RAF, which is the first MAPK in this pathway. Then, RAF phosphorylates and activates MEK1/2, which finally activates ERK1/2 through dual phosphorylation on tyrosine and threonine. ERK1/2 then goes on to activate various substrates downstream like FOS and JUN that ultimately leads to transcriptional activation of genes involved in cell proliferation and survival.

TABLE 1 Different features of RASopathies, including main features, cardiac-specific features, and critical cardiac features.

RASopathy	Main Feature		Cardiac specific Feature		Critical cardiac feature
Noonan syndrome	Short stature, webbed neck, low-set ears, widely spaced eyes, hypertelorism, pectus excavatum/carinatum, cryptorchidism, bleeding diathesis, lymphatic dysplasia		Pulmonary stenosis (PS), hypertrophic cardiomyopathy (HCM)		Atrial septal defect (ASD), ventricular septal defect (VSD), coarctation of the aorta (CoA), critical aortic stenosis (AS)
	Gene	Mutation Type	Mutation Location	Function	Cardiac Implications
Noonan syndrome	PTPN11	Missense, splice site	Exon 3, 7, 8, 12, 13	Encodes for SHP-2 protein which regulates RAS signaling pathway	Pulmonic stenosis (PS), hypertrophic cardiomyopathy (HCM), arrhythmias
	SOS1	Missense, frameshift, splice site, large deletions	Exon 2, 3, 5, 12, 13, 16, 17, 18, 19, 20, 21	Encodes for SOS1 protein which activates RAS signaling pathway	Pulmonic stenosis (PS), hypertrophic cardiomyopathy (HCM), cardiomyopathy, septal defects
	RAF1	Missense	Exon 7, 12, 14	Encodes for RAF1 protein which activates the MEK/ERK signaling pathway	Hypertrophic cardiomyopathy (HCM), pulmonary valve stenosis (PVS), cardiomyopathy
	KRAS	Missense	Exon 2	Encodes for KRAS protein which regulates cell division and differentiation	Hypertrophic cardiomyopathy (HCM)
RASopathy	Main Feature		Cardiac specific Feature		Critical cardiac feature
Cardio-facio-cutaneous syndrome	Short stature, sparse hair, curly hair, prominent forehead, hypertelorism, downward slanting palpebral fissures, ptosis, hearing loss, intellectual disability		Hypertrophic cardiomyopathy (HCM), pulmonary valve stenosis (PVS)		Atrial septal defect (ASD), ventricular septal defect (VSD), critical pulmonary valve stenosis (c-PVS), severe mitral valve disease (MVD)
	Gene	Mutation Type	Mutation Location	Function	Cardiac Implications
Cardio-facio-cutaneous syndrome	BRAF	Missense, frameshift, splice site, large deletions	Exon 5, 8, 11, 15	Encodes for BRAF protein which activates the MEK/ERK signaling pathway	Pulmonic stenosis (PS), hypertrophic cardiomyopathy (HCM), arrhythmias, cardiomyopathy
RASopathy	Main Feature		Cardiac specific Feature		Critical cardiac feature
Costello syndrome	Short stature, coarse facies, curly hair, loose skin, hypertrophic cardiomyopathy, feeding difficulties, intellectual disability, neoplasia		Hypertrophic cardiomyopathy (HCM), pulmonic stenosis (PS)		Atrial septal defect (ASD), ventricular septal defect (VSD), critical pulmonary valve stenosis (c-PVS), severe mitral valve disease (MVD)
	Gene	Mutation Type	Mutation Location	Function	Cardiac Implications
Costello syndrome	HRAS	Missense	Exon 2, 3	Encodes for HRAS protein which regulates cell division and differentiation	Hypertrophic cardiomyopathy (HCM), tachycardia, arrhythmias
RASopathy	Main Feature		Cardiac specific Feature		Critical cardiac feature
Legius syndrome	Café-au-lait macules, lipomas, macrocephaly, learning disabilities, Noonan-like facies		None reported		None reported
	Gene	Mutation Type	Mutation Location	Function	Cardiac Implications
Legius syndrome	SPRED1	Missense, frameshift, splice site, large deletions	Exon 1, 2, 3, 5, 6, 7, 8, 9	Encodes for SPRED1 protein which acts as a negative regulator of RAS signaling pathway	Pulmonic stenosis (PS), hypertrophic cardiomyopathy (HCM), valvular heart disease (VHD)
RASopathy	Main Feature		Cardiac specific Feature		Critical cardiac feature
Neurofibromatosis Type 1	Café-au-lait macules, neurofibromas, Lisch nodules, scoliosis, optic gliomas, learning disabilities, skeletal abnormalities		Pulmonary stenosis (PS)		Atrial septal defect (ASD), ventricular septal defect (VSD), hypertrophic cardiomyopathy (HCM)
	Gene	Mutation Type	Mutation Location	Function	Cardiac Implications
Neurofibromatosis Type 1	NF1	Missense, nonsense, frameshift, splice site, large deletions	Most commonly 17q11.2	Encodes for neurofibromin protein which acts as a negative regulator of RAS signaling pathway	Hypertrophic cardiomyopathy (HCM), pulmonary stenosis (PS), congenital heart defects (CHD)

atrioventricular canal defect, and aortic coarctation, are observed less frequently in NS1 patients (4–7). The second most prevalent cardiovascular anomaly associated with NS1 is HCM, present in approximately 20% of patients. Although NS1 is clinically heterogeneous and can manifest at any age, 80% of NS-1 HCM diagnoses are made early in infancy, and compared to non-syndromic types of HCM, NS1-HCM patients have a greater degree of ventricular hypertrophy, a higher prevalence, and a

more severe pattern of left ventricular outflow tract obstruction (LVOTO). A literature survey indicates that a patient's likelihood of NS1-HCM varies significantly according to the gene mutated in the RAS-MAPK pathway. A few studies suggest an association between DCM and NS1 to some extent, where histology/echocardiography showed hypertrophy of myocardial fibers with focal interstitial fibrosis with no evidence of myocardial disarray. The features were consistent with DCM (8–11).

Noonan syndrome with multiple lentigines (NSML), which is also known as LEOPARD syndrome, has the cardiac manifestation of pulmonary valve stenosis and hypertrophic cardiomyopathy along with brown spots on the skin called lentigines, caused by the mutation in one of four genes: BRAF, MAP2K1, PTPN11, and RAF1 (12–14).

Genes involved in Noonan syndrome

PTPN11 was found to be the most studied gene in NS populations (29 studies vs. 16 studies or fewer for other genes). Possible reasons include that *PTPN11* was the first gene of the RAS/MAPK pathway to be implicated in NS in 2001, while *KRAS* was discovered only five years later, followed by SHP-2. Although *KRAS* was already involved in malignancy disorders through various somatic mutations, its interrelation with NS was found *via* germline mutations in 2006 (15). Subsequently, in 2007, *SOS1, RAF1*, and *MAP2K1* genes were found to be implicated in NS (16), after which *BRAF* (12, 16), *NRAS* (17), and *RIT1* (18) (RAS/MAPK kinase genes) were shown to be involved. Notably, the chronology of discovering the involved genes does not correlate with their frequency or the intensity of the phenotypic manifestations but is merely incidental. The most common gene implicated in the causation of NS is still *PTPN11* (60%), constituting 52.6% of all mutations detected in Noonan patients to date (**Figure 2**). The second most found mutated gene in NS is *SOS1*(16.4% of patients). Furthermore, *RIT1* and *RAF1* have been found to have a prevalence of 8%, making them the third most-involved genes. Therefore, mutations in *PTPN11, SOS1, RAF1, and RIT1* alone comprise 93% of the mutations causing NS. Hence, these genes are included in the first line of genetic screening in patients with the NS phenotype. **Table 2** summarizes the genes and domains involved in RASopathies. *KRAS* (2.8%) and *NRAS* (0.8%) have the lowest incidence among all reported cases of Noonan syndrome caused by the RAS subfamily of genes involved in the RAS/MAPK pathway, in contrast with the *RIT1* gene in the same family. Similarly, *BRAF* constitutes 2.3% among RAF family members compared to the more prevalent *RAF1*. **Table 1** emphasizes the genes involved in different RASopathies and their normal function, mutation type, mutation location, and cardiac implications.

PTPN11 (protein-tyrosine phosphatase, nonreceptor-type 11)

PTPN11 is the most common gene associated with NS and accounts for approximately half of all cases. The *PTPN11* gene (19) has three domains: the more commonly mutated N-amino terminal src-homology 2 (N-SH2) and phospho-tyrosine phosphatase (PTP) domains, and the C-amino terminal src-homology 2 domain (C-SH2) and carboxy-terminal tail (5, 6).

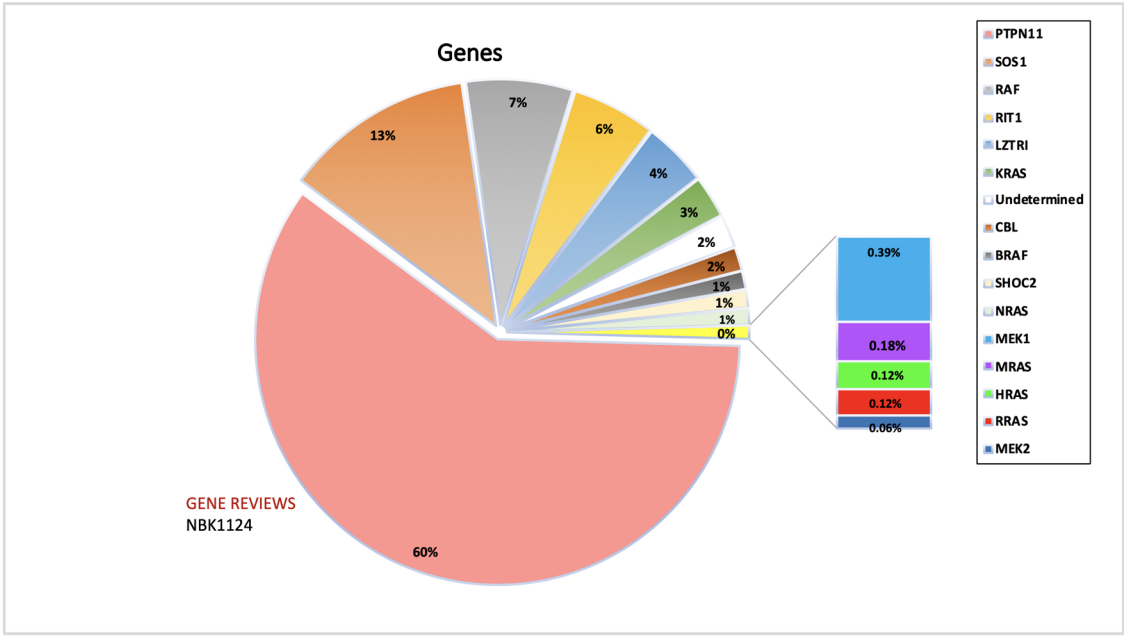

FIGURE 2
The figure represents the information of the genes implicated in NS and associated RASopathies. PTPN11, SOS1 and RAF alone makes up for more than 90% of the total pathogenic mutations. The data is obtained from the NSEuroNet database.

TABLE 2 Common RASopathy-associated mutations.

Component	Gene	Mutation	Domain	Type
Phosphatases	*PPP1CB*	p.P49R	N-terminus	NS
	PTPN11	p.D61G/N/H	N-SH2	NS
		p.Y63C		
		p.Q79R/P		
		p.N308D/S/T	Phosphatase	
		p.Y279C/S		NS-ML
		p.T469M/P		
RAS isoforms	*HRAS*	p.G12S/A/C	RAS	CS
	KRAS	p.V14I		NS
		p.P34R/K		
		p.I36M		
		p.T58I		
		p.G60R/S		
		p.D153V		
	NRAS	p.G60E		
	MRAS	p.G23R/V		
	RRAS	p.G23dup		
	RIT1	p.A57G		
		p.F82l/I/V		
		p.M90I		
		G95A		
Kinases	*BRAF*	p.Q257R/K	CRD	CFC
		p.L597V	Kinase	
	RAF1	p.S257l/K/P	CR2	NS
	MEK1	p.Y130C/N/H	Kinase	CFC
	MEK2	p.F57C/I/V/l	N-terminus	
GEFs	*SOS1*	p.M269T/R	RHO GEF	NS
		p.R552/G/S/K	Allosteric site	
		p.E848K	RAS GEF	
Ubiquitin	*CBL*	p.Y371H/C/N	RING	NSLD
	LZTR1	p.G248R	Kelch	NS

The table presents information about the most frequent recurring changes that occur in known RASopathy genes and specifies the protein domain where the alteration happens. The selection criteria were based on the clinical outcome (phenotype) of the variants. The acronyms used in the table include CFC, cardiofaciocutaneous syndrome; CS, Costello syndrome; NS, Noonan syndrome; NS-LAH, Noonan syndrome with loose anagen hair; NSLD, Noonan syndrome-like disease; NS-ML, Noonan syndrome with multiple lentigines.

PTPN11 codes for protein SHP-2 which is involved in semilunar valvulogenesis, hemopoietic cell differentiation, and mesodermal patterning (20–23). SHP-2 also regulates the cell proliferation, migration, or differentiation processes during the developmental stage (24) and is widely expressed in several tissues, such as the heart, muscles, and brain. SHP-2 is a pivotal protein in the RAS/MAPK cascade. *PTPN11* mutations were mainly seen in cases with pulmonary valve stenosis in NS1 patients (5, 6).

SOS1 (Son of seven less homologs 1)

Mutated *SOS1* (OMIM 182530) is considered the second-most-common genetic aberration associated with NS, causing NS in up to 20% of patients with absent *PTPN11* mutation (25). Its locus is on the 2p22-p21 region, consisting of 23 exons (26, 27) and coding for multiple domains containing: regulatory histone-like folds domain (HF), Dbl homology domains (DH), and Pleckstrin homology domains (PH); catalytic RAS exchanging motif (REM) and Cdc25 domains; helical linker (HL) relating PH and REM, and the Polyproline region (25, 28). SOS1 is a guanine exchange factor (GEF) with a significant role in the RAS/MAPK pathway (26, 27) and mainly implicated in NS patients with ectodermal defects (25, 28–30) and pulmonic stenosis more than that of PTPN1.

KRAS (kirsten rat sarcoma viral oncogene homolog)

The *KRAS* (OMIM 190070) gene is mapped to the 12p12 region and consists of 6 exons coding for the P loop and switch I and switch II domains (15). Gain of function mutations in *KRAS* causes approximately 5% of NS cases in the absence of the PTPN11 mutations (16, 31).

NRAS (neuroblastoma RAS viral oncogene homolog)

The *NRAS* (OMIM 164790) gene locus on 1p13.2 comprises six coding exons (32). *NRAS* mutations are involved in less than 1% of NS cases (17).

RIT1 (Ric-like protein without CAAX motif 1)

The *RIT1* (OMIM 609591) locus on 1q22, consisting of 6 exons, causes hyperactivation of transcription factor *ELK1* in the RAS/MAPK cascade. It is present in 9% of NS cases (18). Prevalence is seen to mainly coexist with cardiac defects such as CHD (94%), HCM (71%), and pulmonic stenosis (65%). This finding was subsequently confirmed by Bertola et al., who found the exact prevalence (9%), and Gos et al., who found a lower mutation rate (3.8%). Those mutation clusters in the G1, Switch I, and more frequently in Switch II domains, were proven to entail a significant activation of the RAS/MAPK pathway by hyper-activating transcription factor *ELK1* (33, 34).

RAF1 (v-RAF-1 murine leukemia viral oncogene homolog 1)

RAF1 (OMIM 164760) locus on 3p25, consisting of 17 exons, codes for protein serine-threonine kinase (35–37) and has three conserved regions. Mutations causing failure of autoinhibition of this gene lead to activation of the RAS/MAPK cascade, causing NS (3%–17% of cases). An association of 80% is found with HCM.

BRAF (V-Raf murine sarcoma viral oncogene homolog B1)

Mutated *BRAF* (OMIM 164757) locus on 7q34 enhances ERK activation (38, 36), causing NS in 1.7%–1.9% of cases.

MAP2K1 (mitogen-activated protein kinase 1)

MAP2K1 (OMIM 176872), with a locus on 15q22, comprises 11 exons encoding the MEK protein, which activates ERK-MAP (39). Among NS cases without *PTPN11* and SOS1 mutations, 4.2% are caused by mutated MAP2K1 (40).

SOS2 (Son of seven less homolog 2)

Mutation of the homolog of *SOS2* (OMIM 601247) locus on 14q21 causes 4% of Noonan cases, closely associated with ectodermal defects like *SOS1* (41).

LZTR1 (leucine-zipper-like transcription regulator 1)

The *LZTR1* gene (OMIM 600574) mapped on 22q11.21, consisting of 21 exons, encodes for a protein of the BTB-ketch superfamily, also implicated in neurofibromatosis (42). However, it is not associated with the RAS/MAPK pathway (41).

A2ML1 [a-2-macroglobulin (A2m)-like-1]

Mutation of *A2ML1* (OMIM 610627), mapped on 12p13 with 35 exons, comprises 1% of Noonan patients negative for other significant genes (43). *A2ML1* is a member of the a-macroglobulin superfamily, localized in the 12p13 region with 35 coding exons, and is a protease inhibitor upstream of the MAPK pathway (44). Nevertheless, how its mutation affects the MAPK pathway requires further explication.

Other genes

Recently implicated rare variants in NS include *RASA2, MAP3K8*, and *SPRY* (45).

Neurofibromatosis type 1 (NF1) and cardiac manifestation

Neurofibromatosis (OMIM 162200) is an autosomal dominant genetic disorder caused by a heterozygous mutation of the NF1 gene located on chromosome 17q11.2. NF1 is a multisystem disease impacting the growth and function of various cell types and organs. Early-onset cerebrovascular disease, pheochromocytomas, and cardiovascular disease frequently cause premature death in individuals with NF1. Neurofibromas, the characteristic tumors of NF1, impact approximately 1/2000 live births (46) and can develop within the heart, obstructing blood flow in the heart or major vessels by compression or invasion, leading to hemorrhage. Fortunately, these are rare complications. NF1 encodes the neurofibromin protein, which belongs to the family of GTPase activating proteins (GAPs) and which negatively regulates RAS signaling. Neurofibromin also positively regulates cyclic adenosine monophosphate (AMP) levels (47, 48). Increased cyclic AMP levels have been associated with reduced cell growth, likely through interference with multiple mitogenic signaling pathways. The most common cardiovascular manifestations of NF1 include vasculopathy (49), hypertension (50), and other congenital heart defects (51). Sørensen found myocardial infarction and cerebrovascular accidents at a younger than-expected age in NF1 patients (52). NF1 vasculopathy includes segmental hypoplasia of the abdominal aorta and fibro cellular intimal proliferation. Both contribute to the luminal stenosis (53), aneurysms, the rupturing of which has been known to cause catastrophic abdominal and retroperitoneal hemorrhage and arteriovenous malformations, and is the second leading cause of death in neurofibromatosis patients (54–56). Coronary heart disease occurs at a higher-than-expected frequency compared with that in the general population, with pulmonary artery stenosis representing 25% of these malformations. Hypertension is common among female NF1 patients during pregnancy (57), and the prevalence increases with age. However, it has not been investigated whether NF1-hypertension is just a coincidental finding often discovered during medical evaluation for other reasons. Based on the previous literature, 10%–15% of NF1 patients have CHD (51). Approximately 50% of NF1 individuals with CHD have PVS. Aortic stenosis, aortic coarctation, atrial septal defects (ASD), and ventricular septal defects (VSD) are detected less frequently in NF-CHDs (58–60).

Genetics of neurofibromatosis type 1

NF1 is a large and complex gene that carries more than 280 kb of genomic DNA, including 57 constitutive exons and other alternatively spliced exons (61). Now, over 2,800 different *NF1* variants have been identified (62). Genetic testing in NF1 is challenging because of the large number of possible mutations in this large gene. Approximately 5% of patients with NF1 have a complete or near-complete deletion of the NF1 gene. These patients display a more severe phenotype, including earlier onset, large load of neurofibromas, greater likelihood of cognitive deficiency, dysmorphic facial features, increased risk of malignancy, and connective tissue involvement, with joint laxity, hyperextensible skin, and mitral valve prolapse. *ADAP2* gene, which has been considered as a modifier of NF1, involved in cardiac development, is a reliable candidate gene for the occurrence of congenital valve defects (63). Additionally, *CENTA2* and *JJAZ1* are two possible candidates for the cardiovascular malformations (64).

Sex dimorphism in RASopathy-induced cardiomyopathy in NS and NF1

The relationship between RASopathies and sex dimorphism is controversial, complex, and likely influenced by many factors.

Studies have suggested that males with NS may be more likely to have more severe cardiac manifestations, including a higher incidence of hypertrophic cardiomyopathy and aortic valve stenosis, compared to females with NS (3, 35, 65). Similarly, few studies indicated that males had a higher incidence of pathogenic variants in the *RAF1* gene, a less common genetic mutation associated with NS (66–69). However, other studies suggested no significant sex differences in the prevalence or severity of cardiac abnormalities in NS patients (16, 70). A retrospective cohort of 412 children with NS by Romano et al. found that female patients had a higher prevalence of pulmonary valve stenosis and a higher incidence of cardiac surgery compared to male patients. These female patients also indicated a higher incidence of composite cardiovascular events compared to male patients (71).

There is limited evidence regarding sex differences in cardiac manifestations of NF1 (72). But a recent study investigated sex differences in cardiac function in NF1 patients with Left Ventricular (LV) dysfunction and found that males had significantly lower Left ventricular ejection fraction (LV EF) and more severe LV dysfunction than females. In addition, males had a higher incidence of LV remodeling and a higher risk of sudden cardiac death than females (73). Similarly, individuals with NF1 found that males were more likely to have cardiac abnormalities than females and that males had a higher incidence of pulmonary stenosis and atrial septal defects (51). On contrary, an older study found that females with NF1 may be more likely to have cardiac abnormalities than males (58).

Current observations indicate that there may be some sex differences in the prevalence or severity of cardiac manifestations in RASopathies. These differences are not always consistent across studies and may be influenced by other factors such as age, genotype, and environmental factors. Additionally, many individuals with RASopathies have a normal cardiac function. However, the mechanisms underlying these sex differences are not well understood. One possible explanation is the differential expression of RAS-MAPK pathway genes in males and females, which could affect the development and progression of cardiomyopathy in RASopathies. Another possible explanation is the influence of sex hormones on cardiac function and remodeling, which could interact with the RAS-MAPK pathway and contribute to sex differences in RASopathy-induced cardiomyopathy. Despite the growing recognition of sex differences in RASopathy-induced cardiomyopathy, there is a lack of sex-specific guidelines for the diagnosis and management of cardiac complications in these disorders. This highlights the need for further research to understand the mechanisms underlying sex differences in RASopathy-induced cardiomyopathy and develop sex-specific management strategies to improve outcomes for both male and female patients.

Age of onset and clinical penetrance of genetic variants in RASopathies

Cardiomyopathy, a common cardiovascular complication in patients with NS and NF1, is caused by genetic mutations in the RAS-MAPK pathway. The age of onset and clinical penetrance of cardiomyopathy differ between NS and NF1. NS typically presents in childhood or adolescence, while NF1 may not present until adulthood. The penetrance of cardiomyopathy is also higher in NS than in NF1. Colquitt et al. in 2014 demonstrated that in NS patients severe HCM has an early onset with an increased risk of long-term morbidities (74). Later many studies confirmed the early onset of HCM (75, 76) as well as pulmonary valve stenosis and arterial septal defect in NS patients (77). In contrast, the prevalence of HCM in NF1 patients was only 2%, with a mean age of onset of 26 years. Also, mutations in the NF1 gene have been associated with a decreased risk of cardiomyopathy (59).

Several genetic variants have been associated with an increased risk of cardiomyopathy in NS and NF1. In NS, mutations in the *PTPN11* and *RAF1* genes have been associated with an increased risk of HCM. Lin et al. in 2000 found that the prevalence of HCM was higher in NS patients with *PTPN11* mutations than in those with *RAF1* mutations (44% vs. 18%). Overall, 9% of the DCM cohort presenting in childhood or adolescence have *RAF1* mutations (59) *PTPN11* had common echocardiography features characterized by pulmonary valve stenosis, while HCM is characterized by *RAF1*. *RAF1* genotypes were shown as prognostic factors, eliciting multiple interventions that may be required for NS patients with severe pulmonary stenosis or myectomy for HCM (77). But a recent study indicated that the proportion of *RIT1* mutation-positive patients who underwent intervention due to cardiovascular disease was significantly higher than that of patients with *PTPN11* mutations (78). A multi-center cohort study to compare the incidence of sudden cardiac death (SCD) and implantable cardioverter-defibrillator (ICD) use between RAS-HCM ($n = 188$) and P-HCM ($n = 567$) patients showed a lower median age for RAS-HCM. Nonarrhythmic deaths occurred primarily in infancy, and SCD primarily in adolescence (79). Another study suggested the possibilities of prenatal RASopathy testing by comparing the genotypic variations from 352 chromosomal microarray negative cases for prenatal RASopathy testing with post-natal cohorts (25 patients with available prenatal information and 108 institutional database genotypes). The study supported the view that a subset of RASopathy genes and variants that are more frequently associated with complex prenatal features such as hydrops/effusions or serious cardiopathy should be considered in the prenatal evaluation (80).

Trametinib, cobimetinib, and binimetinib are examples of medications that have been approved for use in certain tumors to suppress the RAS/MAPK signaling pathway. These medications may benefit NS patients with mutations resulting in gain-of-function alterations in the RAS/MAPK pathway. This has been investigated in mouse models with the *RAF1* mutation, which is present in many NS patients. Mek inhibition during postnatal treatment reversed hypertrophy, restored standard cardiomyocyte size, and lowered fractional shortening toward the target range (81). Since then, there have been several case reports highlighting anecdotal successes with MEK inhibition in NS patients. By now, three groups have described the cases of four patients who, after

using trametinib, showed improvement from NS and HCM (82–84). Studies have also shown that arrhythmia and lymphatic abnormalities resolve after starting MEK inhibition treatment (83, 85, 86). While there are some promising early reports of this medical therapy for a patient population for which it is typically believed that the only treatment option is cardiac transplantation, more research is still required in this area (87).

Our understanding of the molecular basis of RASopathies continues to expand, along with our knowledge of the various clinical manifestations of these disorders, including cardiomyopathy. **Figure 3** indicates the involvement of RAS/MAPK pathway genes in NS and NF1. The age of onset and clinical penetrance of cardiomyopathy in NS and NF1 are important factors that can influence the diagnosis and management of these conditions. However, much is still unknown about the mechanisms underlying the development of cardiomyopathy in RASopathies, and further research is needed to identify novel therapeutic targets and improve outcomes for affected individuals. One potential explanation for the variability in age of onset and clinical penetrance of cardiomyopathy in NS and NF1 is the wide range of genetic mutations that can occur within these genes. As we have seen, specific mutations can result in more severe forms of cardiomyopathy, while others may have little to no effect on the heart. Other genetic and environmental factors may also play a role in determining the severity and timing of cardiomyopathy in these individuals. Another possible explanation is that comorbidities, such as hypertension, diabetes, or obesity, can further exacerbate the risk of developing cardiomyopathy in individuals with RASopathies. It is crucial for clinicians to carefully monitor and manage these conditions to reduce the risk of cardiovascular complications in this patient population.

Despite these challenges, genetic testing and imaging technology advances have greatly improved our ability to diagnose and monitor cardiomyopathy in individuals with RASopathies. Identifying specific genetic mutations associated with cardiomyopathy can help guide treatment decisions and improve outcomes for affected individuals.

De-novo mutations in RAS/MAPK pathway

Since the RAS/MAPK pathway was discovered in humans, the role of these two molecules has been investigated extensively in a wide range of human diseases, including the role of somatic mutations in RAS/MAPK mediated cancer. RAS/MAPK pathway genes are often activated because of germline mutations, referred to as RASopathies, comprising ectodermal and mesodermal development abnormalities and various neoplasia. Interestingly, mutations in RASopathy genes impact different cellular subsets differently, and the phenotype observed in patients varies widely. This phenotype diversity with the same genotype could be due to

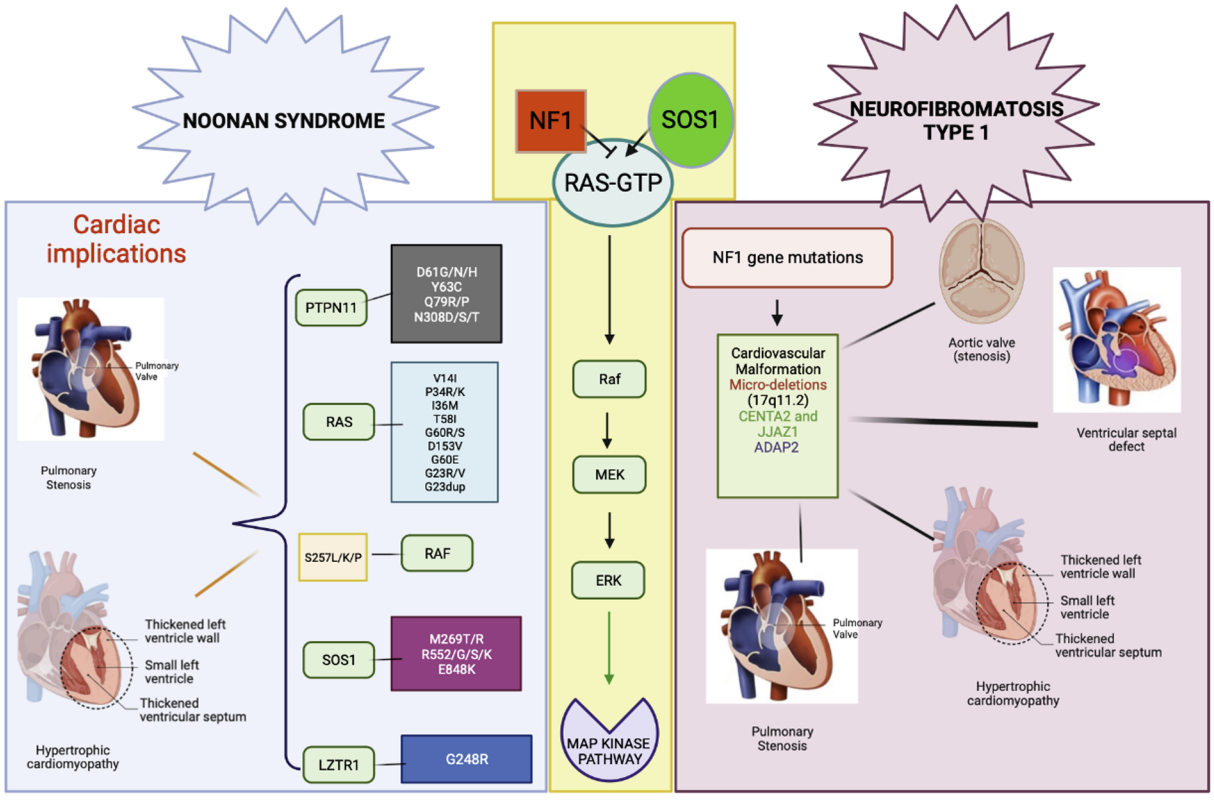

FIGURE 3
RAS/MAPK pathway gene involvement in NS and NF1. Gene variants and cardiac malformations in NS and NF1.

secondary events modified by epigenetic, environmental, and yet undetermined factors. Recent sequencing technology advances have enabled us to decipher many genotype-phenotype mysteries. A recent study discovered *de novo* variants in PTPN11, RAF1, BARF, SHOC2, RASA1, and HRAS in nine sporadic patients, all of whom had cardiovascular abnormalities along with other Noonan syndromic malformations (88). The above study identified six genes harboring eight *de novo* variants. Two patients with Capillary Malformation-Arteriovenous Malformation (CM-AVM had a novel variant in RASA1. The novel missense variant (NM_002890.2: c.2828T>C, p.Leu943Pro) occurred with an amino acid change from a nonpolar amino acid, leucine (Leu), to another nonpolar amino acid, proline (Pro). This study demonstrates the limitation of phenotype-driven genetics testing and the power of family-based NGS for detecting disorders with a clinically atypical presentation and in severely ill infants with CHDs without known genetic cause. Individuals with RASopathies have been linked to various malformations along with cardiovascular problems. Patients with these illnesses may have improved outcomes when the diagnosis is determined based on phenotype and genotype.

Conclusion and perspectives

RASopathies are a group of genetic disorders characterized by gene mutations in the RAS/MAPK signaling pathway. These genetic disorders are associated with a broad range of clinical manifestations, including developmental abnormalities, intellectual disabilities, and cardiac defects. Among these disorders' the most common cardiac abnormalities are pulmonary valve stenosis, septal defects, left-sided lesions, and complex forms with multiple anomalies. Early diagnosis and management of these cardiac abnormalities are critical for improving the overall outcome of individuals with RASopathies. With the development of genomic technologies, more details of genetic mutations that result in RASopathies and associated cardiac abnormalities can be identified. The new advancement will provide valuable insights into the pathophysiology of these disorders and may lead to the development of new therapeutics for these debilitating disorders.

Author contributions

NH and SC conceptualized the idea. NH drafted the manuscript. SC, ZC, and MHC edited the drafts. All authors contributed to the article and approved the submitted version.

Funding

ZC is funded by the National Science Foundation (2025434). SC is funded by the American Heart Association (SDG) and by NHLBI (R01HL152063). MHC, is funded by NHLBI (R01HL152063).

Acknowledgments

The figures 1 and 3 were created using biorendor tool. We gratefully acknowledge Sonia Epstein's help in proofreading the final manuscript.

Conflict of interest

The authors declare that the research was conducted in the absence of any commercial or financial relationships that could be construed as a potential conflict of interest.

Publisher's note

References

1. Tidyman WE, Rauen KA. The RASopathies: developmental syndromes of ras/MAPK pathway dysregulation. *Curr Opin Genet Dev.* (2009) 19(3):230–6. doi: 10.1016/j.gde.2009.04.001

2. Rauen KA. The RASopathies. *Annu Rev Genomics Hum Genet.* (2013) 14:355–69. doi: 10.1146/annurev-genom-091212-153523

3. Gelb BD, Roberts AE, Tartaglia M. Cardiomyopathies in Noonan syndrome and the other RASopathies. *Prog Pediatr Cardiol.* (2015) 39(1):13–9. doi: 10.1016/j.ppedcard.2015.01.002

4. Sanchez-Cascos A. The Noonan syndrome. *Eur Heart J.* (1983) 4(4):223–9. doi: 10.1093/oxfordjournals.eurheartj.a061452

5. Stein-Gerlach M, Wallasch C, Ullrich A. SHP-2, SH2-containing protein tyrosine phosphatase-2. *Int J Biochem Cell Biol.* (1998) 30(5):559–66. doi: 10.1016/s1357-2725(98)00002-8

6. Feng GS. Shp-2 tyrosine phosphatase: signaling one cell or many. *Exp Cell Res.* (1999) 253(1):47–54. doi: 10.1006/excr.1999.4668

7. Shaw AC, Kalidas K, Crosby AH, Jeffery S, Patton MA. The natural history of Noonan syndrome: a long-term follow-up study. *Arch Dis Child.* (2007) 92(2):128–32. doi: 10.1136/adc.2006.104547

8. Takazawa A, Hashimoto A, Aomi S, Imamaki M, Noji S, Koyanagi H, et al. Successful mitral valve plasty for mitral regurgitation combined with dilated cardiomyopathy in Noonan's syndrome. *Nihon Kyobu Geka Gakkai.* (1995) 43(6):894–7.

9. Yu CM, Chow LT, Sanderson JE. Dilated cardiomyopathy in Noonan's syndrome. *Int J Cardiol.* (1996) 56(1):83–5. doi: 10.1016/0167-5273(96)02713-1

10. Kurose A, Oyama K, Murakami Y, Ohyama K, Segawa I, Sawai T, et al. Dilated cardiomyopathy in Noonan's syndrome: a first autopsy case. *Hum Pathol.* (2000) 31(6):764–7. doi: 10.1053/hupa.2000.7635

11. Aljeaid D, Sanchez AI, Wakefield E, Chadwell SE, Moore N, Prada CE, et al. Prevalence of pathogenic and likely pathogenic variants in the RASopathy genes in patients who have had panel testing for cardiomyopathy. *Am J Med Genet A.* (2019) 179(4):608–14. doi: 10.1002/ajmg.a.61072

12. Sarkozy A, Digilio MC, Dallapiccola B. Leopard syndrome. *Orphanet J Rare Dis*. (2008) 3:13. doi: 10.1186/1750-1172-3-13

13. Carcavilla A, Santomé JL, Pinto I, Sánchez-Pozo J, Guillén-Navarro E, Martín-Frías M, et al. LEOPARD Syndrome: a variant of Noonan syndrome strongly associated with hypertrophic cardiomyopathy. *Rev Esp Cardiol*. (2013) 66(5):350–6. doi: 10.1016/j.rec.2012.09.015

14. Wang J, Chandrasekhar V, Abbadessa G, Yu Y, Schwartz B, Kontaridis MI. In vivo efficacy of the AKT inhibitor ARQ 092 in Noonan syndrome with multiple lentigines-associated hypertrophic cardiomyopathy. *PloS One*. (2017) 12(6): e0178905. doi: 10.1371/journal.pone.0178905

15. Carta C, Pantaleoni F, Bocchinfuso G, Stella L, Vasta I, Sarkozy A, et al. Germline missense mutations affecting KRAS isoform B are associated with a severe Noonan syndrome phenotype. *Am J Hum Genet*. (2006) 79(1):129–35. doi: 10.1086/504394

16. Lee BH, Kim JM, Jin HY, Kim GH, Choi JH, Yoo HW. Spectrum of mutations in Noonan syndrome and their correlation with phenotypes. *J Pediatr*. (2011) 159 (6):1029–35. doi: 10.1016/j.jpeds.2011.05.024

17. Cirstea IC, Kutsche K, Dvorsky R, Gremer L, Carta C, Horn D, et al. A restricted spectrum of NRAS mutations causes Noonan syndrome. *Nat Genet*. (2010) 42 (1):27–9. doi: 10.1038/ng.497

18. Aoki Y, Niihori T, Banjo T, Okamoto N, Mizuno S, Kurosawa K, et al. Gain-of-function mutations in RIT1 cause Noonan syndrome, a RAS/MAPK pathway syndrome. *Am J Hum Genet*. (2013) 93(1):173–80. doi: 10.1016/j.ajhg.2013.05.021

19. Schade RW, van't Laar A, Majoor CL, Jansen AP. A comparative study of the effects of cholestyramine and neomycin in the treatment of type II hyperlipoproteinaemia. *Acta Med Scand*. (1976) 199(3):175–80. doi: 10.1111/j.0954-6820.1976.tb06712.x

20. Tang TL, Freeman RM, O'Reilly AM, Neel BG, Sokol SY. The SH2-containing protein-tyrosine phosphatase SH-PTP2 is required upstream of MAP kinase for early Xenopus development. *Cell*. (1995) 80(3):473–83. doi: 10.1016/0092-8674(95)90498-0

21. Qu CK, Yu WM, Azzarelli B, Cooper S, Broxmeyer HE, Feng GS. Biased suppression of hematopoiesis and multiple developmental defects in chimeric mice containing shp-2 mutant cells. *Mol Cell Biol*. (1998) 18(10):6075–82. doi: 10.1128/MCB.18.10.6075

22. Chen B, Bronson RT, Klaman LD, Hampton TG, Wang JF, Green PJ. Mice mutant for egfr and Shp2 have defective cardiac semilunar valvulogenesis. *Nat Genet*. (2000) 24(3):296–9. doi: 10.1038/73528

23. Saxton TM, Ciruna BG, Holmyard D, Kulkarni S, Harpal K, Rossant J. The SH2 tyrosine phosphatase shp2 is required for mammalian limb development. *Nat Genet*. (2000) 24(4):420–3. doi: 10.1038/74279

24. Neel BG, Gu H, Pao L. The 'Shp'ing news: sH2 domain-containing tyrosine phosphatases in cell signaling. *Trends Biochem Sci*. (2003) 28(6):284–93. doi: 10.1016/S0968-0004(03)00091-4

25. Roberts AE, Araki T, Swanson KD, Montgomery KT, Schiripo TA, Joshi VA, et al. Germline gain-of-function mutations in SOS1 cause Noonan syndrome. *Nat Genet*. (2007) 39(1):70–4. doi: 10.1038/ng1926

26. Webb GC, Jenkins NA, Largaespada DA, Copeland NG, Fernandez CS, Bowtell DD. Mammalian homologues of the Drosophila son of sevenless gene map to murine chromosomes 17 and 12 and to human chromosomes 2 and 14, respectively. *Genomics*. (1993) 18(1):14–9. doi: 10.1006/geno.1993.1421

27. Hart TC, Zhang Y, Gorry MC, Hart PS, Cooper M, Marazita ML, et al. A mutation in the SOS1 gene causes hereditary gingival fibromatosis type 1. *Am J Hum Genet*. (2002) 70(4):943–54. doi: 10.1086/339689

28. Lepri F, De Luca A, Stella L, Rossi C, Baldassarre G, Pantaleoni F, et al. SOS1 Mutations in Noonan syndrome: molecular spectrum, structural insights on pathogenic effects, and genotype-phenotype correlations. *Hum Mutat*. (2011) 32 (7):760–72. doi: 10.1002/humu.21492

29. Nimnual A, Bar-Sagi D. The two hats of SOS. *Sci STKE*. (2002) 2002(145):pe36. doi: 10.1126/stke.2002.145.pe36

30. Zenker M, Horn D, Wieczorek D, Allanson J, Pauli S, van der Burgt I, et al. SOS1 Is the second most common Noonan gene but plays no major role in cardio-facio-cutaneous syndrome. *J Med Genet*. (2007) 44(10):651–6. doi: 10.1136/jmg.2007.051276

31. Schubbert S, Zenker M, Rowe SL, Böll S, Klein C, Bollag G, et al. Germline KRAS mutations cause Noonan syndrome. *Nat Genet*. (2006) 38(3):331–6. doi: 10.1038/ng1748

32. Mitchell EL, Jones D, White GR, Varley JM, Santibanez Koref MF. Determination of the gene order of the three loci CD2, NGFB, and NRAS at human chromosome band 1p13 and refinement of their localisation at the subband level by fluorescence in situ hybridisation. *Cytogenet Cell Genet*. (1995) 70(3–4):183–5. doi: 10.1159/000134028

33. Bertola DR, Yamamoto GL, Almeida TF, Buscarilli M, Jorge AAL, Malaquias AC, et al. Further evidence of the importance of RIT1 in Noonan syndrome. *Am J Med Genet A*. (2014) 164A(11):2952–7. doi: 10.1002/ajmg.a.36722

34. Gos M, Fahiminiya S, Poznański J, Klapecki J, Obersztyn E, Piotrowicz M, et al. Contribution of RIT1 mutations to the pathogenesis of Noonan syndrome: four new cases and further evidence of heterogeneity. *Am J Med Genet A*. (2014) 164A (9):2310–6. doi: 10.1002/ajmg.a.36646

35. Pandit B, Sarkozy A, Pennacchio LA, Carta C, Oishi K, Martinelli S, et al. Gain-of-function RAF1 mutations cause Noonan and LEOPARD syndromes with hypertrophic cardiomyopathy. *Nat Genet*. (2007) 39(8):1007–12. doi: 10.1038/ng2073

36. Razzaque MA, Nishizawa T, Komoike Y, Yagi H, Furutani M, Amo R, et al. Germline gain-of-function mutations in RAF1 cause Noonan syndrome. *Nat Genet*. (2007) 39(8):1013–7. doi: 10.1038/ng2078

37. Kobayashi T, Aoki Y, Niihori T, Cavé H, Verloes A, Okamoto N, et al. Molecular and clinical analysis of RAF1 in Noonan syndrome and related disorders: dephosphorylation of serine 259 as the essential mechanism for mutant activation. *Hum Mutat*. (2010) 31(3):284–94. doi: 10.1002/humu.21187

38. Wan PTC, Garnett MJ, Roe SM, Lee S, Niculescu-Duvaz D, Good VM, et al. Mechanism of activation of the RAF-ERK signaling pathway by oncogenic mutations of B-RAF. *Cell*. (2004) 116(6):855–67. doi: 10.1016/s0092-8674(04)00215-6

39. Giroux S, Tremblay M, Bernard D, Cardin-Girard JF, Aubry S, Larouche L, et al. Embryonic death of Mek1-deficient mice reveals a role for this kinase in angiogenesis in the labyrinthine region of the placenta. *Curr Biol*. (1999) 9(7):369–72. doi: 10.1016/s0960-9822(99)80164-x

40. Nava C, Hanna N, Michot C, Pereira S, Pouvreau N, Niihori T, et al. Cardio-facio-cutaneous and Noonan syndromes due to mutations in the RAS/MAPK signalling pathway: genotype-phenotype relationships and overlap with costello syndrome. *J Med Genet*. (2007) 44(12):763–71. doi: 10.1136/jmg.2007.050450

41. Yamamoto GL, Aguena M, Gos M, Hung C, Pilch J, Fahiminiya S, et al. Rare variants in SOS2 and LZTR1 are associated with Noonan syndrome. *J Med Genet*. (2015) 52(6):413–21. doi: 10.1136/jmedgenet-2015-103018

42. Piotrowski A, Xie J, Liu YF, Poplawski AB, Gomes AR, Madanecki P, et al. Germline loss-of-function mutations in LZTR1 predispose to an inherited disorder of multiple schwannomas. *Nat Genet*. (2014) 46(2):182–7. doi: 10.1038/ng.2855

43. Vissers LELM, Bonetti M, Paardekooper Overman J, Nillesen WM, Frints SGM, de Ligt J, et al. Heterozygous germline mutations in A2ML1 are associated with a disorder clinically related to Noonan syndrome. *Eur J Hum Genet*. (2015) 23 (3):317–24. doi: 10.1038/ejhg.2014.115

44. Galliano MF, Toulza E, Gallinaro H, Jonca N, Ishida-Yamamoto A, Serre G, et al. A novel protease inhibitor of the alpha2-macroglobulin family expressed in the human epidermis. *J Biol Chem*. (2006) 281(9):5780–9. doi: 10.1074/jbc.M508017200

45. Chen PC, Yin J, Yu HW, Yuan T, Fernandez M, Yung CK, et al. Next-generation sequencing identifies rare variants associated with Noonan syndrome. *Proc Natl Acad Sci U S A*. (2014) 111(31):11473–8. doi: 10.1073/pnas.1324128111

46. Uusitalo E, Leppävirta J, Koffert A, Suominen S, Vahtera J, Vahlberg T, et al. Incidence and mortality of neurofibromatosis: a total population study in Finland. *J Invest Dermatol*. (2015) 135(3):904–6. doi: 10.1038/jid.2014.465

47. Dasgupta B, Dugan LL, Gutmann DH. A neurofibromatosis-1-regulated pathway is required for learning in Drosophila. *Nature*. (2000) 403(6772):895–8. doi: 10.1038/35002593

48. Guo HF, Tong J, Hannan F, Luo L, Zhong Y. The neurofibromatosis 1 gene product neurofibromin regulates pituitary adenylate cyclase-activating polypeptide-mediated signaling in astrocytes. *J Neurosci*. (2003) 23(26):8949–54. doi: 10.1523/JNEUROSCI.23-26-08949.2003

49. İncecik F, Hergüner ÖM, Alınç Erdem S, Altunbaşak Ş. Neurofibromatosis type 1 and cardiac manifestations. *Turk Kardiyol Dern Ars*. (2015) 43(8):714–6. doi: 10.5543/tkda.2015.27557

50. Nguyen R, Mir TS, Kluwe L, Jett K, Kentsch M, Mueller G, et al. Cardiac characterization of 16 patients with large NF1 gene deletions. *Clin Genet*. (2013) 84 (4):344–9. doi: 10.1111/cge.12072

51. Pinna V, Daniele P, Calcagni G, Mariniello L, Criscione R, Giardina C, et al. Prevalence, type, and molecular Spectrum of NF1 mutations in patients with neurofibromatosis type 1 and congenital heart disease. *Genes (Basel)*. (2019) 10 (9):675. doi: 10.3390/genes10090675

52. Sørensen SA, Mulvihill JJ, Nielsen A. Long-term follow-up of von recklinghausen neurofibromatosis. Survival and malignant neoplasms. *N Engl J Med*. (1986) 314(16):1010–5. doi: 10.1056/NEJM198604173141603

53. Baradhi KM, Bream P. Fibromuscular dysplasia. In: *Statpearls*. Treasure Island (FL): StatPearls Publishing (2022). Available at: http://www.ncbi.nlm.nih.gov/books/NBK493204/ (Accessed February 28, 2023).

54. Keenan RA, Robinson DJ, Briggs PC. Fatal spontaneous retroperitoneal haemorrhage caused by von Recklinghausen's neurofibromatosis. *J R Coll Surg Edinb*. (1982) 27(5):310.

55. Shelton NP. Fatal spontaneous retroperitoneal hemorrhage in a patient with von Recklinghausen's disease. A case report. *J Indiana State Med Assoc*. (1983) 76 (12):831.

56. Poston GJ, Grace PA, Venn G, Spencer J. Recurrent near-fatal haemorrhage in von Recklinghausen's disease. *Br J Clin Pract*. (1990) 44(12):755–6.

57. Friedman JM. Neurofibromatosis 1. In: Adam MP, Everman DB, Mirzaa GM, Pagon RA, Wallace SE, Bean LJ, et al. editors. *Genereviews®*. Seattle (WA): University of Washington (1993). Available at: http://www.ncbi.nlm.nih.gov/books/NBK1109/ (Accessed February 27, 2023).

58. Friedman JM, Arbiser J, Epstein JA, Gutmann DH, Huot SJ, Lin AE, et al. Cardiovascular malformations and other cardiovascular abnormalities in neurofibromatosis 1. *Am J Med Genet*. (2000) 95(2):108–17. doi: 10.1002/1096-8628(20001113)95:2<108::aid-ajmg4>3.0.co;2-0

59. Lin AE, Birch PH, Korf BR, Tenconi R, Niimura M, Poyhonen M, et al. Cardiovascular disease in neurofibromatosis 1: report of the NF1 cardiovascular task force. *Genet Med*. (2002) 4(3):105–11. doi: 10.1097/00125817-200205000-00002

60. Tedesco MA, Di Salvo G, Natale F, Pergola V, Calabrese E, Grassia C, et al. The heart in neurofibromatosis type 1: an echocardiographic study. *Am Heart J*. (2002) 143(5):883–8. doi: 10.1067/mhj.2002.122121

61. Gutmann DH, Wood DL, Collins FS. Identification of the neurofibromatosis type 1 gene product. *Proc Natl Acad Sci U S A*. (1991) 88(21):9658–62. doi: 10.1073/pnas.88.21.9658

62. Prasad BCM, Chandra VVR, Sudarsan A, Kumar PS, Sarma PVGK. Clinical characteristics and NF1 gene mutation analysis of three successive generations in three different Indian families with neurofibromatosis type 1 and peripheral nerve sheath tumours. *J Clin Neurosci*. (2018) 53:62–8. doi: 10.1016/j.jocn.2018.04.006

63. Venturin M, Carra S, Gaudenzi G, Brunelli S, Gallo GR, Moncini S, et al. ADAP2 In heart development: a candidate gene for the occurrence of cardiovascular malformations in NF1 microdeletion syndrome. *J Med Genet*. (2014) 51(7):436–43. doi: 10.1136/jmedgenet-2013-102240

64. Venturin M, Guarnieri P, Natacci F, Stabile M, Tenconi R, Clementi M, et al. Mental retardation and cardiovascular malformations in NF1 microdeleted patients point to candidate genes in 17q11.2. *J Med Genet*. (2004) 41(1):35–41. doi: 10.1136/jmg.2003.014761

65. Tartaglia M, Mehler EL, Goldberg R, Zampino G, Brunner HG, Kremer H, et al. Mutations in PTPN11, encoding the protein tyrosine phosphatase SHP-2, cause Noonan syndrome. *Nat Genet*. (2001) 29(4):465–8. doi: 10.1038/ng772

66. Ratola A, Silva HM, Guedes A, Mota C, Braga AC, Oliveira D, et al. A novel Noonan syndrome RAF1 mutation: lethal course in a preterm infant. *Pediatr Rep*. (2015) 7(2):5955. doi: 10.4081/pr.2015.5955

67. Harms FL, Alawi M, Amor DJ, Tan TY, Cuturilo G, Lissewski C, et al. The novel RAF1 mutation p.(Gly361Ala) located outside the kinase domain of the CR3 region in two patients with Noonan syndrome, including one with a rare brain tumor. *Am J Med Genet A*. (2018) 176(2):470–6. doi: 10.1002/ajmg.a.38569

68. Hagino M, Ota C, Onoki T, Iwasawa S. Male infant with Noonan syndrome with RAF-1 gene mutation who survived hypertrophic cardiomyopathy-induced fatal heart failure and uncontrollable arrhythmias. *BMJ Case Rep*. (2022) 15(9):e250342. doi: 10.1136/bcr-2022-250342

69. Lan J, Zeng T, Liu S, Lan J, Qian L. Noonan syndrome with RAF1 gene mutations in a newborn with cerebral haemorrhage. *Eur J Med Res*. (2022) 27(1):146. doi: 10.1186/s40001-022-00772-2

70. Lee BH, Yoo H-W. Noonan syndrome and RASopathies: clinical features, diagnosis and management. *J Genet Med,*. (2019) 16(1):1–9. doi: 10.5734/JGM.2019.16.1.1

71. Romano A, Kaski JP, Dahlgren J, Kelepouris N, Pietropoli A, Rohrer TR, et al. Cardiovascular safety of growth hormone treatment in Noonan syndrome: real-world evidence. *Endocr Connect*. (2022) 11(1):e210549. doi: 10.1530/EC-21-0549

72. Hamoy-Jimenez G, Elahmar HA, Mendoza M, Kim RH, Bril V, Barnett C. A cross-sectional study of gender differences in quality of life domains in patients with neurofibromatosis type 1. *Orphanet J Rare Dis*. (2022) 17(1):40. doi: 10.1186/s13023-022-02195-y

73. Cutruzzolà A, Irace C, Frazzetto M, Sabatino J, Gullace R, De Rosa S, et al. Functional and morphological cardiovascular alterations associated with neurofibromatosis 1. *Sci Rep*. (2020) 10(1):12070. doi: 10.1038/s41598-020-68908-0

74. Colquitt JL, Noonan JA. Cardiac findings in Noonan syndrome on long-term follow-up. *Congenit Heart Dis*. (2014) 9(2):144–50. doi: 10.1111/chd.12102

75. Lioncino M, Monda E, Verrillo F, Moscarella E, Calcagni G, Drago F, et al. Hypertrophic cardiomyopathy in RASopathies: diagnosis, clinical characteristics, prognostic implications, and management. *Heart Fail Clin*. (2022) 18(1):19–29. doi: 10.1016/j.hfc.2021.07.004

76. Chen H, Li X, Liu X, Wang J, Zhang Z, Wu J, et al. Clinical and mutation profile of pediatric patients with RASopathy-associated hypertrophic cardiomyopathy: results from a Chinese cohort. *Orphanet J Rare Dis*. (2019) 14(1):29. doi: 10.1186/s13023-019-1010-z

77. Sun L, Xie YM, Wang SS, Zhang ZW. Cardiovascular abnormalities and gene mutations in children with Noonan syndrome. *Front Genet*. (2022) 13:915129. doi: 10.3389/fgene.2022.915129

78. Ichikawa Y, Kuroda H, Ikegawa T, Kawai S, Ono S, Kim KS, et al. Cardiac features of Noonan syndrome in Japanese patients. *Cardiol Young*. (2023) 33(4):564–9. doi: 10.1017/S104795112200124X

79. Lynch A, Tatangelo M, Ahuja S, Steve Fan CP, Min S, Lafreniere-Roula M, et al. Risk of sudden death in patients with RASopathy hypertrophic cardiomyopathy. *J Am Coll Cardiol*. (2023) 81(11):1035–45. doi: 10.1016/j.jacc.2023.01.012

80. Scott A, Di Giosaffatte N, Pinna V, Daniele P, Corno S, D'Ambrosio V, et al. When to test fetuses for RASopathies? Proposition from a systematic analysis of 352 multicenter cases and a postnatal cohort. *Genet Med*. (2021) 23(6):1116–24. doi: 10.1038/s41436-020-01093-7

81. Wu X, Simpson J, Hong JH, Kim KH, Thavarajah NK, Backx PH, et al. MEK-ERK pathway modulation ameliorates disease phenotypes in a mouse model of Noonan syndrome associated with the Raf1(L613V) mutation. *J Clin Invest*. (2011) 121(3):1009–25. doi: 10.1172/JCI44929

82. Andelfinger G, Marquis C, Raboisson MJ, Théoret Y, Waldmüller S, Wiegand G, et al. Hypertrophic cardiomyopathy in Noonan syndrome treated by MEK-inhibition. *J Am Coll Cardiol*. (2019) 73(17):2237–9. doi: 10.1016/j.jacc.2019.01.066

83. Meisner JK, Bradley DJ, Russell MW. Molecular management of multifocal atrial tachycardia in Noonan's syndrome with MEK1/2 inhibitor trametinib. *Circ Genom Precis Med*. (2021) 14(5):e003327. doi: 10.1161/CIRCGEN.121.003327

84. Mussa A, Carli D, Giorgio E, Villar AM, Cardaropoli S, Carbonara C, et al. MEK Inhibition in a newborn with RAF1-associated Noonan syndrome ameliorates hypertrophic cardiomyopathy but is insufficient to revert pulmonary vascular disease. *Genes (Basel)*. (2021) 13(1):6. doi: 10.3390/genes13010006

85. Dori Y, Smith C, Pinto E, Snyder K, March ME, Hakonarson H, et al. Severe lymphatic disorder resolved with MEK inhibition in a patient with Noonan syndrome and SOS1 mutation. *Pediatrics*. (2020) 146(6):e20200167. doi: 10.1542/peds.2020-0167

86. Nakano TA, Rankin AW, Annam A, Kulungowski AM, McCallen LM, Hill LR, et al. Trametinib for refractory chylous effusions and systemic complications in children with Noonan syndrome. *J Pediatr*. (2022) 248:81–88.e1. doi: 10.1016/j.jpeds.2022.05.030

87. Wilkinson JD, Lowe AM, Salbert BA, Sleeper LA, Colan SD, Cox GF, et al. Outcomes in children with Noonan syndrome and hypertrophic cardiomyopathy: a study from the pediatric cardiomyopathy registry. *Am Heart J*. (2012) 164(3):442–8. doi: 10.1016/j.ahj.2012.04.018

88. Zheng S, Huang H, Ma L, Zhu T. RASopathies due to de novo pathogenic variants: clinical features, genetic findings and outcomes in nine neonates born with congenital heart defects. *BMC Med Genomics*. (2022) 15(1):184. doi: 10.1186/s12920-022-01336-3

Frontiers in
Cardiovascular Medicine

Innovations and improvements in cardiovascular treatment and practice

Focuses on research that challenges the status quo of cardiovascular care, or facilitates the translation of advances into new therapies and diagnostic tools.

Discover the latest Research Topics

See more →

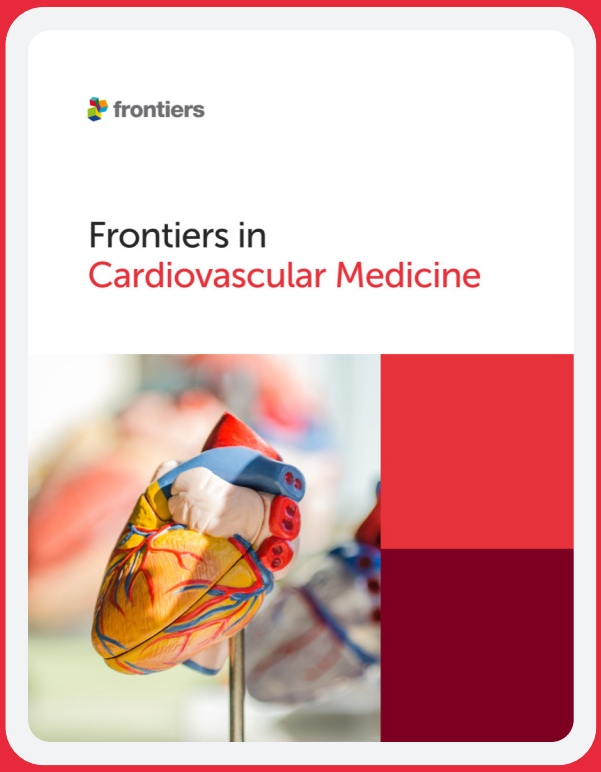

Frontiers

Avenue du Tribunal-Fédéral 34
1005 Lausanne, Switzerland
frontiersin.org

Contact us

+41 (0)21 510 17 00
frontiersin.org/about/contact